University of Alberta

Synthesis and Characterization of Platinum Acetylide Molecules and Macrocycles and Their Circular Dichroism Properties

by

Amber L. Sadowy

A thesis submitted to the Faculty of Graduate Studies and Research
in partial fulfillment of the requirements for the degree of

Master of Science

Department of Chemistry

Edmonton, Alberta
Fall 2007

Your file Votre référence
ISBN: 978-0-494-33338-9
Our file Notre référence
ISBN: 978-0-494-33338-9

ABSTRACT

This thesis will demonstrate the power and limitations of using diphosphine ligand exchange to control the chirality and coordination geometry around the platinum(II) acetylide center of acyclic and cyclic complexes. In one simple step, a *trans*-platinum acetylide complex can be converted to its *cis*-analogue, using either chiral or achiral chelating diphosphine ligands. Conveniently, multiple chiral derivatives can result from a single precursor making this methodology efficient and cost effective.

To increase the scope of these ligand exchange reactions and to study the magnitude of chiral induction provided by the individual diphosphine ligands, three series of acyclic model complexes were synthesized. This study shows that many chelating diphosphine ligands can be used for ligand exchange, and interestingly the CD spectra of these model complexes indicate certain ligands are more effective for chirality transfer than others. Conversely, preliminary studies show *trans*-platinacyclynes are reluctant to undergo the same exchange reactions with chiral diphosphine ligands.

ACKNOWLEDGEMENTS

I would like to thank first and foremost my supervisor Dr. Rik Tykwinski for his enthusiasm and encouragement over the years. I am also thankful for the opportunity to co-author a book chapter with him, an experience that eventually helped in the writing of this thesis and I enjoyed. I will always remember, as well, my attendance at ISNA-12 in Japan as my first international travel experience, which was another fantastic opportunity provided by Rik.

Secondly, I thank the Tykwinski group members, especially, Erin Graham, Shar Ramsaywack and Dan Lehnherr for taking the time and effort to help me edit this thesis, I really appreciate it. I also thank the present members Thanh Luu, Wes Chalifoux, Mojtaba Gholami, Yanqing Pan, Dr. Khalid Azyat and former members and lab mates Jamie Kendall and Andreea Spantulescu for their friendship and help during this time.

The staff at the University of Alberta has also been very helpful during the past three years and I would like to thank, in particular, Wayne Moffat, Ryan Lister and Melanie Kaban in the Analytical and Instrumentation lab for teaching me how to use the CD spectrometer and weighing out so many samples. Dr. Angie Morales-Izquierdo in the Mass Spectrometry lab, Mark Miskolzie in the NMR lab and Drs. Robert McDonald and Michael Ferguson in the X–ray Crystallography lab have also helped me numerous times with my research, which I appreciate tremendously.

Lastly, I must graciously thank my family and friends, in Victoria and Edmonton, for their love and support throughout all my university years, and especially Dana for being my rock. None of this could have been accomplished and wouldn't have been half as fun without them.

TABLE OF CONTENTS

LIST OF TABLES

LIST OF FIGURES

LIST OF SCHEMES

List of Abbreviations

Ac	acetyl
AIBN	azobis(isobutyronitrile)
AFM	atomic force microscopy
AM1	Austin model 1
aq	aqueous
BDPP	2,4-bis(diphenylphosphino)pentane
BINAP	2,2′-bis(diphenylphosphino)-1,1′-binapthyl
bipy	bipyridyl
Bn	benzyl
br	broad
BTAC	benzyltriethylammonium chloride
Bu	butyl
BuLi	butyl lithium
Bz	benzoyl
CD	circular dichroism
CHIRAPHOS	bis(diphenylphosphino)butane
cm	centimeter
Cy	cyclohexyl
dba	dibenzylideneacetone
d	doublet
Trost ligand	1,2-diaminocyclohexane-*N*,*N*′-bis(2′-diphenylphosphino-benzoyl)
DCTB	T-2-(3-(4-*t*-Butyl-phenyl)-2-methyl-2-propenylidene)malononitrile

dec	decomposition
DIOP	4,5-bis(diphenylphosphinomethyl)-2,2-dimethyl-1,3-dioxolane
DME	1,2-dimethoxyethane
DMF	*N*,*N*'-dimethylformamide
dppe	1,2-bis(diphenylphosphino)ethane
dppp	1,3-bis(diphenylphosphino)propane
DUPHOS	1,2-Bis[(2,5)-dimethylphospholano]benzene
EI	electron ionization
Et	ethyl
EtOAc	ethyl acetate
ESI	electrospray
g	gram(s)
GPC	gel permeation chromatography
h	hours
HOMO	highest occupied molecular orbital
HOPG	highly oriented pyrolytic graphite
HRMS	high resolution mass spectroscopy
Hz	hertz
i	iso
IR	infrared
JOSIPHOS	1-[2-(diphenylphosphino)ferrocenyl]ethyldicyclohexylphosphine
K_a	association constant
K_{SV}	Stern–Volmer constant

m	multiplet
M	molar
mg	milligram
MALDI-TOF	matrix-assisted laser desorption/ionization time-of flight
Me	methyl
MHz	megahertz
mL	milliliter
mmol	millimole
Mp	melting point
MS	mass spectroscopy
NBS	*N*-bromosuccinnimide
nm	nanometer
NMR	nuclear magnetic resonance
NORPHOS	2,3-bis(diphenylphosphino)bicyclo[2.2.1]hept-5-ene
ORTEP	Oak Ridge thermal ellipsoid plot
OTf	trifluoromethanesulfonate
PCBM	[6,6]-phenyl-C_{61} butyric acid methyl ester
Ph	phenyl
PhH	benzene
PhMe	toluene
ppm	parts per million
Pr	propyl
PROPHOS	1,2-bis(diphenylphosphino)propane

py	pyridine
ROMP	ring-opening metathesis polymerization
rt	room temperature
s	singlet
SEC	size exclusion chromatography
SPM	shape persistent macrocycle
STM	scanning tunneling microscopy
SYNPHOS	6,6′-bis(diphenylphosphino)-2,2′,3,3′-tetrahydro-5,5′-bi-1,4-benzodioxin
t	triplet
t	tert
TBAF	tetrabutylammonium fluoride
t-Bu	tertiary-butyl
TCB	1,2,4-trichlorobenzene
TES	triethylsilyl
THF	tetrahydrofuran
THP	tetrahyropyranyl
TIPS	triisopropylsilyl
TLC	thin layer chromatography
TMEDA	*N,N,N′,N′*–tetramethylethylenediamine
TMS	trimethylsilyl
TMSCl	trimethylsilyl chloride
tol	toluene
Ts	tosyl (*p*-toluenesulfonyl)

TTF	tris(tetrathiafulvaleno)
UV–vis	ultraviolet–visible
VPO	vapor pressure osmometry
XRD	X–ray diffraction

List of Symbols

Å	angstrom
β_n	natural bite angle
δ	chemical shift
γ	molecular second hyperpolarizability
ε	molar absorptivity
$\Delta\varepsilon$	molar CD or molar extinction
λ	wavelength of emission
λ_{max}	wavelength of maximal absorption
Φ	quantum yield

CHAPTER 1 INTRODUCTION TO SHAPE PERSISTENT MACROCYCLES BASED ON ACETYLENIC SCAFFOLDING*

1.1 INTRODUCTION

Historically, one might argue that the synthesis of many shape persistent macrocycles (SPMs) was initiated through a combination of their enticing symmetrical structures and the synthetic challenge they posed. More recently, however, SPMs have found an important role as functional components in supramolecular chemistry. In comparison to flexible macrocycles, SPMs have been designed to exhibit fewer degrees of conformational flexibility, which greatly facilitates their assembly into highly organized supramolecular systems. From the onset, acetylenic building blocks have played a defining role in the construction of SPMs, and most recently, the evolution of modern metal catalyzed coupling reactions to form sp-sp^2 and sp-sp carbon bonds has greatly advanced this field. Furthermore, SPMs based on acetylenic carbon scaffolding are particularly well suited to applications in supramolecular chemistry, given their synthetic accessibility, rigid or semi-rigid configuration, and lack of steric impedance about the acetylenic units.

The *synthesis* of acetylenic SPMs has been reviewed on a number of occasions, typically with a focus on a particular structural motif, and those molecules based on an arylene ethynylene framework have received enormous attention.[1-13] Likewise, the *use* of acetylenic SPMs in functional systems has also been reviewed, but again typically with respect to a particular molecular design.[5,14-16] In view of previous literature in this area, the goal of this particular chapter will be to integrate the two aspects. First, a general

* A version of this chapter has been submitted for publication in *Modern Supramolecular Chemistry*; Diederich, F.; Stang, P. J.; Tykwinski, R. R., Eds.; Wiley-VCH: Weinheim, in press.

summary of synthetic strategies commonly used for the synthesis of acetylenic SPMs will be described. Second, the implementation of SPMs as building blocks in supramolecular chemistry will be presented, with an emphasis on the synthetic aspects toward the macrocycle intertwined as often as possible. The function of SPMs has been broadly divided into three sections: 1) SPMs used as components of supramolecular assemblies, 2) SPMs used in host–guest systems, and 3) aggregation/adsorption of SPMs, including solution state aggregation, liquid crystallinity, and surface adsorption. Clearly, the substantial breadth of research that has been conducted in the area of acetylenic SPMs prevents a comprehensive description of this research in the confines of a single chapter. Thus, examples have been chosen to highlight the diversity of recent synthetic achievements, as well as the application of SPMs in particular areas of supramolecular chemistry.

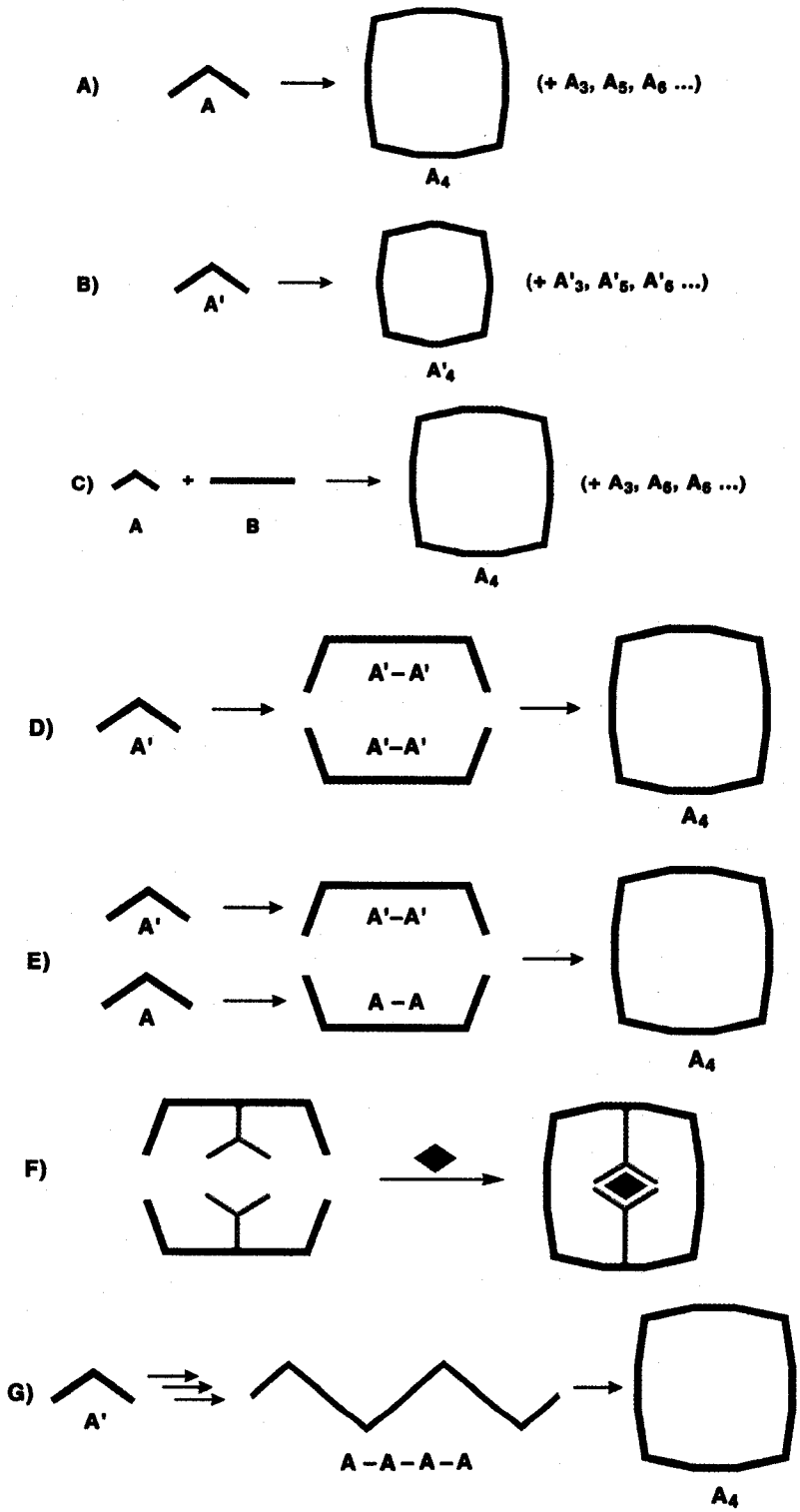

Figure 1.1 Schematic description of synthetic strategies for macrocycle formation.

1.1.1 SPM Synthesis Through Intermolecular Reactions

One of the most straightforward routes to the synthesis of acetylenic SPMs is the one-step **nA** → $\mathbf{A_n}$ approach in which a suitable precursor is subjected to conditions that effect cyclooligomerization (Fig. 1.1A). While often biased to selectively produce a desired cyclic oligomer, other macrocycles are often formed, which can lead to a tedious separation step. As with many macrocyclizations, the success of this strategy benefits from highly dilute conditions that favor the kinetic formation of cyclic products (first order ring closing reaction) over acyclic oligomers (second order reaction). To circumvent the need for extraordinary amounts of solvent to achieve high dilution, many reactions are done under pseudo-high dilution, where one or more of the reactants is added slowly to the reaction mixture. The **nA** → $\mathbf{A_n}$ approach is often used for the synthesis of butadiynyl based macrocycles, in which oxidative acetylenic homocoupling can be relied on for efficient bond formation. This is demonstrated in the synthesis of expanded radialenes **1** to which mesogenic side groups have been appended, as reported by Diederich and coworkers (Scheme 1.1A).[17] In this case, trimer, tetramer, and pentamer macrocycles were observed with the tetramer as the dominant product.

There are a number of variants of oxidative acetylenic homocoupling from which to choose, all based on adaptation of Glaser's original report.[18] Hay (e.g., CuCl, TMEDA, O_2, CH_2Cl_2)[19], Eglinton ($CuSO_4$ or $Cu(OAc)_2$, py),[20,21] and Breslow (CuCl, $CuCl_2$, oxygen free py)[22] conditions are the most commonly encountered. And, more recently, the use of Pd(II) as a co-catalyst in the presence of Cu(I) and O_2 (or an external oxidant such as chloroacetone or I_2) has emerged as an alternative to the traditional Cu(I)/Cu(II) homocoupling based methods.[23] As shown, for example, in the synthesis of TTF based

[18]annulenes **2** and **3** by Iyoda and coworkers (Scheme 1.1B).[24] There seems, unfortunately, to be no real consensus as to predicting which homocoupling protocol stands the best chance of success for a particular target, although it has been shown that reagent solubility, for example, can dictate the success of one method over another.[25]

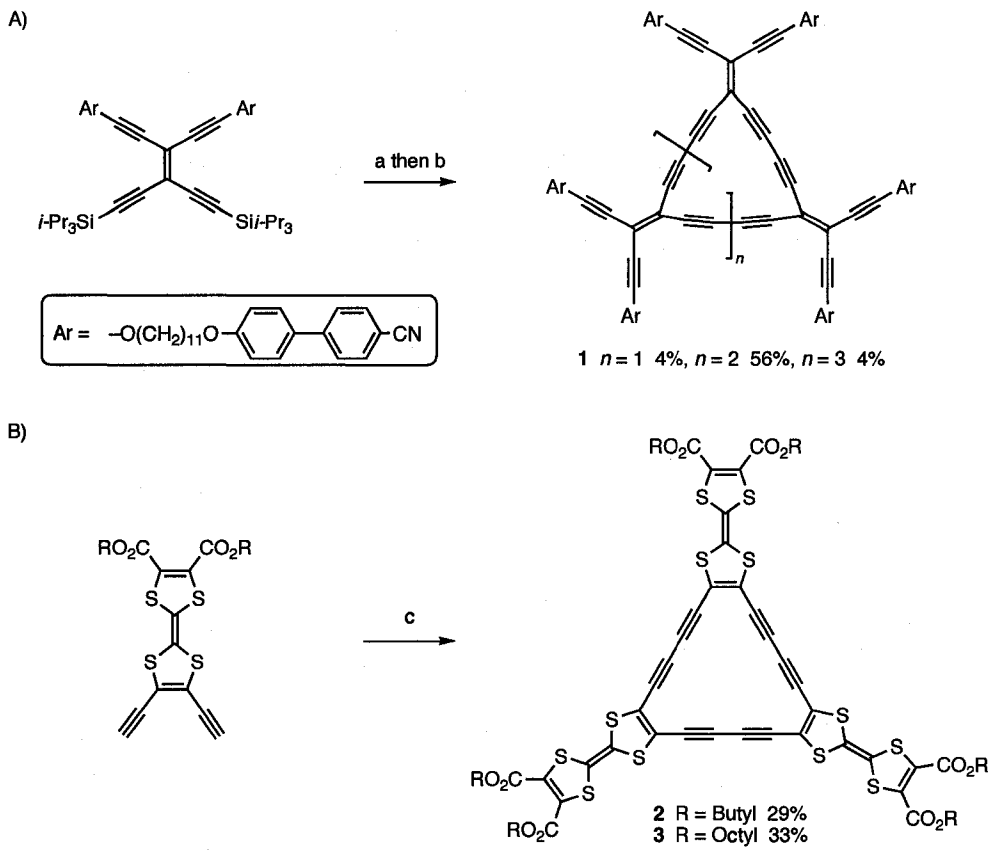

Scheme 1.1 A) Synthesis of radialenes **1** by oxidative acetylenic homocoupling,[17] and B) Synthesis of TTF based [18]annulenes **2** and **3** by Pd-mediated homocoupling.[24] Reagents and conditions: (a) TBAF, THF; (b) $Cu(OAc)_2$, O_2, py/PhH; c) CuI, $PdCl_2(PPh_3)_2$, Et_3N.

The most recent method developed for the **nA** → $\mathbf{A_n}$ approach relies on dynamic covalent bond formation using a metathesis reaction. In this case, reactions are typically under thermodynamic control, providing the potential for increased selectivity in product formation. The initial examples using alkyne metathesis toward the formation of SPMs were reported by Adams, Bunz, and coworkers using the precatalyst $Mo(CO)_6$,[26,27] but

rather low yields of the desired products (**4**) limited general applicability (Scheme 1.2). Recent efforts by Moore and coworkers using a Mo(VI)-alkylidyne catalyst, however, have refined this process such that precipitation driven reactions now provide moderate to excellent results (see Scheme 1.25).[28]

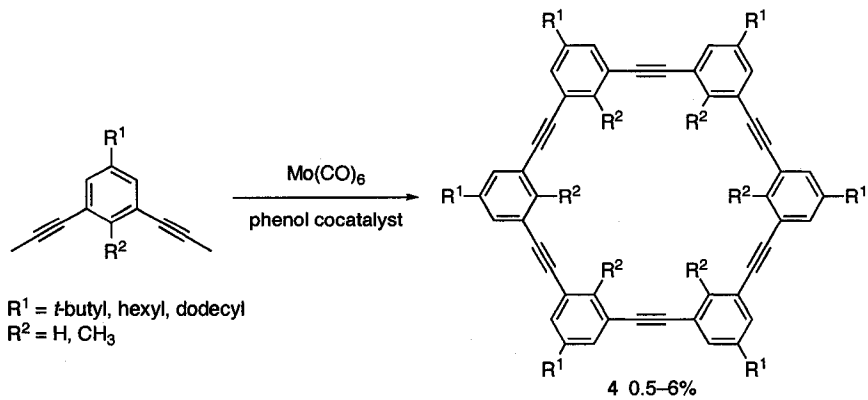

Scheme 1.2 SPM formation by alkyne metathesis.[26]

The **nA** → $\mathbf{A_n}$ approach to macrocycle assembly can also derive from an unsymmetrical, bifunctional precursor (Fig. 1.1B) and often proceeds using a metal catalyzed cross-coupling reaction. This approach was used by Eglinton and coworkers to synthesize the trimeric SPM **5** via a Castro–Stephens coupling starting with the preformed Cu-acetylide **6** (Scheme 1.3).[29] The same product was later synthesized in improved yield by Linstrumelle and coworkers using a Pd-catalyzed Sonogashira coupling, a sequence starting with the *in situ* removal of acetone from **7** under basic conditions to provide the terminal alkyne.[30]

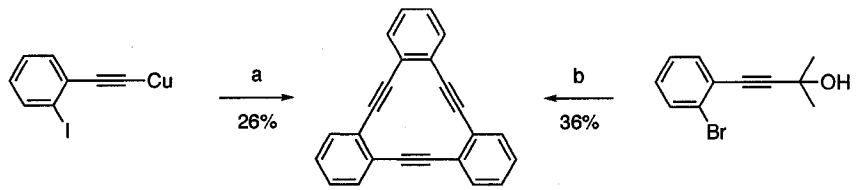

6 5 7

Scheme 1.3 Formation of SPM **5** from unsymmetrical precursors **6** or **7**. Reagents and conditions: (a) py, heat;[29] (b) NaOH, $Pd(PPh_3)_4$, CuI, PhH, BTAC, 85 °C.[30]

A variation of the one-pot approach that has, perhaps, been underdeveloped to date involves the use of multiple components (**A** and **B**), where the geometry of the reactants is designed to provide selectivity toward one macrocyclic product, **nA + nB** → $\mathbf{A_n}$ (Fig. 1.1C). For example, Iyoda and coworkers exploited this approach to form selectively the cyclic trimer **8** based on the combination of a linear acetylene linker and 3,4-diiodothiophene corner piece **9** (Scheme 1.4).[31] Considering that six new carbon-carbon bonds are in formed in this reaction, the overall yield represents an impressive 85% yield for each cross-coupling event.

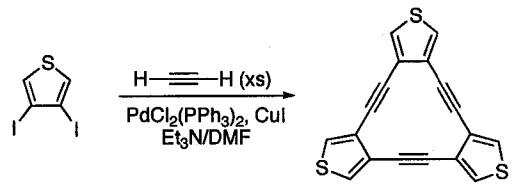

9 8 37%

Scheme 1.4 Formation of SPM **8** via a one-pot, two-component reaction.[31]

A major drawback of the one-pot, one-step approach is the lack of selectivity that is often encountered toward forming a single cyclic oligomer, coupled with a potential lack of control over which oligomer is formed preferentially. To help belay this fact, oligomeric fragments of the desired target are often assembled (Figs. 1.1D and 1.1E) and then combined together in the final step, helping to maximize product formation (e.g., 2(**A–A**) → $\mathbf{A_4}$ or **A–A** + **A'–A'** → $\mathbf{A_4}$). Once again, the ring forming step may be a

homocoupling event as in Figure 1.1D (typically via oxidative acetylenic homocoupling) or the combination of two complimentary pieces as in Figure 1.1E (e.g., via a Sonogashira, Cadiot–Chodkiewicz, or metathesis reaction). Baxter's formation of the pyridine containing macrocycle **10** using the Eglinton reaction provides an example of the former (Scheme 1.5A, see also Fig. 1.3),[32] while Mayor and Shu's use of a Pd-catalyzed Cadiot–Chodkiewicz reaction to combine the two halves (**11** and **12**) of macrocycle **13** demonstrates the latter (Scheme 1.5B, see also Scheme 1.24).[33] The synthesis of these two SPMs provides a salient example of how synthetic yields for macrocycle formation can vary widely, even with the use of a similar strategy.

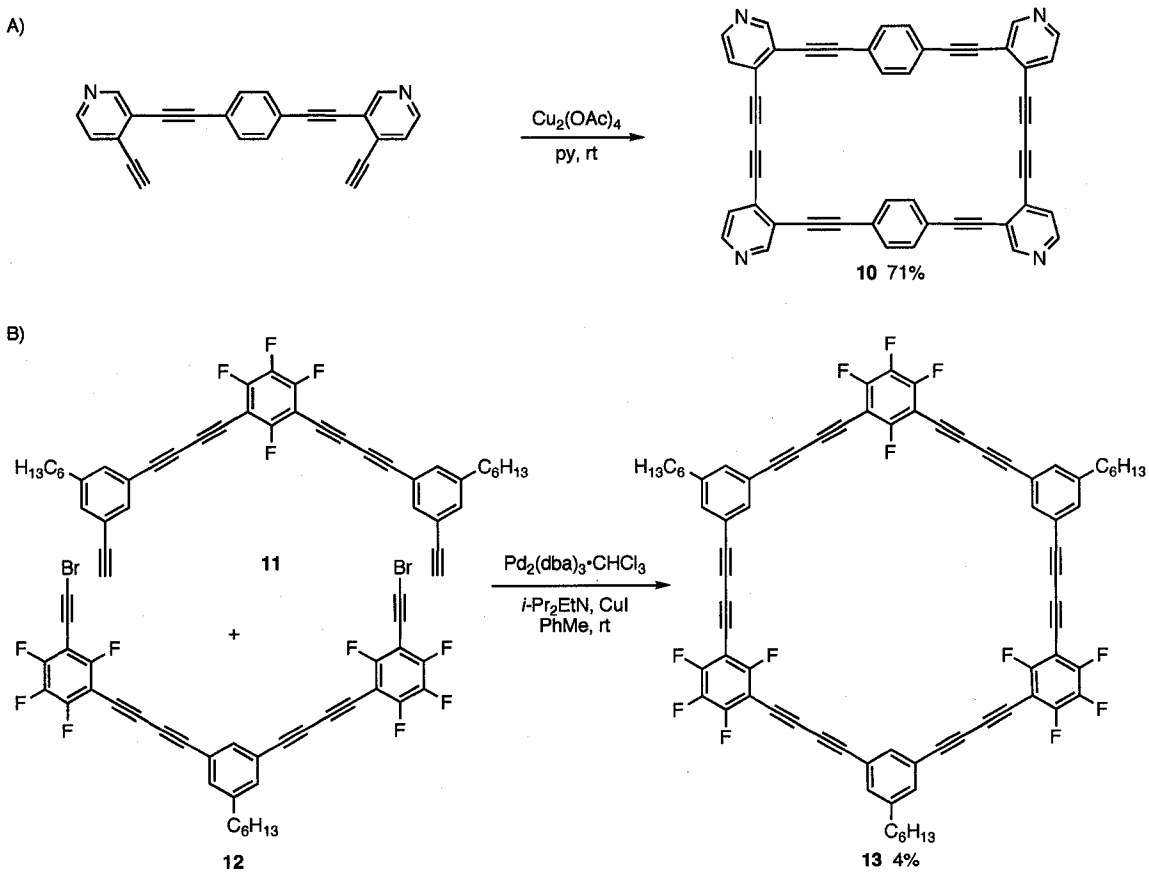

Scheme 1.5 Intermolecular cyclization of preformed oligomeric segments by A) Eglinton homocoupling to form **10**[32] and B) Cadiot–Chodkiewicz heterocoupling to form **13**.[33]

1.1.2 SPM Synthesis Through Intramolecular Reactions

A further improvement on the concept of using preassembled oligomers exploits the involvement of a template (covalent or noncovalent) to "entropically trap" the pieces in a synthetically favorable position (Fig. 1.1F).[34-39] Templation then nominally results in an intramolecular ring-closure reaction, albeit in the case where weaker non-covalent interactions template the fragments together, the definition of intramolecular may not rigorously apply. The concept of templated formation of shape-persistent macrocycles was originally introduced by Sanders and coworkers toward synthesis of porphyrin "dimer" **14** shown in Scheme 1.6, templated by 4,4′-bipyridine.[39-42] In the absence of the 4,4′-bipyridine template, cyclization of **15** under analogous conditions led to a mixture of di- and trimeric macrocycles in reduced yield. In addition, catenation (see Schemes 1.16 and 1.17), metal templation with Pt and Cu (see Schemes 1.17 and 1.21), quadrupolar interactions of aryl and perfluoroaryl groups (see Scheme 1.23 and 1.24) and covalent tethering (see Scheme 1.28) have also been successfully used in the context of templated macrocycle formation.

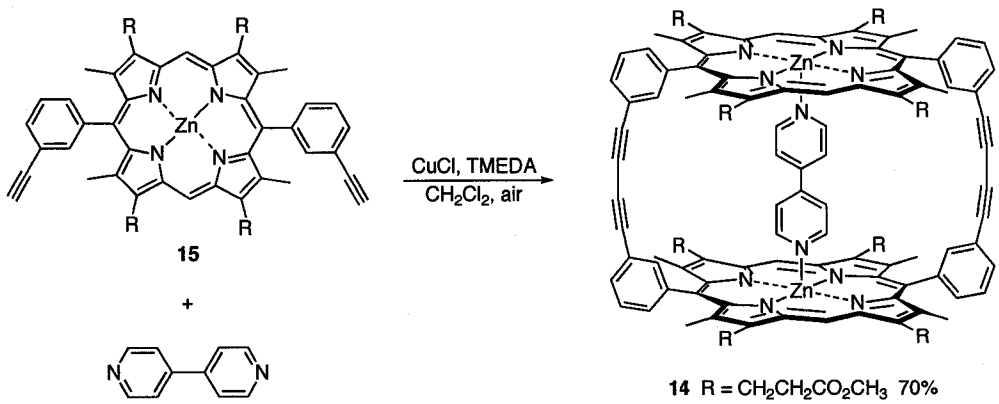

Scheme 1.6 Templated, selective formation of porphyrin "dimer" **14**.[40]

To achieve more precise control over a cyclization process, it is often desirable to reduce the cyclization to a single, intramolecular bond forming reaction, as shown in Figure 1.1G. This approach necessitates the stepwise assembly of an acyclic oligomer lacking only this crucial ring-forming bond. While the synthesis of the requisite precursor can be tedious and time consuming relative to a one-pot cyclooligomerization, the intramolecular nature of the cyclization event ensures the highest selectivity toward formation of a single cyclic product. The route can also result in an increased product yield, although yields can remain frustratingly low. With respect to acetylenic macrocycles, two common approaches will be used to demonstrate this approach. The first involves the use of triazenes as a masking group for aryl iodides, a transformation introduced by Moore and coworkers in 1991.[43] As reported by Yoshida and coworkers, the two "halves" **16** and **17** were assembled separately and then connected through a Sonogashira reaction to give acyclic "octamer" **18** (Scheme 1.7).[44] Three subsequent steps then gave the SPM **19**: 1) reaction of the aryl triazene **18** with I_2 to give the aryl iodide (MeI can also be used[43]), 2) removal of the trimethylsilyl group to provide the terminal alkyne, and 3) ring closure under Sonogashira conditions.

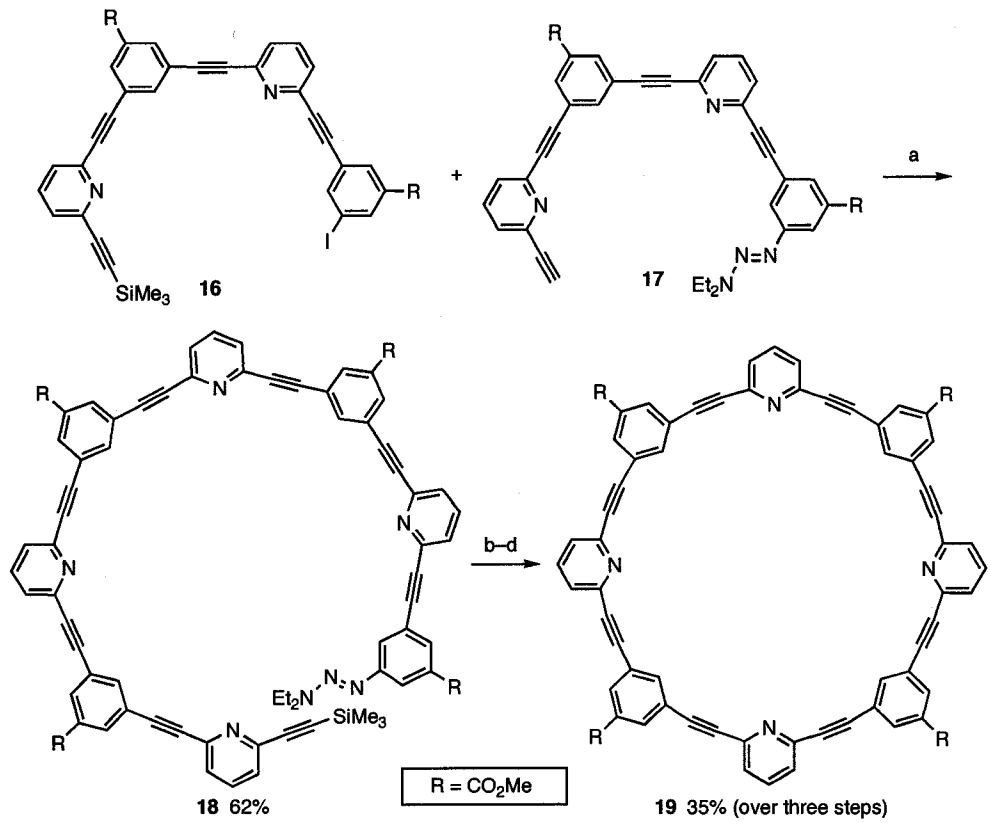

Scheme 1.7 Stepwise formation of SPM **19** using an aryl triazene as a masking group for an aryl iodide.[44] Reagents and conditions: (a) $PdCl_2(PPh_3)_2$, CuI, Et_3N/THF (1:1); (b) I_2, $ClCH_2CH_2Cl$, 80 °C; (c) KOH, MeOH, $CHCl_3$; (d) $PdCl_2(PPh_3)_2$, CuI, Et_3N/THF (1:1).

A second common technique relies on the use of orthogonal alkyne protecting groups, based on the ability to selectively remove a trimethylsilyl (or triethylsilyl) group in the presence of a triisopropylsilyl group (TMS, TES, and TIPS, respectively). The synthesis of tetramer **20** by Tobe and coworkers demonstrates this approach (Scheme 1.8).[45] Starting with **21**, selective removal of the TMS group, with K_2CO_3/MeOH generated the terminal alkyne, which was used without isolation in a Sonogashira reaction with **22**, and this was followed by a second Sonogashira reaction with TMS-acetylene to give **23**. Removal of the TMS group and oxidative homocoupling gave the macrocycle precursor **24**. Finally, the TIPS groups were removed with TBAF, and a

homocoupling reaction gave the desired product **20**. While providing low yield (10%), the preassembly of **24** helped to ensure preferential formation of the desired cyclic tetramer.

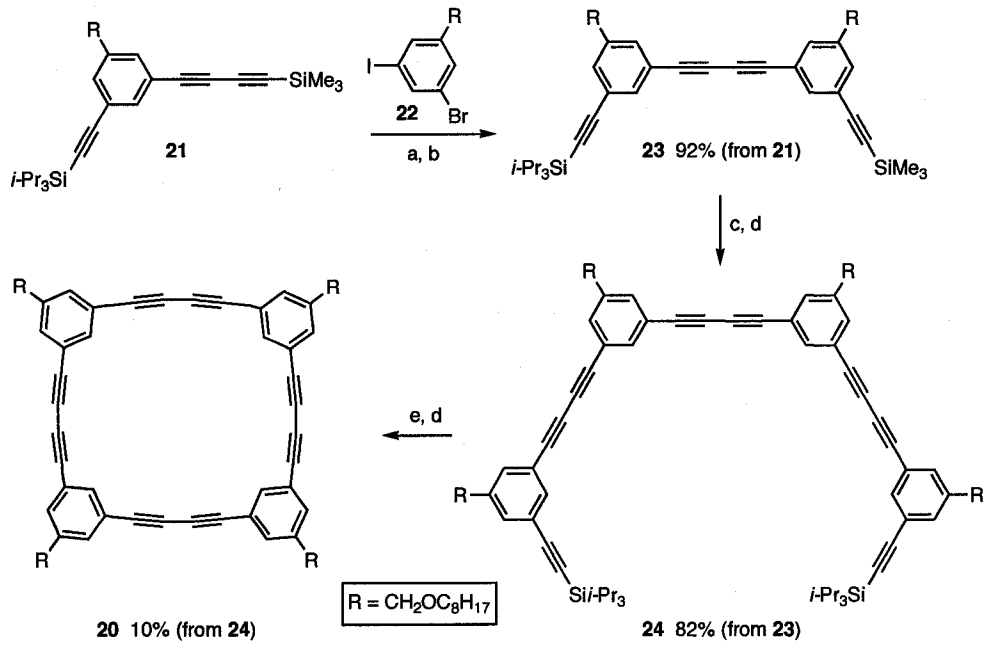

Scheme 1.8 Intramolecular ring closure to provide macrocycle **20**.[45] Reagents and conditions: (a) K_2CO_3, THF, MeOH, rt, then $Pd_2(dba)_3$•$CHCl_3$, CuI, PPh_3, Et_3N, **22**, 50 °C; (b) $Pd_2(dba)_3$•$CHCl_3$, PPh_3, CuI, Et_3N, TMSA, 75 °C; (c) K_2CO_3, THF, MeOH, rt; (d) $Cu(OAc)_2$, py, rt; (e) TBAF, THF, rt.

In a comparison of Cu- versus Pd-homocoupling reactions, Haley and coworkers demonstrated a trend between the selectivity of the ring forming event, the catalyst used, and the ring strain present in the transition state of the bond-forming step.[46,47] The selectivity is demonstrated in the formation of bis[15]- and bis[14]annulenes (**25**, **26** and **27**, **28**) shown in Scheme 1.9, several derivatives of which were explored for self-association (see Fig. 1.4). Briefly, it was shown that intramolecular homocoupling of **29** or **30** under Eglinton conditions gave preferentially the bis[15]annulenes **25** and **26**. This selectivity was ascribed to the nature of the dimeric Cu-acetylide intermediate, which, prior to reductive elimination, is commonly assumed to adopt a pseudo-*trans*-

configuration (Scheme 1.9, inset a). Molecular modeling showed that such an intermediate geometrically favors the formation of the less strained [15]annulenes over the more strained [14]annulenes. Conversely, use of Pd-catalyzed homocoupling conditions with **29** or **30** results in selective formation of the bis[14]annulenes **27** and **28**. In this case, the *cis*-configuration of the Pd-diacetylide intermediate, prior to reductive elimination, is presumably enforced by the chelating bidentate dppe ligand (Scheme 1.9, inset b), and this factor ultimately leads exclusively to formation of the more strained products **27** and **28**.

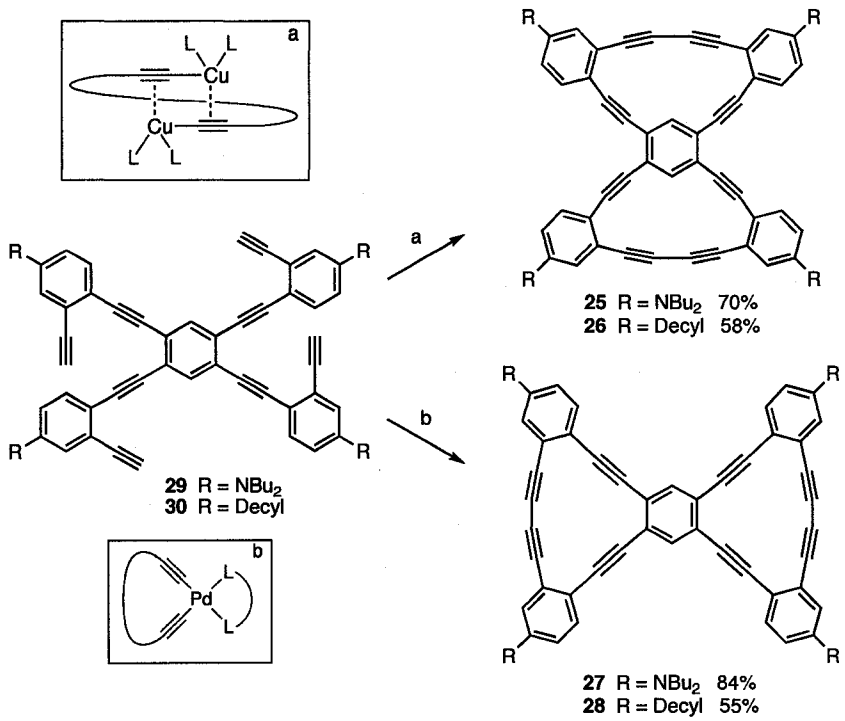

Scheme 1.9 Selective homocoupling based on Cu- or Pd-catalysis, by Haley and coworkers, in the formation of [15]annulenes **25** and **26** and [14]annulenes **27** and **28**.[46] Reagents and conditions: (a) $Cu(OAc)_2$, py, 60 °C; (b) $PdCl_2(dppe)$, CuI, I_2, THF, *i*-Pr_2NH, 50 °C.

Finally, it is worth noting that the formation of acetylenic SPMs on solid support has also been attempted, although to date, success has been limited.[48] Recent advances in the formation of acyclic oligomers by Moore and coworkers, however, suggest that this is a technique that could ultimately lend itself to selective SPM formation, as well as more facile purification.[49]

1.2 SUPRAMOLECULAR SPMS

The use of shape persistent macrocycles in supramolecular chemistry has been limited only by the imagination of those working in this vast area of science. In many cases, a specific component is engineered into the SPM framework to govern directed supramolecular assembly processes, often through metal ion complexation. In other cases, the SPM has been designed with a specific size and/or configuration so that it can act as a host for a guest ion or molecule. Alternatively, intermolecular interactions between the macrocycles themselves afford aggregation that facilitates ordering of the system in the solution state, as liquid crystals, or on surfaces. Salient examples that illustrate some of these design concepts will be discussed below.

1.2.1 SPMs as Components in Supramolecular Assemblies

The placement of a particular functional group into the skeleton of a SPM provides rigid molecules capable of predictable self-assembly in supramolecular systems. To this end, Tykwinski and coworkers have synthesized cross-conjugated macrocycles with exocyclic pyridine donor sites to function as analogues to 4,4′-bipyridine (Scheme 1.10).[50] For example, 3,5-diethynylpyridine, was cross-coupled to vinyl triflate **31** using $Pd(PPh_3)_4$, resulting in the macrocycle precursor **32**. Subsequent desilylation and

oxidative homocoupling under high dilution (0.5 mM) using Hay conditions in CH_2Cl_2 gave SPM **33** in 52% yield.

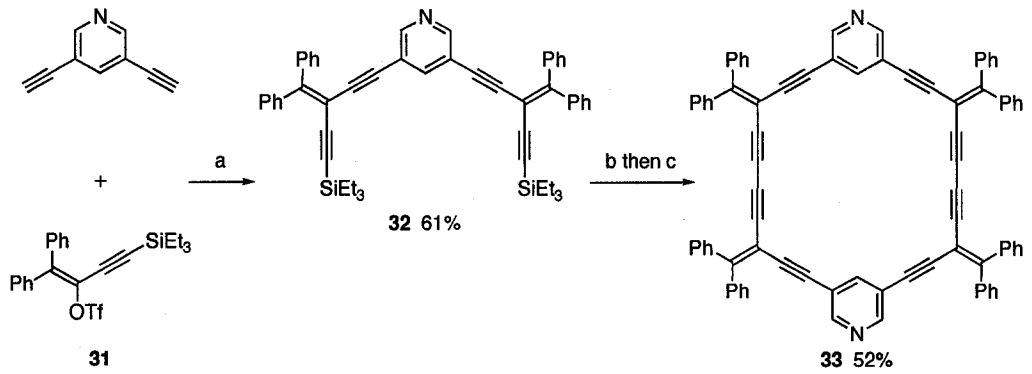

Scheme 1.10 Synthesis of macrocyclic ligand **33**.[50] Reagents and conditions: (a) $Pd(PPh_3)_4$, CuI, Et_2NH, THF, 55 °C; (b) TBAF, THF, rt; (c) CuI, TMEDA, O_2, CH_2Cl_2, rt.

The ability of **33** to function as a component in self-assembly reactions was established through reaction with the Ru-porphyrin **34**, carried out in CH_2Cl_2 at room temperature leading to the desired metal complex **35** (Scheme 1.11).[50,51] While ^1H NMR spectroscopy showed quantitative formation of complex **35**, the isolated yield based on precipitation was only 60%, suggesting weak association between the SPM and the Ru-porphyrins. X–ray crystallographic analysis of **35** subsequently showed that unfavorable steric interactions between the phenyl rings of **35** and the pendent porphyrins were the likely origin of this weak association. The metal-directed, self-assembly of **33** with $Pt(OTf)_2(PEt_3)_2$ gave dimeric assembly **36**.[52] X–ray crystallographic analysis of **36** showed that the macrocyclic ligand **33** had assumed a boat conformation through complexation to Pt (Scheme 1.11, inset). This conformation results in the solid-state formation of bidirectional channels, that incorporate eight molecules of the crystallization solvent $ClCH_2CH_2Cl$ per unit cell. The possible use of this material as a porous solid was

later evaluated using hyperpolarized ^{129}Xe NMR spectroscopy, which demonstrated the permanent porosity of the material even after the removal of the co-crystallized solvent.[53]

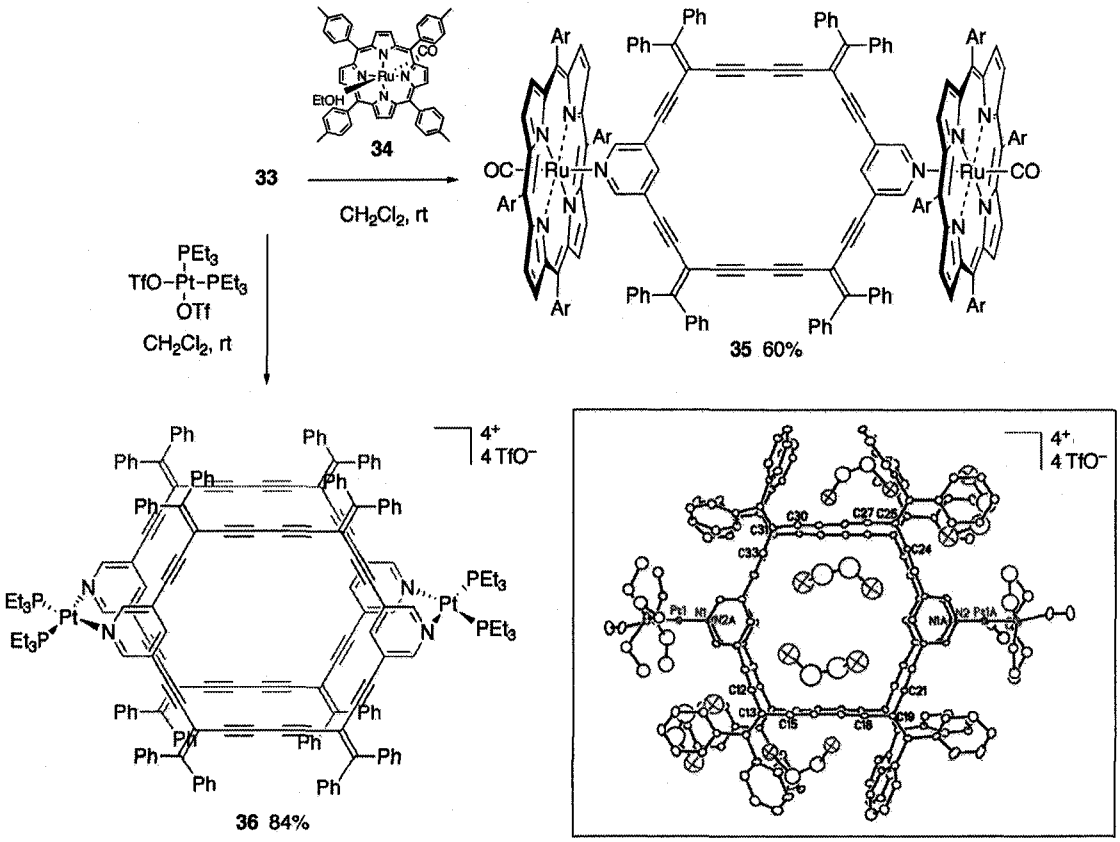

Scheme 1.11 Self-assembly of SPM **33** using an Ru-porphyrin **34** and $Pt(OTf)_2(PEt_3)_2$, resulting in supramolecular complexes **35**[50] and **36**[52]. Inset: solid-state structure of **36** as determined by X–ray crystallography.

In addition to the macrocycles described above, Tykwinski and coworkers have also isolated platinacycles **37–39** based upon the same 3,5-diethynylpyridine subunit and the 1,4-diethynylbenzene subunit (Scheme 1.12).[54-56] The macrocyclic precursors **40–42** were synthesized using a sequence of Pd-catalyzed cross-couplings, then desilylated and subjected to either *trans*- or *cis*-$PtCl_2(PPh_3)_2$ or *cis*-$PtCl_2(PEt_3)_2$, in the presence of CuI in a catalytic amount and high dilution of Et_2NH to afford thermally very stable platinacycles **37–39** in a wide range of yields from 45–71%. Ligand exchange reactions

with bidentate phosphine ligands and **37–39** were also reported for the PPh_3 ligand derivatives due to the increased lability of the ligand vs. PEt_3 (i.e., **38b**). These reactions provide the *cis*-counterparts of **37**, **38a** and **39**, which may be achiral or chiral depending on the phosphine ligand used. Subsequent chapters will provide, in extensive detail, more information of these reactions (see Chapter 2 in particular). The corresponding homocoupled products of **40** and **42** (not shown) via a Hay coupling reaction were also reported to be stable with low solubility (see Scheme 1.10 for the analogous reaction).[56]

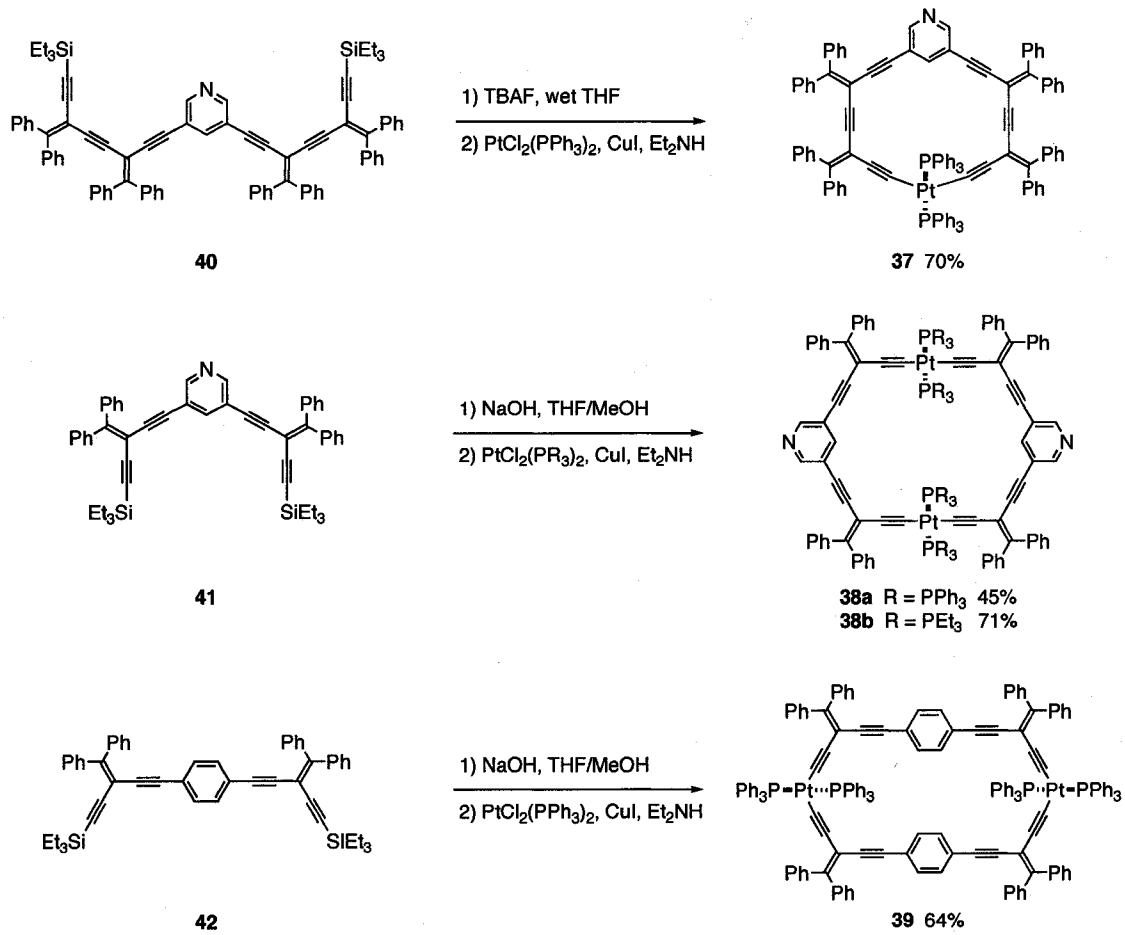

Scheme 1.12 Synthesis of *trans*-platinacycles **37–39** by Pt-acetylide coupling.[54,55]

Lees and Sun have synthesized similar macrocyclic ligands, with *meta*-substituted benzene ring linkers, using Sonogashira and Hay reactions (Scheme 1.13).[57] The reaction of dibromide **43** with terminal diyne **44** led solely to the formation of macrocycle **45**, which was purified easily by recrystallization from CH_2Cl_2. In a manner similar to that described by Tykwinski (see above), oxidative homocoupling of **44** gave the nearly insoluble SPM **46** in only 32% yield, along with oligomeric products. The Re(I) supramolecular transition metal complexes **47** and **48** were then prepared by heating **45** or **46** with the Re(I) diamine complex in THF at reflux. Both the SPMs (**45** and **46**) and their metal complexes (**47** and **48**) showed strong fluorescence in solution.

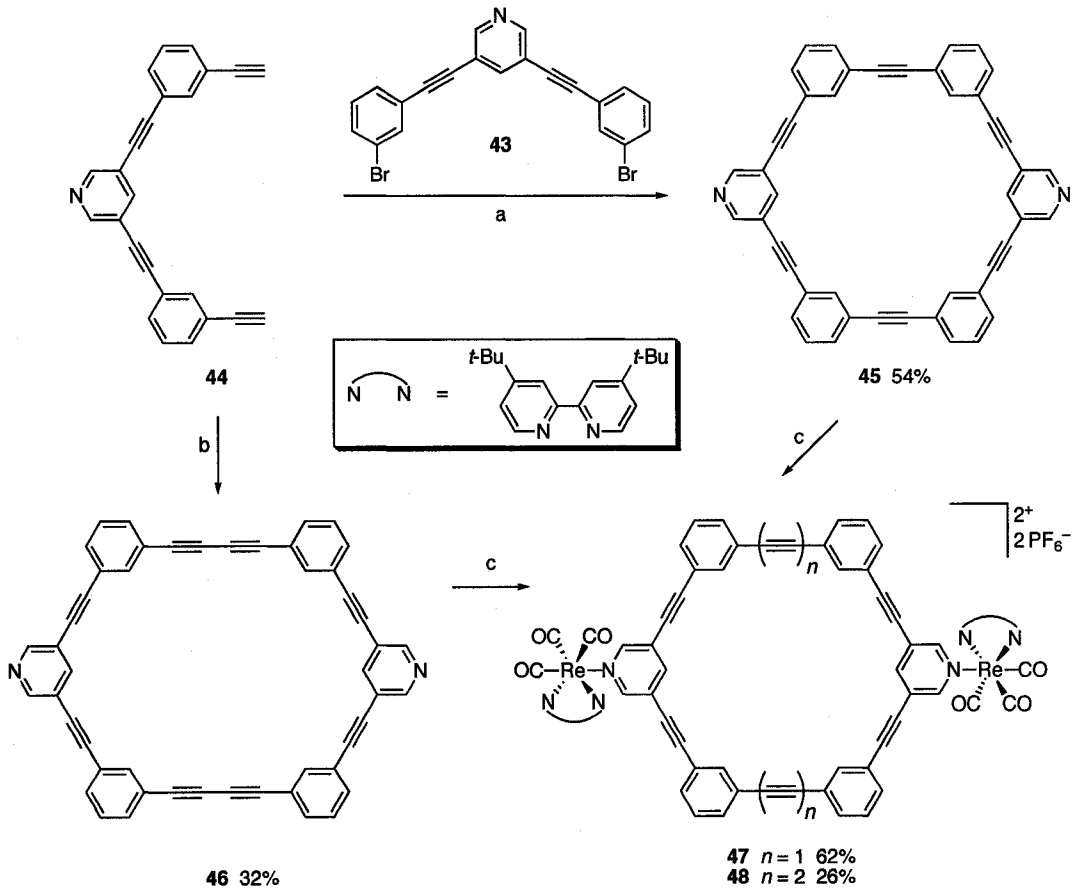

Scheme 1.13 Synthesis of SPMs **45** and **46** and formation of their metal complexes **47** and **48**.[57] Reagents and conditions: (a) $PdCl_2(PPh_3)_2$, CuI, *i*-Pr_2NH, 70 °C, 16 h; (b) CuCl, py, O_2, rt, 30 h; (c) $(CH_3CN)Re(CO)_3$(4,4′-*t*-Bu_2bipy)(PF_6), THF, 60 °C.

The SPMs **49** and **50** with opposing 2,2′-bipyridine donor sites for metal complexation were prepared by Schlüter and coworkers using a Sonogashira reaction to effect ring closure (ring closing bonds indicated[†] in Scheme 1.14A).[58,59] While SPM **49** was formed in a reasonable yield of 28%, macrocycle **50** was inexplicably isolated in a much lower yield (14%) and could not be obtained pure. This disparity in yield for structurally similar macrocycles highlights an example of the unanticipated challenges that often face macrocycle assembly.[60] X–ray crystallographic analysis of **49** and **50** showed that the SPMs are layered in the solid-state, resulting in "channels" that contain both co-crystallized solvent molecules and portions of the flexible side chains. The bipyridine group can rotate freely, allowing for either *exo*- or *endo*-cyclic metal ion complexation. When either **49** or **50** was reacted with $RuCl_2(bipy)_2$, however, only assemblies **51** and **52** formed, with *exo*-cyclicly complexed ruthenium.

[†] This same convention will be used periodically throughout the chapter to show the final ring closing bond.

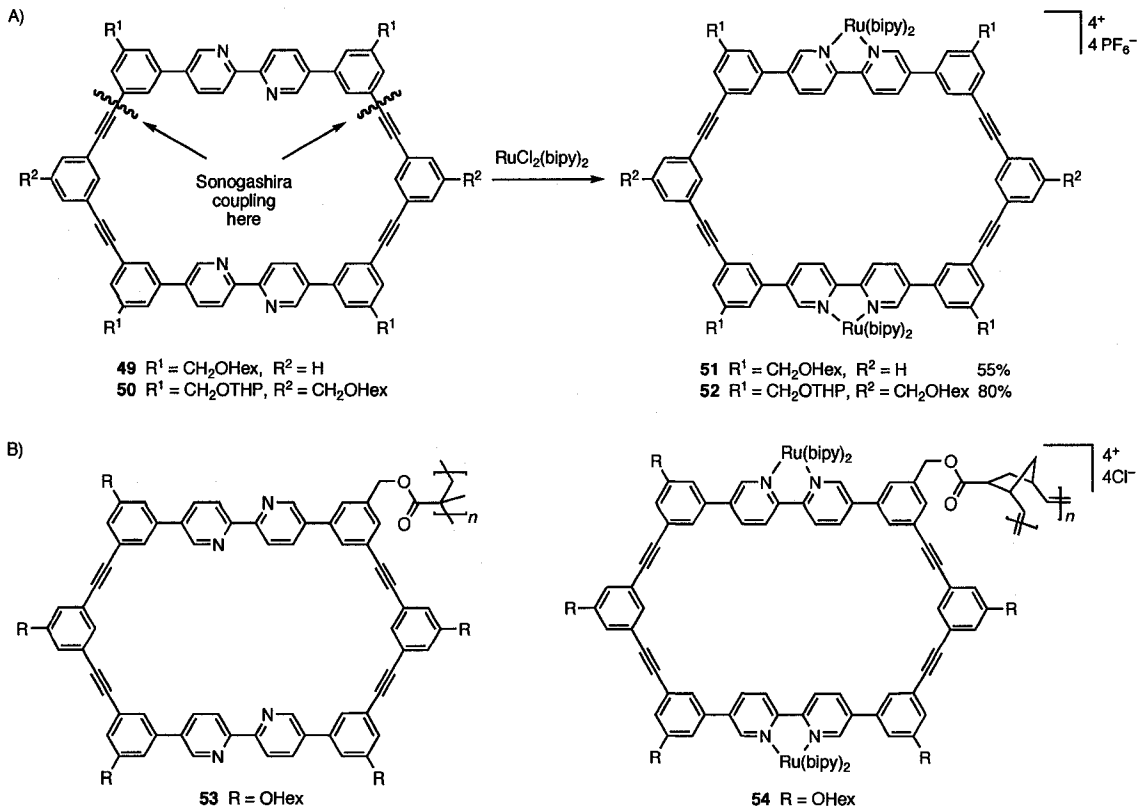

Scheme 1.14 A) SPMs **49** and **50** with opposing bipyridine donor sites and synthesis of their metal complexes **51** and **52**[58] and B) Polymers **53** and **54** formed via free radical polymerization and ring-opening metathesis polymerization, respectively.[59]

This same group has reported one of the most detailed discussions of optimizing the synthesis of SPMs, using the basic macrocyclic structure found in **49** and **50**. The aim was to reduce the number of steps, increase yields, and replace Stille reactions with the more efficient and less toxic Suzuki reactions.[61] The ultimate goal was to convert SPM monomers (not shown) into polymer **53** via free radical polymerization and polymer **54** through ring-opening metathesis polymerization (ROMP) using the Grubbs II catalyst (Scheme 1.14B). In the latter case, the "protected" Ru-complex of the macrocyclic monomer was required for the success of the ROMP reaction.

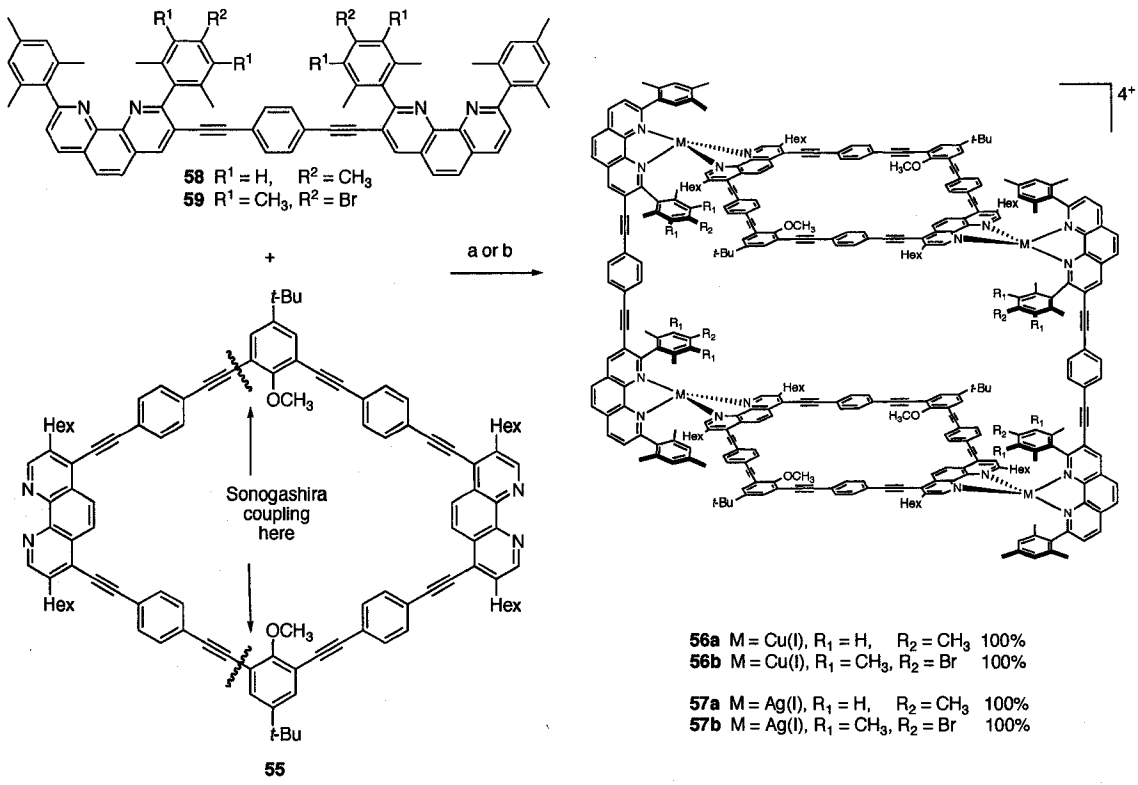

Scheme 1.15 Synthesis of nanoboxes **56–57** using metallosupramolecular assembly.[62] Reagents and conditions: (a) $Cu(MeCN)_4PF_6$, CH_2Cl_2, rt; (b) $AgPF_6$, CH_2Cl_2, rt.

Schmittel and coworkers envisioned the SPM **55**, containing phenanthroline units with *exo*-cyclic binding sites, as the key building block to form supramolecular complexes **56–57** (Scheme 1.15).[62] Macrocycle **55** was obtained in 16% yield through a Sonogashira reaction,[63] and simply dissolving **55** with either components **58** or **59** in the presence of $Cu(MeCN)_4PF_6$ in CH_2Cl_2 at room temperature gave quantitative self-assembly to the phenanthroline nanoboxes **56a** or **56b**. The authors relied on the use of steric and electronic effects from bulky aryl substituents at one end of the phenanthroline ligand **58** or **59** to thermodynamically and kinetically direct coordination toward the desired heteroleptic Cu(I) complexes.[64] Although X–ray crystallographic analysis could not be done for boxes **56a** and **56b**, spectroscopic analysis and MM+ calculations suggested an internal volume of >5000 $Å^3$. The self-assembly reaction of **55** with $AgPF_6$

gave the analogous supramolecular structures **57a** and **57b**. Conversion between the Ag(I) complexes **57a** or **57b** to the Cu(I) complexes **56a** or **56b**, respectively, could be accomplished through the addition of CuI to a solution of the former at room temperature. Regeneration of the Ag(I) nanoboxes **57a** and **57b** from **56a** or **56b** could then be achieved through the addition of excess AgCN. SPM **55** was also used for the formation of a supramolecular nanobasket (not shown).[65]

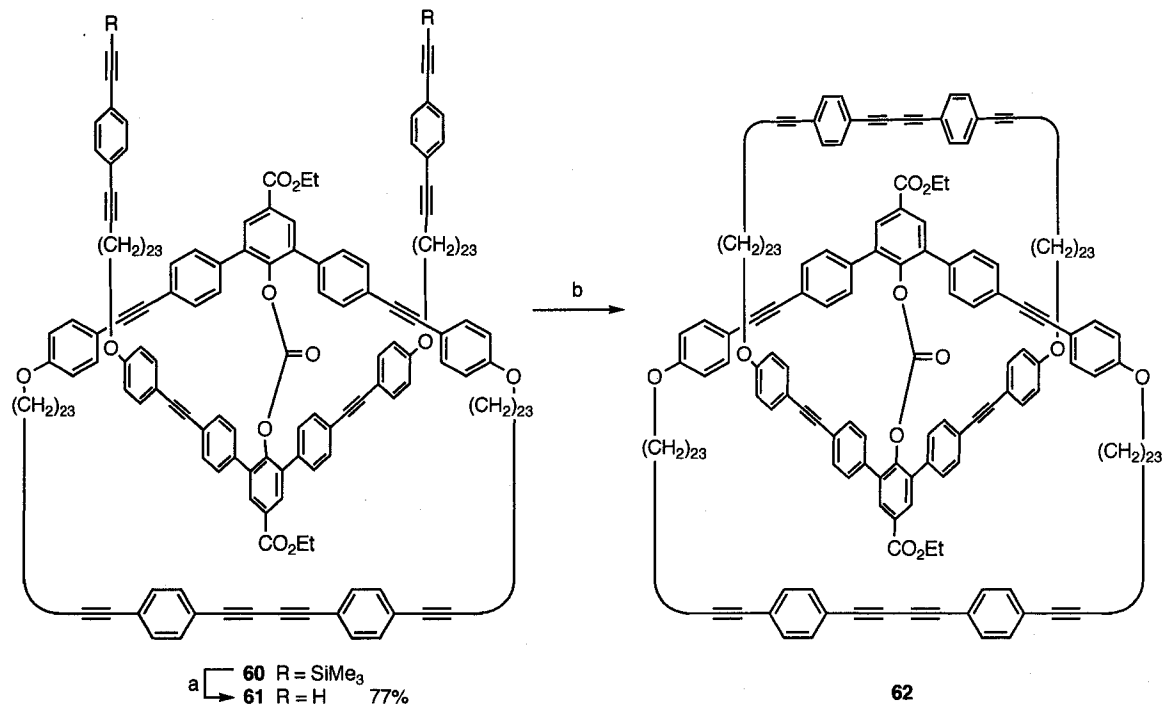

Scheme 1.16 Synthesis of precatenane **62** by carbonate templated oxidative dimerization.[66] Reagents and conditions: (a) KOH, EtOH, THF; (b) CuCl, $CuCl_2$, py, rt.

Macrocycles with acetylenic subunits have been used a great deal in the formation of catenantes. Two pertinent examples will be described here. Using the preorganization concept pioneered by Sauvage and Dietrich–Buchecker,[67] Godt and Ünsal have reported the synthesis of a [2]catenane with 87-membered, non-interacting rings (Scheme 1.16).[66] Synthesis of the [2]catenane began with the formation of **60** in which the two "halves" of the catenane are connected by a covalent carbonate template. Subsequent to desilylation,

the terminal diyne **61** was subjected to acetylenic homocoupling under Breslow conditions and gave a mixture of the intended precatenane **62** and the non-catenated dimer (not shown) in a 2.6:1 ratio (90% combined yield). This mixture was subjected to carbonate cleavage with TBAF in THF, liberating the free [2]catenane in 63% yield (not shown). This synthesis was highly efficient, purification was simple, and large-scale reactions could be performed easily.

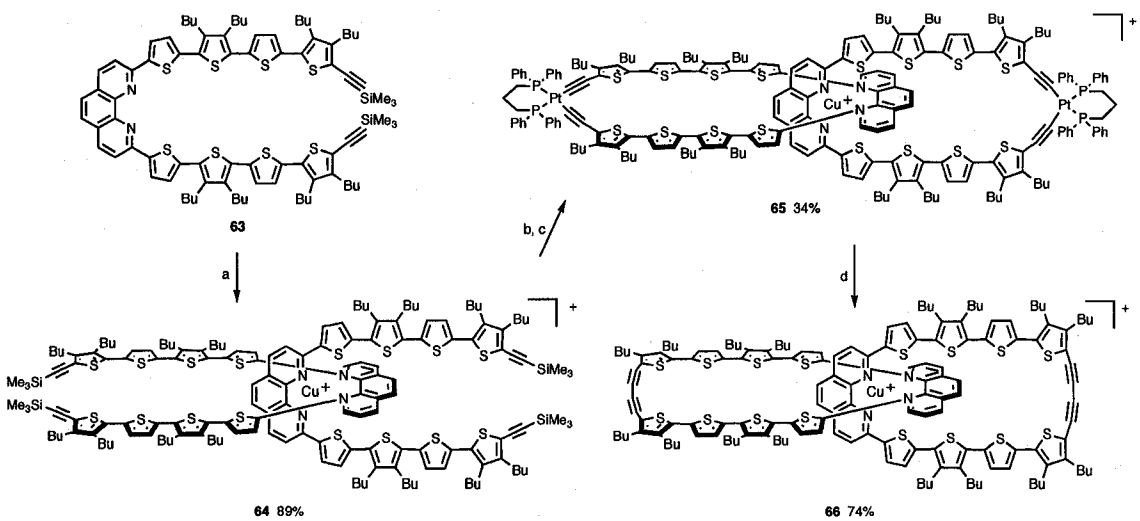

Scheme 1.17 Synthesis of conjugated Cu(I) catenate **66** using metal templation and Pt reductive elimination.[68] Reagents and conditions: (a) $Cu(CH_3CN)_4BF_4$; (b) CsF; (c) *cis*-$PtCl_2$(dppp), rt, Et_3N, PhMe, 60 h; (d) I_2, THF.

Bäuerle and coworkers have synthesized a "π-conjugated" catenane, utilizing Cu(I) templation and a newly developed method for acetylenic homocoupling based on the reductive elimination of platinum to generate the desired C–C bond formation (Scheme 1.17).[68] The C-shaped **63** was first preorganized around Cu(I), resulting in the homoleptic bis-phenanthroline complex **64**. After removal of the four TMS groups with CsF, macrocyclization with *cis*-$PtCl_2$(dppp) led to the catenate **65**. The Pt-corners were reductively eliminated with I_2 in THF, leading to catenate **66**. Decomplexation with KCN gave the Cu-free "π-conjugated oligothiophene-based" catenane in good yield (not

shown). It is worth noting that in smaller interlocked π-conjugated catenane synthesized by this same group, Cu(I) demetalation was impossible, and therefore the Cu-free catenanes were not isolated.[69]

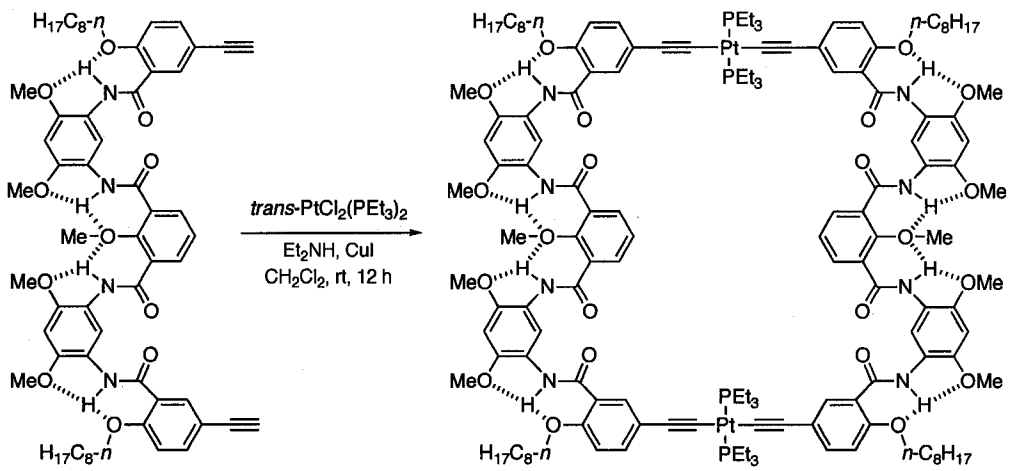

Scheme 1.18 Synthesis of rigid hydrogen-bonded SPM **67**.[70]

In an interesting application of Pt-acetylide chemistry, Li and coworkers have used a preorganization concept to facilitate the self-assembly of SPM **67** (Scheme 1.18). The planar zig-zag precursor is stabilized through repeated, intramolecular three-center hydrogen bonding, and its rigid structure presents both acetylene groups aligned on the same side of the molecule. With this orientation, the formation of **67** in the presence of *trans*-$PtCl_2(PEt_3)_2$ and CuI should have been greatly favored, but the authors report an unexpectedly low yield of 18% for the cyclization step.[70]

1.2.2 SPMs in Host–Guest Systems

The ability to selectively functionalize SPMs, coupled with their preorganized nature makes them quite useful as molecular hosts for a wide variety of guests. One of the first examples capitalizing on this concept came from Diederich and coworkers, who synthesized a family of chiral binaphthyl-derived hosts including triangular, square and rectangular derivatives (for example **68–73**, Fig. 1.2) via a one pot (**nA** → $\mathbf{A_n}$) Hay reaction. They subsequently studied the molecular recognition of these SPMs with carbohydrates. The smaller SPM **71** was capable of selective carbohydrate recognition with several glucopyranosides, with modest enantioselectivity observed in some cases. Later generations of SPMs built on this same concept, incorporated larger carbon scaffolds and modified receptor sites, such as the phosphate ester **73** shown below, a molecule that bonded selectively to disaccharides.[71-74]

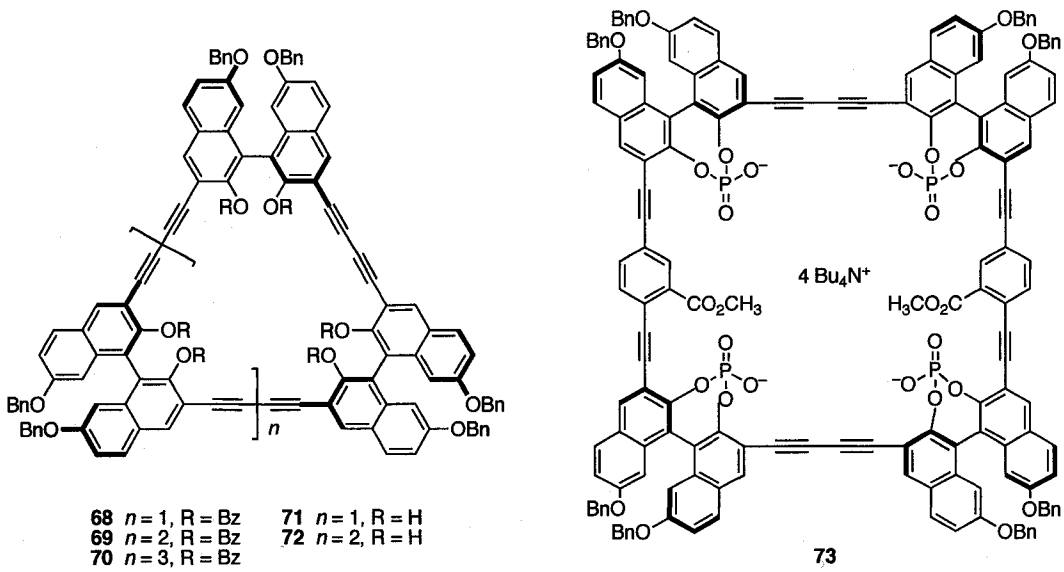

68 $n = 1$, R = Bz **71** $n = 1$, R = H
69 $n = 2$, R = Bz **72** $n = 2$, R = H
70 $n = 3$, R = Bz

73

Figure 1.2 Examples of Diederich's saccharide receptors **68–72**[73,74] and disaccharide receptor **73**[71,72] based on *R*-binaphthol.

Kawase, Oda and coworkers have synthesized a unique series of belt shaped paraphenylacetylene macrocycles **74–77** (Scheme 1.19A) and studied their host-guest supramolecular chemistry. The precursor polyenes **78–81** were synthesized using a modified McMurry reaction, and a subsequent bromination/dehydrobromination sequence with *t*-BuOK gave the desired SPMs **74–77**. A 4:1 mixture of **78/80** gave the corresponding mixture of SPMs **74** and **76** that could be separated by GPC, while pure samples of **79** and **81** could be obtained to provide **75** and **77** directly.[75,76] Using the same bromination/dehydrobromination procedure, SPMs **82–84** were synthesized with 1,4- or 2,6-naphthylene units, respectively, at opposing positions (Scheme 1.19B).

SPMs **74** and **82** have a diameter of 1.31 nm that is suitable for inclusion of C_{60}, while that of **84** (1.41 nm) is nearly perfect for inclusion of C_{70}.[77,78] The **84**$\supset C_{60}$ and **84**$\supset C_{70}$ complexes are extremely stable, with association constants (K_a) of roughly 1×10^5 and 1×10^6 dm^3mol^{-1} and Stern–Volmer constants (K_{SV}) of 2.6×10^5 and 4.3×10^6 dm^3mol^{-1}, respectively. Using competitive complexation experiments, the selectivity of **84** for C_{70} vs. C_{60} was determined to be >10:1.[77] Multicomponent onion-type complexes were then prepared, with two SPMs encompassing a single fullerene molecule, such as **83**$\supset$**82**$\supset C_{60}$ and **77**$\supset$**74**$\supset C_{60}$ (not shown) (Scheme 1.19B).[79] Initially, it was thought that charge-transfer interactions were the main driving force for fullerene-nanoring complexation. Recent studies have, however, shown that electrostatic and van der Waals energies are more significant than charge-transfer energies, and electrostatic interactions are now considered the most likely driving force for the observed complexation.[80]

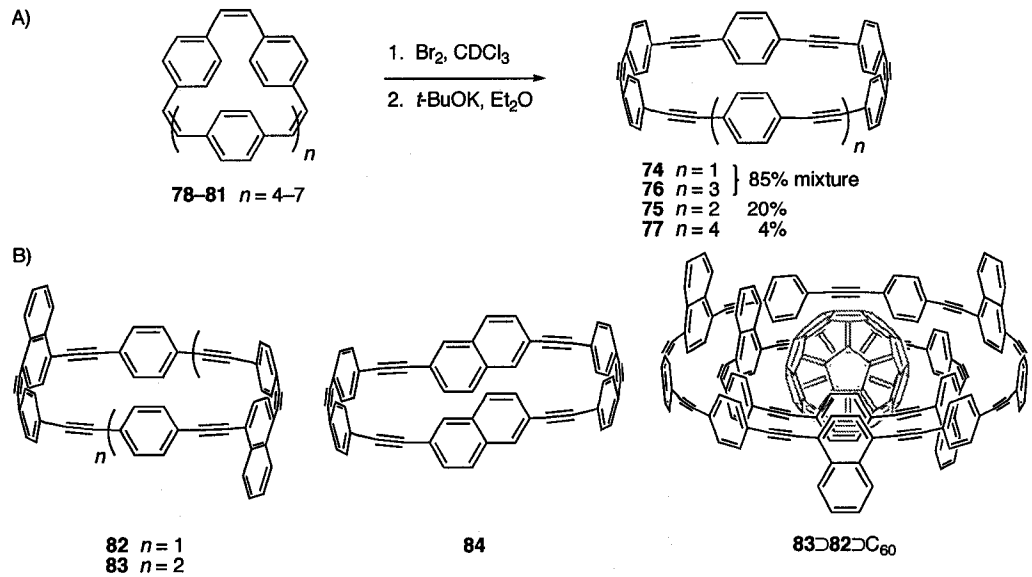

Scheme 1.19 A) Synthesis of paraphenylacetylene SPMs **74–77** through bromination/dehydrobromination[76] and B) molecular structure of SPMs **82–84**[77] and onion complex **83⊃82⊃**C_{60}.[79]

The binding of metal ions is a common use of SPMs in supramolecular chemistry. Toward this goal, Baxter has synthesized multiple *ortho*-fused arylene-ethynylene SPMs using either Hay or Eglinton reactions (Fig. 1.3). Macrocycle **85** was formed using Hay conditions and molecular modeling studies suggested the 2,2′-bipyridine rings are in a cisoid conformation. This places all four nitrogen lone pair electrons oriented toward the interior cavity, promoting the coordination of metal ions of a comparable size. UV–vis and fluorescence spectroscopy showed that **85** responded to only four of the 22 metal cations tested: Co(II), Ni(II), Cu(II) and Zn(II). Furthermore, the signal output was dependent on the metal cation, making **85** a possible multisubstrate, multiple readout ion sensor.[81] Macrocycles **86** and **87** were the first reported 2,2′-bipyridyl twistophanes with a 6,6′-connection, and the synthetic yield of SPM **86** was marginally higher under Hay (13%) than Breslow conditions (9%). SPM **86** acted as a fluorescence-quenching sensor for Cu(II) and Ag(I), while **87** functioned as a sensor only for Cu(II).[82] Baxter

synthesized SPM **10** in 71% yield using Eglinton conditions,[32] the coordination preference of **10** for metal ions was determined as Pd(II) > Co(II) ≈ Ni(II) ≈ Ag(I) > Fe(II) ≈ Hg(II). SPM **88** was synthesized in good yield (46%) using Eglinton conditions and was reported as the first SPM combining thienyl (electron donor) and pyridyl (electron acceptor) units. Metal binding studies showed that **88** binds preferentially to metal cations in roughly the same order as **10**: Pd(II) >> Ni(II) > Co(II) > Ag(I) > Hg(II).[83] Finally, Baxter and Dali-Youcef used the Stephens-Castro reaction for cyclotrimerization to **89**, formed in only 5% yield. This unexpected low yield was attributed to the linear and/or cross-linked nature of the cuprate intermediate making formation of the final bond unfavorable. Nevertheless, macrocycle **89** was found to be a highly selective fluorescence quenching sensor for Pd(II).[84]

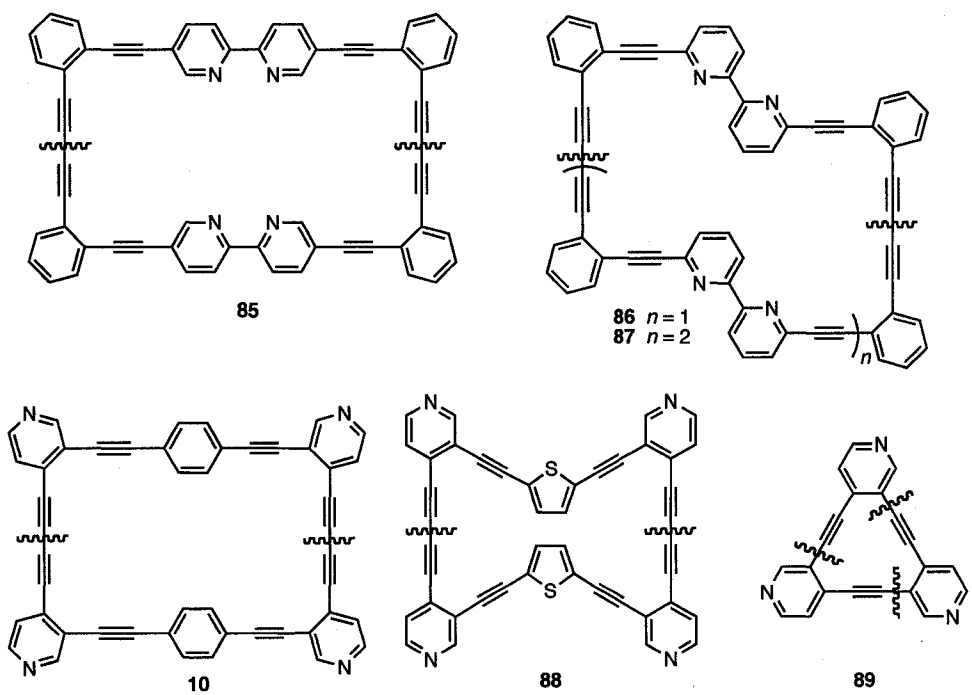

Figure 1.3 Baxter's *ortho*-fused SPMs **10** and **85–89** used for metal ion binding.[32,81-84]

Using the Sonogashira reaction, Yoshida and coworkers have reported the stepwise synthesis of SPM **90**, which was then converted to its butyl ester **91** (Scheme 1.20).[85] X–ray crystallographic analysis confirmed that **91** had a completely planar structure, with acetylenic bond angles of 168.7 and 171.0°. The macrocycle shows unusually intense fluorescence (λ_{em} = 355 nm, Φ = 0.18, CH_2Cl_2), and the emission maximum shifted dramatically to 433 nm (Φ = 0.41) upon the addition of $SbCl_5$. Based on the ^1H NMR and UV–vis spectroscopic analyses, the luminophor was predicted to be the 1:1 complex **92**. Interestingly, no other metal investigated showed any effect on the fluorescence, making **91** a potentially useful ion sensor for toxic Sb(V).

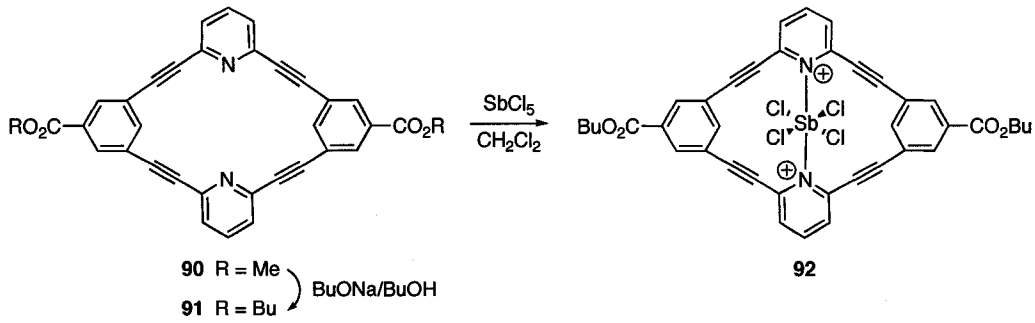

Scheme 1.20 SPMs **90–91** and the complex with Sb(V) (**92**).[85]

Fallis and Heuft have used a metal templated synthesis to form the helical 1,10-phenanthroline-capped metal complexed SPMs **93** and **94** (Scheme 1.21) and their demetalated analogues (not shown). The addition of $Cu(OAc)_2$ (0.5 equiv) to a solution of **95** in pyridine and diethyl ether templated the formation of intermediate **96**. Following the addition of excess $Cu(OAc)_2$ (5.5 equiv), the Cu(I) complexed SPM **93** was isolated in an excellent yield of 84%. Treatment of **93** with aqueous KCN then provided the Cu-free SPM in 70% yield (not shown). The *N,N*-dibutylamine substituted analogue **94** was formed in an analogous manner and taken on directly to the Cu-free SPM (39%) in a one-

pot procedure. It was shown by variable temperature ^{13}C NMR spectroscopy that the helical Cu(I) complex **94** had a barrier to racemization of 4 kcal mol^{-1} higher than the Cu-free analogue.[86]

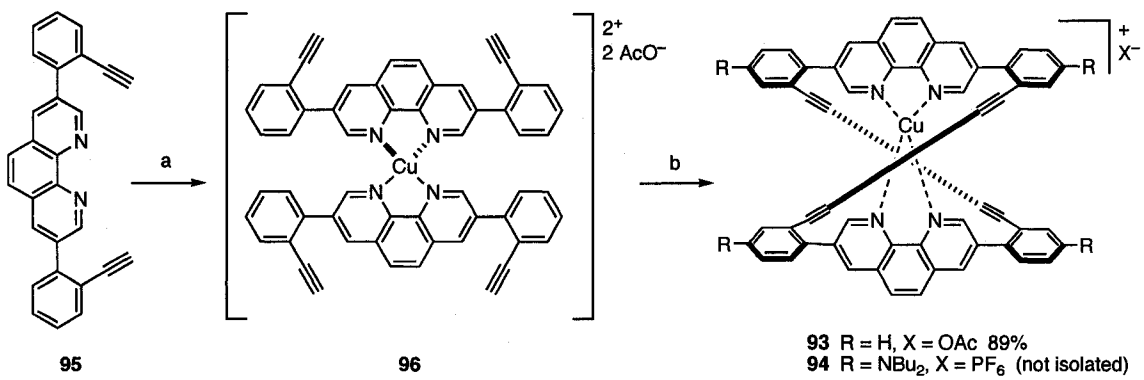

Scheme 1.21 Templated, one-pot synthesis of helical 1,10-phenanthroline SPMs.[86] Reagents and conditions: (a) $Cu(OAc)_2$ (0.5 equiv), Et_2O/py, 2 h; (b) $Cu(OAc)_2$ (5.5 equiv), Et_2O/py.

MacLachlan and coworkers have formed large SPMs **97–99** using a simple, one-pot, template-free, [3+3] Schiff-base condensation procedure (Scheme 1.22). The yields of the macrocycles were 40–68% and no evidence of acyclic oligomer or polymer formation was observed. This is presumably due to the reversibility of the imine condensation, which allows the most thermodynamically stable product to ultimately form, in this case the [3+3] macrocycles. These SPMs bind to a number of metal ions, but coordination to Zn(II) proved to be the most interesting. Pure **97–99** are weakly fluorescent in THF (Φ = 0.13–0.15), but the Zn-complexes in THF at reflux to form **100–102** drastically increases the emission quantum yield (Φ = 0.86–0.92). This enhanced luminescence is attributed formation of a more rigid macrocycle after the binding of Zn(II) to the three host sites. The emission spectra of **100–102** are almost identical, and it was therefore suggested that the luminescence is localized to the site of metal complexation with little or no electronic coupling through the conjugated backbone of the

molecule.[87] Strong solution state aggregation was later reported for **100** (as well as a branched alkyl derivative, not shown) based on intermoledular Zn···O interactions between the molecules.[88]

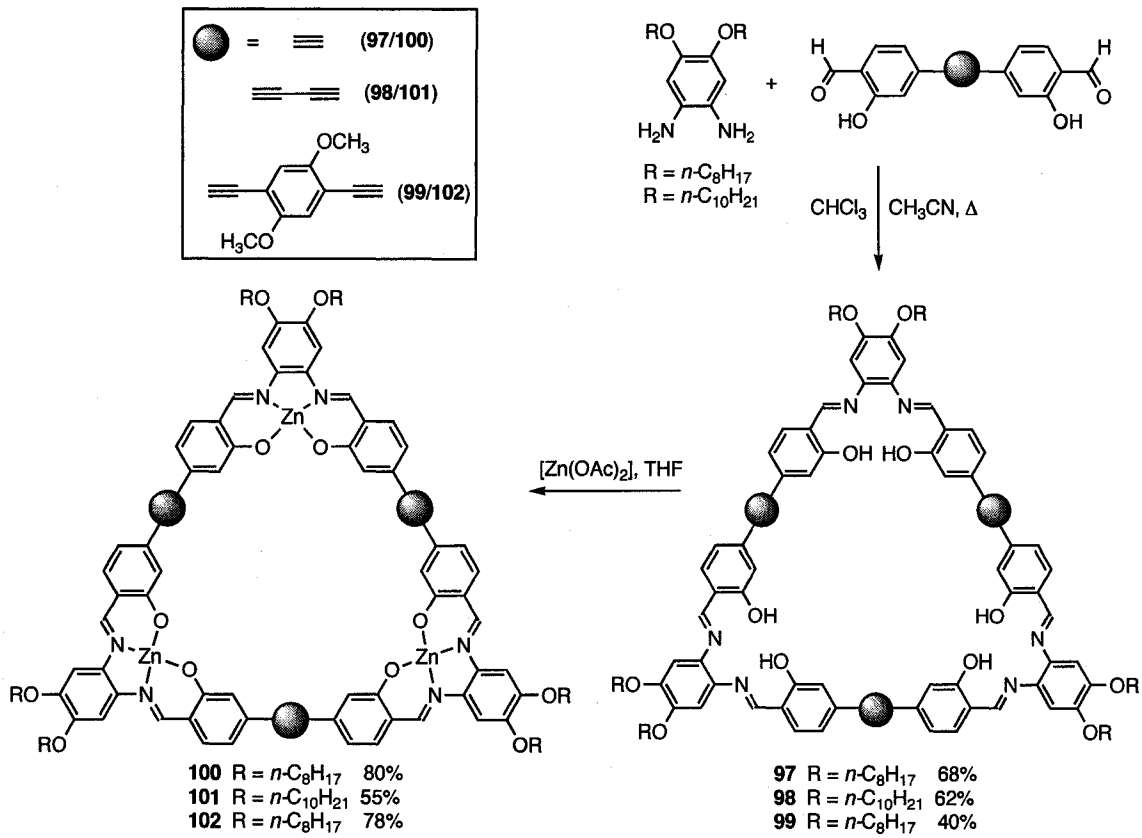

Scheme 1.22 Synthesis of Schiff base SPMs **97–99** and their complexation with Zn(II) (**100–102**).[87]

1.2.3 Aggregation and Surface Chemistry of SPMs

The organization of SPMs into well-defined structures has been one of the most common goals toward their application to supramolecular chemistry. The typically flat conjugated skeleton of acetylenic SPMs facilitates intermolecular self-association, and a number of other secondary bonding interactions can be used to augment the aggregation

process. Incorporation of long pendent alkyl chains about the disc-like structure of SPMs can lead to columnar, discotic liquid crystals (LC), as well as the ability to form highly ordered monolayers on surfaces such as HOPG. The role of SPMs in such applications is described in this section.

1.2.3.1 Aggregation of SPMs

Marsella and coworkers have reported SPM formation based on quadrupole enhanced self-assembly in solution (Scheme 1.23A).[89] While solid-state packing based on aryl–perfluoroaryl interactions (Ar_H–Ar_F) is a well established supramolecular motif,[90,91] it was interesting to see these electrostatic interactions manifested in the *solution state* cyclization formation of **103–105** and then **106–107**. Using Sonogashira conditions in THF and pseudo high dilution conditions to reduce polymer formation, a mixture of terminal diynes **108** and **109** and diiodides **110** or **111** were reacted. Macrocycles **103–105** were formed in yields of 12, 10 and 30%, respectively, and the higher yield of **105** was taken as evidence of the ability of Ar_H–Ar_F electrostatic interactions to template the cyclization. The generality of this outcome was explored through the competitive coupling of diiodides **110** and **111** with terminal diyne **112** under the same conditions (Scheme 1.23B). An enhanced yield was again observed for the Ar_H–Ar_F SPM **106** (26%) in comparison to that of the Ar_H–Ar_H SPM **107** (10%). A stepwise cross-coupling was proposed, in which equilibrium was established between a folded and open intermediate. When both Ar_H and Ar_F were present, the folded intermediate facilitated cyclization.

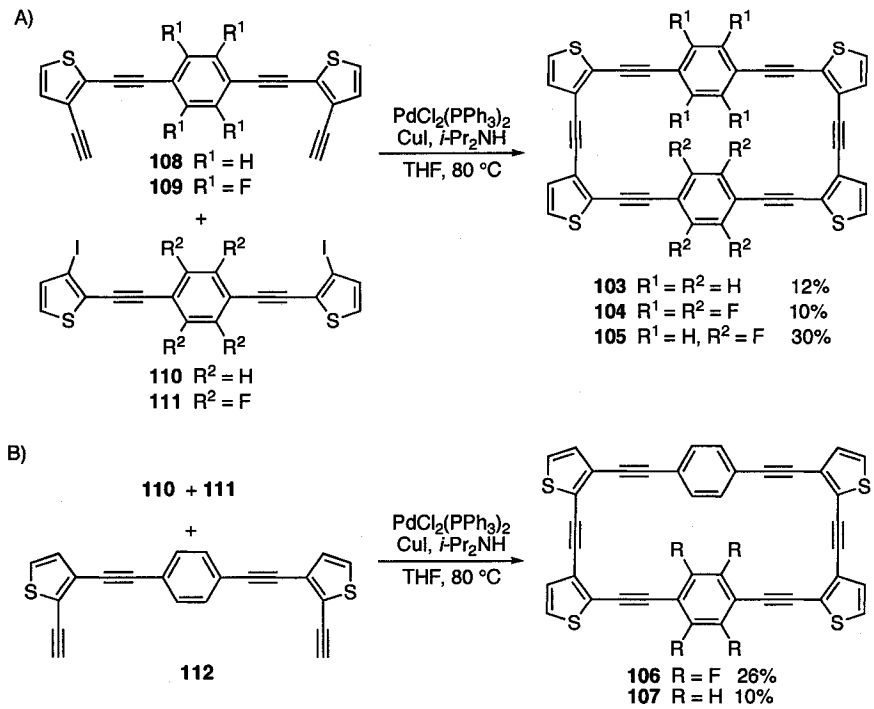

Scheme 1.23 Synthesis of SPMs **103–107**.[89]

SPM **13** was designed by Shu and Mayor to foster intermolecular aggregation based on Ar_H–Ar_F interactions and was synthesized via two different routes.[33] The first strategy coupled two halves of the macrocycle using a modified Cadiot–Chodkiewicz reaction, yielding 4% of macrocycle **13** after a difficult purification process (see Scheme 1.5B). The second strategy coupled dibromide **113** with diyne **114** under the same Cadiot–Chodkiewicz conditions, affording **13** in 7% yield after GPC purification (Scheme 1.24). While the overall yield of the second strategy was slightly lower than that of the first, product isolation in this case was much easier and more efficient, making synthesis through the pentamer **113** preferred. MALDI-TOF MS of **13** identified signals consistent with aggregation, and a study of concentration dependence using ^{1}H NMR spectroscopy showed a consistent upfield shift in the proton signals of the benzene

moiety, indicative of face-to-face aggregation due to π–π stacking.[92-98] The size of these aggregates was not, however, determined.

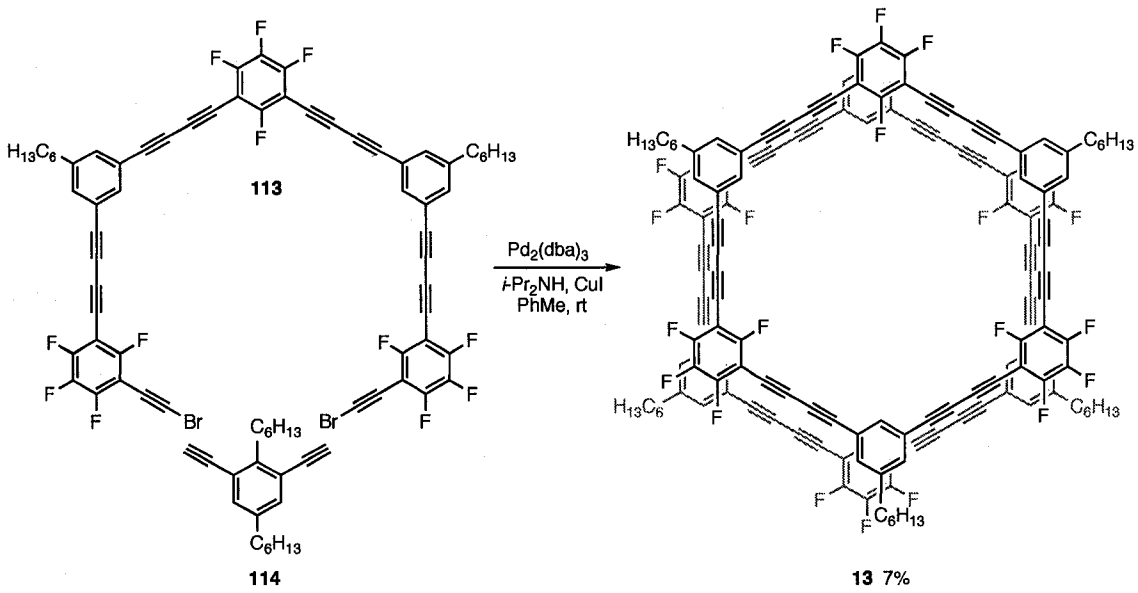

Scheme 1.24 Synthesis of SPM **13** by a Pd-catalyzed Cadiot–Chodkiewicz reaction.[33]

Tobe and coworkers have synthesized butadiyne-bridged SPMs **115–118** via an intramolecular Eglinton reaction to effect ring closure in yields of 27–50% (Fig. 1.4).[92,96, 99] Aggregation studies between electron poor SPMs **117–118** and electron rich SPMs **115–116** show results that are in many ways analogous to those arising from Ar_F–Ar_H quadrupole–quadrupole interactions as described above. Since this interaction requires mutual overlap of the aromatic rings, it is not unexpected to find SPMs with more interaction sites formed heteroaggregates more readily (i.e., **116** and **118** vs. **115** and **117**). Pyridinophanes **117** and **118** also efficiently serve as a host for the tropylium cation, forming 1:1 and 2:1 complexes.

Haley and coworkers have explored aggregation of isomeric SPMs with charge distribution biased by strong electron donors and acceptors. For example, [15]- and

[14]annulenes **119–122** all form dimers in a range of solvents, but the [15]annulenes **119** and **120** consistently show association constants about one order of magnitude higher than the analogous [14]annulenes **121** or **122** (Fig. 1.4).[47]

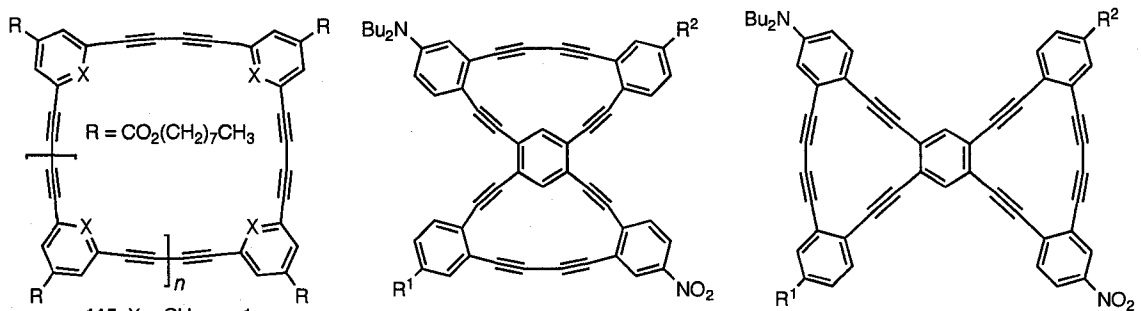

115 X = CH, n = 1
116 X = CH, n = 3
117 X = N, n = 1
118 X = N, n = 3

119 $R^1 = NBu_2$, $R^2 = NO_2$
120 $R^1 = NO_2$, $R^2 = NBu_2$

121 $R^1 = NBu_2$, $R^2 = NO_2$
122 $R^1 = NO_2$, $R^2 = NBu_2$

Figure 1.4 SPMs **115–118** synthesized by Tobe and coworkers[99] and SPMs **119–122** synthesized by Haley and coworkers.[47]

Tetrathiafulvalene (TTF) based [18]annulenes **123** and **124** (Fig. 1.5) have been synthesized via cyclooligomerization (see Scheme 1.1B), while the [12]annulene **125** was formed under Sonogashira conditions using a terminal diyne and a diiodide (not shown).[24] All three SPMs show strong self-aggregation in benzene and toluene, but not in $CDCl_3$, CD_2Cl_2 and THF-d_8. STM measurements carried out on samples of **123** and **124**, which were deposited from dilute CH_2Cl_2 solutions onto a Au(111) surface, show them to have similar dimensions of about 2.2 nm long and 0.2–0.25 nm high.

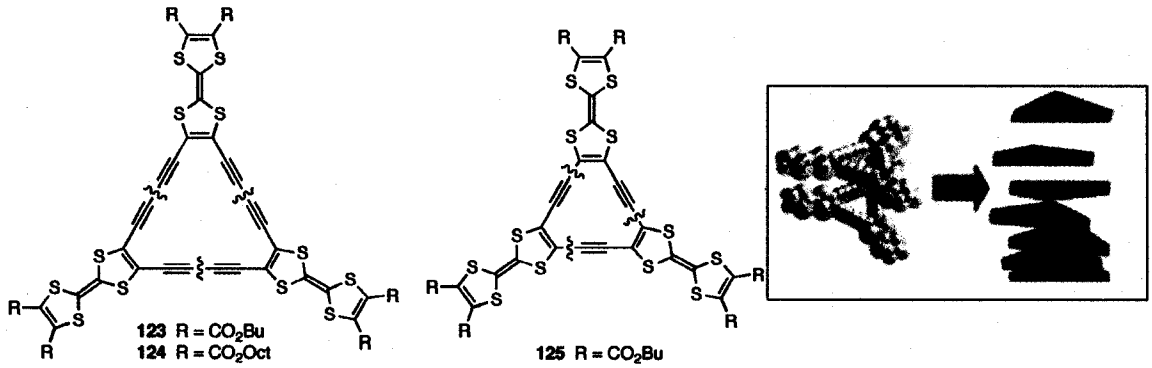

Figure 1.5 TTF[18]annulenes **123** and **124** and TTF[12]annulene **125** synthesized by Iyoda and coworkers.[24] Inset: schematic representation of their self-assembly. Reprinted with permission from *Org. Lett.* **2006**, *8*, 1917-1920. Copyright 2006 American Chemical Society.

Helicene based SPM (*M,M,M*)-**126**, as well as all other possible stereoisomers, have been synthesized by Yamaguchi and coworkers using a Sonogashira reaction of the corresponding diiodide and terminal diyne (Fig. 1.6).[95] Self-aggregation of these SPMs was evident in concentration dependent ^{1}H NMR spectroscopic studies in $CDCl_3$ (0.1 and 10 mM). Dimer formation (even in benzene) was observed by vapor pressure osmometry (VPO), but higher aggregation was not. The dimerization appeared to depend substantially on the configuration of the helicene units: (*M,M,M*)-**126** and (*M,M,M*)-**126** > (*M,P,M*)-**126** and (*M,P,M*)-**126** > (*M,M,M*)-**126** and (*P,P,P*)-**126** > (*M,P,M*)-**126** and (*P,M,P*)-**126**.

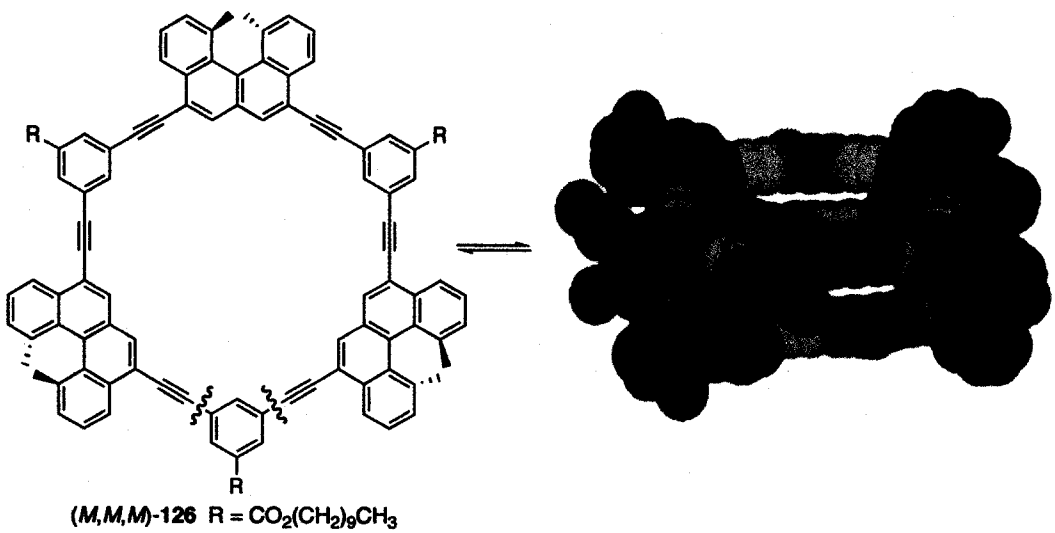

Figure 1.6 SPM (*M,M,M*)-**126** and the structure of the dimer from Amber* calculations.[95] Reprinted with permission from *Org. Lett.* **2001**, *3*, 1097-1099. Copyright 2001 American Chemical Society.

It was later shown that an amine derivative of (*M,M,M*)-**126** could be oxidatively dimerized using MnO_2 in toluene to provide azo-linked *cis*- and *trans*-(*M,M,M*)/(*M,M,M*)-**127**, respectively (Fig. 1.7).[100] These isomers were easily separated by GPC and their stereochemistry was determined by UV–vis spectroscopy. Isomerization was not observed for the isomers upon heating or irradiation. VPO studies in $CHCl_3$ indicated *trans*-(*M,M,M*)/(*M,M,M*)-**127** was monomeric below 0.01 mM and dimeric above 2 mM. On the other hand, *cis*-(*M,M,M*)/(*M,M,M*)-**127** was a trimeric aggregate below 1 mM and polymeric above 1 mM. These observations were explained based on the conformation of the isomers, as depicted in Figure 1.7. Intramolecular or bimolecular aggregates are not possible for *cis*-(*M,M,M*)/(*M,M,M*)-**127** due to the rigidity of the azo group at 120°, therefore two *cis* molecules cannot exist in the same plane. These findings provided a new motif for selective self-assembly of bimolecular π-π interactions of helicenes.

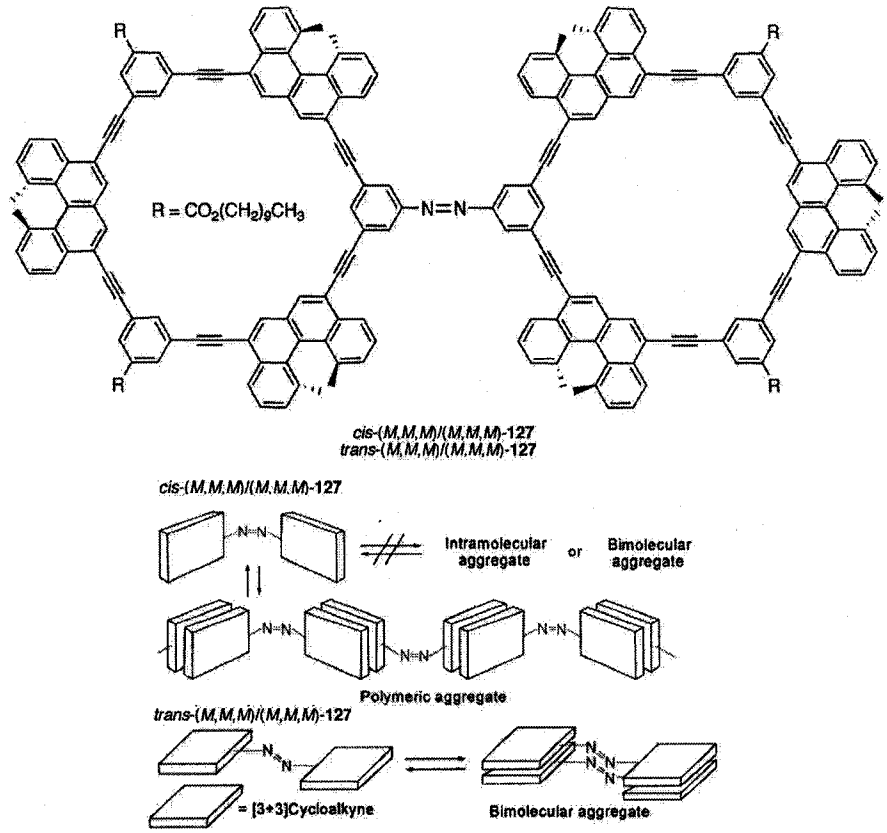

Figure 1.7 Structure of *cis*- and *trans*-(*M*,*M*,*M*)/(*M*,*M*,*M*)-**127** (top) and schematic description of their aggregation behavior (bottom).[100] Reprinted with permission from *J. Am. Chem. Soc.* **2003**, *125*, 9268-9269. Copyright 2003 American Chemical Society.

Höger and coworkers have recently observed that the free-base derivative of pyridinium SPM **128** (Fig. 1.8) shows only weak aggregation in solution, forming tubular structures.[101] Once the pyridyl groups were alkylated to form the cationic species **128**, however, well defined dimers were formed, even at very low concentrations. This behavior was explained through a conformational locking of the SPM into a boat conformation that directs the pyridinium groups toward the center of the dimer to accommodate the bromide ions. Ultimately, this hinders any further aggregation from either the top or bottom of the system.

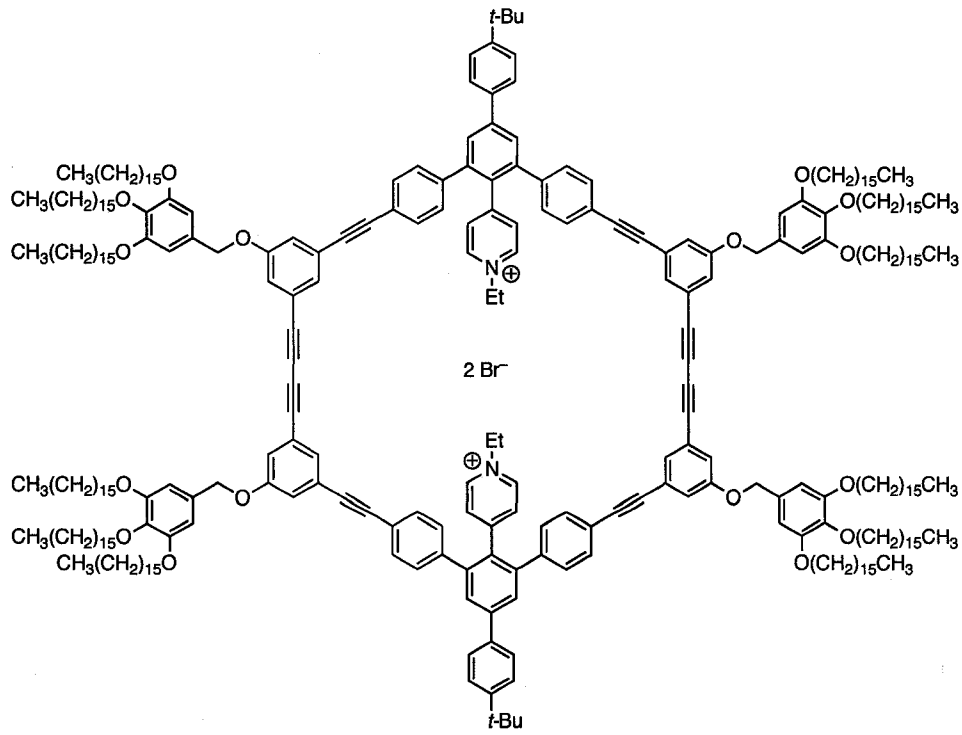

128

Figure 1.8 Cationic SPM **128**.[101]

Alkyne metathesis reactions have emerged as an efficient and effective means of forming macrocycles. In the case of acetylenic SPMs, Adams, Bunz and coworkers were the first to employ alkyne metathesis (see Scheme 1.2). Moore and coworkers have subsequently refined this strategy capitalizing on the selective formation of the thermodynamically favored product under equilibrium control using precipitation-driven alkyne metathesis.[102] These reactions were typically high yielding, and could be scaled up to provide gram quantities of the desired SPM. For example, reaction of **129** using EtC≡Mo[NAr(*t*-Bu)]$_3$ as a catalyst in the presence of *p*-nitrophenol gave **130** in 81% isolated yield on a milligram reaction scale and an amazing 77% yield on a gram scale (Scheme 1.25).[28,103] SPM **130** was shown to form aggregates in solution, especially in polar solvents such as acetone.[104] An analogous metathesis reaction gave tetrameric

carbazole based SPM **131** in 84% yield as the sole product. This SPM self-assembled into nanofibrils using the sol-gel method, driven by the favorable π-π-stacking of the planar macrocycles and hydrophobic interactions between the alkyl side chains.[105] The related SPM **132** also aggregated to give nanofibrils, that when fabricated into thin films, could be used in the detection of explosives (e.g., TNT) based on fluorescence quenching.[106]

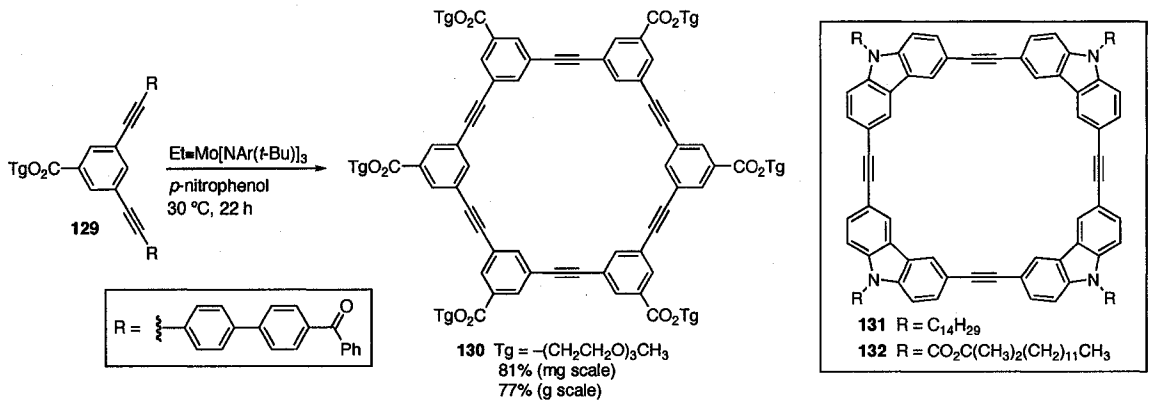

Scheme 1.25 Synthesis of SPM **130** synthesized by alkyne metathesis.[28,103] Inset: molecular structures of SPMs **131** and **132**.[105,106]

Moore and Zhao have also reported the use of imine metathesis for the synthesis of SPM **133** in almost quantitative yield from **134** and **135** (Scheme 1.26).[107] It had been previously shown that SPM **133** aggregates into columnar assemblies in acetonitrile,[108] a phenomenon driven by the solvophobically favored aromatic stacking. It was thus proposed that once formed under the metathesis reaction conditions, **133** was stabilized by the free energy gained from the intermolecular aggregation. This makes aggregates the thermodynamically most stable species and shifts the metathesis equilibrium in favor of cyclization. This "aggregation driven" formation of macrocycles presents a powerful new strategy for high yield formation of SPMs. The same group also reported the quantitative formation of SPM **133** via a simple condensation of an amine and an aldehyde to introduce the imine bond.[109]

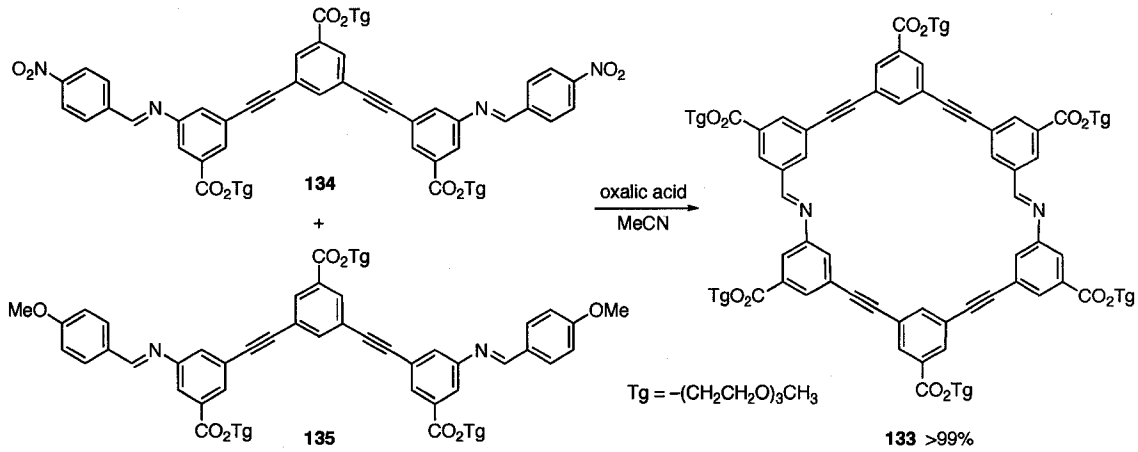

Scheme 1.26 Synthesis of **133** by imine metathesis.[107]

In contrast to the work just described, in which aggregation facilitates product formation, aggregation can also lead to the demise of SPMs as a result of intermolecular close contacts that lead to polymerization. For example, Tobe and coworkers have described the unusual spontaneous polymerization of hexameric SPM **136**, at room temperature, while the tetramer (**137**) and octamer (**138**) were quite stable (Fig. 1.9).[45] Thus, in cases where the isolation of a SPM with butadiynyl groups proves challenging, it is wise to consider both if the SPM was formed and if it was stable.

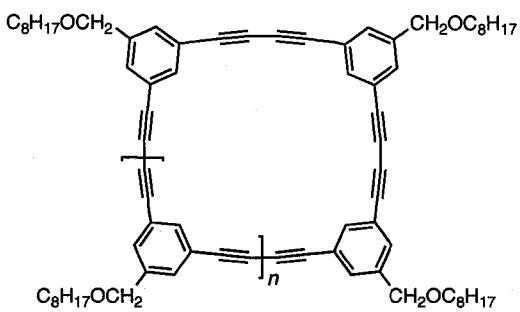

137 $n = 1$; **136** $n = 3$; **138** $n = 5$

Figure 1.9 Tetramer **137**, hexamer **136** and octamer **138** SPMs synthesized by Tobe and coworkers.[45]

1.2.3.2 Liquid Crystalline SPMs

The formation of liquid crystals (LC) from suitably functionalized acetylenic SPMs has often been the motivation for their synthesis. A number of groups have sought to capitalize on the planar or nearly planar disk-like geometry of SPMs toward the formation one-dimensional columnar stacks based on a combination of π–π stacking, van der Waals, dipole, and hydrophobic interactions. For example, Heiney, Moore and coworkers have reported the high-resolution X–ray diffraction analysis (XRD) of a tubular, discotic LC based on SPM **139**, which has been synthesized via a Sonogashira reaction (Fig. 1.10).[109] These studies reveal an unanticipated distortion and doubling of an underlying hexagonal lattice with $b \approx 2a$ as shown in Figure 1.10, suggesting that the unit cell must contain two crystallographically inequivalent molecules A and B. To determine the degree to which ions could be integrated into the columnar structure, SPM **139** was doped with AgOTf (1, 2, or 4 wt%) and examined via powder XRD. At 4%, columnar order is essentially destroyed, but at 1 and 2%, order is maintained and there is strong evidence that the silver and triflate ions are located within the center of the channels, offering a potential anisotropic LC ionic conductor.

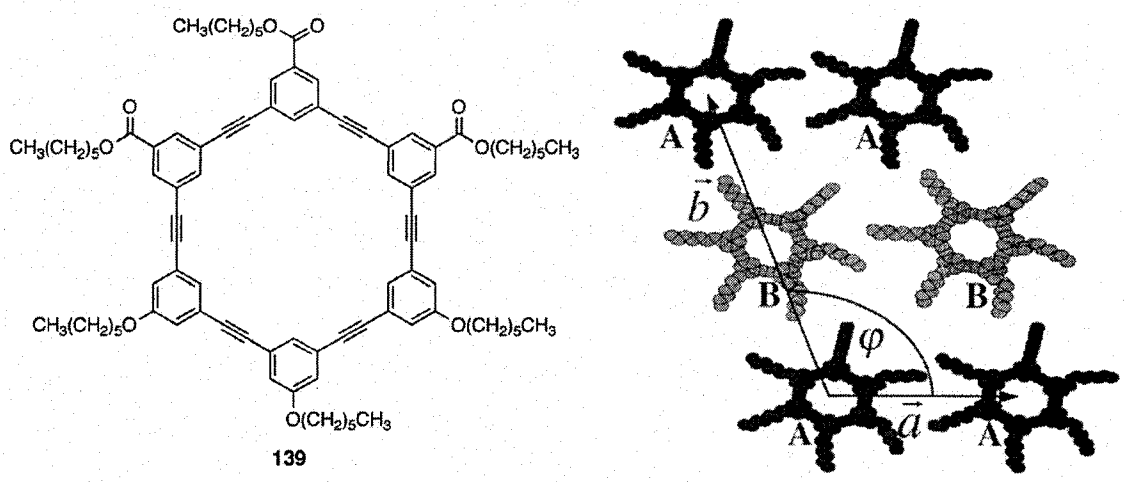

Figure 1.10 Liquid crystalline SPM **139** and its molecular arrangement in the unit cell.[109] Reprinted with permission from O. Y. Mindyuk, M. R. Stetzer, P. A. Heiney, J. C. Nelson, J. S. Moore, *Adv. Mater.* **1998**, *10*, 1363-1366.

Tew and coworkers have reported *ortho*-phenylene ethynylene SPMs **140–142** with discotic LC properties (Fig. 1.11).[110] All attempts at the formation of **140–142** through the metathesis approach were discouraging; **142** could not be synthesized while **140** and **141** were formed as mixtures. Ultimately, an intramolecular Sonogashira reaction was used. X–ray diffraction shows that symmetric **140** and **141** self-assemble into highly ordered columnar structures, while asymmetric macrocycle **141** is less ordered. The most significant difference between the *meta*-phenylene ethynylene SPMs reported by Moore (e.g., **130**) and **140–142** is the size of the central cavity, which is ca. 8 Å for **139** (H to H) compared to 2.4 Å for **140**.[111] Because columnar assembly is thought to be inhibited by large internal voids, the small cavity size of **140–142** favors self-assembly.

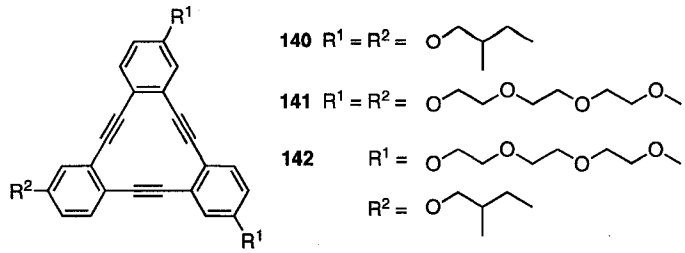

Figure 1.11 *Ortho*-phenylene ethynylene SPMs **140–142** synthesized by Tew and coworkers.[110]

As described above, the common design of a discotic LC integrates the (semi)rigid core of an SPM with flexible side chains about the periphery. An interesting twist of this concept was introduced by Höger and coworkers: Would a LC material arise from an SPM with flexible side groups that fill the *inside* of the macrocycle? SPM **143** was synthesized to probe the idea of an *inverted* LC, using an acetylenic homocoupling reaction to combine the two halves (Fig. 1.12).[112] X–ray crystallography shows that the alkyl chains are arranged within the macrocyclic framework, and the compound forms a mesophase at 185 °C that becomes isotropic at 207 °C. The long alkyl chains of **143** occupy an adaptable position on the SPM core, however, that could place them either inside or outside the cavity in the LC. It is thus unclear whether **143** represented a true inverted LC. SPMs **144–148** have subsequently been synthesized by an analogous sequence and also show thermotropic mesophases.[113,114] Given that the long alkyl chains in this case are constrained directionally into the interior of the SPM, as shown crystallographically for **144** (Fig. 1.12, inset), the formation of inverted LCs is established. Preliminary guidelines toward the formation of inverted LCs have arisen from this study. First, there must be alkyl substituents that have the potential to fill the internal void, and second, SPMs must not contain bulky extraannular substituents that cause the molecules to become interlocked.[113]

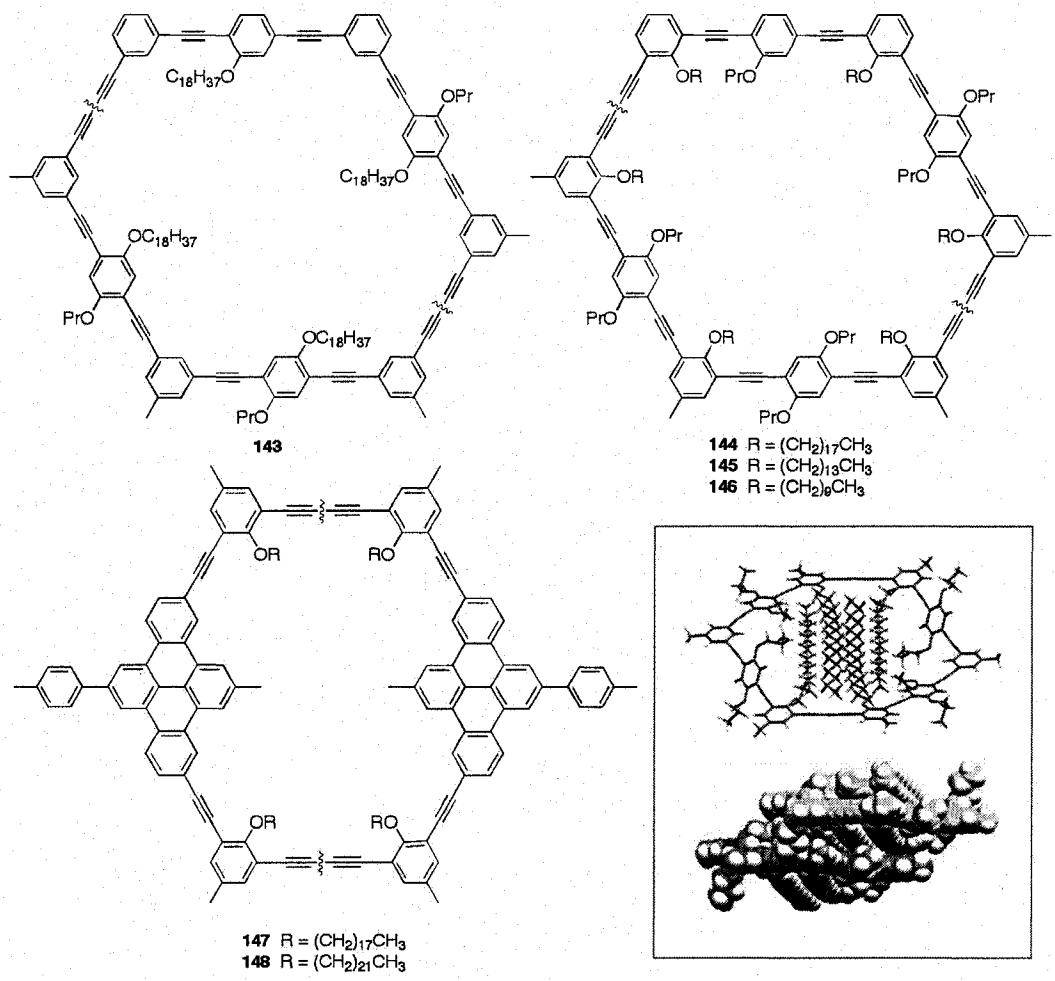

Figure 1.12 Macrocycles **143–148** exhibit inverted discotic liquid crystal properties. Inset: crystal structure of **144**. Reprinted with permission from S. Höger, X. H. Cheng, A.-D. Ramminger, V. Enkelmann, A. Rapp, M. Mondeshki, I. Schnell, *Angew. Chem. Int. Ed.* **2005**, *44*, 2801-2805.

1.2.3.3 Adsorption of SPMs on Surfaces

With the recent surge in surface analysis techniques, the characterization of surface adsorbed SPMs has blossomed. This is particularly true for the use of scanning tunneling microscopy (STM), where the conjugated core of the SPM is expected to show a higher tunneling efficiency than nonconjugated portions (e.g., pendent alkyl groups), facilitating analysis.[115] Because the same intermolecular forces that provide for solution

state aggregation and/or liquid LC formation can also be exploited to organize SPMs onto surfaces, it is perhaps not surprising that structural motifs for surface adsorbed SPMs are often similar to those described in Sections 1.2.3.1 and 1.2.3.2.

Tobe and coworkers have synthesized SPMs **149** and **150**, using the *in situ* deprotection Pd(0)-catalyzed cross-coupling protocol developed by Linstrumelle (Scheme 1.27).[30,116] The cyclization of tetrabromotolan **151** with diethynylbenzene **152** in the presence of the phase-transfer catalyst $CH_3N[(CH_2)_7CH_3]_3Cl$ afforded **149** in 9% yield, while the same protocol with **153** gave **150** in 5% yield.[117] It was demonstrated that **149** and **150** formed specific topologies at the liquid/solid interface (TCB/HOPG), designated as a Kagomé lattice for **149** (Scheme 1.27, inset A) and a honeycomb structure for **150** (Scheme 1.27, inset B).[118] The rarely observed Kagomé lattice is very interesting due to its relevance in the field of spin-frustrated magnetic materials. Only a handful of 3D crystals have shown this lattice packing, and **149** is the first 2D network to be reported with this motif. Whereas the rhomboid shaped SPM **149** shows a corner sharing hexagonal packing pattern, triangular **150** has side-sharing hexagonal packing. For both SPMs, the alkyl chains run almost perpendicular to the sides of the SPM framework, and each core thus obeys the symmetry aspects of their respective networks.

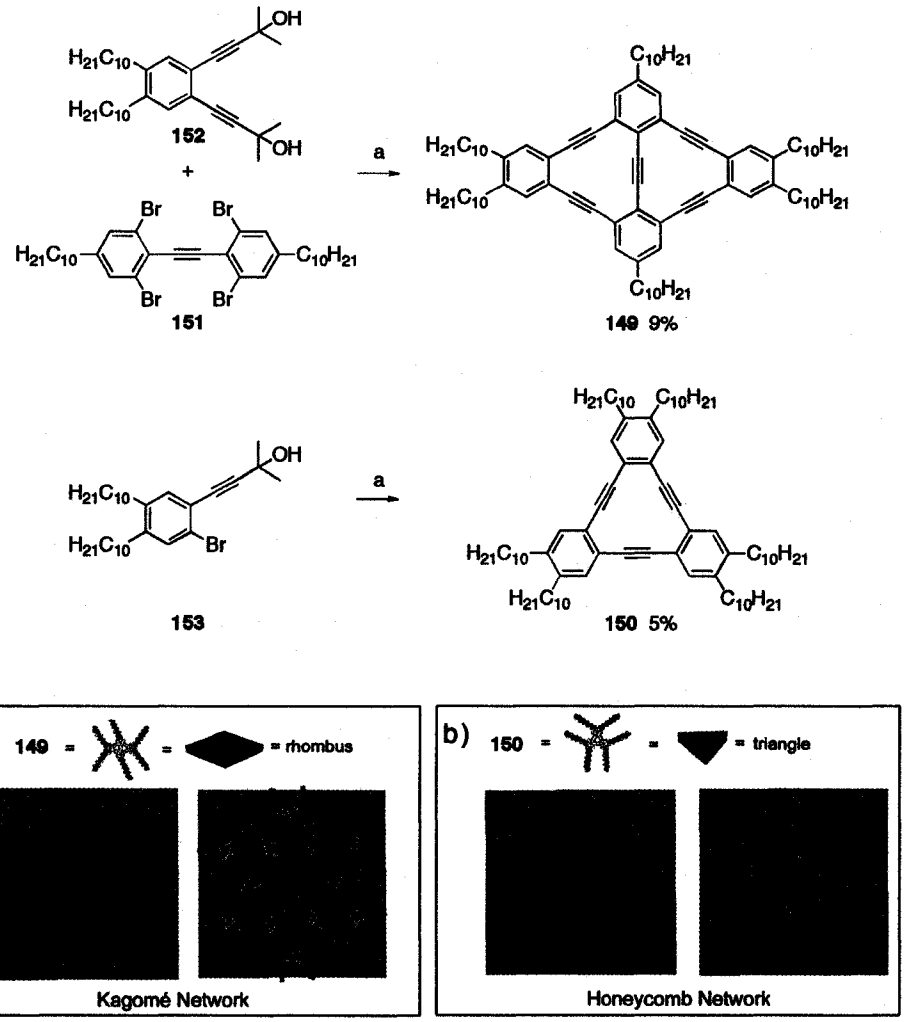

Scheme 1.27 Synthesis of macrocycles **149** and **150**.[117] Reagents and conditions: (a) $Pd(PPh_3)_4$, CuI, PPh_3, KOH, PhH, $CH_3N[(CH_2)_7CH_3]_3Cl$, reflux.[118] Insets: a) Schematic representation of the dense packing of *ideal* rhombic plates (left) and of networks of **149** (right); b) Schematic representation of the dense packing of *ideal* triangular plates (left) and networks of **150** (right).[118]

Höger and coworkers have used SPMs **154–157** to establish that the size of a rigid macrocycle should be balanced against the presence of flexible extra- and intraannular groups that decorate the core periphery (Scheme 1.28).[119,120] SPMs with both ester (**154** and **155**) and carboxylic acid (**156**) groups form well-ordered, structured monolayers on an HOPG surface (Scheme 1.28, inset a), whereas those containing intraannular thiol

groups (**157**) form self-assembled monolayers on Au(111) (Scheme 1.28, inset b). The ring closing step to **154–157** relied on acetylenic homocoupling of the two halves of the macrocycle, which typically provided only moderate yields. In an effort to increase the quantity of these macrocycles available for study, the covalent template approach has been applied, converting **158** to **159** and **160** in excellent yields over the three steps.[121] Unlike **154–157**, however, attempts to melt the template-bound SPMs **159** and **160** into a LC phase were unsuccessful. The lack of LC behavior was attributed to the presence of the biphenylene bridge, which is longer than the diameter of macrocycle and therefore results in a non-planar conformation. Efforts then turned to the adsorption of **159** and **160** onto the surface of HOPG. STM has established that the SPMs are planarized on the HOPG surface, and that the biphenylene bridge is also adsorbed onto the surface. Modeling studies have been used to show that in the absence of the solid support, the molecules prefer a nonplanar conformation and only become planar when adsorbed.

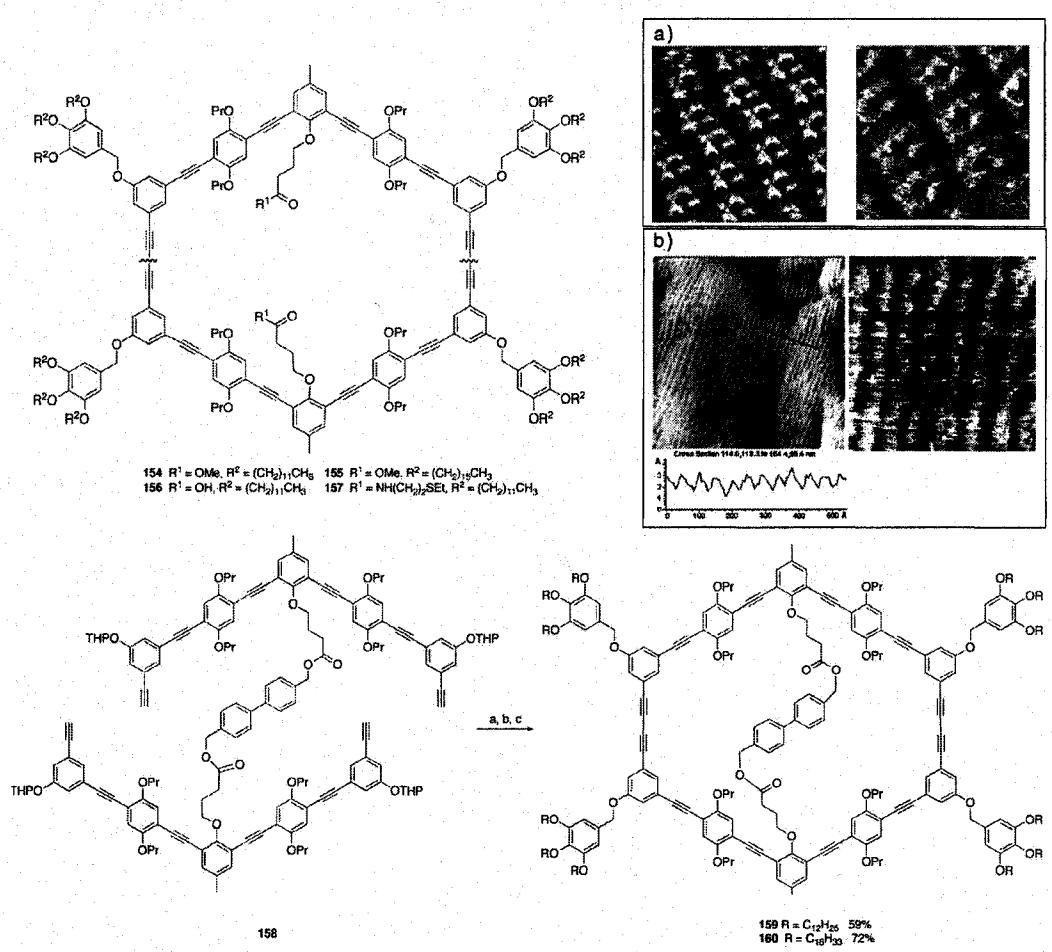

Scheme 1.28 Structure of SPMs **154**–**157**[119,120] and templated synthesis of **159** and **160**.[121] Reagents and conditions: (a) CuCl, $CuCl_2$, py, 81%; (b) *p*-TsOH, MeOH, $CHCl_3$, 99%; (c) $ClCH_2Ph(OR)_3$, K_2CO_3, DMF, 59% (159) and 72% (160). Inset a) STM images of **154** at the liquid/solid (1-phenyloctane/HOPG) interface, 17.7 × 17.7 nm^2 (left) and 12.7 × 12.7 nm^2 (right); Reprinted with permission from *J. Am. Chem. Soc.* **2004**, *126*, 214-222. Copyright 2004 American Chemical Society. Inset b) STM images of SAMs of **157** on Au(111) at the air-substrate interface, 200 × 200 nm^2 and z-profile taken along the black line showing a row width of 5 ± 0.4 nm (left). The same SAMs at higher magnification at the vacuum-substrate interface, 40 × 40 nm^2 (right); Reprinted with permission from *Langmuir* **2004**, *20*, 2781-2784. Copyright 2004 American Chemical Society.

STM has also been used to characterize SPM **161** (Fig. 1.13A) and **161**/C_{60}, after assembling highly ordered arrays from 1,2,4-trichlorobenzene (TCB) onto a HOPG surface.[122] Monolayers of pure **161** exhibit perfect ordering over a relatively large area, but only two alkyl chains for each extraannular side group are observed. The STM image

of the ordered array of **161**/C_{60} at high resolution displays well-ordered bright spots, vastly different from the STM images of pure **161**. The C_{60} molecules are not sequestered inside of the macrocycle, but are located at the sides of the macrocycle near the bithiophene units. This observation indicates that the driving force for the supramolecular assembly is the donor-acceptor interaction between the C_{60} and bithiophene groups rather than C_{60} and the uncovered HOPG surface inside macrocycle **161**.

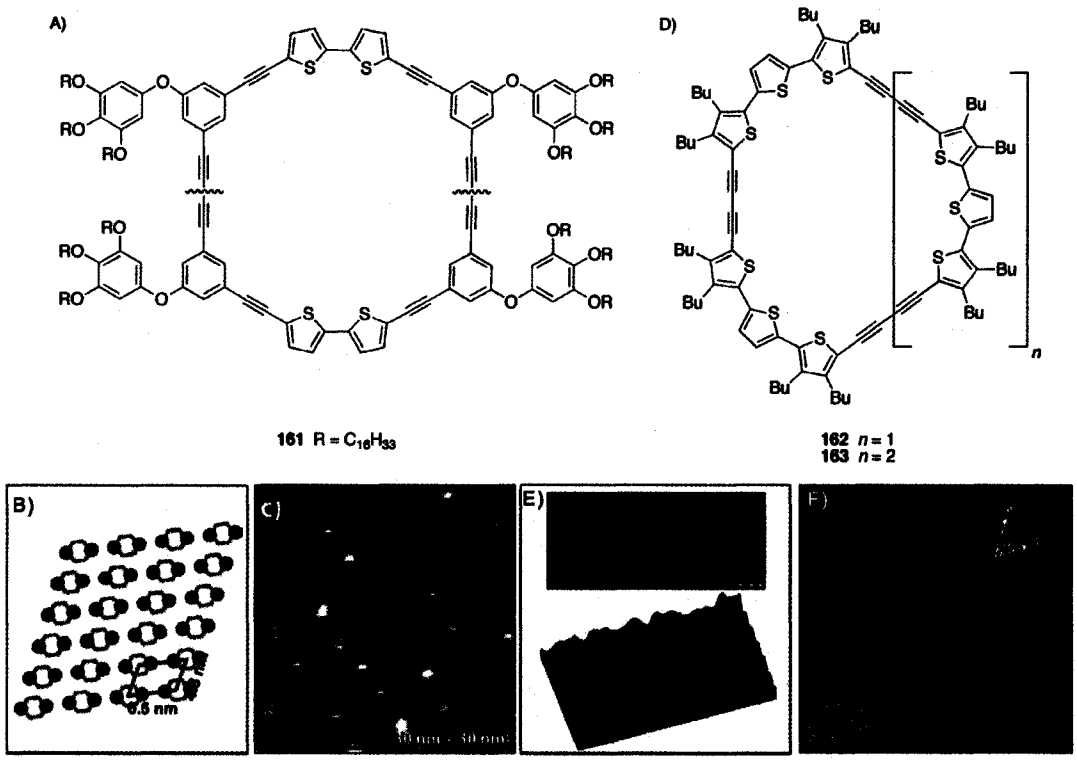

Figure 1.13 A) SPM **161**;[122] B) A proposed structural model for **161**/C_{60} on HOPG; C) A high resolution STM image (30 x 30 nm^2) of an ordered array with **161**/C_{60} on HOPG showing the adsorption site of C_{60} on the macrocycle **161**. Both images reprinted with permission from *J. Amer. Chem. Soc.* **2006**, *128*, 4218-4219. Copyright 2006 American Chemical Society; D) Oligiothiophene SPMs **162** and **163**;[123,124] E) Short-range ordering at solution/HOPG interface of SPM **162** from top view and 3D side view; F) short-range ordering at the solution/HOPG interface for SPM **163**; Both images reprinted with permission from E. Mena-Osteritz, P. Bäuerle, *Adv. Mater.* **2001**, *13*, 243-246.

The synthesis of SPMs **162** and **163** (Fig. 1.13B) has been reported by Bäuerle and coworkers.[123] Characterization of **162** and **163** by STM at the solution/HOPG

interface shows that both SPMs self-assemble to form well-ordered, stable hexagonal arrays.[124] The STM image of **162** shows the unique "donut-like" molecular shape of macrocycle **162** from a top and 3D side view. The images agree with the semiempirical calculations that predict a "spider-like" conformation for the SPM, with the butyl side chains bent downwards. The STM image of **163** displays a cycle divided into two halves. This substructure corresponds to the electron density distribution of the HOMO–1 for **163**, where one nodal plane results in two "C-shaped" pieces of the macrocycle. The cyclic structure and highly ordered self-assembly of these molecules lend themselves to the possible formation of channels or nanotubes.

Schlüter and coworkers have synthesized a number of macrocycles (**164–165**) with either one or two (opposing) terpyridine groups (Figure 1.14), and provide an excellent comparison of the synthetic efficiency of routes used for their formation.[60] The periphery of the macrocycles have been decorated with different flexible side chains, and physical properties were assessed as a function of the nature and number of side chains. It is interesting to note that while all SPMs with one terpyridine group (**164**) are nicely crystalline, those with two are not. X–ray crystallographic characterization of three derivatives provide insight into the packing effects of the various pendent alkyl chains as well as the propensity to adsorb onto the surface of HOPG. For one derivative of **164** (n = 0, $R^1 = R^2 = OC_6H_{13}$, $R^3 = H$, $R^4 = C_6H_{13}$), an ordered, albeit loosely packed, molecular arrangement was observed by STM on the HOPG surface. Crystallographic analysis shows that the SPM is not planar, however, a fact that likely makes surface adsorption entropically "expensive", and thus limited resolution of their analysis.

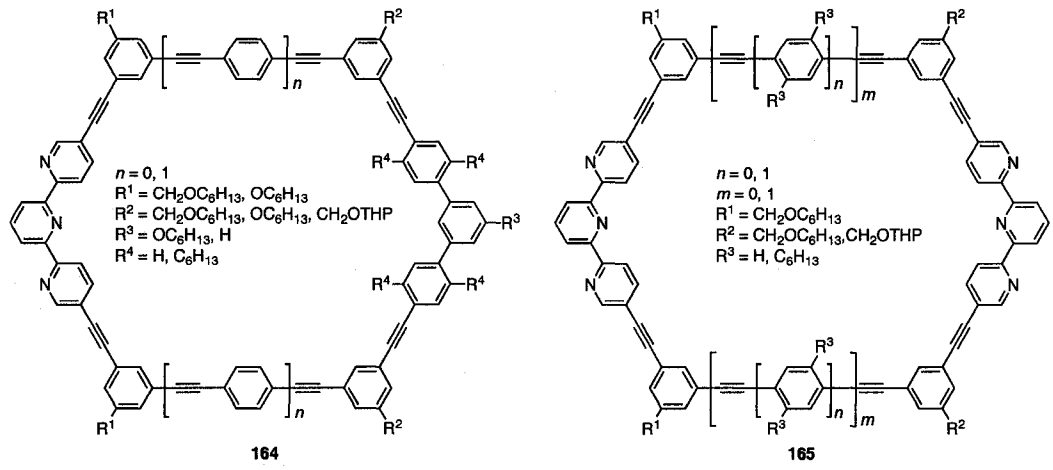

Figure 1.14 SPMs **164** and **165** synthesized by Schlüter and coworkers.[60]

1.3 CONCLUSIONS

Whether by more traditional means such as acetylenic homocoupling or by more modern metathesis reactions, the synthesis of SPMs for use in supramolecular chemistry continues to evolve at an ever increasing pace. Modern metal mediated coupling techniques have helped to improve many ring forming reactions, but it has been the imagination of the chemists involved that has been the most significant advance. Once considered only structural curiosities, acetylene SPMs have now evolved into building blocks for an incredible range of functional materials. The synthesis of acetylenic SPMs and their applications to supramolecular chemistry will no doubt continue to challenge and fascinate chemists who cannot resist their allure.

1.4 REFERENCES

1. Zhang, W.; Moore, J. S. *Angew. Chem. Int. Ed.* **2006**, *45*, 4416-4439.

2. Zhao, D.; Moore, J. S. *Chem. Commun.* **2003**, 807-818.

3. Young, J. K.; Moore, J. S. *Modern Acetylene Chemistry*; Diederich, F.; Stang, P. J.; Eds.; Wiley-VCH: Weinheim, 1995; Chapter 12.

4. Höger, S. *Angew. Chem. Int. Ed.* **2005**, *44*, 3806-3808.

5. Höger, S. *Acetylene Chemistry*; Diederich, F.; Stang, P. J.; Tykwinski, R. R.; Eds.; Wiley-VCH: Weinheim, 2005; Chapter 10.

6. Jones, C. S.; O'Connor, M. J.; Haley, M. M. In *Acetylene Chemistry*; Diederich, F.; Stang, P. J.; Tykwinski, R. R.; Eds.; Wiley-VCH, Weinheim: 2005; Chapter 8.

7. Höger, S. *J. Polym. Sci., Part A: Polym. Chem.* **1999**, *37*, 2685-2698.

8. Tahara, K.; Tobe, Y. *Chem. Rev.* **2006**, *106*, 5274-5290.

9. Spitler, E. L.; Johnson II, C. A.; Haley, M. M. *Chem. Rev.* **2006**, *106*, 5344-5386.

10. Nielsen, M. B.; Diederich, F. *Chem. Rev.* **2005**, *105*, 1837-1867.

11. Marsden, J. A.; Palmer, G. J.; Haley, M. M. *Eur. J. Org. Chem.* **2003**, 2355-2369.

12. Grave, C.; Schlüter, A. D. *Eur. J. Org. Chem.* **2002**, 3075-3098.

13. *Modern Cyclophane Chemistry*; Gleiter, R.; Hopf, H., Eds.; Wiley-VCH: Weinheim, 2004.

14. Cheng, X. H.; Ju, X. P.; Hoeger, S. *Chin. J. Org. Chem.* **2006**, *26*, 733-743.

15. Höger, S. *Chem. Eur. J.* **2004**, *10*, 1320-1329.

16. Yamaguchi, Y.; Yoshida, Z. *Chem. Eur. J.* **2003**, *9*, 5430-5440.

17. Nielsen, M. B.; Schreiber, M.; Baek, Y. G.; Seiler, P.; Lecomte, S.; Boudon, C.; Tykwinski, R. R.; Gisselbrecht, J. P.; Gramlich, V.; Skinner, P. J.; Bosshard, C.; Günter, P.; Gross, M.; Diederich, F. *Chem. Eur. J.* **2001**, *7*, 3263-3280.

18. (a) Glaser, C. *Ber. Dtsch. Chem. Ges.* **1869**, *2*, 422-424; (b) For an excellent review, see: Siemsen, P.; Livingston, R. C.; Diederich, F. *Angew. Chem. Int. Ed.* **2000**, *39*, 2632-2657.

19. Hay, A. S. *J. Org. Chem.* **1962**, *27*, 3320-3321.

20. Eglinton, G.; Galbraith, A. R. *J. Chem. Soc.* **1959**, 889-896.

21. Eglinton, G.; Galbraith, A. R. *Chem. Ind.* **1956**, 737-738.

22. Okrongly, D.; Denmeade, S. R.; Chiang, M. Y.; Breslow, R. *J. Am. Chem. Soc.* **1985**, *107*, 5544-5545.

23. Rossi, R.; Carpita, A.; Bigelli, C. *Tetrahedron Lett.* **1985**, 26, 523-526.

24. Enozawa, H.; Hasegawa, M.; Takamatsu, D.; Fukui, K.; Iyoda, M. *Org. Lett.* **2006**, *8*, 1917-1920.

25. Tobe, Y.; Utsumi, N.; Nagano, A.; Sonoda, M.; Naemura, K. *Tetrahedron* **2001**, *57*, 8075-8083.

26. Ge, P.-H.; Fu, W.; Herrmann, W. A.; Herdtweck, E.; Campana, C.; Adams, R. D.; Bunz, U. H. F. *Angew. Chem. Int. Ed.* **2000**, *39*, 3607-3610.

27. Pschirer, N. G.; Fu, W.; Adams, R. D.; Bunz, U. H. F. *Chem. Commun.* **2000**, 87-88.

28. Zhang, W.; Moore, J. S. *J. Am. Chem. Soc.* **2004**, *126*, 12796-12796.

29. Campbell, I. D.; Eglinton, G.; Henderson, W.; Raphael, R. A. *Chem. Commun.* **1966**, 87-89.

30. Huynh, C.; Linstrumelle, G. *Tetrahedron* **1988**, *44*, 6337-6344.

31. Iyoda, M.; Vorasingha, A.; Kuwatani, Y.; Yoshida, M. *Tetrahedron Lett.* **1998**, *39*, 4701-4704.

32. Baxter, P. N. W. *Chem. Eur. J.* **2003**, *9*, 2531-2541.

33. Shu, L.; Mayor, M. *Chem. Commun.* **2006**, 4134-4136.

34. For an excellent recent example, see: Hoffmann, M.; Wilson, C. J.; Odell, B.; Anderson, H. L. *Angew. Chem. Int. Ed.* **2007**, *46*, 3122-3125.

35. Laughrey, Z. R.; Gibb, B. C. *Top. Curr. Chem.* **2005**, *249*, 67-125.

36. Dietrich-Buchecker, C.; Colasson, B. X.; Sauvage, J.-P. *Top. Curr. Chem.* **2005**, *249*, 261-283.

37. Godt, A. *Eur. J. Org. Chem.* **2004**, 1639-1654.

38. Anderson, S.; Anderson, H. L. *Templated Organic Synthesis*; Diederich, F.; Stang, P. J.; Eds.; Wiley-VCH, Weinheim, 2000; p. 1-38.

39. Anderson, S.; Anderson, H. L.; Sanders, J. K. M. *Acc. Chem. Res.* **1993**, *26*, 469-475.

40. Anderson, H. L.; Sanders, J. K. M. *Angew. Chem. Int. Ed. Engl.* **1990**, *29*, 1400-1403.

41. Anderson, H. L.; Sanders, J. K. M. *J. Chem. Soc., Chem. Commun.* **1989**, 1714-1715.

42. Walter, C. J.; Anderson, H. L.; Sanders, J. K. M. *J. Chem. Soc., Chem. Commun.* **1993**, 458-460.

43. Moore, J. S.; Weinstein, E. J.; Wu, Z. *Tetrahedron Lett.* **1991**, *32*, 2465-2466.

44. Yamaguchi, Y.; Kobayashi, S.; Miyamura, S.; Okamoto, Y.; Wakamiya, T.; Matsubara, Y.; Yoshida, Z. *Angew. Chem. Int. Ed.* **2004**, *43*, 366-369.

45. Nomoto, A.; Sonoda, M.; Yamaguchi, Y.; Ichikawa, T.; Hirose, K.; Tobe, Y. *J. Org. Chem.* **2006**, *71*, 401-404.

46. Marsden, J. A.; Miller, J. J.; Haley, M. M. *Angew. Chem. Int. Ed.* **2004**, *43*, 1694-1697.

47. Marsden, J. A.; Miller, J. J.; Shirtcliff, L. D.; Haley, M. M. *J. Am. Chem. Soc.* **2005**, *127*, 2464-2476.

48. Shortell, D. B.; Palmer, L. C.; Tour, J. M. *Tetrahedron* **2001**, *57*, 9055-9065.

49. Elliott, E. L.; Ray, C. R.; Kraft, S.; Atkins, J. R.; Moore, J. S. *J. Org. Chem.* **2006**, *71*, 5282-5290.

50. Campbell, K.; McDonald, R.; Tykwinski, R. R. *J. Org. Chem.* **2002**, *67*, 1133-1140.

51. A similar SPM based on isopropylidene subunits gave the analogous complex **35**, see ref. 50.

52. Campbell, K.; Kuehl, C. J.; Ferguson, M. J.; Stang, P. J.; Tykwinski, R. R. *J. Am. Chem. Soc.* **2002**, *124*, 7266-7267.

53. Campbell, K.; Ooms, K. J.; Wasylishen, R. E.; Tykwinski, R. R. *Org. Lett.* **2005**, *7*, 3397-3400.

54. Campbell, K.; McDonald, R.; Ferguson, M. J.; Tykwinski, R. R. *Organometallics* **2003**, *22*, 1353-1355.

55. Campbell, K.; McDonald, R.; Ferguson, M. J.; Tykwinski, R. R. *J. Organomet. Chem.* **2003**, *683*, 379-387.

56. Campbell, K. Ph.D. thesis, University of Alberta, Edmonton, AB, 2004.

57. Sun, S.-S.; Lees, A. J. *Organometallics* **2001**, *20*, 2353-2358.

58. Henze, O.; Lentz, D.; Schäfer, A.; Franke, P.; Schlüter, A. D. *Chem. Eur. J.* **2002**, *8*, 357-365.

59. Henze, O.; Lentz, D.; Schluter, A. D. *Chem. Eur. J.* **2000**, *6*, 2362-2367.

60. Grave, C.; Lentz, D.; Schäfer, A.; Samori, P.; Rabe, J. P.; Franke, P.; Schlüter, A. D. *J. Am. Chem. Soc.* **2003**, *125*, 6907-6918.

61. Opris, D. M.; Franke, P.; Schlüter, A. D. *Eur. J. Org. Chem.* **2005**, 822-837.

62. Schmittel, M.; Ammon, H.; Kalsani, V.; Wiegrefe, A.; Michel, C. *Chem. Commun.* **2002**, 2566-2567.

63. Schmittel, M.; Ammon, H. *Synlett* **1999**, 750-752.

64. Schmittel, M.; Ganz, A. *Chem. Commun.* **1997**, 999-1000.

65. Kalsani, V.; Ammon, H.; Jäckel, F.; Rabe, J. P.; Schmittel, M. *Chem. Eur. J.* **2004**, *10*, 5481-5492.

66. Ünsal, Ö.; Godt, A. *Chem. Eur. J.* **1999**, *5*, 1728-1733.

67. Dietrich-Buchecker, C. O.; Hemmert, C.; Khémiss, A.-K.; Sauvage, J.-P. *J. Am. Chem. Soc.* **1990**, *112*, 8002-8008.

68. (a) Bäuerle, P.; Ammann, M.; Wilde, M.; Götz, G.; Mena-Osteritz, E.; Rang, A.; Schalley, C. A. *Angew. Chem. Int. Ed.* **2007**, *46*, 363-368; (b) For a review of Pt-acetylide macrocycles, see: Kaiser, A.; Bäuerle, P. *Top. Curr. Chem.* **2005**, *249*, 127-201.

69. Ammann, M.; Rang, A.; Schalley, C. A.; Bäuerle, P. *Eur. J. Org. Chem.* **2006**, 1940-1948.

70. Zhu, J.; Wang, X.-Z.; Chen, Y.-Q.; Jiang, X.-K.; Chen, X.-Z.; Li, Z.-T. *J. Org. Chem.* **2004**, *69*, 6221-6227.

71. Droz, A. S.; Neidlein, U.; Anderson, S.; Seiler, P.; Diederich, F. *Helv. Chim. Acta.* **2001**, *84*, 2243-2289.

72. Droz, A. S.; Diederich, F. *J. Chem. Soc., Perkin Trans. 1* **2000**, 4224-4226.

73. Bähr, A.; Droz, A. S.; Püntener, M.; Neidlein, U.; Anderson, S.; Seiler, P.; Diederich, F. *Helv. Chim. Acta* **1998**, *81*, 1931-1963.

74. Anderson, S.; Neidlein, U.; Gramlich, V.; Diederich, F. *Angew. Chem. Int. Ed.* **1995**, *34*, 1596-1600.

75. Kawase, T.; Darabi, H. R.; Oda, M. *Angew. Chem. Int. Ed. Engl.* **1996**, *35*, 2664-2666.

76. Kawase, T.; Ueda, N.; Tanaka, K.; Seirai, Y.; Oda, M. *Tetrahedron Lett.* **2001**, *42*, 5509-5511.

77. Kawase, T.; Tanaka, K.; Seirai, Y.; Shiono, N.; Oda, M. *Angew. Chem. Int. Ed.* **2003**, *42*, 5597-5600.

78. Association constants (K_a) were determined by absorption spectroscopy and Stern–Völmer constants (K_{SV}) by fluorescence specroscopy.

79. Kawase, T.; Tanaka, K.; Shiono, N.; Seirai, Y.; Oda, M. *Angew. Chem. Int. Ed.* **2004**, *43*, 1722-1724.

80. Kawase, T.; Oda, M. *Pure Appl. Chem.* **2006**, *78*, 831-839.

81. Baxter, P. N. W. *J. Org. Chem.* **2001**, *66*, 4170-4179.

82. Baxter, P. N. W. *Chem. Eur. J.* **2002**, *8*, 5250-5264.

83. Baxter, P. N. W. *J. Org. Chem.* **2004**, *69*, 1813-1821.

84. Baxter, P. N. W.; Dali-Youcef, R. *J. Org. Chem.* **2005**, *70*, 4935-4953.

85. Kobayashi, S.; Yamaguchi, Y.; Wakamiya, T.; Matsubara, Y.; Sugimoto, K.; Yoshida, Z. *Tetrahedron Lett.* **2003**, *44*, 1469-1472.

86. Heuft, M. A.; Fallis, A. G. *Angew. Chem. Int. Ed.* **2002**, *41*, 4520-4523.

87. Ma, C.; Lo, A.; Abdolmaleki, A.; MacLachlan, M. J. *Org. Lett.* **2004**, *6*, 3841-3844.

88. Ma, C. T. L.; MacLachlan, M. J. *Angew. Chem. Int. Ed.* **2005**, *44*, 4178-4182.

89. Marsella, M. J.; Wang, Z.-Q.; Reid, R. J.; Yoon, K. *Org. Lett.* **2001**, *3*, 885-887.

90. Coates, G. W.; Dunn, A. R.; Henling, L. M.; Dougherty, D. A.; Grubbs, R. H. *Angew. Chem. Int. Ed. Engl.* **1997**, *36*, 248-251.

91. Coates, G. W.; Dunn, A. R.; Henling, L. M.; Ziller, J. W.; Lobkovsky, E. B.; Grubbs, R. H. *J. Am. Chem. Soc.* **1998**, *120*, 3641-3649.

92. Tobe, Y.; Utsumi, N.; Kawabata, K.; Nagano, A.; Adachi, K.; Araki, S.; Sonoda, M.; Hirose, K.; Naemura, K. *J. Am. Chem. Soc.* **2002**, *124*, 5350-5364.

93. Lin, C.-H.; Tour, J. *J. Org. Chem.* **2002**, *67*, 7761-7768.

94. Höger, S.; Bonrad, K.; Mourran, A.; Beginn, U.; Möller, M. *J. Am. Chem. Soc.* **2001**, *123*, 5651-5659.

95. Nakamura, K.; Okubo, H.; Yamaguchi, M. *Org. Lett.* **2001**, *3*, 1097-1099.

96. Tobe, Y.; Utsumi, N.; Nagano, A.; Naemura, K. *Angew. Chem. Int. Ed.* **1998**, *37*, 1285-1287.

97. Shetty, A. S.; Zhang, J.; Moore, J. S. *J. Am. Chem. Soc.* **1996**, *118*, 1019-1027.

98. Zhang, J.; Moore, J. S. *J. Am. Chem. Soc.* **1992**, *114*, 9701-9702.

99. Tobe, Y.; Nagano, A.; Kawabata, K.; Sonoda, M.; Naemura, K. *Org. Lett.* **2000**, *2*, 3265-3268.

100. Saiki, Y.; Sugiura, H.; Nakamura, K.; Yamaguchi, M.; Hoshi, T.; Anzai, J. *J. Am. Chem. Soc.* **2003**, *125*, 9268-9269.

101. Klyatskaya, S.; Dingenouts, N.; Rosenauer, C.; Müller, B.; Höger, S. *J. Am. Chem. Soc.* **2006**, *128*, 3150-3151.

102. Zhang, W.; Brombosz, S. M.; Mendoza, J. L.; Moore, J. S. *J. Org. Chem.* **2005**, *70*, 10198-10201.

103. Zhang, W.; Moore, J. S. *J. Am. Chem. Soc.* **2005**, *127*, 11863-11870.

104. Lahiri, S.; Thompson, J. L.; Moore, J. S. *J. Am. Chem. Soc.* **2000**, *122*, 11315-11319.

105. Balakrishnan, K.; Datar, A.; Zhang, W.; Yang, X. M.; Naddo, T.; Huang, J. L.; Zuo, J. M.; Yen, M.; Moore, J. S.; Zang, L. *J. Am. Chem. Soc.* **2006**, *128*, 6576-6577.

106. Naddo, T.; Che, T.; Zhang, W.; Balakrishnan, K.; Yang, X.; Yen, M.; Zhao, J.; Moore, J. S.; Zang, L. *J. Am. Chem. Soc.* **2007**, *129* , 6978-6979.

107. Zhao, D.; Moore, J. S. *Macromolecules* **2003**, *36*, 2712-2720.

108. Zhao, D.; Moore, J. S. *J. Org. Chem.* **2002**, *67*, 3548-3554.

109. Mindyuk, O. Y.; Stetzer, M. R.; Heiney, P. A.; Nelson, J. C.; Moore, J. S. *Adv. Mater.* **1998**, *10*, 1363-1366.

110. Seo, S. H.; Jones, T. V.; Seyler, H.; Peters, J. O.; Kim, T. H.; Chang, J. Y.; Tew, G. N. *J. Am. Chem. Soc.* **2006**, *128*, 9264-9265.

111. Zhang, J.; Moore, J. S. *J. Am. Chem. Soc.* **1994**, *116*, 2655-2656.

112. Höger, S.; Enkelmann, V.; Bonrad, K.; Tschierske, C. *Angew. Chem. Int. Ed.* **2000**, *39*, 2268-2270.

113. Höger, S.; Cheng, X. H.; Ramminger, A.-D.; Enkelmann, V.; Rapp, A.; Mondeshki, M.; Schnell, I. *Angew. Chem. Int. Ed.* **2005**, *44*, 2801-2805.

114. For a more detailed discussion of the LC and surface chemistry of SPMs such as **147–148**, see: Cheng, X.; Ver Heyen, A.; Mamdouh, W.; Uji-i, H.; De Schryver, F.; Höger, S.; De Feyter, S. *Langmuir* **2007**, *23*, 1281-1286.

115. De Feyter, S.; Gesquière, A.; Abdel-Mottaleb, M. M.; Grim, P. C. M.; De Schryver, F. C.; Meiners, C.; Sieffert, M.; Valiyaveettil, S.; Müllen, K. *Acc. Chem. Res.* **2000**, *33*, 520-531.

116. Ohkita, M.; Ando, K.; Suzuki, T.; Tsuji, T. *J. Org. Chem.* **2000**, *65*, 4385-4390.

117. Sonoda, M.; Sakai, Y.; Yoshimura, T.; Tobe, Y.; Kamada, K. *Chem. Lett.* **2004**, *33*, 972-973.

118. Furukawa, S.; Uji-i, H.; Tahara, K.; Ichikawa, T.; Sonoda, M.; De Schryver, F. C.; Tobe, Y.; De Feyter, S. *J. Am. Chem. Soc.* **2006**, *128* , 3502-3503.

119. Fischer, M.; Lieser, G.; Rapp, A.; Schnell, I.; Mamdouh, W.; De Feyter, S.; De Schryver, F. C.; Höger, S. *J. Am. Chem. Soc.* **2004**, *126*, 214-222.

120. Borissov, D.; Ziegler, A.; Höger, S.; Freyland, W. *Langmuir* **2004**, *20*, 2781-2784.

121. Ziegler, A.; Mamdouh, W.; Heyen, A. V.; Surin, M.; Uji-i, H.; Abdel-Mottaleb, M. M. S.; De Schryver, F. C.; De Feyter, S.; Lazzaroni, R.; Höger, S. *Chem. Mater.* **2005**, *17*, 5670-5683.

122. Pan, G.-B.; Cheng, X.-H.; Höger, S.; Freyland, W. *J. Am. Chem. Soc.* **2006**, *128*, 4218-4219.

123. Krömer, J.; Rios-Carreras, I.; Fuhrmann, G.; Musch, C.; Wunderlin, M.; Debaerdemaeker, T.; Mena-Osteritz, E.; Bäuerle, P. *Angew. Chem. Int. Ed.* **2000**, *39*, 3481-3486.

124. Mena-Osteritz, E.; Bäuerle, P. *Adv. Mater.* **2001**, *13*, 243-246.

CHAPTER 2 SYNTHESIS AND CHARACTERIZATION OF ACYCLIC PLATINUM ACETYLIDE COMPLEXES

2.1 INTRODUCTION

As introduced in Chapter 1 chiral macrocycles and, in particular, metal-acetylide containing macrocycles are very popular in supramolecular chemistry. Metal-directed self-assembly reactions are frequently used to prepare supramolecular frameworks such as molecular squares,[1-5] cages[6-11] and polymeric and dendrimeric molecules.[12,13] Examining the effects of incorporating chirality into systems of this type has grabbed the interest of many chemists over the last few years.[14-16] Promising results have been reported for these materials in various enantioselective processes such as asymmetric catalysis,[17,18] chemical sensing[19,20] and selective guest inclusion.[21] In the assembly of these systems, common chiral building blocks such as ones based upon binaphthyl are typically introduced early in the macrocycle synthesis. Inefficient use of these costly chiral reagents can make this methodology expensive, therefore introducing chirality last is an attractive prospect.

The Tykwinski group has recently reported the use of ligand exchange to control the coordination geometry about a Pt(II) acetylide center. In one simple step, a *trans*-Pt-acetylide complex is converted to its *cis*-analogue by substituting two PPh_3 ligands with a chiral or achiral chelating diphosphine ligand. Conveniently, multiple chiral derivatives can be formed from a single achiral precursor, and since chirality is introduced in the final step, this process is usually much more cost effective than other methodologies. This initial work provides the motivation for this thesis and important points of this study are provided next.

The synthesis of *trans*-Pt-acetylide macrocycles **37**, **38a** and **39** has been described in Section 1.2.1 and their ligand exchange reactions are shown in Scheme 2.1.[22] Chelating diphosphine ligands dppee **200**, *S*,*S*-, or *R*,*R*-CHIRAPHOS **201** (see Fig. 2.2) have been used to form *cis*-Pt-acetylide macrocycles **202–207** in good to excellent yield after reaction times of 3–5 days. These reactions demonstrate the divergent generation of either achiral or chiral macrocycles, or both enantiomers if necessary, in a single step from a single precursor. Reactions are performed by simply dissolving the macrocycle in CH_2Cl_2 with the corresponding ligand and then allowing the mixture to stir at room temperature until the reaction is complete.

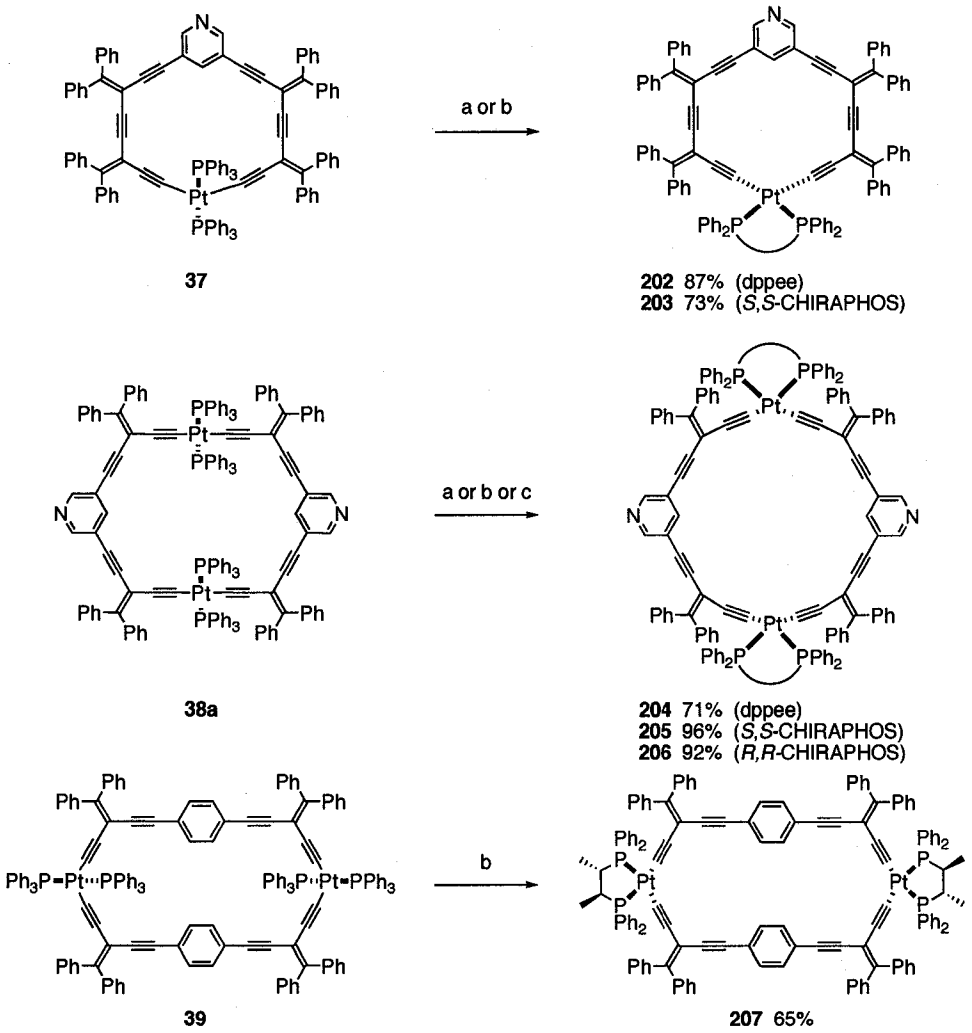

Scheme 2.1 Synthesis of *cis*-Pt-acetylide macrocycles **202–207**. Reagents and conditions: (a) dppee **200**, CH_2Cl_2, rt; (b) *S,S*-CHIRAPHOS **201**, CH_2Cl_2, rt; (c) *R,R*-CHIRAPHOS **201**, CH_2Cl_2, rt.

This study was also extended to acyclic complexes, also containing *trans*-Pt-acetylides with PPh_3 ligands. Molecules of this type were used as model systems for ligand exchange, because they were synthesized much easier and ligand exchanges occurred much faster. The *trans*-Pt-acetylide complexes **208** and **209** have been reported to undergo ligand exchange with dppee **200** and *S,S*-CHIRAPHOS **201** to form the *cis*-Pt-acetylide complexes **210–212** in good to excellent yield in less than 1 day or in some cases minutes (Scheme 2.2).[23,24]

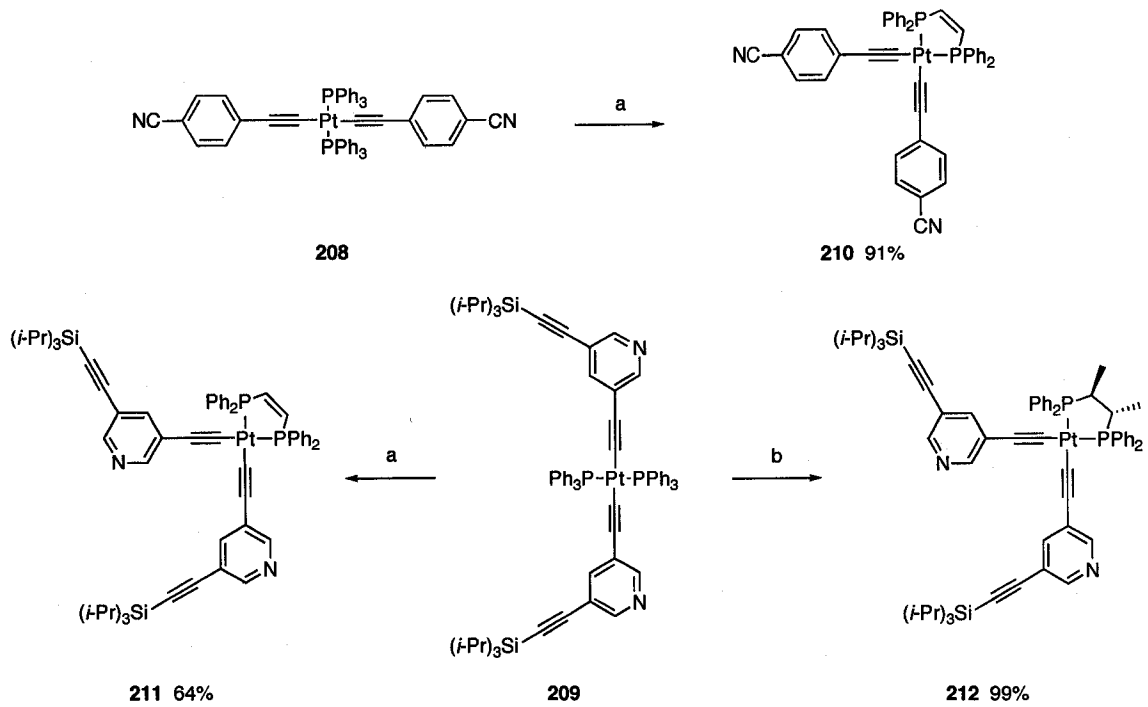

Scheme 2.2 Synthesis of acyclic *cis*-Pt-acetylide complexes **210–212**. Reagents and conditions: (a) dppee **200**, CH_2Cl_2, rt; (b) *S*,*S*-CHIRAPHOS **201**, CH_2Cl_2, rt.

The *trans*-Pt-acetylide complex **213** has also been reported to undergo ligand exchange quickly with dppee **200** and *S*,*S*-CHIRAPHOS **201** to form *cis*-Pt-acetylide complexes **214** and **215** in good to excellent yield and has been repeated with similar results for this current study (Scheme 2.3).[22,24]

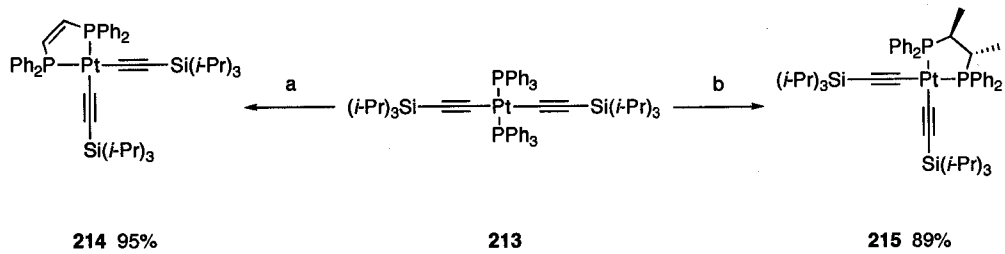

Scheme 2.3 Synthesis of *cis*-Pt-acetylide complexes **214** and **215**. Reagents and conditions: (a) dppee **200**, CH_2Cl_2, rt; (b) *S*,*S*-CHIRAPHOS **201**, CD_2Cl_2, rt.

It was established that the ligand exchange reactions described above can be very conveniently monitored by ^{31}P NMR spectroscopy as shown with the example in Figure 2.1 reacting *trans*-Pt-acetylide complex **213** with dppee **200**. The top figure is a ^{31}P NMR spectrum of the reaction mixture after 5 minutes in $CDCl_3$. The growth of the pseudo–t signal at ~52 ppm ($^1J_{P-Pt}$ = 2197 Hz) of the product **214** in conjunction with the less intense pseudo–t signal at ~21 ppm ($^1J_{P-Pt}$ = 2728 Hz) of the starting material **213**, the appearance of the free PPh_3 signal at –4 ppm, and disappearance of the dppee **200** signal at –22 ppm indicate the reaction has fully consumed all the dppee **200** available. To maximize the yield of the *cis*-Pt-acetylide complex **214** excess dppee **200** was added, resulting in the middle ^{31}P NMR spectrum. Now the *trans*-Pt-acetylide complex **213** has been consumed leaving only signals of the product **214**, free PPh_3 and excess dppee **200**. After purification, the bottom ^{31}P spectrum of pure **214** was obtained. As the *trans*-Pt-acetylide complexes are transformed into the *cis*-Pt-acetylide complexes typically a deshielding of the phosphorous atoms occurs as well as a decrease in the $^1J_{P-Pt}$ coupling constant from ~2600–2800 Hz to ~2100–2300 Hz. These values are typical for *trans*-bis(alkynyl) and well as *cis*-bis(alkynyl) complexes.[25] The remainder of this chapter will focus on the synthesis and characterization of acyclic molecules of this type, and their ligand exchange reactions with chelating diphosphine ligands.

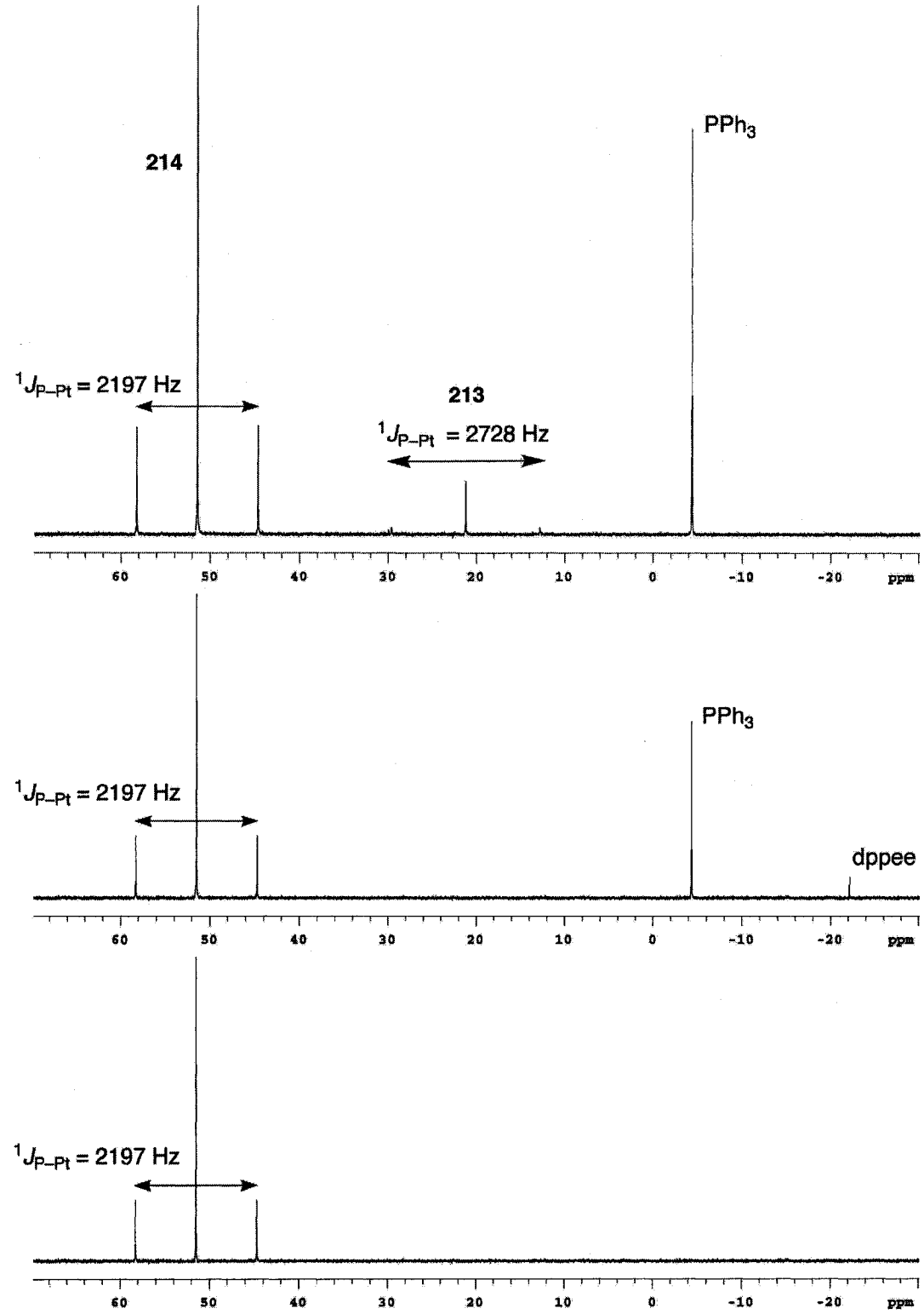

Figure 2.1 $^{31}P\{^{1}H\}$ NMR spectra (162 Hz, $CDCl_3$) following the reaction of **213** with dppee **200** to form **214**. (Top) ^{31}P NMR spectrum of the reaction mixture after less than 5 minutes; (Middle) ^{31}P NMR spectrum after excess dppee **200** is added to consume **213**; (Bottom) ^{31}P NMR spectrum of purified *cis*-Pt-acetylide complex **214**.

2.2 Results and Discussion

2.2.1 Synthesis and Characterization of trans-Pt-Acetylide Complexes

For the purposes of this research project *trans*-Pt-TIPS-monoyne complex **213** and *trans*-Pt-tolyl-monoyne complex **216** were chosen as the precursors for two series of ligand exchange reactions.[26,27] From previous experience it was known that ligand exchange does not occur with *trans*-Pt-acetylide complexes containing PEt_3 ligands. Therefore PPh_3 ligands were necessary for ligand exchange due to their increased labiality. The synthesis of *trans*-Pt-acetylide complexes requires a terminal acetylene, and therefore in the case of **217** desilylation with TBAF in wet THF at room temperature prior to coupling was necessary (Scheme 2.4). The appropriate terminal acetylene, triisopropylacetylene (TIPSA) or desilylated **217**, was subsequently added to a degassed solution of either *cis*- or *trans*-$PtCl_2(PPh_3)_2$ **218** in Et_2NH. A catalytic amount of CuI was added, the flask sealed under a nitrogen atmosphere and then was allowed to stir at room temperature for typically 14 hours. Temperatures of 50–55 °C were previously reported for this reaction,[24] but room temperature was found to work well in these cases. After work-up, *trans*-Pt-acetylide complexes **213** and **216** were purified by either column chromatography or by precipitation from a CH_2Cl_2 solution by the addition of hexanes or Et_2O. They were isolated as colourless (**213**) or yellow (**216**) stable solids in good yield.

Compounds **213** and **216** have low solubility in organic solvents, which makes the characterization of **216** impossible by mass spectrometry. On the other hand, this limited solubility allows for the growth of single crystals of **216** suitable for X–ray crystallographic analysis (see Chapter 2.2.4). Both compounds **213** and **216** have been characterized by ^{1}H, ^{13}C, ^{31}P NMR and IR spectroscopies and display typical *trans*-Pt-

acetylide $^1J_{P-Pt}$ coupling constants of 2728 and 2660 Hz in their respective ^{31}P NMR spectra (see Table 2.1). It is possible to use *cis*-$PtCl_2(PPh_3)_2$ for these reactions because the usually resulting *trans*-Pt-acetylide complexes are thermodynamically more stable than their *cis*-analogues, therefore, rearrangement about the Pt center occurs, even at room temperature.

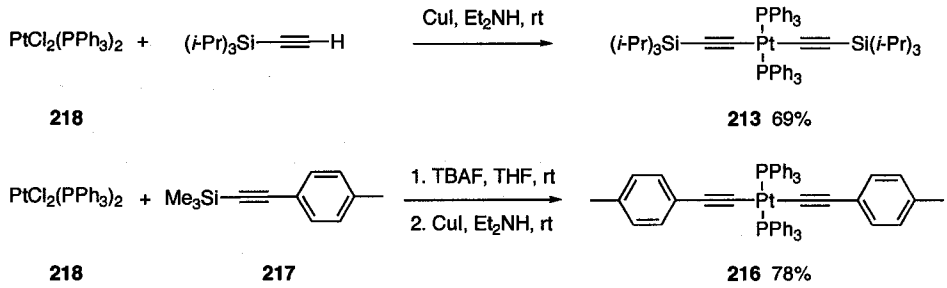

Scheme 2.4 Synthesis of *trans*-Pt-acetylide complexes **213** and **216**.

2.2.2 Synthesis and Characterization of cis-Pt-Acetylide Complexes

Ligand exchange reactions were performed on *trans*-Pt-acetylide complexes **213** and **216** with chelating diphosphine ligands **200**, **201** and **219–222** (Figure 2.2) resulting in two series, the *cis*-Pt-TIPS-monoyne complexes **214**, **215**, **223–226** and the *cis*-Pt-tolyl-monoyne complexes **227–232** (Scheme 2.5). This conversion to product was performed easily by adding one equivalent of the appropriate ligand to a solution of either **213** or **216** and stirring the reaction mixture until the ^{31}P NMR spectra indicated the reaction was complete. Solutions of $CHCl_3$, $CDCl_3$, CH_2Cl_2 or CD_2Cl_2 were all found to work equally as well, but dry CH_2Cl_2 was typically used in an effort to reduce the presence of impurities in the reaction mixtures and for economical reasons. All reactions on a ~20 mg scale proceeded quickly at room temperature, usually within hours, but to ensure the reactions were complete they were occasionally allowed to react overnight. Upon completion of the reaction, solvent removal followed by purification via column

chromatography led to the isolation of the desired *cis*-Pt-acetylide complex. First, a less polar eluent was used to remove free PPh_3 and the excess ligand, followed by a polar eluent to provide the product. Pure *cis*-Pt-monoyne complexes **214**, **215**, **223–232** were thus obtained in good to excellent yield. Chromatographic purification using alumina was found to work better for the *cis*-Pt-tolyl monoyne complexes **227–232**, while silica worked best for the *cis*-Pt-TIPS-monoyne complexes **214**, **215**, **223–226**.

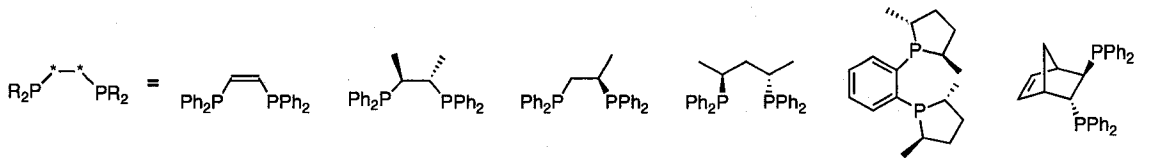

200 (dppee) **201** (*S,S*-CHIRAPHOS) **219** (*R*-PROPHOS) **220** (*S,S*-BDPP) **221** (*R,R*-Me-DUPHOS) **222** (*R,R*-NORPHOS)

Figure 2.2 Chelating diphosphine ligands **200**, **201**, **219–222** used for ligand exchange.

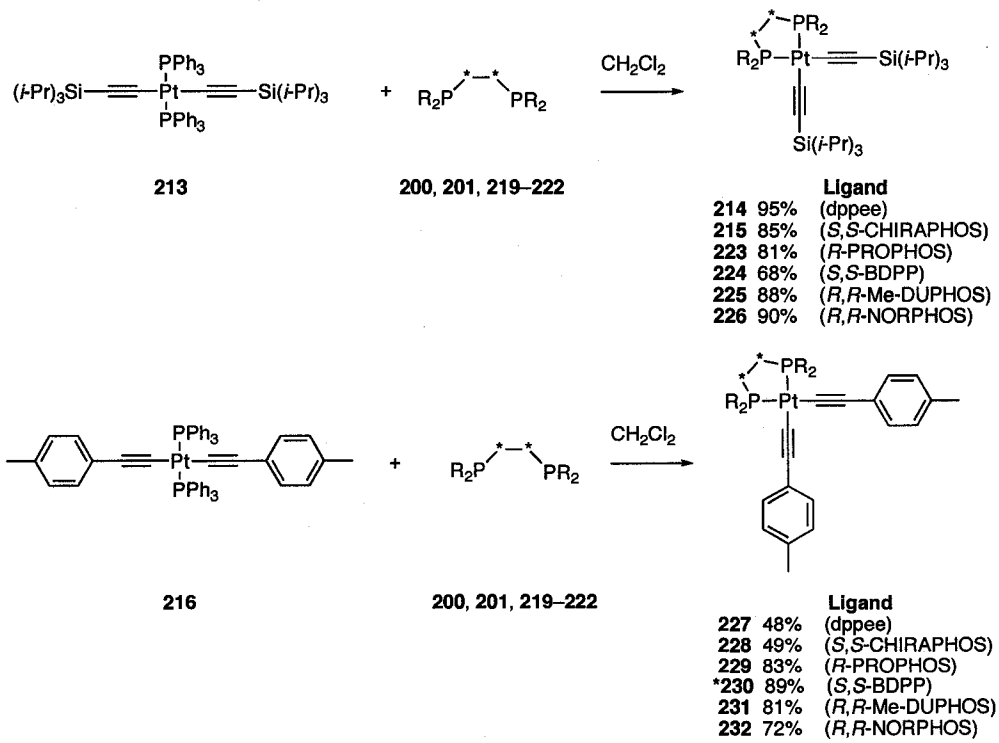

Scheme 2.5 Synthesis of *cis*-Pt-TIPS-monoyne complexes **214**, **215**, **223–226** and *cis*-Pt-tolyl-monoyne complexes **227–232**. (For compound denoted with *, see text for an explanation.)

Ligand exchange with *S,S*-CHIRAPHOS **201**, *S,S*-BDPP **220** and *R,R*-NORPHOS **222** with *trans*-Pt-diyne complex **233** (provided by Mr. Thanh Luu) occurred in the same manner as described above for the monoyne complexes, leading to *cis*-Pt-diyne complexes **234–236** in good yield (Scheme 2.6). These ligands were chosen because they appeared the most effective in chirality transfer for the monoyne systems, based upon CD spectroscopic analysis (see Section 2.2.5). Compounds **234** and **236** were purified and isolated by silica gel column chromatography, while compound **235** was purified by precipitation from the reaction solvent by the addition of hexanes after solvent reduction, then isolated by filtration. Purification by precipitation was found to be very efficient for many acyclic complexes. Typically purification of the *cis*-Pt-acetylide complexes was attempted by precipitation first and then if unsuccessful chromatography was used.

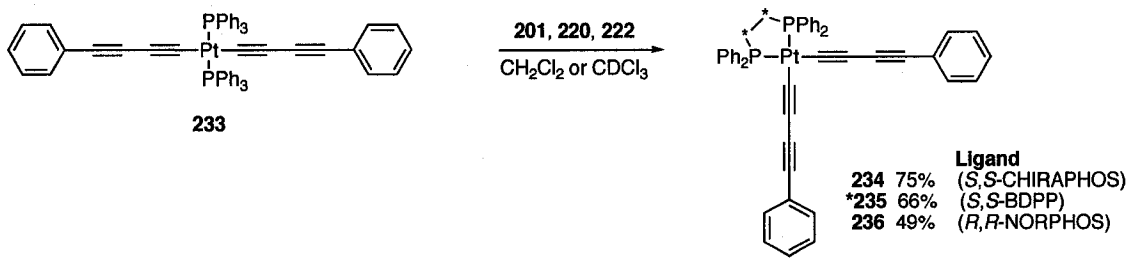

Scheme 2.6 Synthesis of chiral *cis*-Pt-diyne complexes **234–236**. (For compound denoted with *, see text for an explanation.)

A ligand exchange with *S,S*-CHIRAPHOS **201** and *trans*-Pt-triyne complex **237** (provided by Mr. Thanh Luu) was also carried out in CD_2Cl_2 in under 30 minutes. Purification by silica gel chromatography afforded pure *cis*-Pt-triyne complex **238** in excellent yield (Scheme 2.7). To date this is the only triyne derivative synthesized, but the series will be extended in the near future.

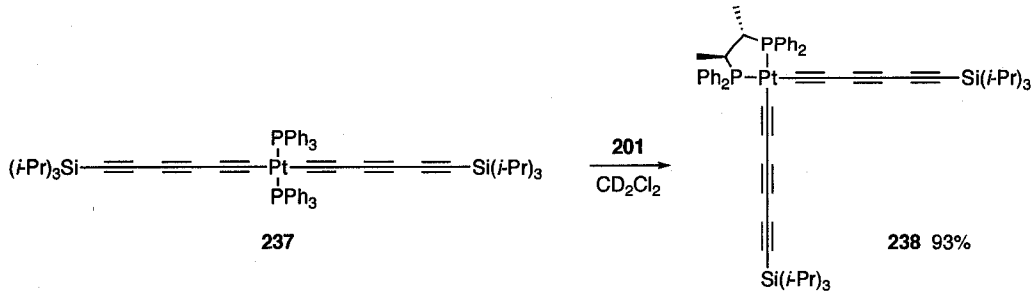

Scheme 2.7 Synthesis of *cis*-Pt-triyne complex **238**.

All *cis*-Pt-acetylide complexes have been fully characterized by ^{1}H, ^{31}P and ^{13}C NMR, and IR spectroscopies, mass spectral analysis and microanalysis where possible. In most cases, the ^{31}P NMR spectra were the most informative. The pseudo–t signal in the ^{31}P NMR spectra for all of the *cis*-Pt-acetylide complexes synthesized have $^{1}J_{P-Pt}$ coupling constants in the expected range of 2100–2300 Hz, with two exceptions (See Table 2.1).

First, in the ^{31}P NMR spectra of *R*-PROPHOS and *R,R*-NORPHOS containing compounds (**223**, **226**, **229**, **232** and **236**), two pseudo–dt patterns are observed, due to the inequivalent phosphorous atoms and the resulting $^{3}J_{P-P}$ coupling. A second anomaly was found for *S,S*-BDPP containing compounds **230** and **235** which have coupling constants of 2585 and 2510 Hz, respectively, which are more characteristic of *trans*-Pt-acetylide complexes. The ESI and MALDI mass spectral analysis of **230** and **235** is also unusual with signals at *m/z* 1837 and 1771 corresponding to $[2M + Ag]^{+}$ and $[2M]^{+}$, respectively. These observations indicate **230** and **235** may not have the expected *cis*-Pt-acetylide conformation as depicted in Schemes 2.5 and 2.6, but rather a dimeric Pt containing complex with two bridging *S,S*-BDPP ligands (Figure 2.3). This structure, with a *trans*-Pt-acetylide configuration, would be consistent with the higher than expected $^{1}J_{P-Pt}$ coupling constants of **230** and **235**, as well as the mass spectral data. This

dimeric species was not observed for the *S,S*-BDPP containing *cis*-Pt-TIPS-monoyne complex **224** likely due to the steric demand of the TIPS groups.

Table 2.1 *trans*- and *cis*-Pt-acetylide complexes ^{31}P $\{^1H\}$ NMR chemical shifts (ppm) and $^1J_{P-Pt}$ coupling constants (Hz), in $CDCl_3$.

Compound	^{31}P $\{^1H\}$ δ / ppm	^{31}P $\{^1H\}$ $^1J_{P-Pt}$ / Hz*	Compound	^{31}P $\{^1H\}$ δ / ppm	^{31}P $\{^1H\}$ $^1J_{P-Pt}$ / Hz*
trans-			**227**	53.1	2276
213[†24]	21.2	2719	**228**	44.2	2234
216	19.7	2660	**229**[§]	51.7	2285
233[†28]	19.3	2525		34.3	2259
237[†28]	19.2	2571	**230/239**	26.9	2585
cis-			**231**	66.4	2206
214[†24]	52.0	2208	**232**[§]	12.0	2280
215[†22]	46.4	2194		11.2	2280
223[§]	51.3	2206	**234**	41.9	2236
	34.2	2191	**235/240**	26.9	2510
224	5.7	2134	**236**	11.3	2294
225	65.3	2134		10.6	2294
226[§]	11.2	2213	**238**	41.9	2236
	10.3	2211			

* all peaks have a pseudo–t multiplicity, † in CD_2Cl_2, § $^3J_{P-P}$ coupling constants are omitted,

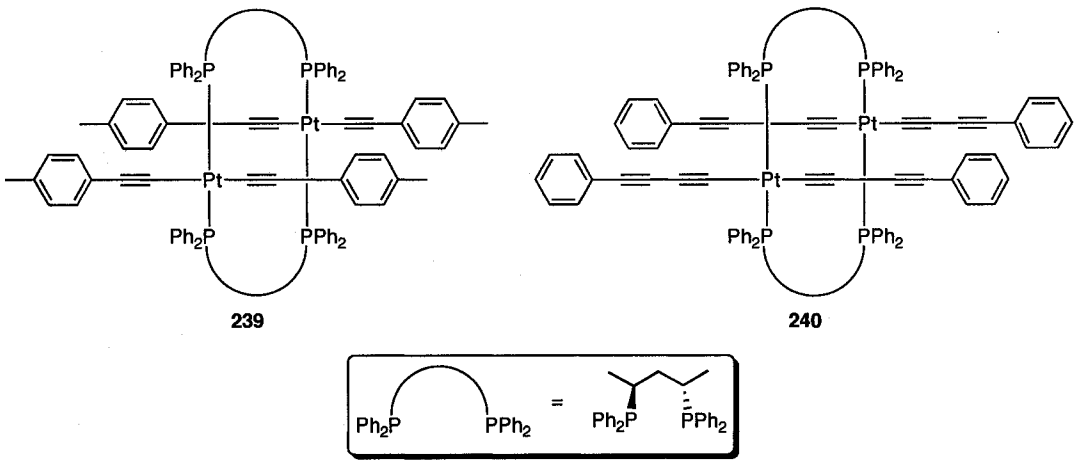

Figure 2.3 Possible dimeric structures of compounds **239** and **240** based upon experimental evidence.

The ^{13}C NMR spectroscopic analysis of the *cis*-Pt-acetylide complexes proved to be difficult due to the complex splitting pattern caused by the magnetically inequivalent phosphorus atoms and platinum coupling. The analysis was significantly more complicated for the *R*-PROPHOS and *R,R*-NORPHOS containing compounds **223**, **226**, **229**, **232** and **236**, where the phosphorus atoms are chemical shift inequivalent. For the *cis*-Pt-monoyne complexes **223**, **226**, **229**, **232**, ^{1}H and ^{31}P decoupled ^{13}C NMR spectra were recorded, drastically simplifying the ^{13}C NMR spectral analysis. This approach, i.e., ^{13}C $\{^{1}H, ^{31}P\}$ NMR spectra, would be recommended for similar compounds synthesized in the future, to allow for a more meaningful analysis.

The α-acetylide carbon signal in *cis*-Pt-acetylide complexes ($L_2Pt(C{\equiv}CR)_2$) are assigned as a doublet of doublets (dd) with a *cis* $^{2}J_{C-P}$ coupling constant of 4–48 Hz and *trans* $^{2}J_{C-P}$ coupling constant of 133–169 Hz. For the *cis*-Pt-TIPS-monoyne complexes **214**, **215**, **223–226** this carbon has a chemical shift of 122–129 ppm, while for the *cis*-Pt-tolyl-monoyne, diyne and triyne complexes **227–232**, **234–236** and **238** this carbon is shielded to 101–107 ppm (See Table 2.2). Due to poor signal to noise in all of the ^{13}C NMR spectra, the $^{1}J_{C-Pt}$ coupling constant to the α-acetylide carbon is not observed. To confirm its presence and the signal assignment, however, a ^{1}H and ^{31}P decoupled ^{13}C NMR spectrum of compound **231** was recorded until this coupling constant was visible. This experiment conclusively assigned this resonance as a pseudo–ddt with $^{1}J_{C-Pt}$ = 1105 Hz. In spectra with lesser signal to noise, this signal is thus expected to be observed as a doublet of doublets.

The β-acetylide carbon of ($L_2Pt(C{\equiv}CR)_2$) is observed for all of the *cis*-Pt-acetylide complexes at 92–112 ppm with *trans* $^{2}J_{C-P}$ coupling constants between 3 and 40 Hz, *cis*

$^2J_{C-P}$ coupling constants less than 5 Hz (not always observed) and $^2J_{C-Pt}$ coupling constants between 229 and 307 Hz (observed when there is sufficient signal to noise, see Table 2.2 for more details). Compounds **229**, **230/239** and **235/240**, however, do not follow these trends. In the case of the *S,S*-BDPP containing compounds **230/239** and **235/240** this is probably due to their dimeric structure, but in the case of compound **229** it is unclear why the trend is not followed.

Table 2.2 ^{13}C NMR spectral data for the α- and β-acetylide carbon of ($L_2Pt(C{\equiv}CR)_2$), in $CDCl_3$

Compound	α-acetylide carbon		β-acetylide carbon			
	δ (ppm), Obs. Mult.	$^2J_{C-P}$(*trans*), (*cis*) / Hz	δ (ppm), Obs. Mult.	$^2J_{C-Pt}$* / Hz	$^3J_{C-P}$(*trans*) / Hz	$^3J_{C-P}$(*cis*)* / Hz
214	122.9, dd	139, 15	109.3, ddt	229	27	1.6
215**	—	—	108.6, d	240	—	—
223	125.5, dd	136, 14	109.6, ddt	274	27	2.4
	124.5, dd	135, 14	108.9, ddt	273	27	2.3
224	124.9, dd	136, 20	107.1, dt	241	28	—
225	128.9, dd	133, 14	109.2, dt	267	29	—
226	126.0, dd	169, 48	107.4, dt	277	2.9	—
	122.3, dd	135, 15	107.1, dt	278	2.8	—
227	101.5, dd	150, 15	111.6, d	—	32	—
228	105.3, dd	145, 16	110.3, ddt	307	35	2.9
229	111.8, dd	85, 3.0	103.6, dt	275	15	—
	111.5, dd	86, 2.7				
230/239§	111.9, s	—	107.9, d	—	30	—
231	106.3, dd	143, 15	111.9, dt	302	35	—
232	101.5, dd	145, 3.9	109.9, d	—	12	—
	101.3, dd	145, 4.1	109.5, d	—	9.3	—
234	106.2, dd	144, 16	92.3, d	—	36	—
235/240 §	95.7, d	103	107.7, d	—	15	—
236	102.2, dd	144, 6.9	92.2, dd	—	9.6	2.8
	102.0, dd	144, 7.0	92.0, dd	—	9.2	2.8
238	103.3, dd	143, 16	92.3, dd	—	40	4.3

* where observed, ** in CD_2Cl_2 and ^{31}P decoupled, see Reference 21, § likely *trans*-Pt-acetylide complex, see text and Figure 2.3

2.2.3 Additional Chelating Diphosphine Ligands Tested

In addition to the chelating ligands described above, chiral ligands **241–245** have also been used in ligand exchange reactions (Figure 2.4). *S,S*-DIOP **241** and *R*-BINAP **242** were the first chiral ligands tried after CHIRAPHOS **201** because they are among the most inexpensive and popular diphosphine ligands. Unfortunately, reaction of *S,S*-DIOP **241** with *trans*-Pt-acetylide complex **213** resulted in a mixture of unidentified products based on the ^{31}P NMR spectrum, while no reaction was observed for *R*-BINAP **242** and *R*-SYNPHOS **243**, even after heating and long reaction times. In the ^{31}P NMR spectra of these latter two reactions, only the free *R*-BINAP (**242**) or *R*-SYNPHOS (**243**) ligands at –13 ppm and *trans*-Pt-acetylide complex **213** at 21.2 ppm (pseudo–t, $^{1}J_{P-Pt}$ = 2728 Hz) were present, with no sign of free PPh_3 at –4 ppm. The Trost ligand **244** and JOSIPHOS derived ligand **245** were observed to exchange with **213** based on the ^{31}P NMR spectra, which showed new signals at 22.2 and 21.8 ppm (pseudo–t, $^{1}J_{P-Pt}$ = 2719, 2725 Hz) and 20.2 and 0.5 ppm (pseudo–dt, $^{1}J_{P-Pt}$ = 2267, 2205 Hz, $^{3}J_{P-P}$ = 25, 25 Hz), respectively. Based upon the $^{1}J_{P-Pt}$ coupling constant alone, either a *trans*-Pt-acetylide complex or possibly bridged product is formed with Trost ligand **244** and a *cis*-Pt-acetylide complex is formed with **245**, but for practical and economical reasons further studies with these ligands were abandoned.

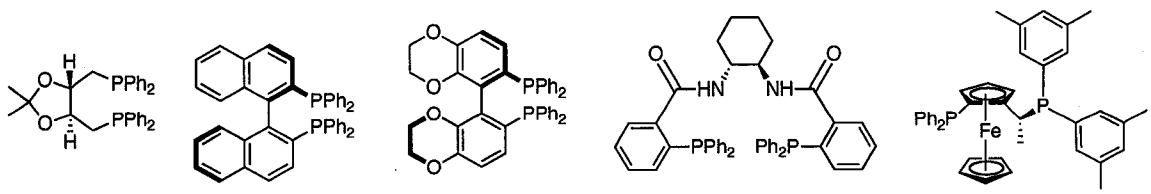

241 (*S,S*-DIOP) **242** (*R*-BINAP) **243** (*R*-SYNPHOS) **244** (*R,R*-DACH-Phenyl Trost Ligand) **245** (*R-S*-JOSIPHOS derivative)

Figure 2.4 Other chiral chelating diphosphine ligands used **241–245**.

2.2.4 Solid State Properties of Selected trans- and cis-Pt-Acetylide Complexes

In addition to the spectroscopic characterization in solution, the solid–state structural properties of *trans*-Pt-tolyl-monoyne complex **216** and *R,R*-Me-DUPHOS containing *cis*-Pt-tolyl-monoyne complex **231** were examined. Single crystals suitable for X–ray crystallographic analysis of **216** were grown by the slow diffusion of Et_2O into a CH_2Cl_2 solution at 4 °C. Crystals of **231** were grown by slow evaporation of a CH_2Cl_2 and acetone solution at room temperature. The ORTEP drawings are shown in Figures 2.5 and 2.6 and selected bond lengths and angles for **213**, **216**, **215** and **231** are compared in Table 2.3.

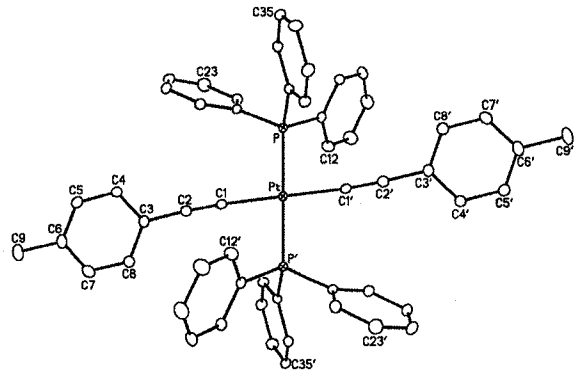

Figure 2.5 ORTEP drawing of *trans*–$(PPh_3)_2Pt(C{\equiv}C–p–CH_3–C_6H_4)_2$, **216**. Thermal ellipsoids are drawn at the 20% probability level.

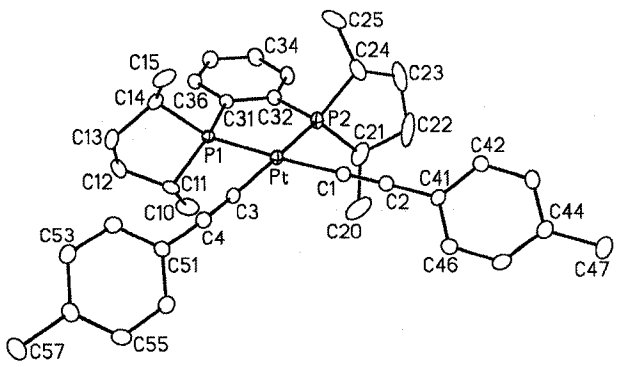

Figure 2.6 ORTEP drawing of *cis*–(*R,R*-Me-DUPHOS)Pt(C≡C-*p*-CH_3–$C_6H_4)_2$ **231**. Thermal ellipsoids are drawn at the 20% probability level.

Compounds **213** and **215** have been selected for comparison to **216** and **231** because their X–ray crystallographic analyses have been previously reported and they are similar in structure to **216** and **231**, respectively. The bond lengths and angles for **213** and **216** are very comparable, with less than 2% deviation between values. The ≡C–Pt–C≡ angles are linear at 180°, but a slight deviation from the square planar geometry about the Pt center is seen with C(1)–Pt–P angles of ~94° and C(1)–Pt–P' angles of ~86°. More significant deviations between *S,S*-CHIRAPHOS and *R,R*-Me-DUPHOS containing compounds **215** and **231** might be expected, but the selected bond lengths are still within 2% of each other. On the other hand, there is a large difference between the bond angles of these compounds, as depicted in Figure 2.7. The ≡C–Pt–C≡ bond angle is much larger for **231** at ~94° compared to ~88° for **215**, and consequently, the C(1)–Pt–P(2) and C(3)–Pt–P(1) bond angles are smaller for **231** at ~90° compared to ~93° for **215**. Interestingly, the P–Pt–P bond angle for both complexes is ~86°. When comparing bond lengths of *trans*- vs. *cis*-Pt-acetylide complexes, the only noteworthy difference is between the Pt–P bonds where the *cis*-Pt-acetylide bonds are consistently shorter.

Table 2.3 A comparison of selected bond lengths and angles for **213**, **216**, **215** and **231**.

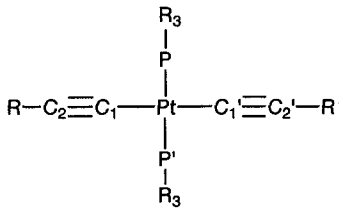

trans

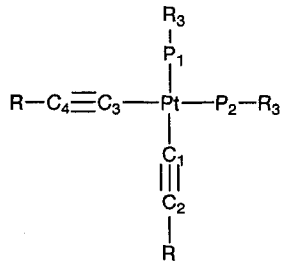

cis

	213[24]	**216**	**215**[22]	**231**
Bond Lengths, Å				
Pt–C(1)	2.005(4)	2.021(4)	2.008(2)	2.014(4)
Pt–C(3)	–	–	2.006(2)	2.035(4)
C(1)–C(2)	1.207(6)	1.192(5)	1.203(4)	1.209(5)
C(3)–C(4)	–	–	1.202(4)	1.187(6)
Pt–P or Pt–P(1)	2.2973(8)	2.2862(10)	2.2777(6)	2.2571(10)
Pt–P(2)	–	–	2.2679(7)	2.2513(10)
Bond Angles, °				
≡C–Pt–C≡	180.0	180.0(2)	87.93(9)	93.86(14)
C(1)–Pt–P or C(1)–Pt–P(2)	93.75(10)	93.95(11)	92.15(6)	89.74(11)
P–Pt–P	180.0	180.0	86.29(2)	86.78(4)
C(1)–Pt–P' or C(3)–Pt–P(1)	86.25(10)	86.05(11)	93.83(7)	89.66(10)

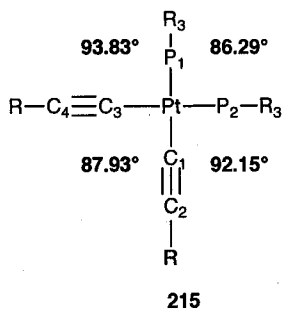

215

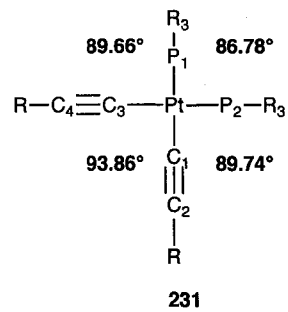

231

Figure 2.7 Schematic representation of bond angles for **215** and **231**.

2.2.5 Electronic Properties of Chiral Acyclic cis-Pt-Acetylide Complexes

2.2.5.1 Pure Ligand and *cis*-Pt-TIPS-Monoyne Complexes

The UV–vis spectra were recorded for pure ligands **201**, **219–222**, and all show a high energy absorption between 254 and 263 nm corresponding to the π–π* transition for the phenyl chromophores with $\varepsilon < 16000\ M^{-1}\ cm^{-1}$. These absorptions are also present in all of the *cis*-Pt-acetylide complexes synthesized with these ligands (Fig. 2.8). The circular dichroism (CD) spectral analysis of the pure ligands *R*-PROPHOS (**219**) and *S,S*-BDPP (**220**) show weak signals at 228 and 243 nm, respectively, while the CD spectra of *S,S*-CHIRAPHOS (**201**), *R,R*-Me-DUPHOS (**221**) and *R,R*-NORPHOS (**222**) contain stronger signals at 229, 317 and 233 nm, respectively. All five ligands show at least one cross-over point in the range of 236–275 nm, in their CD spectra. In all cases the absolute signal intensity of the pure ligand for absorptions >225 nm are less than $\Delta\varepsilon = 11\ M^{-1}\ cm^{-1}$. See Table 2.4 for UV–vis and CD spectral data for the free ligands as well as the chiral *cis*-Pt-acetylide complexes discussed below.

cis-Pt-TIPS-monoyne complexes **215**, **223**, **224**, **225** and **226** all have two absorption maxima in their UV–vis spectra, the lower energy absorption is observed between 293 and 301 nm attributed to the MLCT absorption, and the higher energy absorption is observed between 257 and 268 nm attributed to the π–π* transition for the phenyl chromophores of the ligands (see Figures 2.10–2.14). In the CD spectra, only the *S,S*-CHIRAPHOS and *R,R*-NORPHOS containing compounds **215** and **226** show any remarkable features. Both have a weak low energy band at 291 and 288 nm, respectively, and a strong high energy bisignate band at 254 and 253 nm, respectively. These correspond to the lower and higher energy absorption in the UV–vis spectra. The other

cis-Pt-TIPS-monoyne complexes either do not contain a bisignate band (**225**) or a very weak signal in the higher energy region (**223** and **224**). The *R,R*-NORPHOS containing compound **226** had the most intense signal in the CD spectrum of $\Delta\varepsilon = 28\ M^{-1}\ cm^{-1}$ (240 nm)*, and the *S,S*-CHIRAPHOS containing compound **215** had the second largest signal of $\Delta\varepsilon = 13\ M^{-1}\ cm^{-1}$ (268 nm). For a comparison of CD spectra for all *cis*-Pt-TIPS-acetylide compounds see Figure 2.15.

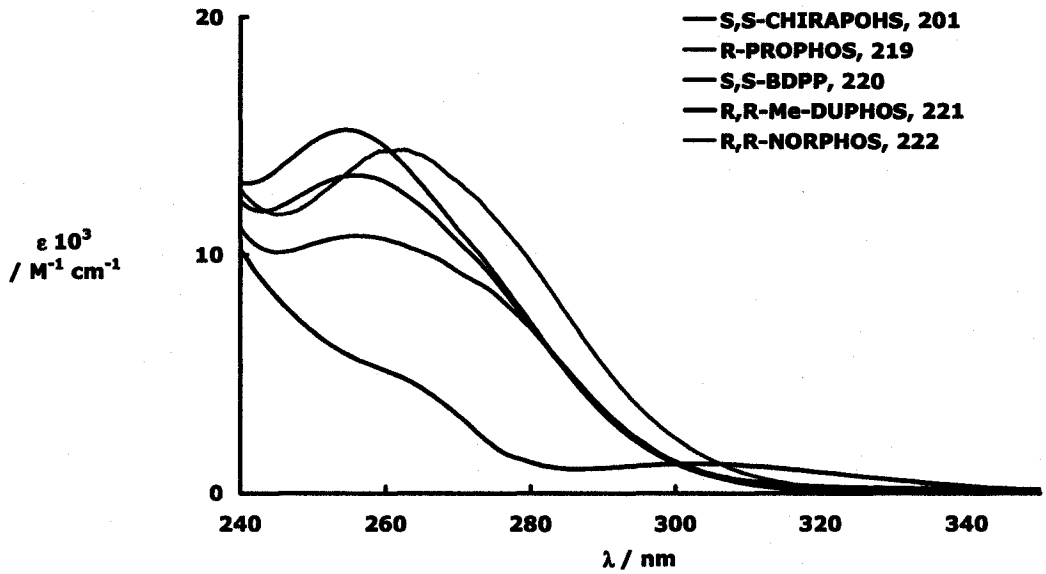

Figure 2.8 UV–vis spectra of chiral diphosphine ligands **201, 219–222** in CH_2Cl_2.

* All Δε indicated are absolute values.

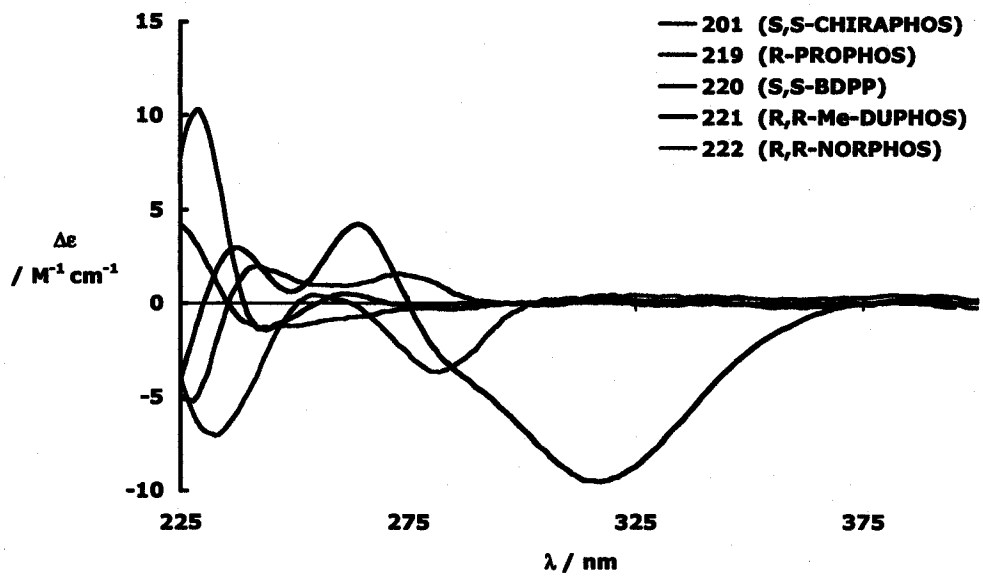

Figure 2.9 CD spectra of chiral diphosphine ligands **201**, **219–222** in CH_2Cl_2.

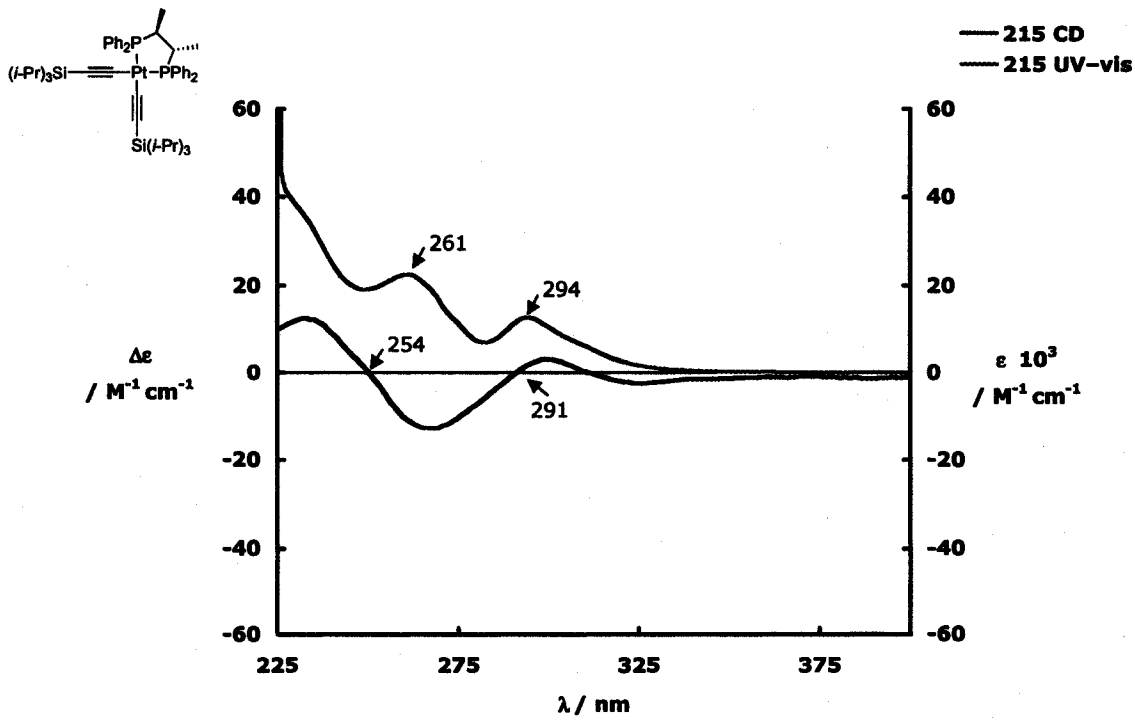

Figure 2.10 CD and UV–vis spectra for **215** in CH_2Cl_2.

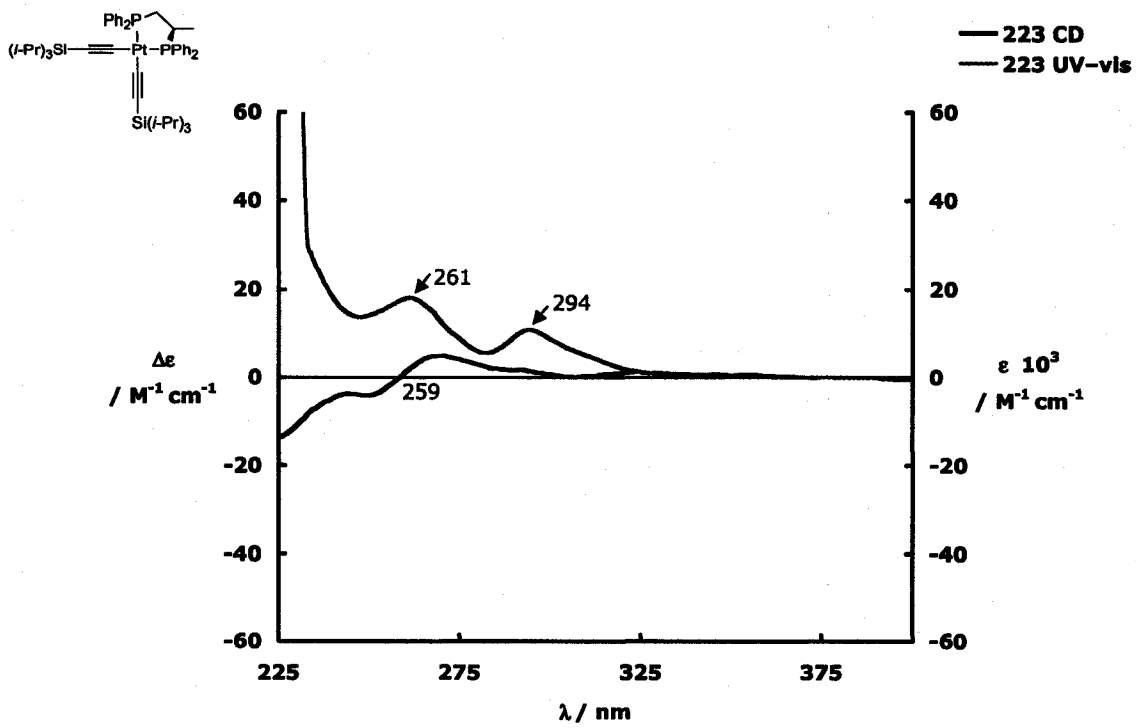

Figure 2.11 CD and UV–vis spectra for **223** in CH_2Cl_2.

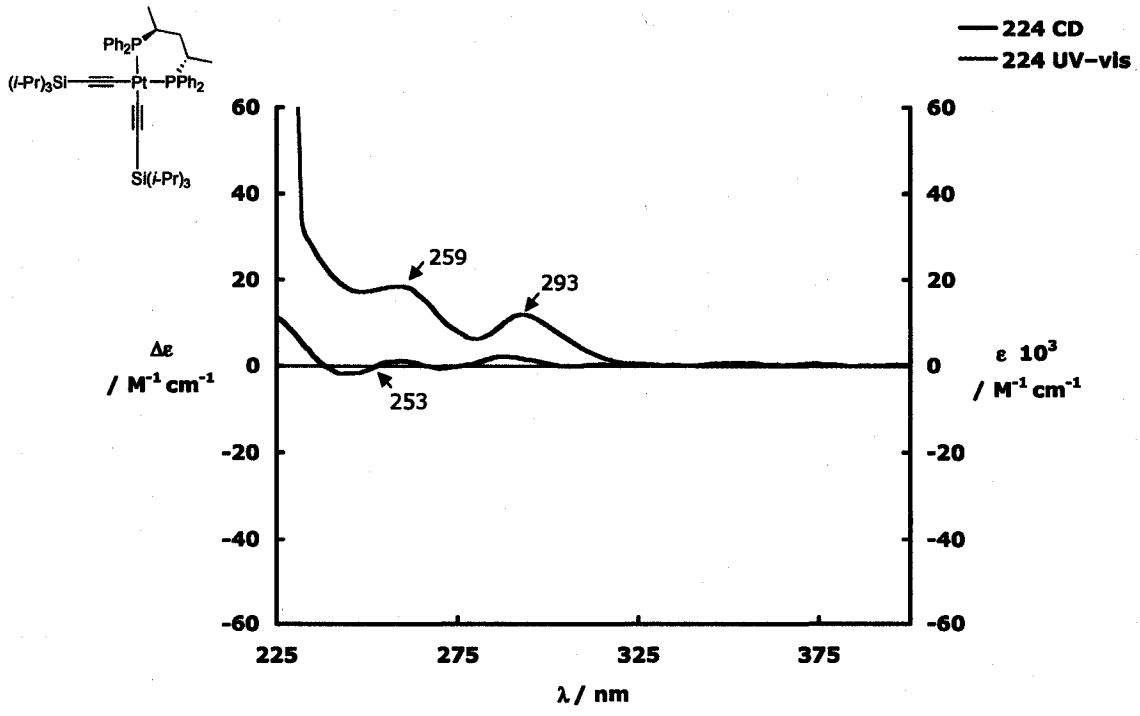

Figure 2.12 CD and UV–vis spectra for **224** in CH_2Cl_2.

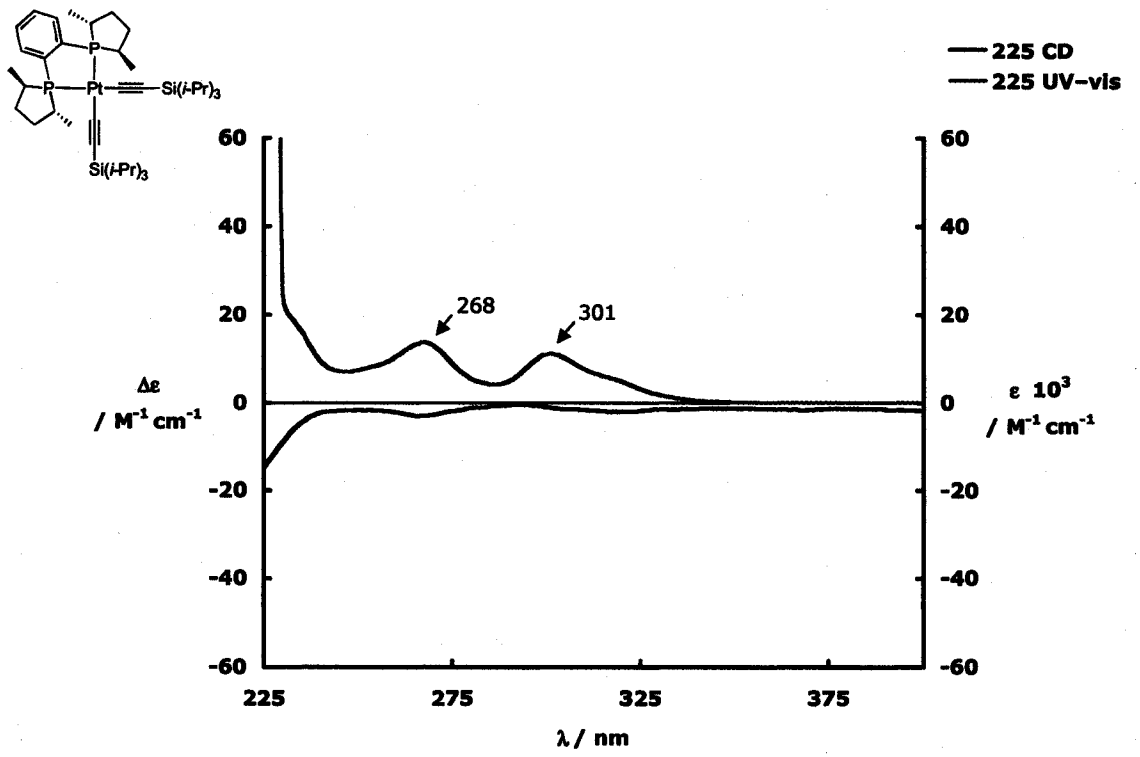

Figure 2.13 CD and UV–vis spectra for **225** in CH_2Cl_2.

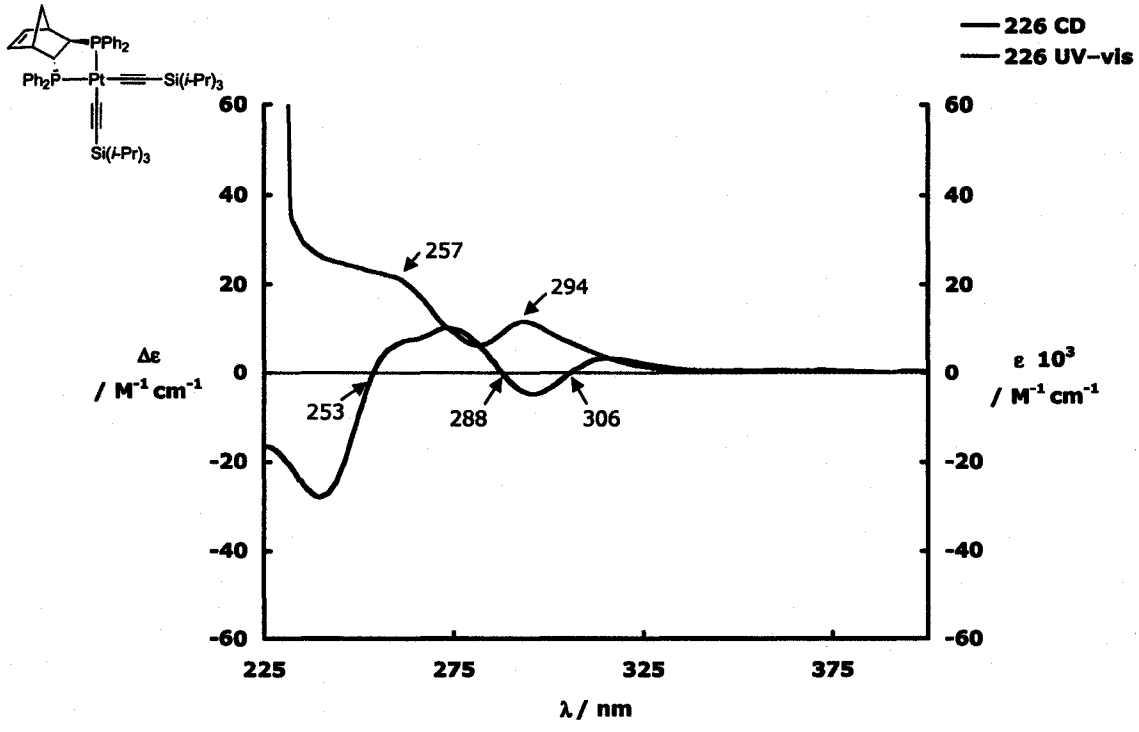

Figure 2.14 CD and UV–vis spectra for **226** in CH_2Cl_2.

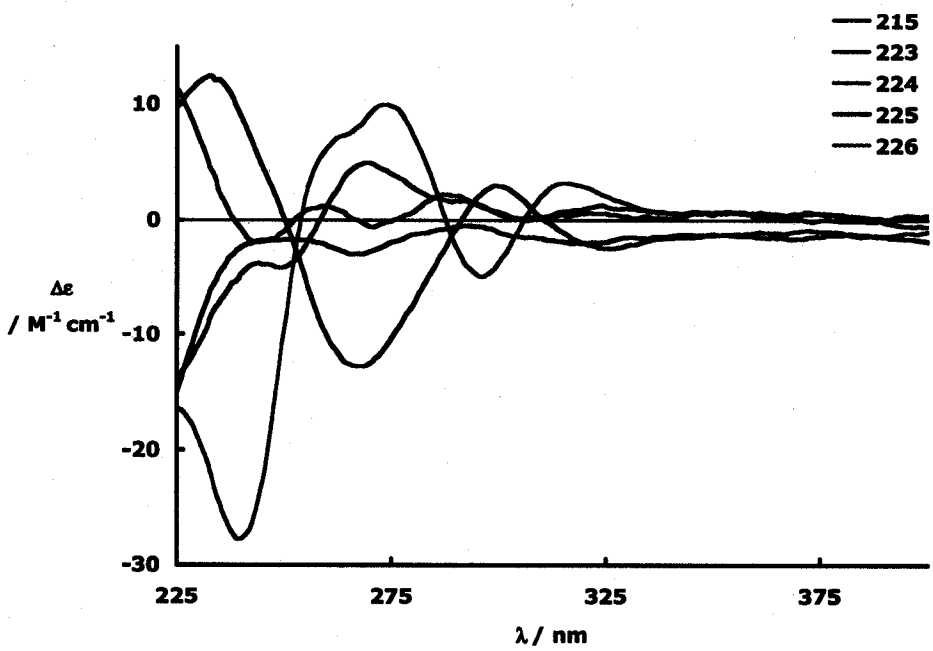

Figure 2.15 CD spectra of chiral *cis*-Pt-TIPS-monoyne complexes **215, 223–226** in CH_2Cl_2.

2.2.5.2 *cis*-Pt-Tolyl-Monoyne Complexes

Similar to the *cis*-Pt-TIPS-monoyne complexes discussed above, *cis*-Pt-tolyl-monoyne complexes **228, 229, 231** and **232** all have two absorption maxima in their UV–vis spectra, the lower energy absorption is observed between 290 and 325 nm attributed to the MLCT absorption, and the higher energy absorption is observed between 257 and 268 nm presumably due to the π–π^* transition for the phenyl chromophores of the ligands (see Figures 2.16–2.19). None of these complexes have a signal in their CD spectra corresponding to the lower energy absorption, while only the *R,R*-Me-DUPHOS containing compound **231** does *not* contain a bisignate band corresponding to the higher energy absorption. These bisignate signals are observed at 252, 252 and 253 nm for compounds **228, 229** and **232**. Again the *R,R*-NORPHOS containing compound **232** had

the strongest signal at $\Delta\varepsilon = 53\ M^{-1}\ cm^{-1}$ (240 nm), followed by *S,S*-CHIRAPHOS, then *R*-PROPHOS containing compounds **228** and **229** with signals of $\Delta\varepsilon = 25$ and $9\ M^{-1}\ cm^{-1}$ (241 and 235 nm, see Figure 2.20 for a comparison of *cis*-Pt-tolyl-acetylide complex CD spectra). Figure 2.21 is included as an example of the relationship between enantiomeric *S,S*-**215** and *R,R*-**215**, where form and intensity are mirrored.

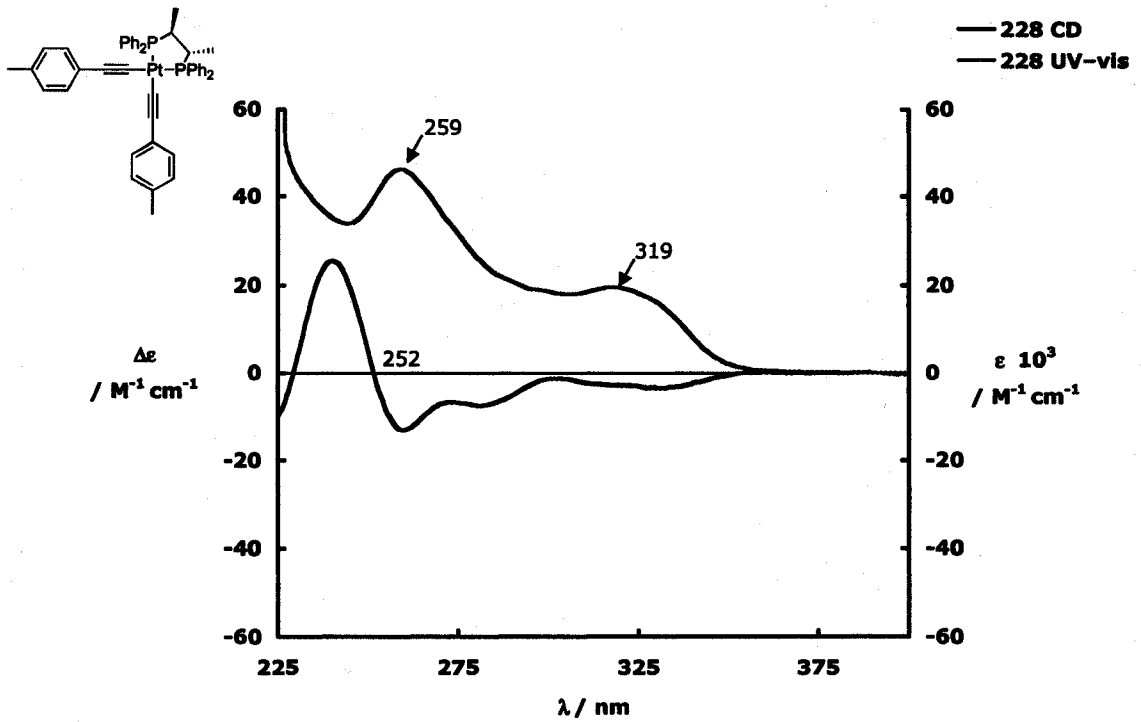

Figure 2.16 CD and UV–vis spectra for **228** in CH_2Cl_2.

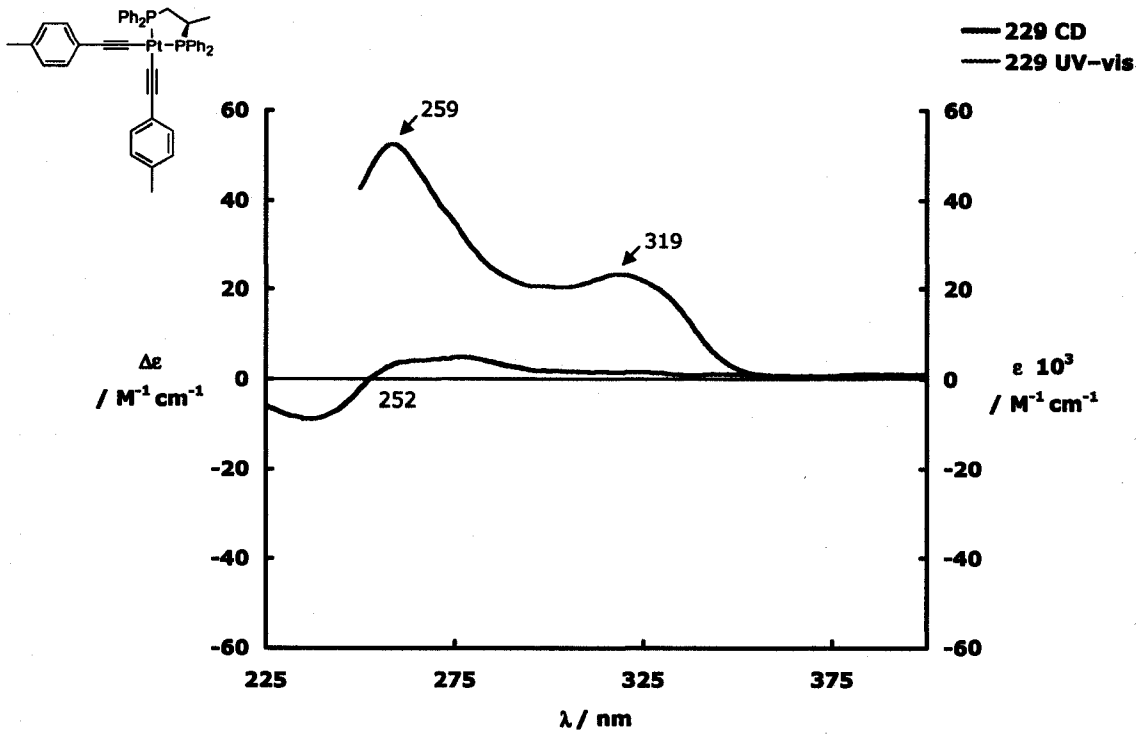

Figure 2.17 CD and UV–vis spectra for **229** in CH_2Cl_2.

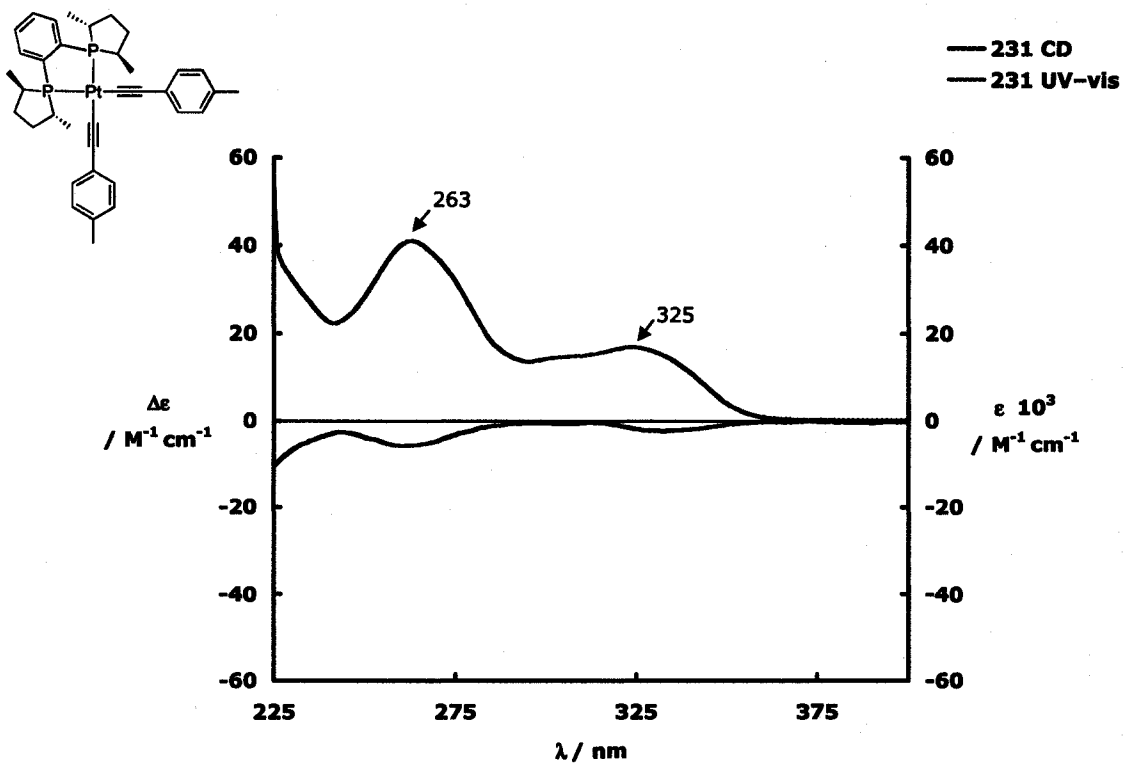

Figure 2.18 CD and UV–vis spectra for **231** in CH_2Cl_2.

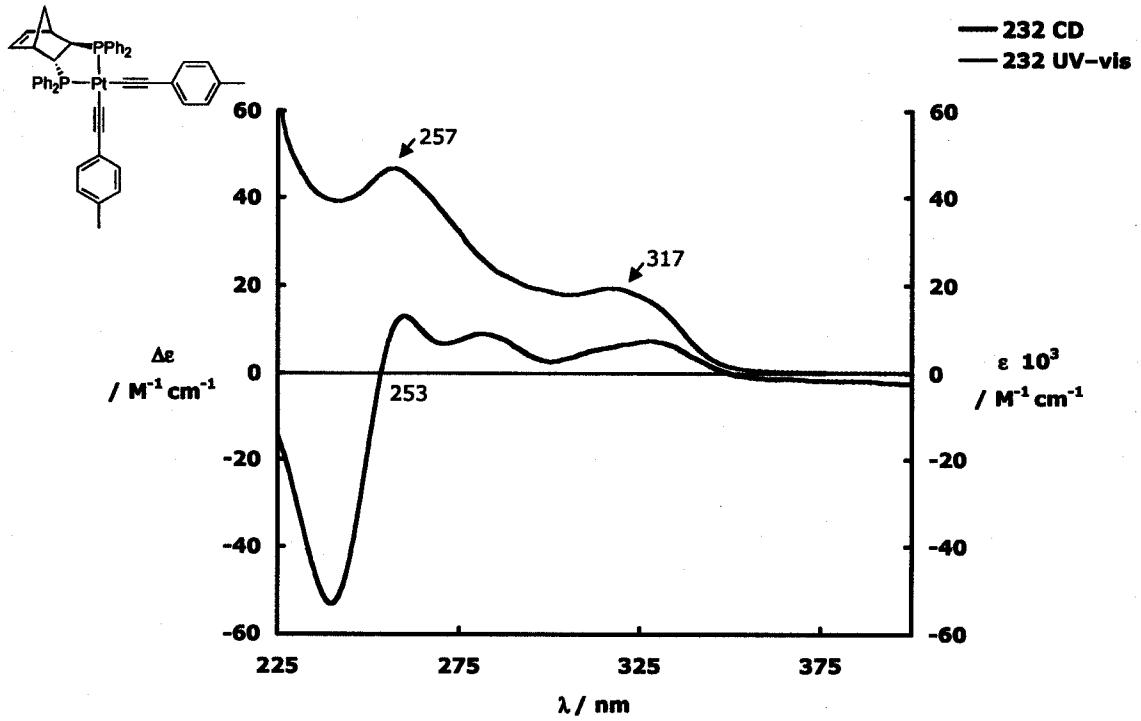

Figure 2.19 CD and UV–vis spectra for **232** in CH_2Cl_2.

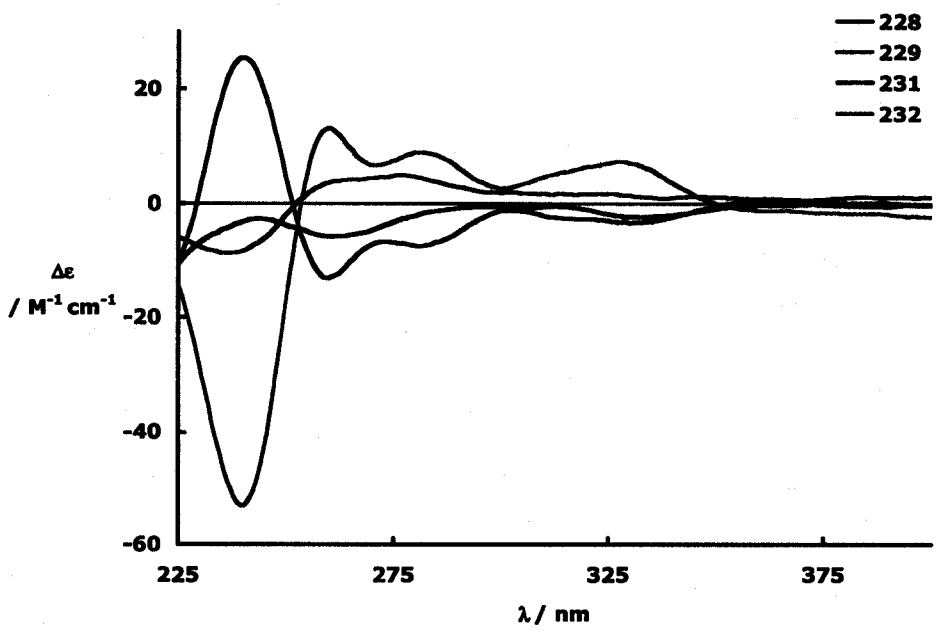

Figure 2.20 CD spectra of chiral *cis*-Pt-tolyl-monoyne complexes **228–232** in CH_2Cl_2.

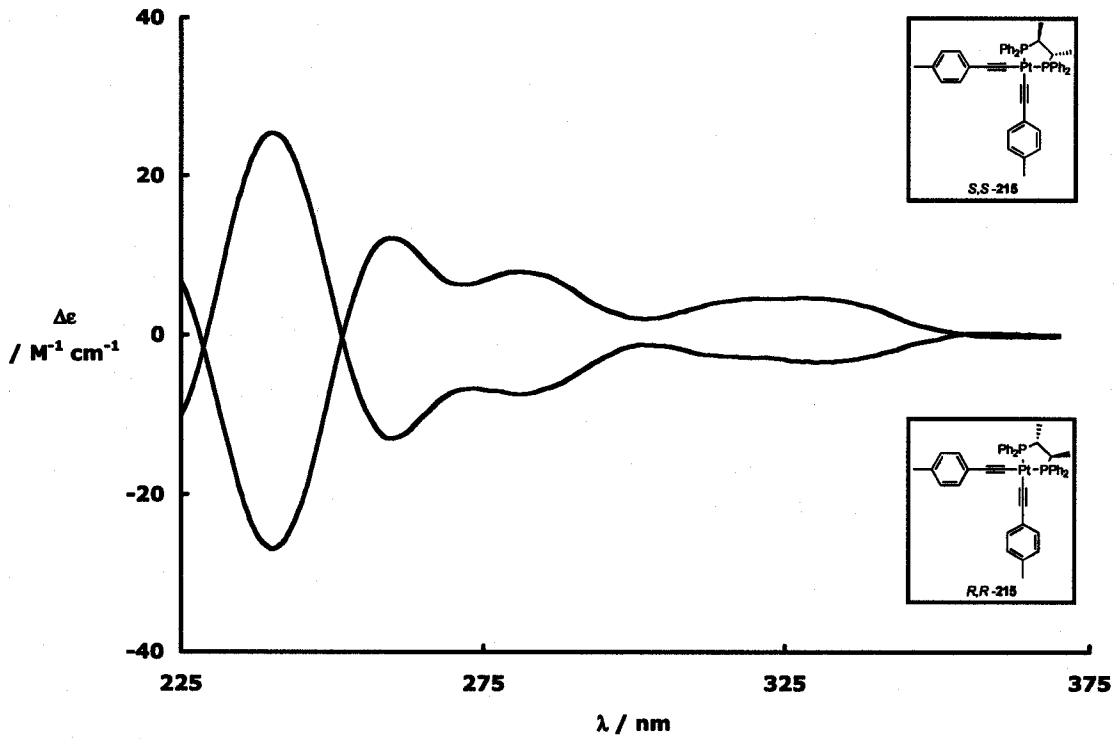

Figure 2.21 CD spectra of enantiomers *S,S*-**215** and *R,R*-**215** in CH_2Cl_2.

2.2.5.3 *cis*-Pt-Diyne and Triyne Complexes

The *cis*-Pt-diyne complexes **234** and **236** both have multiple absorptions in the UV–vis spectra with high energy absorptions between 245 and 263 nm and the lowest energy absorption for both is 337 nm (Figures 2.22 and 2.23). The CD spectra of compounds **234** and **236** have a bisignate signal observed at 257 nm that do not correspond directly to the high energy absorptions in their UV–vis spectra. Of these two compounds the *R,R*-NORPHOS containing compound **236** has the strongest signal of $\Delta\varepsilon = 28\ M^{-1}\ cm^{-1}$ (276 nm) compared to the *S,S*-CHIRAPHOS containing **234** with a moderate signal of $\Delta\varepsilon = 14\ M^{-1}\ cm^{-1}$ (244 nm).

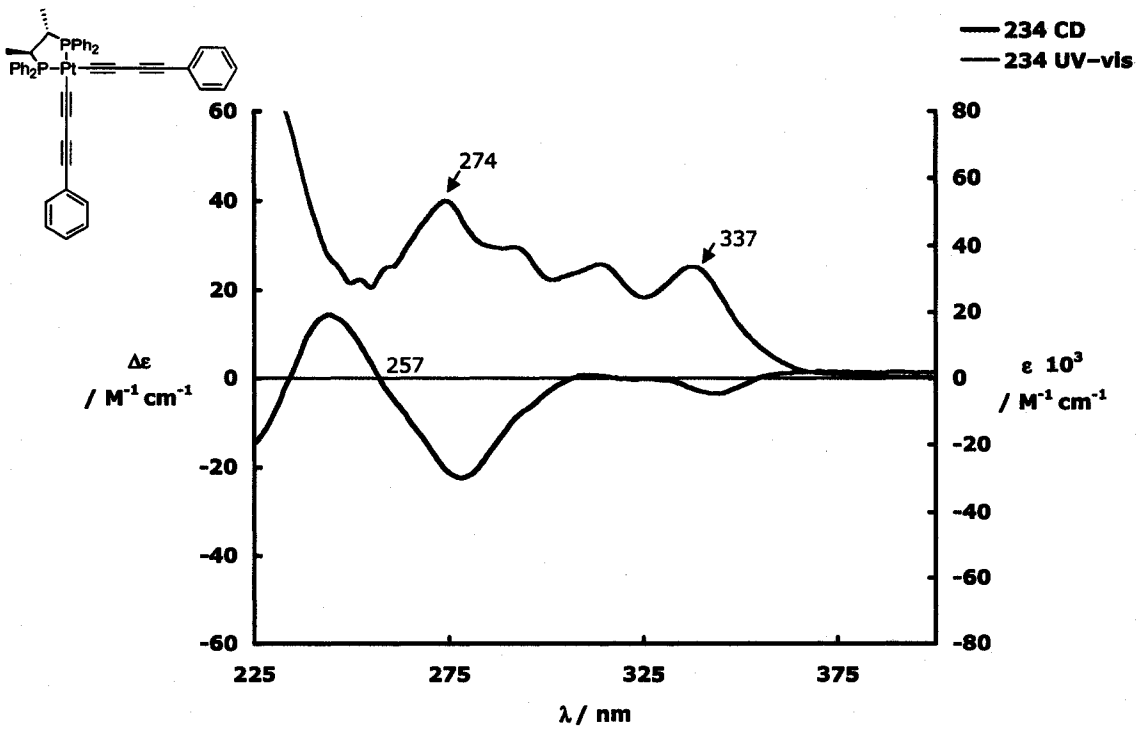

Figure 2.22 CD and UV–vis spectra for **234** in CH_2Cl_2.

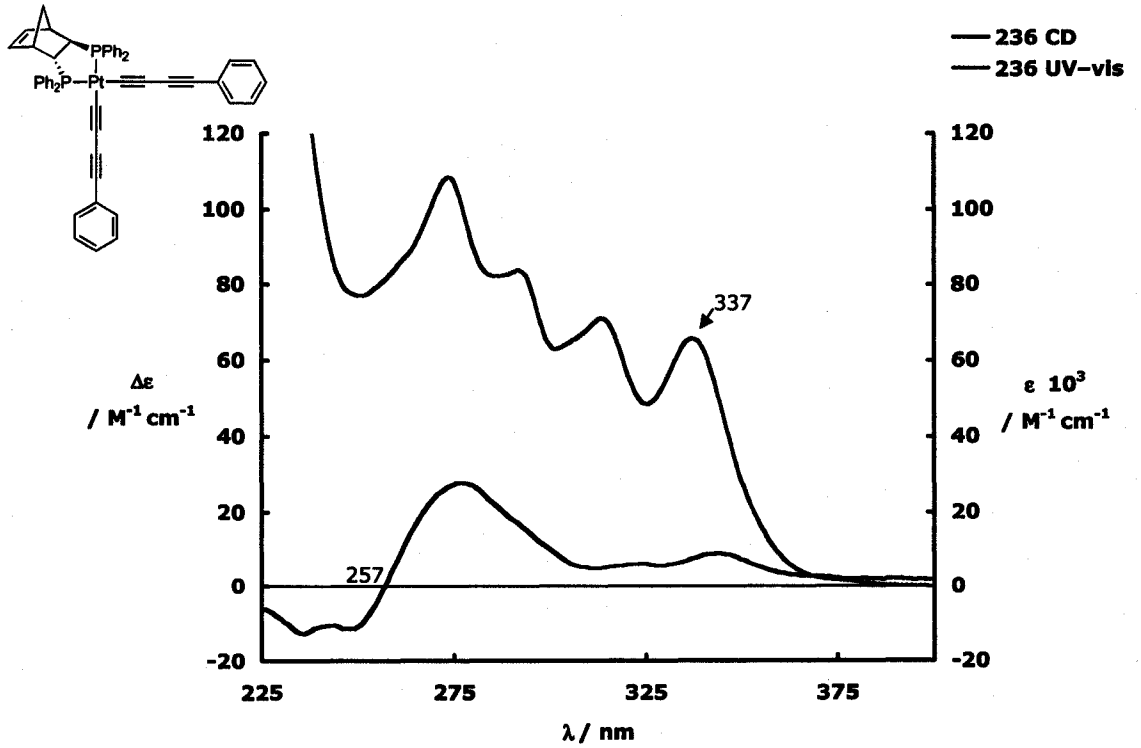

Figure 2.23 CD and UV–vis spectra for **236** in CH_2Cl_2.

The *S,S*-CHIRAPHOS containing *cis*-Pt-triyne complex **238**, as expected, has the highest and lowest energy absorptions (λ = 241 and 359 nm) observed for these acyclic *cis*-Pt-acetylide complexes, due to the extended conjugation of the molecule (Figure 2.24). Three cross-over points are observed in the CD spectrum at 243, 260 and 295 nm, two of which correspond to intense UV–vis absorptions at 241 and 291 nm. The bisignate band at 243 nm has the most intense signal of $\Delta\varepsilon = 27\ M^{-1}\ cm^{-1}$ (234 nm) but unfortunately to date other *cis*-Pt-triyne complexes containing other chiral ligands for comparison have not yet been synthesized.

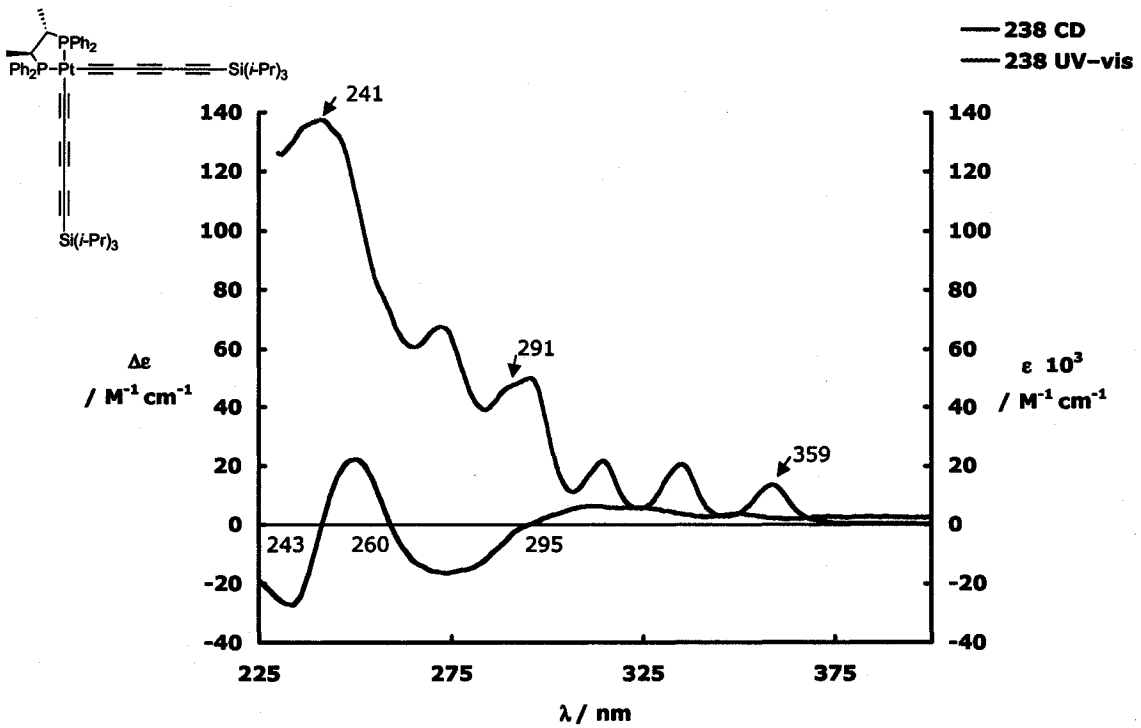

Figure 2.24 CD and UV–vis spectra for **238** in CH_2Cl_2.

Table 2.4 UV–vis and CD spectral data for free ligands and chiral *cis*-Pt-acetylide complexes.

Compound	UV–vis	CD	
	λ (ε) / nm (M^{-1} cm^{-1})	$\lambda_{max\ or\ min}$ ($\Delta\varepsilon$) / nm (M^{-1} cm^{-1})	$\lambda_{(where\ \Delta\varepsilon = 0)}$ / nm
201	258 (11000)	229 (10), 244 (–1.4), 262 (0.5)	239, 255
219	254 (15200)	228 (–5.2), 241 (2.0), 274 (1.6)	236
220	256 (13300)	243 (–1.3)	236
221	263 (4800)	237 (3.0), 264 (4.3), 317 (–9.5)	230, 275
222	262 (14400)	233 (–7.1), 254 (0.4), 282 (–3.7)	250, 263
215	261 (22600), 294 (12500)	233 (12), 268 (–13), 300 (3.0)	254, 291
223	261 (18100), 294 (10900)	251 (–4.0), 270 (5.0), 295 (1.6)	259
224	259 (18400), 293 (12000)	244 (–1.8), 260 (1.1), 290 (2.1)	253
225	268 (13600), 301 (11000)	268 (–3.0)	—
226	257 (22100), 294 (11500)	240 (–28), 262 (7.1), 277 (9.4), 296 (–5.0), 315 (3.2)	253, 288, 306
228	259 (46300), 318 (19500)	241 (25), 260 (–13), 282 (–7.4)	252
229	259 (52700), 319 (23500)	235 (–8.8), 262 (3.8), 277 (4.9)	252
230/239	268 (35600), 290 (21400), 349 (23000)	229 (12), 244 (–0.8), 265 (13), 284 (6.7), 299 (–3.6), 332 (3.7), 357 (–16)	291, 308, 343
231	263 (40900), 325 (16900)	263 (–5.8), 232 (–2.4)	—
232	257 (46300), 317 (18400)	240 (–53), 260 (13), 283 (8.8), 328 (7.3)	253
234	245 (35600), 251 (29500), 274 (53400), 292 (39500), 314 (34600), 337 (33800)	244 (14), 279 (–22), 345 (–3.4)	257
235/240	281 (33000), 302 (26600), 317 (23100), 355 (25200)	235 (12), 262 (13), 278 (16), 318 (–4.4), 364 (–17)	301
236	263 (87800), 273 (108000), 292 (83800), 314 (71000), 337 (65700)	263 (–13), 249 (–11), 276 (28), 324 (6.2), 345 (8.9)	257
238	241 (137000), 257 (78300), 272 (64500), 291 (47400), 295 (49900), 315 (21500), 335 (20600), 359 (13500)	234 (–27), 250 (22), 273 (–16), 311 (6.3)	243, 260, 295

2.2.5.4 Anomalous *S,S*-BDPP Containing Complexes

The electronic properties of *S,S*-BDPP containing compounds **230/239** and **235/240** have not been discussed above because of their presumed dimeric bridged structure (as discussed in Section 2.2.2). Analysis of the UV–vis spectra shows that both compounds posses an additional higher energy absorption, found at 349 and 355 nm, respectively (Figures 2.25 and 2.26). A possible explanation for this is extended conjugation through the Pt due to the possible *trans*-Pt-acetylide configuration, as a result of the bridging diphosphine ligand. Without an X–ray crystallographic analysis the actual structure cannot yet be confirmed.

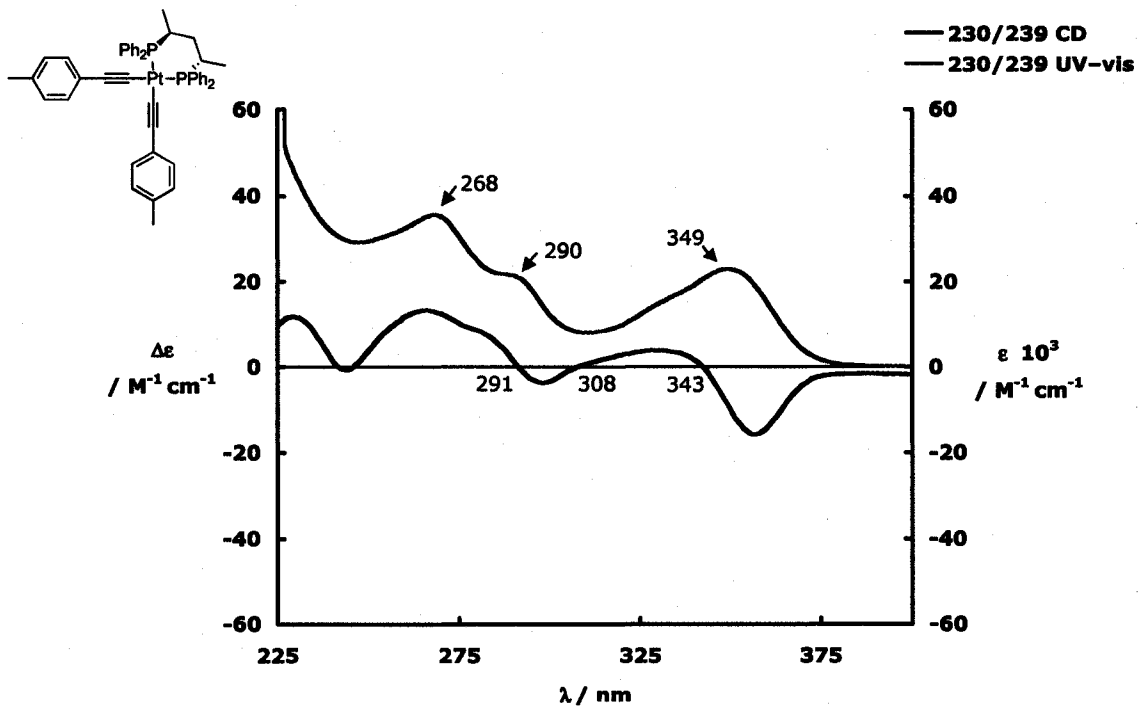

Figure 2.25 CD and UV–vis spectra for **230/239** in CH_2Cl_2.

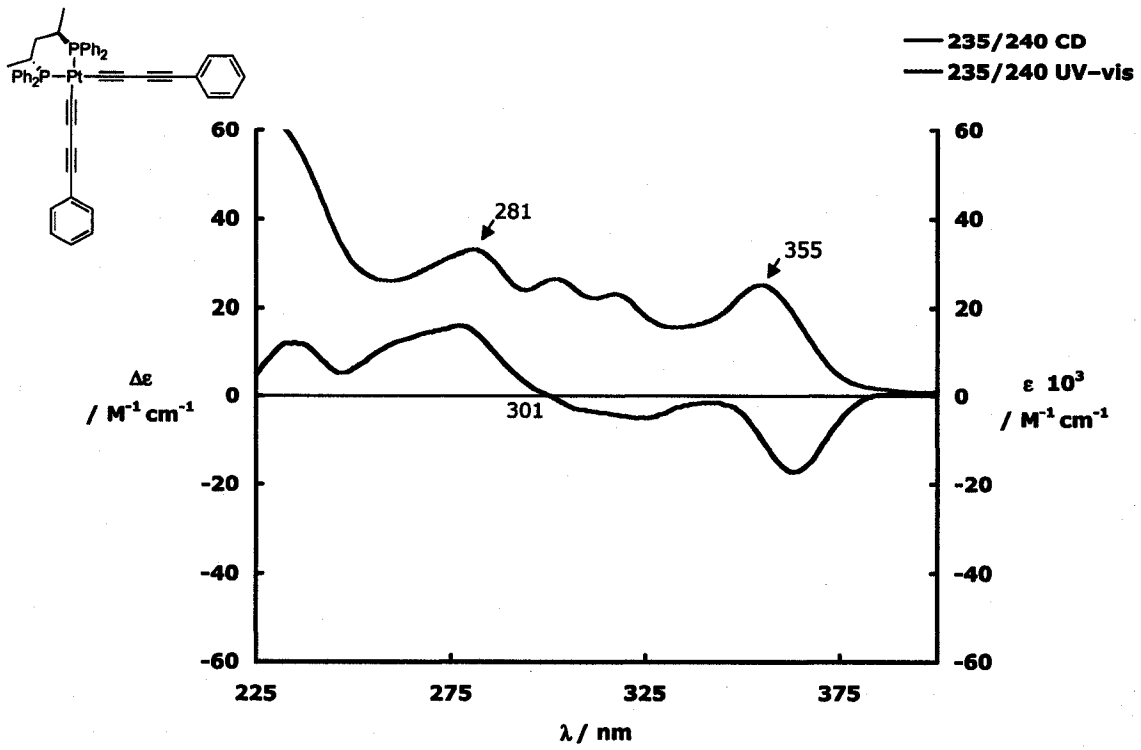

Figure 2.26 CD and UV–vis spectra for **235/240** in CH_2Cl_2.

2.2.5.5 Natural Bite Angle of Chelating Diphosphine Ligands

The most obvious trend to examine in this study is a relationship between the natural bite angle (β_n) of the chelating diphosphine ligands and other observables such as the success of the ligand exchange reactions and spectroscopic properties. Based upon literature values,[29-31] the most representative natural bite angle of each diphosphine ligand was plotted against the $^1J_{P-Pt}$ coupling constant, the ^{31}P chemical shift, and highest energy Δε of the *cis*-Pt-TIPS-monoyne complexes **214**, **215**, **223–226** and *cis*-Pt-tolyl-monoyne complexes **227–232**. These plots did not, however, reveal any meaningful trends. This analysis also did little to explain the reluctance of *R*-BINAP **242** and *R*-SYNPHOS **243** to undergo exchange reactions (see Appendix D for more details).

2.3 CONCLUSIONS

Two complete acyclic chiral *cis*-Pt-monoyne series **215**, **223–226** and **228–232**, as well as acyclic chiral *cis*-Pt-diyne **234**, **236** and *cis*-Pt-triyne **238** complexes have been synthesized using the simple ligand exchange of two PPh_3 ligands for a chelating diphosphine ligand, transforming the achiral *trans*-Pt-acetylide complex precursor into a chiral *cis*-Pt-acetylide complex. All *cis*-Pt-acetylide complexes were formed in good to excellent yield as stable solids and their circular dichroism properties were studied. The magnitude of $\Delta\varepsilon$ in the CD spectra, corresponding to the transfer of chirality from the chiral ligand to the conjugated system, was highly dependant on the chiral ligand present in the complex, ranging from zero to 53 M^{-1} cm^{-1}. Consistently, *R,R*-NORPHOS **222** was most effective in chirality transfer to the molecules, followed by *S,S*-CHIRAPHOS **201**. Ligands *R*-PROPHOS **219** and *R,R*-Me-DUPHOS **221** provided little or no chirality transfer to the chromophores studied, as evaluated by CD spectroscopy. Unexpectedly, *S,S*-BDPP **220** appeared to form dimeric species when reacted with the relatively planar *trans*-Pt-tolyl-monoyne complex **216** and *trans*-Pt-phenyl-diyne complex **233**. Overall, these model compounds have provided a tremendous amount of information pertaining to the scope of ligand exchange and efficiency of chirality transfer which can now be applied to macrocyclic compounds with desirable supramolecular properties.

2.4 REFERENCES

1. Mukherjee, P. S.; Das, N.; Kryschenko, Y. K.; Arif, A. M.; Stang, P. J. *J. Am. Chem. Soc.* **2004**, *126*, 2464-2473.
2. You, C.-C.; Würthner, F. *J. Am. Chem. Soc.* **2003**, *125*, 9716-9725.
3. Yamamoto, T.; Arif, A. M.; Stang, P. J. *J. Am. Chem. Soc.* **2003**, *125*, 12309-12317.
4. Forniés, J.; Gómez, J.; Lalinde, E.; Moreno, M. T. *Chem. Eur. J.* **2004**, *10*, 888-898.
5. Ferrer, M.; Rodriguez, L.; Rossell, O. *J. Organomet. Chem.* **2003**, *681*, 158-166.
6. Mukherjee, P. S.; Das, N.; Stang, P. J. *J. Org. Chem.* **2004**, *69*, 3526-3529.
7. Su, C.-Y.; Cai, Y.-P.; Chen, C.-L.; Smith, M. D.; Kaim, W.; zur Loye, H.-C. *J. Am. Chem. Soc.* **2003**, *125*, 8595-8613.
8. Chand, D. K.; Fujita, M.; Biradha, K.; Sakamoto, S.; Yamaguchi, K. *Dalton Trans.* **2003**, 2750-2756.
9. Kumazawa, K.; Biradha, K.; Kusukawa, T.; Okano, T.; Fujita, M. *Angew. Chem. Int. Ed.* **2003**, *42*, 3909-3913.
10. Müller, I. M.; Spillmann, S.; Franck, H.; Pietschnig, R. *Chem. Eur. J.* **2004**, *10*, 2207-2213.
11. Baldini, L.; Ballester, P.; Casnati, A.; Gomila, R. M.; Hunter, C. A.; Sansone, F.; Ungaro, R. *J. Am. Chem. Soc.* **2003**, *125*, 14181-14189.
12. Le Bouder, T.; Maury, O.; Bondon, A.; Costuas, K.; Amouyal, E.; Ledoux, I.; Zyss, J.; Le Bozec, H. *J. Am. Chem. Soc.* **2003**, *125*, 12284-12299.

13. Rao, C. N. R.; Natarajan, S.; Vaidhyanathan, R. *Angew. Chem. Int. Ed.* **2004**, *43*, 1466-1496.

14. Mamula, O.; von Zelewsky, A. *Coord. Chem. Rev.* **2003**, *242*, 87-95.

15. Telfer, S. G.; Kuroda, R. *Coord. Chem. Rev.* **2003**, *242*, 33-46.

16. Campbell, K.; Tykwinski, R. R. In *Carbon-Rich Compounds*; Haley, M. M.; Tykwinski, R. R.; Eds.; Wiley-VCH: Weinheim, 2006; pp 229-294.

17. Lee, S. J.; Hu, A. G.; Lin, W. B. *J. Am. Chem. Soc.* **2002**, *124*, 12948-12949.

18. Jiang, H.; Hu, A. G.; Lin, W. B. *Chem. Commun.* **2003**, 96-97.

19. Lin, J.; Zhang, H.-C.; Pu, L. *Org. Lett.* **2002**, *4*, 3297-3300.

20. Lee, S. J.; Lin, W. B. *J. Am. Chem. Soc.* **2002**, *124*, 4554-4555.

21. Müller, C.; Whiteford, J. A.; Stang, P. J. *J. Am. Chem. Soc.* **1998**, *120*, 9827-9837.

22. Campbell, K.; Johnson II, C. A.; McDonald, R.; Ferguson, M. J.; Haley, M. M.; Tykwinski, R. R. *Angew. Chem. Int. Ed.* **2004**, *43*, 5967-5971.

23. Campbell, K. Ph.D. thesis, University of Alberta, Edmonton, AB, 2004.

24. Campbell, K.; McDonald, R.; Ferguson, M. J.; Tykwinski, R. R. *J. Organomet. Chem.* **2003**, *683*, 379-387.

25. Whiteford, J. A.; Lu, C. V.; Stang, P. J. *J. Am. Chem. Soc.* **1997**, *119*, 2524-2533.

26. Sonogashira, K.; Fujikura, Y.; Yatake, T.; Toyoshima, N.; Takahashi, S.; Hagihara, N. *J. Organomet. Chem.* **1978**, *145*, 101-108.

27. Sonogashira, K.; Yatake, T.; Tohda, Y.; Takahashi, S.; Hagihara, N. *J. Chem. Soc., Chem. Commun.* **1977**, 291-292.

28. Luu, T. Ph. D. thesis, University of Alberta, Edmonton, AB, 2007.

29. van Leeuwen, P.; Kamer, P. C. J.; Reek, J. N. H.; Dierkes, P. *Chem. Rev.* **2000**, *100*, 2741-2769.

30. Dierkes, P.; van Leeuwen, P. *J. Chem. Soc., Dalton Trans.* **1999**, 1519-1529.

31. del Rio, I.; de Lange, W. G. J.; van Leeuwen, P.; Claver, C. *J. Chem. Soc., Dalton Trans.* **2001**, 1293-1300.

CHAPTER 3 PLATINACYCLE SYNTHESES

3.1 INTRODUCTION

As discussed in the previous chapter, ligand exchange with two PPh_3 ligands on a Pt(II) acetylide center for a chelating diphosphine ligand, easily converts the coordination geometry about platinum from *trans* to *cis* for acyclic compounds. Thus, the next logical step was to extend this study to cyclic molecules, platinacycles. The introductory discussion of acetylenic macrocycles in Chapter 1 has highlighted the importance of this class of macrocycle in supramolecular chemistry. This would also be a good opportunity to use chiral diphosphine ligand exchange as a simple and cost effective method for introducing chirality into a macrocyclic complex. Therefore, my project turned to the synthesis of macrocycle **300** (Figure 3.1), then to synthesize a series chiral macrocycles using chiral ligands (**201**, **219–222**), and finally to study their optical properties using CD spectroscopy. CD spectroscopy ideally would provide some insight into the magnitude of chiral induction provided by the chiral ligand, and subsequently a comparison between the macrocyclic and acyclic series could be accomplished. Platinacycle **300** was designed based upon established chemistry in the Tykwinski group[1-4] and was chosen based on its potential for use in asymmetric catalysis after ligand exchange. Lin and coworkers have reported chiral platinacycles with internal hydroxyl groups that were successfully used for the asymmetric catalysis of the reduction of aldehydes to secondary alcohols.[5-8] Therefore, incorporation of methoxy groups into the targeted macrocycle **300**, was ultimately expected to afford chiral derivatives that could be tested as hosts for asymmetric catalysis.

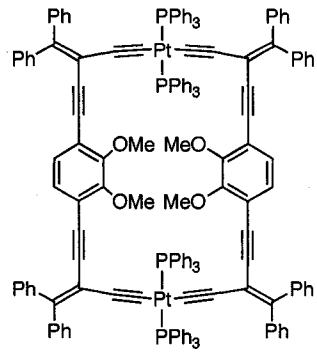

300

Figure 3.1 Targeted platinacycle **300**.

3.2 Results and Discussion

3.2.1 Synthesis of Macrocycle Building Blocks

The synthesis of the macrocycle precursor **301** (see Scheme 3.3) began with veratrole **302**, as described by the optimized procedure followed by Swager and Zhu (Scheme 3.1).[9,10] A two-step sequence of monolithiation and quenching with trimethylsilyl chloride (TMSCl) to **303**, was reported to be higher yielding and procedurally easier than a single-step double lithiation of **302**.[11] First, veratrole **302** was added to a solution of dry hexanes and TMEDA and stirred at room temperature for 30 minutes. Then, BuLi was slowly added and the mixture allowed to stir overnight. After cooling the mixture to –78 °C, TMSCl was slowly added. Once the reaction mixture was warmed to room temperature, the reaction was quenched with water. Purification via silica gel chromatography yielded **304** as a colourless oil, which was subjected to the second lithiation step, which followed the same course as the first. Compound **303** was initially isolated as a colourless oil after silica gel chromatography but eventually solidified.

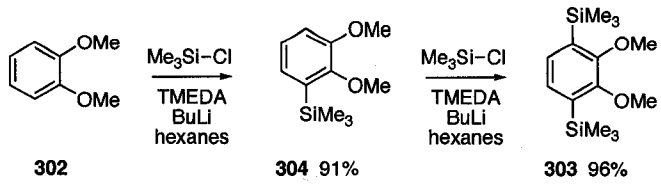

302 304 91% 303 96%

Scheme 3.1 Synthesis of 1,4-bis-(trimethylsilyl)-2,3-dimethoxybenzene **303**.

Iodination[10] of **303** was performed in dichloromethane at 0 °C with iodine monochloride, resulting in the diiodide **305** as a yellow oil (observed to solidify at 4 °C) in good yield after purification by silica gel chromatography (Scheme 3.2). Diiodide **305** was then coupled to TMS–acetylene under modified Sonogashira conditions as described by Swager and Zhu, using $Pd(PPh_3)_4$ as a catalyst and CuI as a cocatalyst in a solution of degassed toluene and Et_2NH for 3 days at 65 °C. The resulting diacetylide **306** was isolated as a yellow oil in good yield after purification via silica gel chromatography.

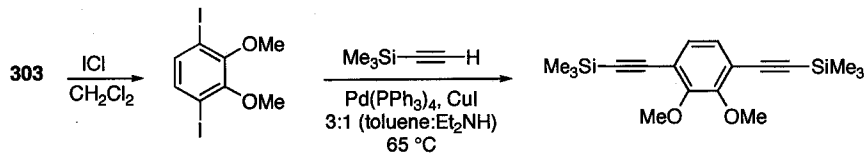

305 67% 306 51%

Scheme 3.2 Synthesis of bis(TMS–acetylene) **306**.

Diacetylene **306** was desilylated using TBAF in wet THF, and then cross-coupled to vinyl triflate **307**,[12] using $Pd(PPh_3)_4$ and CuI in the presence of Et_2NH in THF at 55 °C for 3 days (Scheme 3.3). The resulting macrocyclic precursor **301** was isolated as a bright yellow solid and purified by either silica gel column chromatography or by precipitation from a minimal amount of CH_2Cl_2 by the addition of hexanes. Compound **301** was easily prepared multiple times, usually on a 500 mg scale, with yields close to 60%.

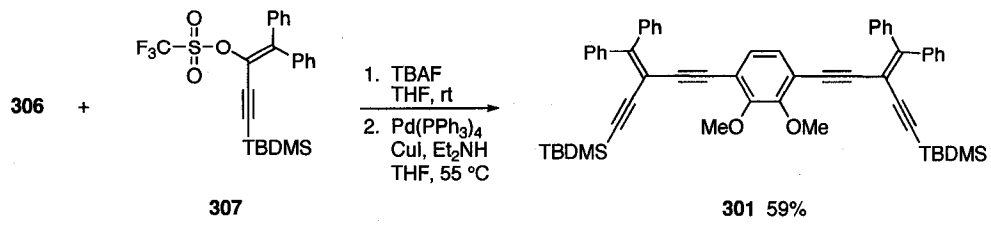

Scheme 3.3 Synthesis of macrocyclic precursor **301**.

3.2.2 Macrocyclization

The coupling of compound **301** with *cis*-$PtCl_2(PPh_3)_2$ to form the desired macrocycle **300** was attempted multiple times and unfortunately led to only asmall amount (9 mg) of the product isolated. A typical reaction (Scheme 3.4) began with the terminal alkyne which was formed by reaction of **301** with TBAF, following work-up, the crude product was added to a degassed solution of Et_2NH (300 mL). Then, after an additional 15–30 min of degassing, *cis*-$PtCl_2(PPh_3)_2$ was added, followed by a catalytic amount of CuI. The flask was then sealed under nitrogen and heated to 55 °C. The solution was too dilute to monitor directly by TLC, making it difficult to determine the end point of the reaction. Therefore, after 4–5 days, the reaction was cooled to room temperature and a 1:1 mixture of Et_2O and CH_2Cl_2 (100 mL) was added, this solution was then washed with water and plenty of saturated aqueous NH_4Cl to remove all of the Et_2NH. The solvent was then removed with no heat (from previous experience decomposition occurs at high temperatures[13]) until 1–2 mL of a dark brown solution remained. TLC analysis of the resulting solution showed multiple spots, therefore isolation by chromatography was not deemed a reasonable option. It had been determined that the best technique to isolate other Pt-acetylide complexes pure was to use hexanes or Et_2O to cause precipitation from the reaction solution. This approach was

attempted with macrocycle **300**, and typically a small amount of fine precipitate was observed. Isolation by filtration however resulted in nominal amounts of yellow precipitate.

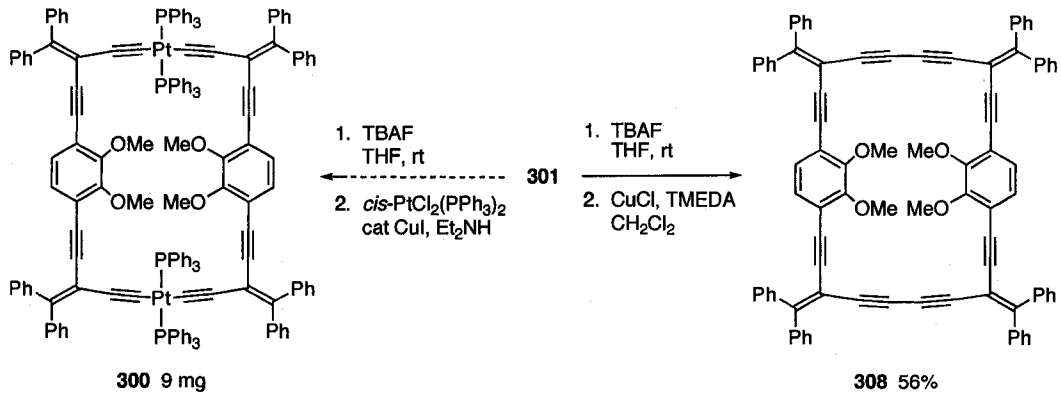

Scheme 3.4 Synthesis of macrocycles **300** and **308**.

In an effort to optimize the macrocyclization conditions further reactions were preformed with the following conditions: a) 250 mL of Et_2NH and a catalytic amount of CuCl at 55 °C, b) 250 mL of Et_2NH and a catalytic amount of CuCl at room temperature, c) 50 mL of Et_2NH and a catalytic amount of CuCl at 55 °C, d) 50 mL of CH_2Cl_2, 5 mL of Et_2NH and a catalytic amount of CuI at 55 °C, e) 250 mL of CH_2Cl_2, 5 mL of Et_2NH and a catalytic amount of CuI at 55 °C. For all trials, removal of the organic solvent was always preformed without heating and the solution was never allowed to go to dryness. In all cases, similar results were observed, either a brownish-orange solid was precipitated or a bright yellow solid was observed in solution but was too fine to be isolated. Only 9 mg of **300** was isolated and used for characterization, and interestingly this was filtered from the organic/aqueous interface during the work-up of one of the reactions. The ^1H NMR spectrum showed the expected methoxy proton signal at 3.57 ppm and signals that integrated for 104 protons in the aromatic region. The ^{31}P NMR

spectrum also looked promising with a pseudo–t observed at 19 ppm with a $^{1}J_{P-Pt}$ coupling constant of 2634 Hz, indicating a *trans*-Pt-acetylide configuration. This evidence in conjunction with a signal at *m/z* 2616.8 in the MALDI spectrum (M^{+}) proved that platinacycle **300** was successfully synthesized. Unfortunately, a useful ^{13}C NMR spectrum was not obtained due to insufficient solubility and lack of sample.

Using a crude sample of the platinacycle **300** dissolved in $CDCl_3$ in an NMR tube, *S,S*-CHIRAPHOS **201** was added and the reaction was monitored. After less than 30 minutes the *trans*-Pt-acetylide pseudo–t signal at 19 ppm in the ^{31}P NMR spectrum disappeared and a *cis*-Pt-acetylide signal appeared at 47 ppm with a $^{1}J_{P-Pt}$ coupling constant of 2290 Hz, typical for a *cis*-Pt-acetylide configuration. In addition to the clean and quick conversion of the *trans*- to *cis*-Pt-acetylide macrocycle, the release of free PPh_3 at –4 ppm was also observed. This reaction indicates that if macrocycle **300** could be isolated in substantial quantities, ligand exchange reactions with chelating diphosphine ligands could easily be performed en route to its potential use in asymmetric catalysis. Due to time constraints and scarcity of starting materials, however, optimization of the synthesis and isolation of **300** was discontinued and other options were explored, which are discussed below.

With the discouraging results in the synthesis of platinacycle **300**, the formation of macrocycle **308** through a Hay homocoupling reaction was attempted (Scheme 3.4). After desilylation of the precursor **301** with TBAF in THF and aqueous work-up, the terminal alkyne was added to 150 mL of dry CH_2Cl_2 without further purification. A prepared mixture of CuCl, TMEDA in CH_2Cl_2 was then slowly added and the resulting solution was allowed to stir at room temperature for 3 days. Subsequent to work-up, the

volume of the organic layer was reduced to approximately 5 mL, and 2–3 mL of acetone was added. This induced precipitation of a bright yellow solid that was filtered to give **308** in 56% yield. This product could however only be characterized by ^{1}H NMR spectroscopy, where the expected methoxy protons appear at 3.79 ppm and signals in the aromatic region integrate for 48 protons. Additional characterization was prevented by the low solubility of macrocycle **308** (only minimal solubility was observed in CH_2Cl_2 and $CHCl_3$). On multiple occasions macrocycle **308** was observed to slowly precipitate out of a CD_2Cl_2 solution in the NMR tube as a fluffy, yellow solid. To further purify the compound this solid was filtered and dried. This was repeated twice but the purified solid was even less soluble making characterization more difficult. Mass spectrometry was also unsuccessful for the characterization of this compound, using numerous solvents, heat and sonication in an attempt to dissolve the compound.

3.2.3 Other Macrocycles

With the problems associated with the isolation of the targeted macrocycle **300**, a synthesis of the redesigned macrocycle **309**, was attempted using compound **306**. This macrocycle has an increased interior size when compared to **300**, therefore if the problems encountered in the synthesis of **300** were due to the steric demands of the interior methoxy groups, this should help. Instead of cross-coupling the bis(TMS–acetylide) **306** with the vinyl triflate **307**, 3-bromoiodobenzene **310** was used under the same Sonogashira conditions (Scheme 3.5). This successfully led to dibromide **311** as a bright yellow solid after isolation by precipitation from a CH_2Cl_2 solution by the addition of Et_2O and hexanes. Unfortunately, the coupling of TMS–acetylene to the dibromide **311** did not proceed as easily as the other Pd catalyzed reactions described, for unknown

reasons. The first attempt used excess TMS–acetylene, catalytic $Pd(PPh_3)_4$ and CuI in the presence of Et_2NH in dry THF at 55 °C for 5 days, resulting in **312** in 38% yield, isolated as a brown oil. In an attempt to increase the yield, a second reaction was preformed using Et_3N and a reduced reaction time of 3 days. This unfortunately decreased the yield to 8%. Using the same conditions as the first trial but changing the catalyst to $PdCl_2(PPh_3)_2$ yielded **312** in only 20%. Reasoning that heat may be the problem, a reaction using the conditions of the first trial was run again, but at room temperature for 7 days, but again a low yield was obtained, 28%. Decreasing the reaction time to 1 day, and using Et_3N and $PdCl_2(PPh_3)_2$ at room temperature resulted in only the starting dibromide **311** being recovered. This reaction would have been further optimized if not for time constraints, and unfortunately only an ^1H NMR spectrum of pure **312** was obtained.

The macrocyclization to form **309** showed promising initial results, based upon one reaction using the small amount of **312** available. After desilylation of **312** with TBAF in wet THF, the terminal alkyne was added to a degassed solution of *cis*-$PtCl_2(PPh_3)_2$ and catalytic CuI under high dilution in Et_2NH. A small amount of macrocycle was isolated following work-up by precipitation from a CH_2Cl_2 solution by the addition of Et_2O and a crude ^{31}P NMR spectrum was obtained showing a pseudo–t at 20 ppm with a $^1J_{P-Pt}$ coupling constant of 2646 Hz. Even though macrocycle **309** could not be fully characterized, this macrocyclization appeared to work better than the original targeted macrocycle **300**. *S,S*-CHIRAPHOS **201** was added to the solution of **309** in the NMR tube and the pseudo–t at 20 ppm disappeared within 30 minutes of shaking and a new pseudo–t appeared at 47 ppm with a $^1J_{P-Pt}$ coupling constant of 2287 Hz along with

the free PPh_3 signal at –4 ppm. These observations are consistent with ligand exchange to form the *cis*-Pt-acetylide macrocycle from the *trans*-Pt-acetylide macrocycle. Isolation of the *cis*-Pt-acetylide macrocycle was not done since the crude ^{31}P NMR spectrum contained multiple impurity peaks. Additional investigation is suggested for this macrocycle.

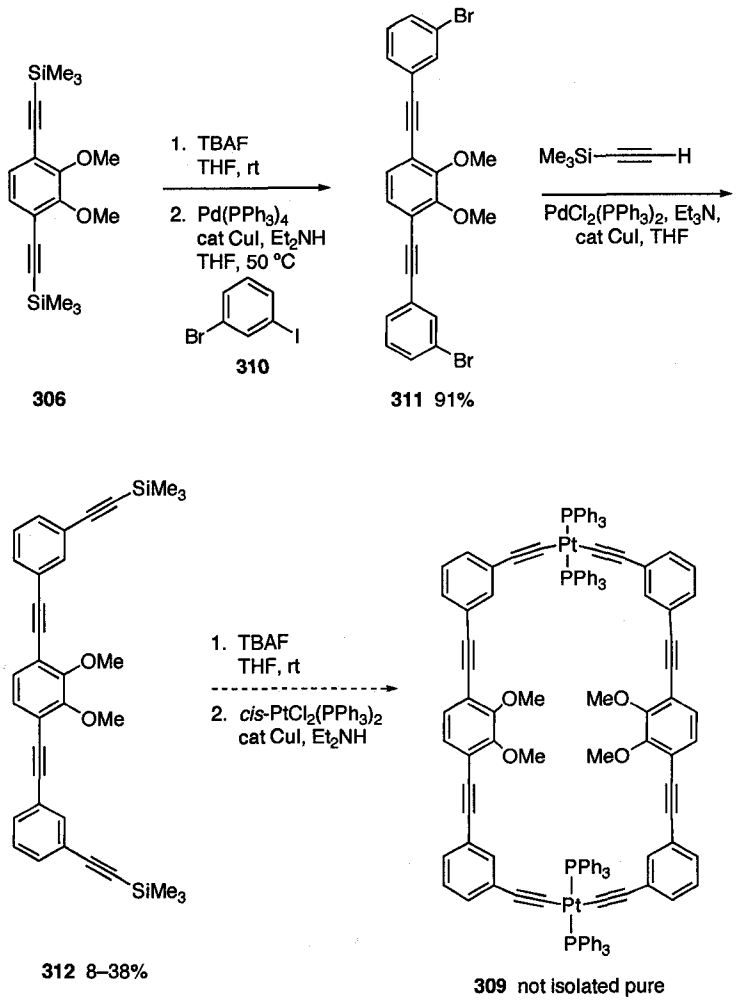

Scheme 3.5 Attempted synthesis of macrocycle **309**.

The next macrocycle synthesis attempt again used starting materials that were readily available. Compound **301** was cross-coupled a second time with vinyl triflate **307**, to form the macrocycle precursor **313** (Scheme 3.6), in moderate yield as a bright yellow

solid after isolation by silica gel chromatography. Compound **313** was partially characterized by ^{1}H NMR and IR spectroscopies and then carried forward. After desilylation of **313** with TBAF in wet THF, formation of the Pt-acetylide macrocycle **314** using typical conditions resulted in the isolation of two unknown compounds (19% and 15%). The ^{31}P NMR spectrum for the first unknown showed only a singlet at 44 ppm while the second unknown showed no signals in the ^{31}P NMR spectrum. The ^{1}H NMR spectra of both unknowns did not show the presence of the methoxy hydrogens at approximately 4 ppm. This synthesis was performed only once and further investigation into the identity of the unknowns was not carried out since they were not the targeted product.

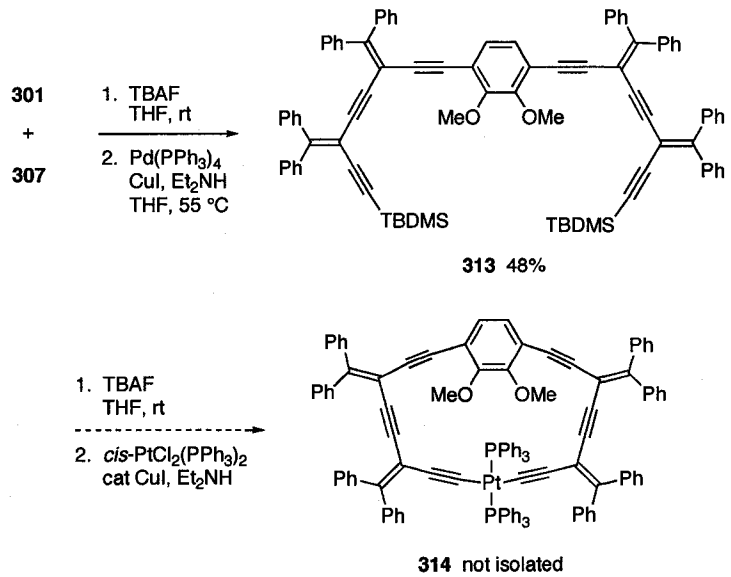

Scheme 3.6 Attempted synthesis of **314**.

The macrocyclization of the tetrayne **315** (provided by Mr. Mojtaba Gholami) gave some unusual results (Scheme 3.7). The first reaction was performed under typical Pt-acetylide coupling conditions and resulted in the isolation of 8 mg of a yellow solid

tentatively assigned as **316** on the basis of a pseudo–t observed in the ^{31}P NMR spectrum at 20 ppm with a $^{1}J_{P-Pt}$ coupling constant of 2072 Hz. This coupling constant is low for a typical *trans*-Pt-acetylide, expected at ~2700 Hz, so it is possible that **316** was isolated with a *cis*-Pt-acetylide conformation. A second attempt at the synthesis of **316** gave unexpectedly different results. Gratifyingly, 58 mg of a brown-orange solid was isolated (68%) but the ^{31}P NMR spectrum was different. Now the only signal present was a pseudo–t at 15 ppm with a $^{1}J_{P-Pt}$ coupling constant of 3672 Hz, which was much higher than the expected ~2700 Hz. Characterization of this compound was attempted by mass spectrometry, but both electrospray and MALDI analyses were inconclusive, showing the largest fragment to be *m/z* 2088, when the expected ion peak was *m/z* 1350. The ^{1}H NMR spectrum was not helpful for identification because only phenyl protons are present in the molecule. Therefore as the ^{31}P NMR spectrum indicated a pure compound, *S,S*-CHIRAPHOS **201** was added to the NMR tube. This was done expecting that the isolation of the product after ligand exchange could be used to determine the identity of the precursor. Gratifyingly, the ^{31}P NMR spectrum showed the disappearance of the pseudo–t at 15 ppm, and the appearance of a pseudo–t at 47 ppm with $^{1}J_{P-Pt}$ coupling constant of 2289 Hz, which was characteristic of a *cis*-Pt-acetylide complex. There was also the appearance of free PPh_3 at –4 ppm. Based upon the ^{31}P NMR spectrum, this new complex, assumed to be the *cis*-Pt-acetylide **317**, was formed cleanly. Unfortunately, when isolation was attempted using a silica gel plug, the compound was lost, possibly due to its insolubility. Regrettably, only a limited amount of **315** was available so further reactions could not be preformed.

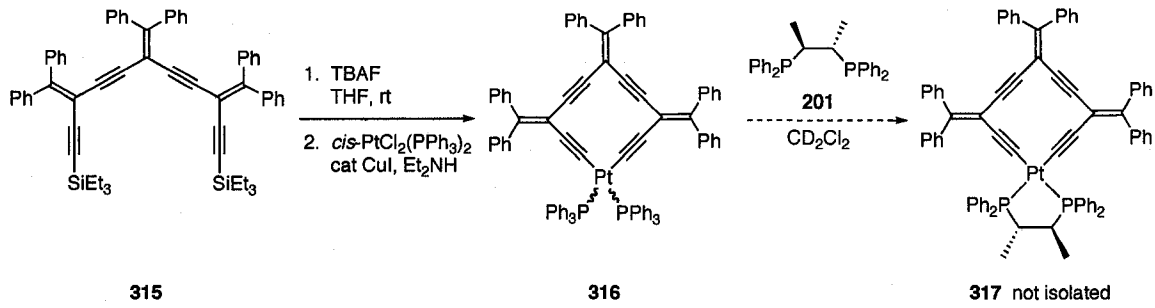

Scheme 3.7 Attempted synthesis of chiral macrocycle **317**.

3.3 CONCLUSIONS

Macrocycle building blocks **301**, **303**, **304**, **306**, and **311** have been fully characterized by ^{1}H, and ^{13}C NMR and IR spectroscopies, melting point, mass spectrometry and elemental analysis. And macrocycles **300** and **308** have been partially characterized by ^{1}H and ^{31}P NMR (for **300**) and IR spectroscopies, melting point and mass spectrometry (for **300**). The targeted macrocycles proved to be difficult to isolate pure and in a large enough quantity to be useful for phosphine ligand exchange.

3.4 REFERENCES

1. Campbell, K.; Tiemstra, N. M.; Prepas-Strobeck, N. S.; McDonald, R.; Ferguson, M. J.; Tykwinski, R. R. *Synlett* **2004**, 182-186.

2. Campbell, K.; Johnson II, C. A.; McDonald, R.; Ferguson, M. J.; Haley, M. M.; Tykwinski, R. R. *Angew. Chem.* **2004**, *43*, 5967-5971.

3. Campbell, K.; McDonald, R.; Tykwinski, R. R. *J. Org. Chem.* **2002**, *67*, 1133-1140.

4. Campbell, K.; McDonald, R.; Ferguson, M. J.; Tykwinski, R. R. *J. Organomet. Chem.* **2003**, *683*, 379-387.

5. Lee, S. J.; Hu, A. G.; Lin, W. B. *J. Am. Chem. Soc.* **2002**, *124*, 12948-12949.

6. Lee, S. J.; Lin, W. B. *J. Am. Chem. Soc.* **2002**, *124*, 4554-4555.

7. Jiang, H.; Hu, A. G.; Lin, W. B. *Chem. Commun.* **2003**, 96-97.

8. Hua, J.; Lin, W. B. *Org. Lett.* **2004**, *6*, 861-864.

9. Zhu, Z. G.; Swager, T. M. *Org. Lett.* **2001**, *3*, 3471-3474.

10. Zhou, Q.; Carroll, P. J.; Swager, T. M. *J. Org. Chem.* **1994**, *59*, 1294-1301.

11. Pring, B. G. *Acta Chem. Scand.* **1973**, *27*, 3873-3880.

12. Stang, P. J.; Fisk, T. E. *Synthesis* **1979**, 438-440.

13. Campbell, K. Ph.D. thesis, University of Alberta, Edmonton, AB, 2004.

CHAPTER 4 CHIRAL LIGAND EXCHANGE WITH *trans*-PLATINACYCLYNES

4.1 INTRODUCTION

In collaboration with Dr. Micheal M. Haley and Dr. Charles A. Johnson II from the University of Oregon, ligand exchange reactions were preformed on the benzene- and pyridine-based *trans*-platinacyclynes **400–402** (Fig. 4.1).

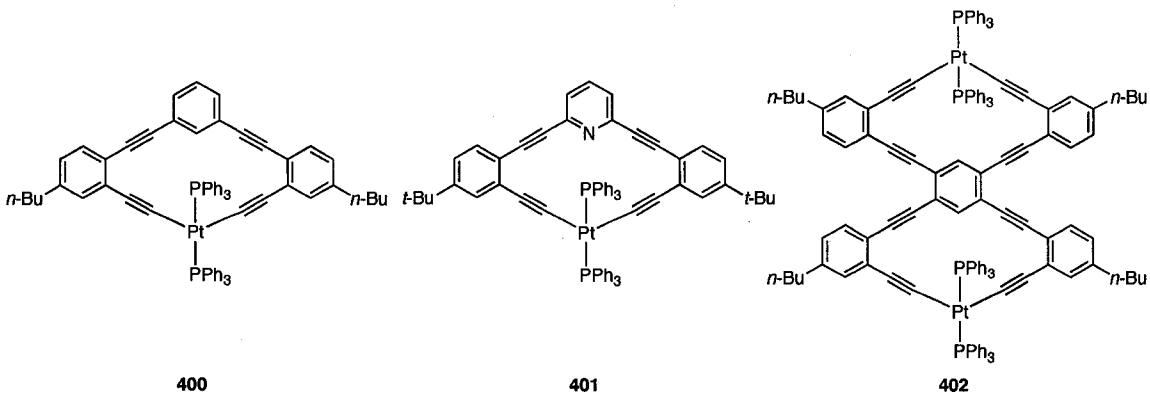

Figure 4.1 *trans*-platinacyclynes **400–402**.

trans-Platinacyclynes **400** and **401** were prepared (at the University of Oregon) by selectively removing the TMS, which is more labile than the TIPS protecting group, on the appropriate diyne **403** or **404**, with K_2CO_3 as a mild base (Scheme 4.1).[1,2] The terminal alkyne was then carried forward without purification to be cross-coupled with either 1,3-diiodobenzene or 2,6-dibromopyridine in the presence of $Pd(PPh_3)_4$, CuI, and $(i\text{-Pr})_2NH$ in THF at 50 °C. This led to the isolation of α,ω-polyynes **405** and **406** in moderate yield. Desilylation of the two TIPS groups with TBAF, followed by the amine-mediated oxidative metallacyclization reaction with *trans*-$PtCl_2(PPh_3)_2$, CuI and Et_2NH, formed platinacyclynes **400** and **401** in moderate to good yield. A pseudo–t due to the $^1J_{P-Pt}$ coupling was observed in the ^{31}P NMR spectra of **400** and **401** at 17 and 18

ppm in $CDCl_3$, respectively, with coupling constants of 2631 and 2716 Hz (values typical for *trans*-Pt-acetylide complexes with PPh_3 ligands).[3-6] The *trans*-Pt-acetylide complexes preferentially formed under the amine-mediated metallacyclization, even with the use of *cis*-$PtCl_2(PPh_3)_2$. The use of CuI, which promotes the isomerization through a reversible ethynyl transfer between Pt and Cu, PPh_3 over PEt_3, and heat encourage the formation of the more thermodynamically favoured *trans*-Pt-acetylide complex over the *cis*-Pt-acetylide complex.[5,6]

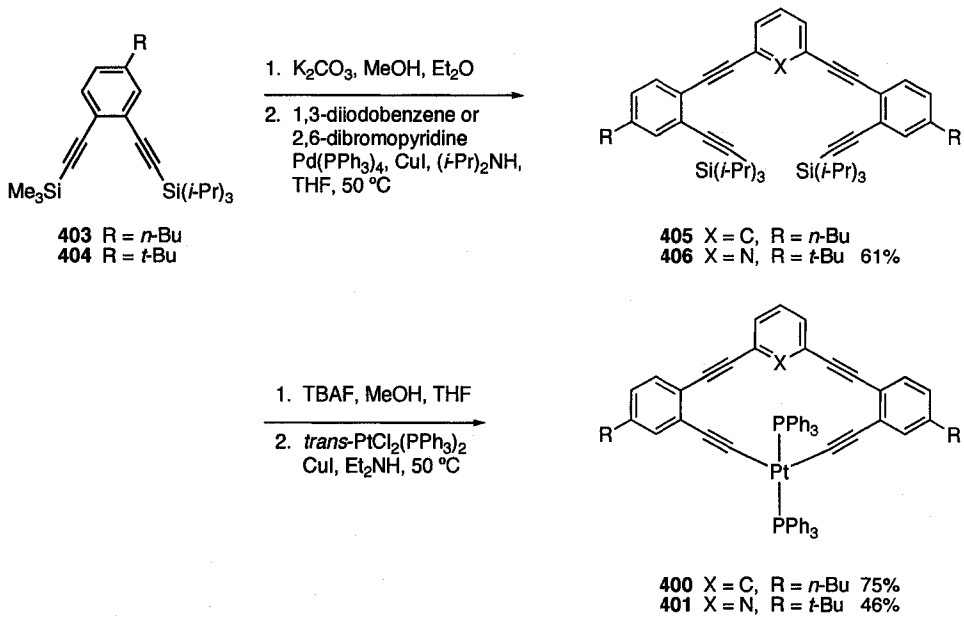

403 R = *n*-Bu
404 R = *t*-Bu

405 X = C, R = *n*-Bu
406 X = N, R = *t*-Bu 61%

400 X = C, R = *n*-Bu 75%
401 X = N, R = *t*-Bu 46%

Scheme 4.1 Synthesis of *trans*-platinacyclynes **400** and **401**.

The same synthetic strategy was used to form the *trans*-bisplatinacyclyne **402**, beginning with the common diyne precursor **403** followed by the cross-coupling of the terminal alkyne intermediate with 1,2,4,5-tetraiodobenzene, leading to octayne **407** in good yield (Scheme 4.2). The same metallacyclization procedure with *trans*-$PtCl_2(PPh_3)_2$ and **407** led to the isolation of **402** as a bright yellow solid with low solubility in nearly

all organic solvents. A $^{1}J_{P-Pt}$ coupling constant of 2629 Hz was observed for the ^{31}P NMR signal at 17 ppm in $CDCl_3$, confirming the *trans*-Pt-acetylide configuration.

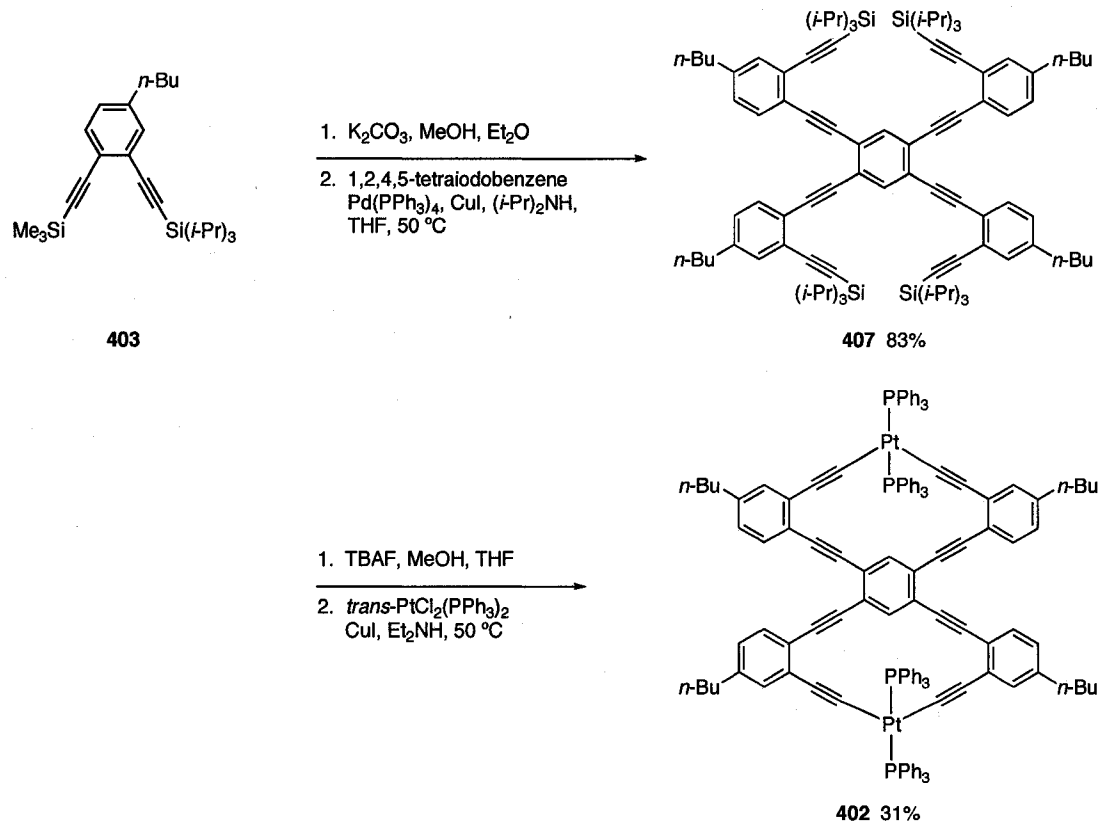

Scheme 4.2 Synthesis of *trans*-platinacyclyne **402**.

cis-Pt-acetylide complexes bearing PPh_3 or PPh_2 ligands have been previously synthesized by Haley and coworkers using Sn transmetallation with either *cis*-$PtCl_2(PPh_3)_2$ or $PtCl_2$(dppe). The use of *cis*-$PtCl_2(PPh_3)_2$ resulted in low yields of the desired *cis*-Pt-acetylide complexes due to the tendency of the bulky PPh_3 ligands to initiate isomerization to the corresponding *trans*-Pt-acetylide complex. The best yields were obtained with $PtCl_2$(dppe), where the chelating diphosphine ligand prevents isomerization to the *trans*-Pt-acetylide complex.

The only previously reported ligand exchange reaction to be performed on a similar *trans*-platinacyclyne is shown below in Scheme 4.3.[4,7] Compound **408** and *S,S*-

CHIRAPHOS **201** were dissolved in CH_2Cl_2 and stirred at room temperature for 3 days, then purification by column chromatography on alumina afforded **409** in good yield. Using ^{31}P NMR spectral analysis, the *cis*-Pt-acetylide configuration was confirmed by the appearance of a pseudo–t at 45 ppm ($^1J_{P-Pt}$ = 2226 Hz) and the free PPh_3 signal at –4 ppm in addition to the disappearance of the pseudo–t at 19 ppm ($^1J_{P-Pt}$ = 2617 Hz) as **408** was consumed. The major difference between **409** and the compounds to be used for ligand exchange in this study **400–402**, is the substitution pattern on the central aromatic ring, which is *ortho* in the case of **409** and *meta* for **400–402**. Based upon the successful formation of **409** ligand exchange reactions with **400–402** were expected to occur easily, albeit with longer reaction times compared to the acyclic derivatives described previously in Chapter 2.

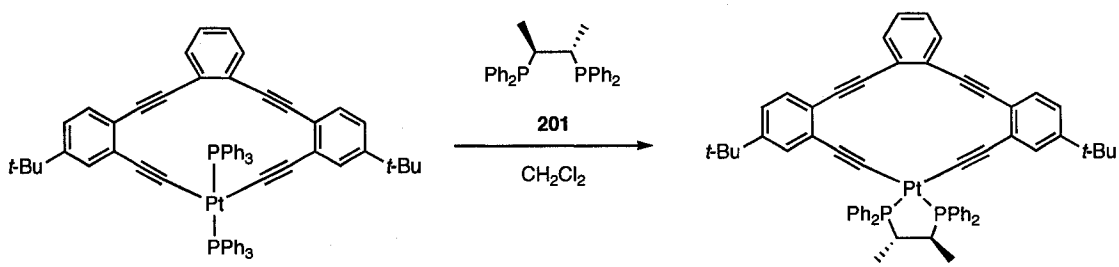

408 **409** 83%

Scheme 4.3 Synthesis of *cis*-platinacyclyne **409**.

4.2 Results and Discussion

4.2.1 Synthesis of Chiral cis-Platinacyclynes

The first ligand exchange reaction attempted was with *trans*-platinacyclyne **400** and *S,S*-CHIRAPHOS **201** in CH_2Cl_2 under a nitrogen atmosphere (Scheme 4.4). An oxygen free atmosphere was essential for long reaction times to prevent the formation of phosphorus oxide impurities. The reaction was monitored frequently by reducing the volume of the reaction mixture, adding $CDCl_3$ and obtaining a ^{31}P NMR spectrum, and after 3 days the presence of both the *cis*-platinacyclyne **410** at 46 ppm (pseudo–t, $^1J_{P-Pt}$ = 2232 Hz) and the starting material **400** at 17 ppm (pseudo–t, $^1J_{P-Pt}$ = 2631 Hz) was observed. At this point, a second equivalent of *S,S*-CHIRAPHOS **201** was added and the reaction was allowed to stir for an additional 7 days. In an attempt to complete the reaction, for at least 1 hour per day the reaction mixture was sonicated in a warm water bath at ~50 °C. The reaction was discontinued when the ^{31}P NMR spectrum did not show any improvement in the ratio of starting material to product, which was ca. 3:1 (**410**:**400**). Separation by column chromatography on silica gel, required 3:1 hexanes:CH_2Cl_2 to remove PPh_3, *S,S*-CHIRAPHOS **201**, and *trans*-platinacyclyne **400**, then 1:1 hexanes:EtOAc to remove the product **410**. Unfortunately, the ^{31}P NMR spectrum of the isolated product **410** showed that the sample was not entirely pure, several small impurities were still present (probably phosphorus oxides), but these were easily removed by the addition of hexanes to the NMR solution to precipitate out the product. After filtration, pure **410** was isolated as a white solid with a yield of 44%.

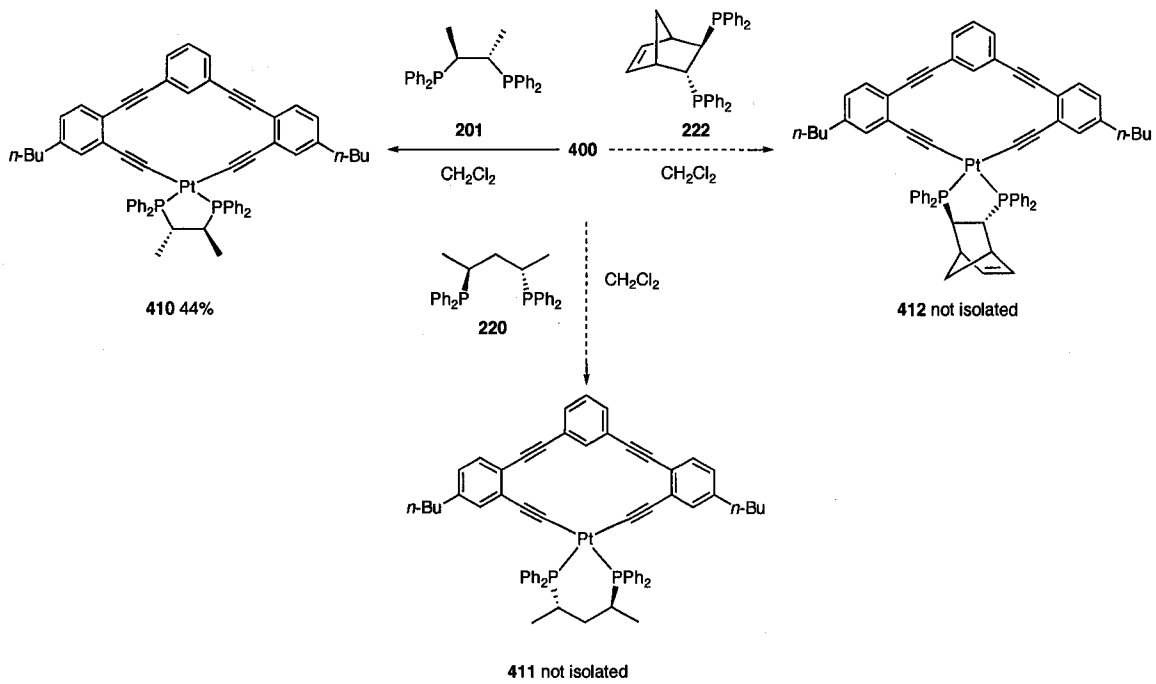

Scheme 4.4 Synthesis of *cis*-platinacyclynes **410–412**.

Using the same *trans*-platinacyclyne **400**, ligand exchange reactions were attempted with *S,S*-BDPP **220** and *R,R*-NORPHOS **222** (Scheme 4.4). In the case of *cis*-platinacyclyne **411**, after 5 days of stirring at room temperature in CH_2Cl_2 under a nitrogen atmosphere, a signal for the product, presumably, was observed at 26 ppm (pseudo–t, $^1J_{P-Pt}$ = 2572 Hz) in the ^{31}P NMR spectrum, with a substantial amount of *trans*-platinacyclyne **400** still present at 17 ppm (pseudo–t, $^1J_{P-Pt}$ = 2631 Hz). A second equivalent of *S,S*-BDPP **220** was added and the reaction was stirred under nitrogen at 50 °C for 22 days. At this time the ^{31}P NMR spectrum contained a number of additional peaks, but the product **411** was still observed and only a small amount of starting material **400** remained. From previous experience, precipitation from a CH_2Cl_2 solution with hexanes or Et_2O was the easiest way to isolate the product, but in this case no precipitation occurred. Column chromatography was therefore used, and separation on

silica gel using 2:1 hexanes:CH_2Cl_2, then EtOAc, gave a slightly cleaner mixture, with the product **411** still present. When a second separation was performed, however, the product was lost for unknown reasons. Interestingly, as was the case of the *S,S*-BDPP ligand bearing **230/239** and **235/240** complexes, the $^1J_{P-Pt}$ coupling constant in the ^{31}P NMR spectrum was near 2500 Hz for **411** rather than the expected coupling of ~2200 Hz, suggesting the same dimerization as described previously (Section 2.2.2).

A similar situation can be described for the reaction of *R,R*-NORPHOS **222** with *trans*-platinacyclyne **400** (Scheme 4.4). In this case, the reaction was carried out twice with identical results. After 16 days under nitrogen, with or without heat, and using greater than two equivalents of *R,R*-NORPHOS **222**, both reactions would only go to about 40% completion. A signal for the presumed product was observed as a pseudo–dt at 14 and 13 ppm ($^1J_{P-Pt}$ = 2277 and 2268 Hz) in the ^{31}P NMR spectrum. Unfortunately, isolation via precipitation from a CH_2Cl_2 solution with hexanes or Et_2O and column chromatography on silica gel did not lead to the isolation of *cis*-platinacyclyne **412**.

The formation of *cis*-platinacyclyne **413** proceeded in a similar manner to that of *cis*-platinacyclyne **410** (Scheme 4.5). After an initial reaction time of 10 days at room temperature in CH_2Cl_2 under a nitrogen atmosphere, both the starting material **401** at 20 ppm (pseudo–t, $^1J_{P-Pt}$ = 2716 Hz) and the product **413** at 52 ppm (pseudo–t, $^1J_{P-Pt}$ = 2271 Hz) were both observed in the ^{31}P NMR spectrum. Thus, a second equivalent of *S,S*-CHIRAPHOS **201** was added, and after an additional 10 days at 50 °C, the greenish-black solution was concentrated (even though the reaction was only about 80% complete) and purified by passing the mixture through a silica gel plug with 1:1 hexanes:CH_2Cl_2 then EtOAc. Precipitation from a CH_2Cl_2 solution with hexanes and filtration gave pure **413**

as a beige solid in 29% yield. The initial attempt of this reaction was performed in a NMR tube and the greenish-black reaction mixture was left in the fridge for a period of months and unfortunately decomposition occurred during that time.

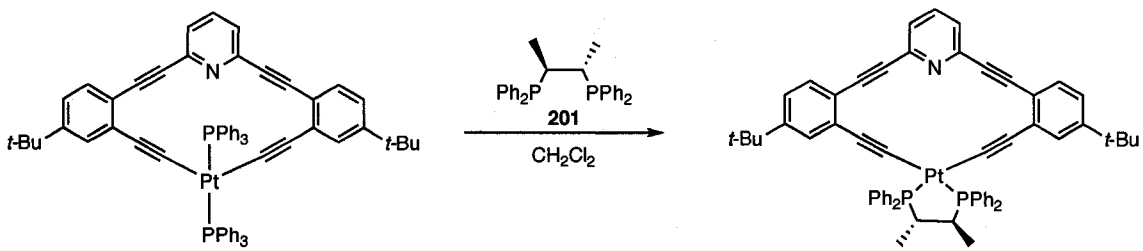

401 **413** 29%

Scheme 4.5 Synthesis of *cis*-platinacyclyne **413**.

A ligand exchange reaction with *S,S*-CHIRAPHOS **201** was also tried with *trans*-bisplatinacyclyne **402** (Scheme 4.6). The reaction was done under similar conditions as described above but in $CDCl_3$ at room temperature. After 7 days, the reaction appeared to be almost complete with the signal for *cis*-bisplatinacyclyne **414** observed at 47 ppm (pseudo–t, $^1J_{P-Pt}$ = 2291 Hz) and the resonance of the starting material **402** at 17 ppm ($^1J_{P-Pt}$ coupling constant was too weak to observe) all but absent in the ^{31}P NMR spectrum. Separation by column chromatography using silica gel resulted only in the recovery of 3 mg of the *trans*-bisplatinacyclyne **402** starting material as a yellow solid, identified by ^{31}P NMR spectroscopy with a chemical shift of 17 ppm (pseudo–t, $^1J_{P-Pt}$ = 2629 Hz). The product may have been lost due to its insolubility. Prior to the attempted chromatographic separation, precipitation with hexanes or Et_2O was not attempted, and this may have been a better technique for purification of this material. Additional ligand exchange reactions with *trans*-platinacyclynes **400–402** were limited by the amount of sample available for study.

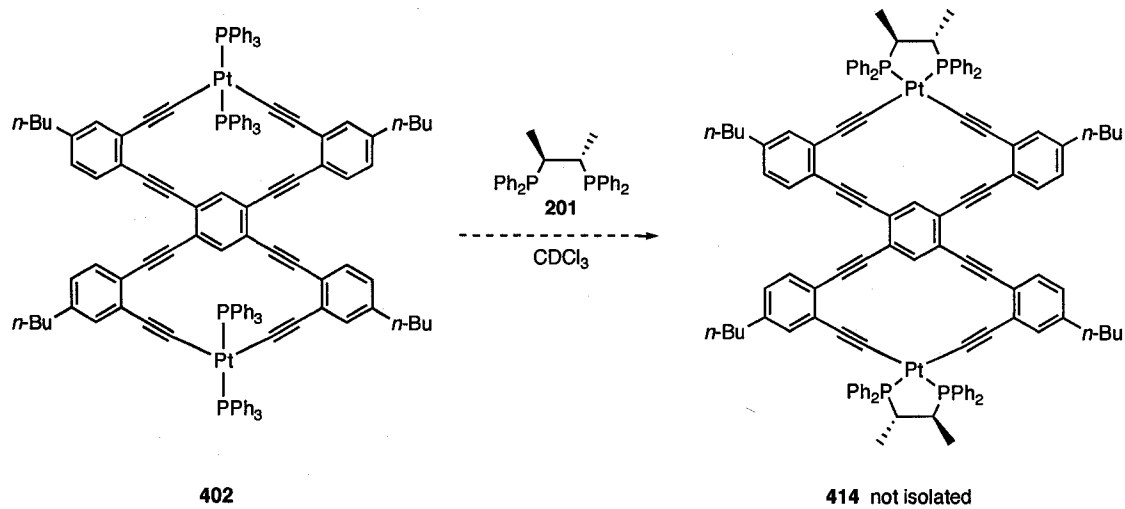

402 **414** not isolated

Scheme 4.6 Attempted synthesis of *cis*-bisplatinacyclyne **415**.

4.2.2 Electronic Properties of Chiral cis-Platinacyclynes

The only compounds characterized by UV–vis and CD spectroscopies are **410** and **413** and these results have been compared to the literature values,[4,7] for the previously reported chiral *cis*-platinacyclyne **409**. The UV–vis spectrum of complex **409** shows a low energy absorption maxima at 347 nm (ε = 20300 M^{-1} cm^{-1}). Similarly, the UV–vis spectra of *cis*-platinacyclyne **410** (Figure 4.2) and **413** (Figure 4.3) both show low energy absorption maxima at 348 nm (ε = 13000 M^{-1} cm^{-1}) and 337 nm (ε = 26900 M^{-1} cm^{-1}), respectively.

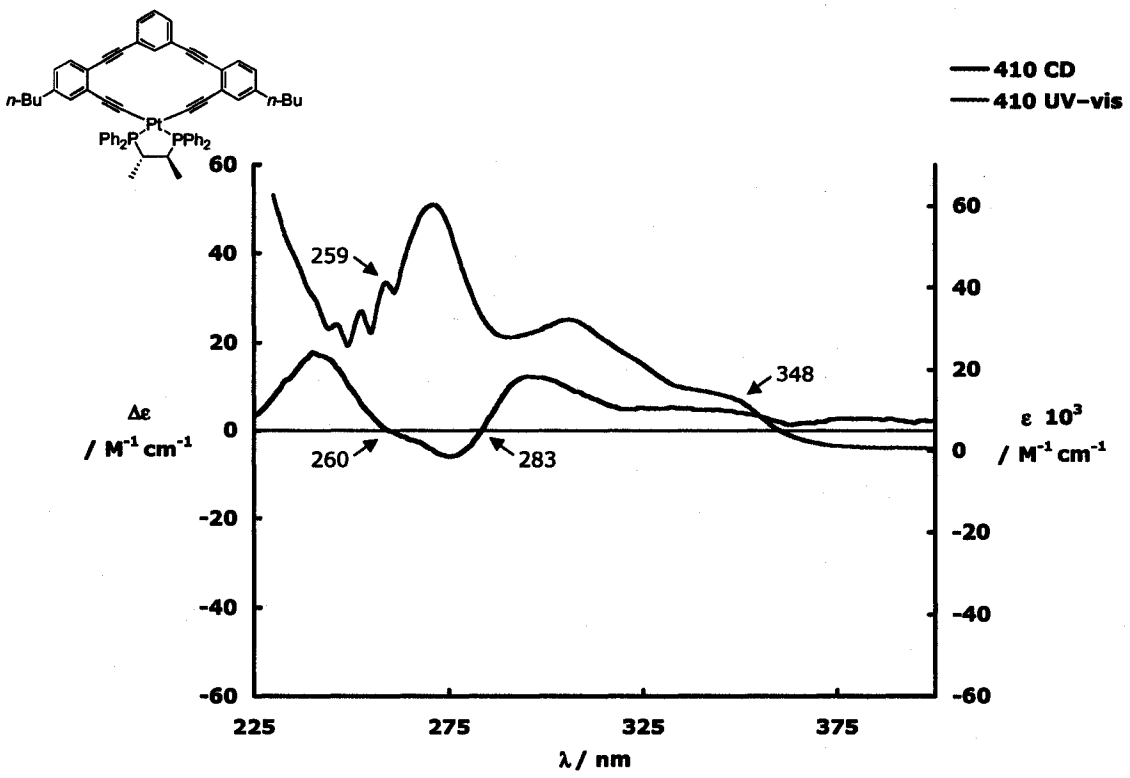

Figure 4.2 CD and UV–vis spectra for **410** in CH_2Cl_2.

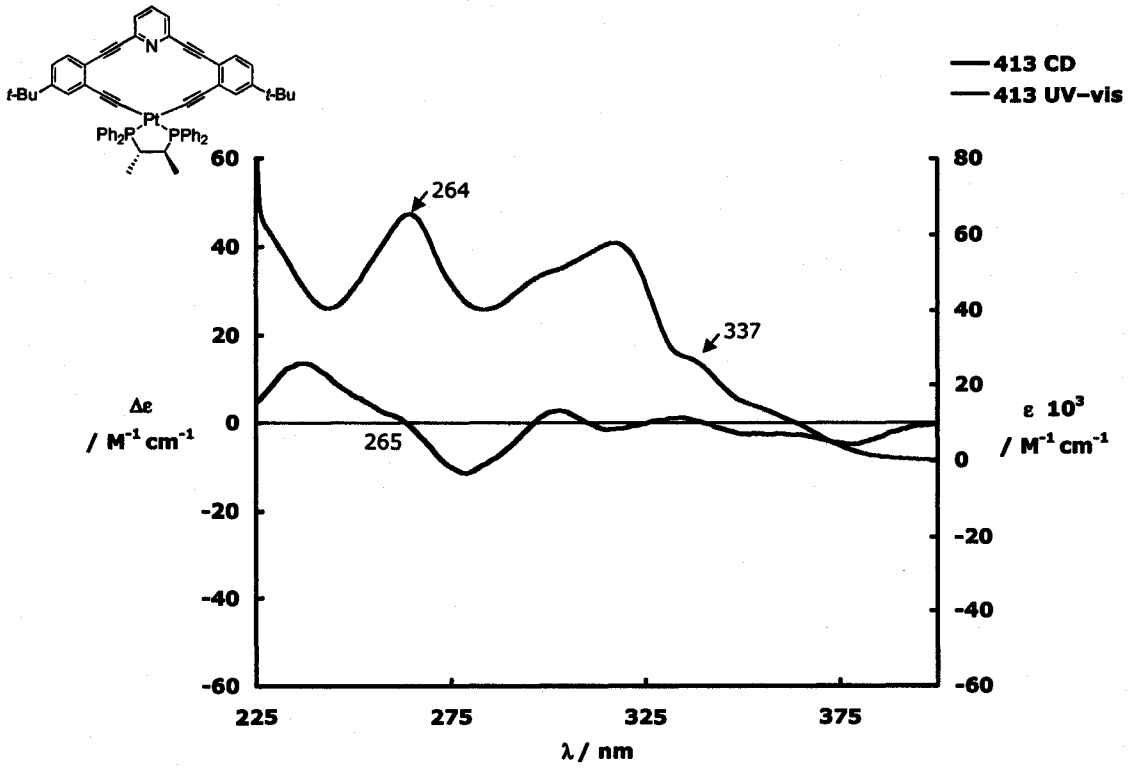

Figure 4.3 CD and UV–vis spectra for **413** in CH_2Cl_2.

The CD spectrum of *S,S*-CHIRAPHOS containing *cis*-platinacyclyne **409**, was reported to have a weak, high energy bisignate signal centered at about 250 nm ($\Delta\varepsilon$ = 24 M^{-1} cm^{-1}).[4,7] This was assumed to be due to the electronic transitions of the chiral, chelating *S,S*-CHIRAPHOS ligand **201** attached to the platinum center. It was speculated that for efficient chirality transfer from the chiral array of phenyl groups on the diphosphine ligand to the acetylenic chromophore bonded to platinum, the chromophore must be rigid but still retain adequate conformational mobility. This explains the weak signal of **409** in the CD spectrum, where this mobility is not substantial. Additional evidence to support this explanation is observed in the CD spectra of *S,S*-CHIRAPHOS containing platinacyclynes **410** and **413** (Figures 4.2 and 4.3), where again weak, high energy signals are centered at 260 nm ($\Delta\varepsilon$ = 17 M^{-1} cm^{-1}) and 265 nm ($\Delta\varepsilon$ = 14 M^{-1} cm^{-1})* respectively.

4.3 Conclusions

This chapter has demonstrated a possible limitation to the use of chelating diphosphine ligand exchanges to convert *trans*-Pt-acetylide macrocycles to their *cis*-counterparts. This conversion has not been effective for these particular cyclic compounds **400–402** as had been demonstrated for others, such as, for example **408**. Based upon the ^{31}P NMR spectra of the reaction mixtures, all of the ligand exchange reactions described above in this chapter went only partially to completion, even after several days. Nonetheless, *S,S*-CHIRAPHOS **201** containing *cis*-platinacyclynes **410** and **413** were isolated and fully characterized. Ironically, the first chelating diphosphine ligand chosen for the ligand exchange reaction, *S,S*-CHIRAPHOS, proved to be the most

* $\Delta\varepsilon$ values discussed are for the absolute maximum of their respective bisignate signal.

successful when compared to *S,S*-BDPP **220** and *R,R*-NORPHOS **222**. To explain these observations, it is possible that the *trans*-platinacyclynes are so thermodynamically stable due to the less strained geometry, that ligand exchange to the *cis*-platinacyclynes is energetically unfavourable. Analysis of the CD spectroscopic data of the isolated complexes, demonstrated the ability of *S,S*-CHIRAPHOS to weakly transfer chirality to the conjugated molecular framework of the Pt-acetylide macrocycles.

For all of these reactions, conversion between the use of CH_2Cl_2 and $CHCl_3$ (and their deuterated analogues) resulted in no apparent difference in reactivity or decomposition. The most significant concern was the prevention of phosphorus oxide formation in the reaction mixture due to exposure of the reaction to atmospheric oxygen. This can be circumvented by making sure the reaction mixture is continuously under a positive nitrogen atmosphere. Additional studies with these platinacyclynes are suggested to optimize the reaction conditions, isolation process and expand the ligand scope.

4.4 References

1. Johnson II, C. A.; Haley, M. M.; Rather, E.; Han, F.; Weakley, T. J. R. *Organometallics* **2005**, *24*, 1161-1172.
2. Johnson, C. A.; Haley, M. M., University of Oregon, *unpublished results.*
3. Campbell, K.; McDonald, R.; Ferguson, M. J.; Tykwinski, R. R. *J. Organomet. Chem.* **2003**, *683*, 379-387.
4. Campbell, K.; Johnson II, C. A.; McDonald, R.; Ferguson, M. J.; Haley, M. M.; Tykwinski, R. R. *Angew. Chem.* **2004**, *43*, 5967-5971.
5. Cross, R. J.; Davidson, M. F. *J. Chem. Soc., Dalton Trans.* **1986**, 1987-1992.

6. Sonogashira, K.; Yatake, T.; Tohda, Y.; Takahashi, S.; Hagihara, N. *J. Chem. Soc., Chem. Commun.* **1977**, 291-292.

7. Campbell, K. Ph.D. thesis, University of Alberta, Edmonton, AB, 2004.

8. Johnson II, C. A.; Baker, B. A.; Berryman, O. B.; Zakharov, L. N.; O'Connor, M. J.; Haley, M. M. *J. Organomet. Chem.* **2006**, *691*, 413-421.

CHAPTER 5 CONCLUSIONS AND FUTURE WORK

5.1 CONCLUSIONS

The main focus of this thesis has been to establish the potential, as well as the limitations of the recently reported diphosphine ligand exchange reactions. These ligand exchange reactions transform *trans*-Pt-acetylide complexes to their *cis*-analogues, via the exchange of two PPh_3 ligands for an achiral or chiral chelating diphosphine ligand. Using this simple methodology to introduce chirality has enormous potential for the economical formation of chiral *cis*-Pt-acetylide macrocycles. Of the chiral ligands tested *S,S*-CHIRAPHOS (**201**) and *R,R*-NORPHOS (**222**), appear to be the most efficient for chirality transfer in monoyne (**214**, **215**, **223–232**), diyne (**234–236**) and triyne (**238**) systems based upon CD spectroscopic analysis.

Although, the transformation from the *trans*-Pt-acetylide complexes to their *cis*-analogues was very efficient for the acyclic complexes, this was not the case for the strained *trans*-platinacyclynes **400–402**, where reaction times of weeks, heating, and sonication could not force the ligand exchange reactions to completion. The first ligand of choice, *S,S*-CHIRAPHOS **201**, however, was determined to undergo ligand exchange with these strained macrocycles the most effectively, allowing for the characterization of two new chiral macrocycles **410** and **413**.

5.2 FUTURE WORK

The obvious extension of this project would be to extend the scope and more rigorously determine the limitations of the chelating diphosphine ligands suitable for this procedure and in particular for ligand exchange in macrocyclic systems. It has been

determined a limitation is present for these reactions since *S,S*-DIOP **241**, *R*-BINAP **242** and *R*-SYNPHOS **243** were unsuccessful, as discussed in Section 2.2.3. Some examples of commercially available ligands **500–505** that could be explored are shown below in Figure 5.1. Both enantiomers of each ligand are available and in some cases the $P(tol)_2$, PMe_2, PEt_2 and $P(cyclohexane)_2$ derivatives are also available. Therefore the number of possible ligands is quite broad. It has been shown that ligand exchange from *trans*-Pt-acetylide complexes containing PEt_3, do not efficiently undergo this transformation, but it has not been determined if the chiral (or achiral) chelating diphosphine ligand itself can contain groups other than PPh_2. The only ligand tried in this regard is *R,R*-Me-DUPHOS **221**, and was successful in the synthesis of *cis*-Pt-monoyne complexes **225** and **231**. These encouraging results increase the number of potentially useful ligands available for this reaction, such as **501** for example.

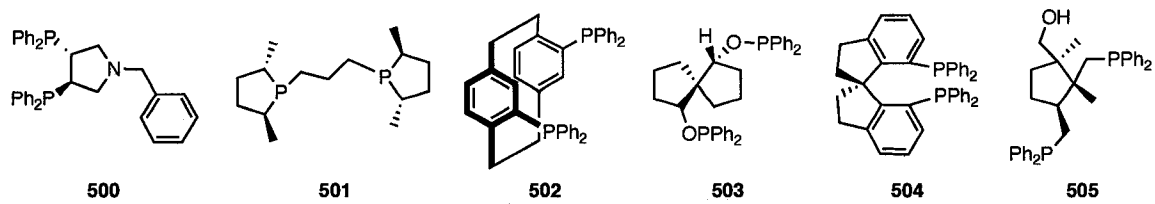

500 **501** **502** **503** **504** **505**

Figure 5.1 Potential chiral chelating diphosphine ligands **500–505**.

The other extension of this research project would be to synthesize a full series of macrocycles containing the same chiral chelating diphosphine ligands used in this study. A CD spectroscopic analysis would determine if the ligands are as effective in chirality transfer for cyclic systems as observed for the acyclic model complexes. Work has already begun on macrocycles with a conjugated scaffolding, such as **506** containing *trans*-Pt-acetylide functionality, as shown in Scheme 5.1. Preliminary ligand exchange reactions leading to the formation of chiral *cis*-Pt-acetylide macrocycles **507** have shown

promising results as discussed in Chapter 3. The synthesis of the macrocycle building blocks has also been discussed, but more synthetic optimization for the cyclization is still needed.

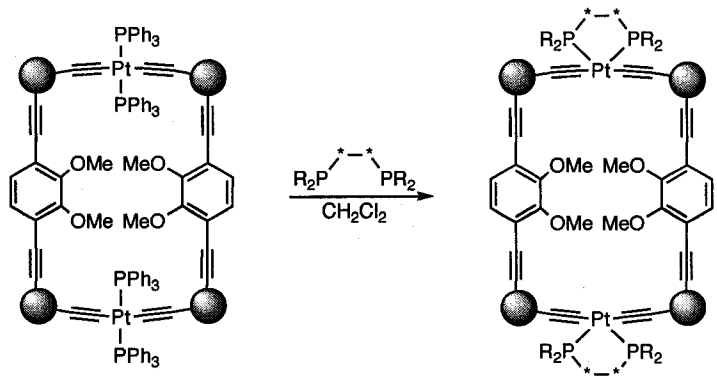

506 507

Scheme 5.1 Schematic chiral chelating diphosphine ligand exchange on *trans*-Pt-acetylide macrocycle **506** leading to chiral *cis*-Pt-acetylide macrocycle **507**.

Once chiral macrocycles of this type have been synthesized and the "best" chiral chelating diphosphine ligand has been determined based upon the CD spectroscopic analysis of the acyclic model and macrocyclic complexes, at least one chiral macrocycle should be tested for its effectiveness in asymmetric catalysis. The presence of methoxy groups in **507** allows for the prospect of asymmetric catalysis with the prototypical diethylzinc addition to aromatic aldehydes **508** in the presence of, for example, Ti(O*i*Pr)$_4$ (Scheme 5.2).[1-4] It would be interesting to observe whether or not the macrocycle Ti(IV) complexes generate chiral secondary alcohols such as **509** in high yield, chemoselectivity, and enantioselectivity.

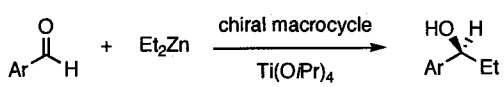

508 509

Scheme 5.2 Asymmetric catalysis testing for chiral macrocycles.

5.3 REFERENCES

1. Lee, S. J.; Hu, A. G.; Lin, W. B. *J. Am. Chem. Soc.* **2002**, *124*, 12948-12949.

2. Lee, S. J.; Lin, W. B. *J. Am. Chem. Soc.* **2002**, *124*, 4554-4555.

3. Jiang, H.; Hu, A. G.; Lin, W. B. *Chem. Commun.* **2003**, 96-97.

4. Hua, J.; Lin, W. B. *Org. Lett.* **2004**, *6*, 861-864.

CHAPTER 6 EXPERIMENTAL SECTION

6.1 GENERAL DETAILS

Column chromatography: Aluminum oxide, neutral, Brockman 1, 150 mesh from *Aldrich Chemical Company, Inc.* (5% water) or silica gel–60 (230–400 mesh) from *General Intermediates of Canada* or *Silicycle.* Thin layer chromatography (TLC): Aluminum sheets coated with *aluminum oxide* 60 F_{254} from *EM Separations* or plastic sheets coated with *silica gel* G UV_{254} from *Macherey–Nagel*: visualization by UV light. Mp.: *Fisher–Johns* apparatus; uncorrected. IR spectra: *Nic–Plan IR Microscope* (as cast from CH_2Cl_2). ^1H–, ^{13}C–, ^{31}P–NMR: *Varian–400* at 27 °C in $CDCl_3$, CD_2Cl_2; solvent peaks (7.24, 5.32 for ^1H and 77.00, 53.80 for ^{13}C, respectively) as reference and H_3PO_4 as ^{31}P reference. EI MS (70 eV): *Kratos MS 50* instrument. ESI MS (*m/z*): *Micromass Zabspec oaTOF* or *PE Biosystems Mariner TOF* instruments; solvents as noted. MALDI MS (*m/z*): *PE Voyager Elite* instrument in reflectron mode with delayed extraction; matrices as noted; solvent $ClCH_2CH_2Cl$. Elemental analyses were performed by the Microanalytical Service, Department of Chemistry, University of Alberta.

For IR data, useful functional groups and 3–4 of the strongest absorptions are reported, including but not limited to C–H, C=C and C≡C bond stretches. All solvent ratios are volume:volume, unless otherwise noted. For simplicity, the coupling constants of the aryl protons for *para*-substituted phenyl groups have been reported as pseudo first-order, even though they are second-order (AA'BB') spin systems. ^{13}C NMR spectra are broadband decoupled. Coupling constants *J* are reported as observed. For simplicity all J_{C-Pt} coupling constants have not been reported in the ^{13}C NMR spectra (where applicable). For mass spectral analyses, low-resolution data are provided in cases when

M^+ is not the base peak; otherwise, only high-resolution data are provided. Crystallographic data for unpublished compounds is available from the X–ray Crystallography Laboratory, Department of Chemistry, University of Alberta.

Circular dichroism spectra were recorded at 20.0 °C, from 550–220 nm with 330 increments, on an *OLIS DSM* 17 CD, Cary-17 Conversion spectrometer/circular dichroism module, On-Line Instruments Inc. with a 1 mm (Hellma) cuvette. Previous to each recording the sample chamber was purged with nitrogen. Spectra were recorded as ellipticity, θ, in units of millidegrees and then converted to molar CD, Δε, using the equation $\Delta\varepsilon = \theta / (32982 * c * l)$, where Δε is the difference in molar absorptivity for oppositely polarized light expressed in M^{-1} cm^{-1}, c is the concentration of the sample (mol L^{-1}), and l is the path length through the cell (cm).[1]

Solutions for CD spectroscopy were prepared by dissolving a known amount (in aluminum weighing boats) of pure, dry sample (as determined by ^1H and ^{31}P NMR spectra) in dry volumetric flasks with dry CH_2Cl_2 for concentrations in the μM range. Prior to running a sample the cuvette was rinsed three times with dry CH_2Cl_2, then rinsed three times with the sample solution. Three replicates were recorded, then averaged and smoothed with *OLIS Globalworks* to produce the final spectrum. Data analysis of CD spectra proceeded after the CH_2Cl_2 background was subtracted and CD units were converted to Δε for the three replicates, each replicate was smoothed, then the wavelength and Δε of the peaks and troughs were recorded. To ensure the data was statistically equivalent, the standard deviation of replicates was calculated and any results

>20% standard deviation were discarded.* The raw data of the replicates were then averaged, converted to $\Delta\varepsilon$ and smoothed to produce one averaged spectrum. Final data was then exported to *Microsoft Excel* and graphed.

UV–vis spectra: *Varian Cary 400* Scan Spectrometer at room temperature; λ_{max} in nm (ε in L mol^{-1} cm^{-1}), with a 1 cm quartz cuvette. The same solutions used for CD spectroscopy were used for UV–vis spectroscopy and the appropriate dilutions were prepared to result in absorbencies in the 0.2–4.0 range. CD and UV–vis samples were recorded the same day. To ensure the data was statistically equivalent, the standard deviation of three replicates was calculated and any results >10% were discarded. The raw data of the replicates were then averaged, to produce one spectrum.

General Experimental Methods.

Reagents were purchased reagent grade from commercial suppliers and used without further purification. THF was distilled from sodium/benzophenone ketyl, hexanes and CH_2Cl_2 were distilled from CaH_2 immediately prior to use. Compounds **305**,[2] **307**,[3] were prepared as previously reported. All Pd-catalyzed cross-coupling reactions were performed in standard, dry glassware under an inert atmosphere of N_2. Degassing of solvents was accomplished by vigorously bubbling N_2 through the solutions for at least 1 hour. Anhydrous $MgSO_4$ or Na_2SO_4 was used as drying agents after aqueous workup. Evaporation and concentration *in vacuo* was achieved at H_2O–aspirator pressure.

---

*Compounds **223, 224, 225** and **231** did not have a significant peak in the CD spectrum, therefore large statistical errors (>20%) were calculated, despite this, the raw data was averaged and smoothed. For compounds **223**, **235**, **413** and free ligands **201**, **219–222** only two replicates were averaged to obtain the UV–vis and CD spectra.

General Procedure A – Desilylation. The appropriate trimethyl–, triethyl– or tertbutyldimethylsilyl–protected alkyne was dissolved in wet THF (10 mL). TBAF (ca. 2.2 equiv) was added, and the resulting solution was stirred, in the presence of air at room temperature, until TLC analysis indicated complete conversion to the desilylated intermediate. Et_2O (25 mL) and CH_2Cl_2 (25 mL) were added, and the resulting solution was washed with saturated NH_4Cl (2 × 25 mL) and dried ($MgSO_4$). The solvent was reduced to ca. 1 mL and the deprotected alkyne was carried on, with no further purification, to the next reaction.

General Procedure B – Palladium-Catalyzed Cross-Coupling. The respective terminal acetylene (ca. 2.3 mmol) was added with Et_2NH or Et_3N (4 mL) to a solution of the appropriate vinyl triflate or aryl halide (1.1 equiv per terminal acetylene) and dry THF (50 mL) and was degassed for 1 hour. $Pd(PPh_3)_4$ or $PdCl_2(PPh_3)_2$ (ca. 0.05 equiv per coupling event) and CuI (ca. 0.15 equiv per coupling event) were sequentially added, then the flask was sealed under N_2 and stirred at the temperature indicated in the individual procedure until TLC analysis no longer showed the presence of the starting material (2–3 days). Reactions performed at elevated temperatures were sealed under N_2 for heating. After cooling to room temperature, Et_2O (50 mL) and CH_2Cl_2 (50 mL) were added and the resulting solution was washed with H_2O (2 × 100 mL), satd. aq. NH_4Cl (4 × 100 mL), dried, and the solvent removed *in vacuo*. Column chromatography (silica gel) and/or precipitation yielded the desired product.

General Procedure C – Formation of Platinum-Acetylide Complexes. The appropriate terminal acetylene (ca. 0.5 mmol) was dissolved in Et_2NH (50 mL) and *cis*- or *trans*-$PtCl_2(PPh_3)_2$ (1 equiv) was added. The resulting solution was degassed for at least 1 hour and CuI (ca. 0.05 equiv) was added. The reaction mixture was sealed under N_2 and stirred at the temperature indicated in the individual procedure until TLC analysis or ^{31}P NMR spectroscopic analysis indicated the deprotected acetylene was entirely consumed. After cooling to room temperature, Et_2O (50 mL) and CH_2Cl_2 (50 mL) were added and the resulting solution was washed with H_2O (2 × 50 mL), satd. aq. NH_4Cl (4 × 50 mL) and dried. Solvent removal using *no heat* and purification by precipitation and/or chromatography gave the desired Pt-acetylide complex. Macrocyclization reactions were performed at much higher dilution as indicated in the individual procedures. Any ^{13}C NMR spectral assignments that are tentative, due to limited amount of sample, complex splitting patterns, overlapping signals or poor signal to noise ratio, have been underlined in the individual experimental write-ups.

6.2 Experimental Details for Chapter 2

trans-$(PPh_3)_2Pt(C{\equiv}C{-}Si(i\text{-}Pr_3))_2$ (213)

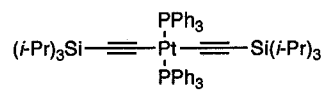

213

An excess of triisopropylsilylacetylene (200 mg, 0.25 mL, 1.1 mmol) was added to a degassed solution of *cis*-$PtCl_2(PPh_3)_2$ **218** (190 mg, 0.24 mmol) in Et_2NH (50 mL). A catalytic amount of CuI (5 mg, 0.03 mmol) was added and the mixture was stirred at rt under N_2 for 36 h. Work-up proceeded according to the general procedure C and

precipitation from a CH_2Cl_2 solution with Et_2O afforded **213** (180 mg, 69%) as a white solid. Mp >210 °C (dec.), (lit. 205 °C (dec.)). Spectral data for compound **213** were consistent with that reported, see: K. Campbell, R. McDonald, M. Ferguson, R. R. Tykwinski, *J. Organomet. Chem.* **2003**, *683*, 379-387.

***cis*–(dppee)Pt(C≡C–Si(*i*-Pr)$_3$)$_2$ (214)**

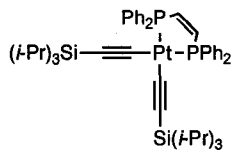

214

cis-1,2-Bis(diphenylphosphino)ethylene **200** (9.2 mg, 0.023 mmol) was added to a solution of **213** (23 mg, 0.021 mmol) in dry CH_2Cl_2 (10 mL). The mixture was stirred at rt for 48 h. Solvent removal followed by purification via column chromatography (silica gel, CH_2Cl_2/hexanes 1:1) afforded **214** (19 mg, 95%) as a white solid. Mp 245 °C (dec.), lit. 250 °C (dec.). Spectral data for compound **214** were consistent with that reported, see: K. Campbell, R. McDonald, M. Ferguson, R. R. Tykwinski, *J. Organomet. Chem.* **2003**, *683*, 379-387.

***cis*–(*S*,*S*-CHIRAPHOS)Pt(C≡C–Si(*i*-Pr)$_3$)$_2$ (215)**

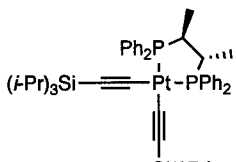

215

(2*S*,3*S*)-Bis(diphenylphosphino)butane **201** (10 mg, 0.024 mmol) was added to a solution of **213** (26 mg, 0.024 mmol) in dry CH_2Cl_2 (10 mL). The mixture was stirred at rt for 3 h. Solvent removal followed by purification via column chromatography (silica gel,

CH_2Cl_2/hexanes 1:1) afforded **215** (20 mg, 85%) as a white solid. Mp 225 °C (dec.), lit. 218 °C (dec.). Spectra data for compound **215** were consistent with that reported, see: K. Campbell et al., *Angew. Chem. Int. Ed.* **2004**, *43*, 5967-5971.

***trans*–$(PPh_3)_2Pt(C{\equiv}C–p–CH_3–C_6H_4)_2$ (216)**

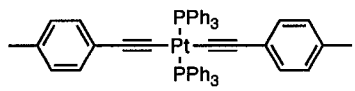

216

Trimethylsilylethynyltoluene **217** (86 mg, 0.45 mmol) was deprotected as described in general procedure A for 1 h. The resulting deprotected alkyne was added to a degassed solution of *cis*-$PtCl_2(PPh_3)_2$ **218** (84 mg, 0.11 mmol) in Et_2NH (50 mL). A catalytic amount of CuI (5 mg, 0.03 mmol) was added and the mixture was stirred at rt under N_2 for 48 h. Work-up proceeded according to the general procedure C and precipitation from a CH_2Cl_2 solution with Et_2O afforded **216** (82 mg, 78%) as a yellow solid. Mp 215 °C (dec.). R_f = 0.69 (CH_2Cl_2/hexanes 2:1, alumina). IR (CH_2Cl_2, cast) 3055, 2110 cm^{-1}; ^1H NMR (400 MHz, $CDCl_3$) δ 7.84–7.74 (m, 12H), 7.41–7.33 (m, 18H), 6.72 (d, J = 8.0 Hz, 4H), 6.19 (d, J = 8.0 Hz, 4H), 2.17 (s, 6H); ^{13}C {^1H} NMR (100 MHz, $CDCl_3$) δ 135.0 (t, J_{C-P}=6 Hz), 134.0, 131.4 (t, $^1J_{C-P}$= 29 Hz), 130.6, 130.2, 127.6 (t, J_{C-P}=5.3 Hz), 125.5, 113.1, 109.3, 21.1; ^{31}P {^1H} NMR (162 MHz, $CDCl_3$) δ 19.7 (pseudo–t, $^1J_{P-Pt}$ = 2660 Hz).

Single crystals of **216** for X–ray crystallography were grown by layering a CH_2Cl_2 solution of **216** with Et_2O and allowing slow diffusion at 4 °C. X–ray crystallographic data for **216**: $C_{54}H_{44}P_2Pt$ (formula weight 949.92) crystallized in the monoclinic space group $P2_1/n$ (an alternate setting of $P2_1/c$ [No. 14]) with a = 13.6022(8) Å, b = 8.5341(5)

Å, c = 18.0885(11) Å, β = 90.4470(10)°; V = 2099.7(2) Å^3; Z = 2; ρ_{calcd} = 1.502 g cm^{-3}; μ = 3.455 mm^{-1}; T = –80 °C; $R_1(F)$ = 0.0250 (7335 reflections with $F_o^2 \geq 2\sigma(F_o^2)$, and $wR_2(F_o^2 \geq -3\sigma(F_o^2))$ = 0.0736 for all 15514 unique data.

cis–(_R_-PROPHOS)Pt(C≡C–Si(_i_-Pr)$_3$)$_2$ (223)

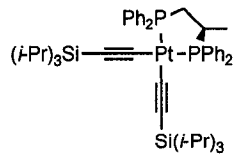

223

(_R_)-1,2-Bis(diphenylphosphino)propane **219** (9.3 mg, 0.022 mmol) was added to a solution of **213** (20 mg, 0.019 mmol) in dry CH_2Cl_2 (10 mL). The mixture was stirred at rt for 5 h. Solvent removal followed by purification via gradient column chromatography (silica gel, CH_2Cl_2/hexanes 1:1 to CH_2Cl_2) afforded **223** (15 mg, 81%) as a white solid. Mp 265–269 °C. R_f = 0.56 (CH_2Cl_2/hexanes 2:1). UV–vis (CH_2Cl_2) λ_{max} (ε) 261 (18100), 294 (10900) nm; IR (CH_2Cl_2, cast) 3055, 2938, 2860, 2049 cm^{-1}; ^{1}H NMR (400 MHz, $CDCl_3$) δ 8.21–8.16 (m, 2H), 8.08–8.03 (m, 2H), 7.86–7.71 (m, 2H), 7.77–7.72 (m, 2H), 7.47–7.28 (m, 12H), 2.97–2.81 (m, 1H), 2.56–2.31 (m, 2H), 0.93–0.78 (m, 45H); ^{13}C {^{1}H, ^{31}P} NMR (100 MHz, $CDCl_3$) δ 135.5, 134.2, 133.4, 133.3, 132.2, 132.1, 131.4, 131.2, 131.0, 130.9, 130.8, 130.54, 130.49, 130.2, 129.1, 128.7, 128.6, 128.5, 128.3, 128.2, 125.7, 124.7, 109.8, 109.0, 36.6, 34.3, 19.05, 19.04, 19.0 (br), 16.2, 11.98, 11.95; ^{31}P {^{1}H} NMR (162 MHz, $CDCl_3$) δ 51.3 (pseudo–dt, $^3J_{P-P}$ = 6.9 Hz, $^1J_{P-Pt}$ = 2206 Hz), 34.2 (pseudo–dt, $^3J_{P-P}$ = 7.3 Hz, $^1J_{P-Pt}$ = 2191 Hz). ESI HRMS ($ClCH_2CH_2Cl$, AgOTf added) calcd. for $C_{49}H_{68}P_2PtSi_2$•Ag ([M + Ag]$^+$) 1076.3034, found 1076.3036. Anal. calcd. for $C_{49}H_{68}P_2PtSi_2$: C, 60.66; H, 7.06. Found: C, 60.51; H, 7.13.

***cis*–(*S*,*S*-BDPP)Pt(C≡C–Si(*i*-Pr)$_3$)$_2$ (224)**

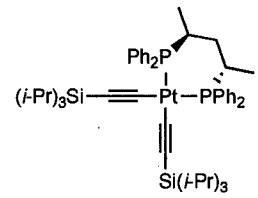

224

(2*S*,4*S*)-2,4-Bis(diphenylphosphino)pentane **220** (13 mg, 0.031 mmol) was added to a solution of **213** (33 mg, 0.031 mmol) in dry CH_2Cl_2 (10 mL). The mixture was stirred at rt for 19 h. Solvent removal followed by purification via gradient column chromatography (silica gel, CH_2Cl_2/hexanes 1:1 to CH_2Cl_2) afforded **224** (21 mg, 68%) as a white solid. Mp 260–263 °C. R_f = 0.51 (CH_2Cl_2/hexanes 2:1). UV–vis (CH_2Cl_2) λ_{max} (ε) 259 (18400), 293 (12000) nm; IR (CH_2Cl_2, cast) 2923, 2055 cm^{-1}; ^{1}H NMR (400 MHz, $CDCl_3$) δ 8.06–8.03 (m, 4H), 7.73–7.69 (m, 4H), 7.42–7.41 (m, 6H), 7.33–7.22 (m, 6H), 2.68 (br, s, 2H), 2.07 (app tt, J_{H-P} = 20 Hz, J_{H-H} = 5.7 Hz, 2H), 0.97 (d, J = 7.0 Hz, 3H) 0.94 (d, J = 7.0 Hz, 3H), 0.81 (d, J = 7.2 Hz, 18H), 0.80 (d, J = 7.2 Hz, 18H), 0.69 (septet, J = 7.1 Hz, 6H); ^{13}C {^{1}H} NMR (100 MHz, $CDCl_3$) δ 134.9 (pseudo–t, J_{C-P} = 5.4 Hz), 134.0 (pseudo–t, J_{C-P} = 4.9 Hz), 131.0 (pseudo–t, J_{C-P} = 19 Hz), 130.5 (pseudo–t, J_{C-P} = 19 Hz), 130.0 (d, J_{C-P} = 9.5 Hz), 129.8, 129.3 (pseudo–t, J_{C-P} = 20 Hz), 128.0 (pseudo–t, J_{C-P} = 5 Hz), 127.5 (pseudo–t, J_{C-P} = 5 Hz), 124.9 (dd, $^2J_{C-P}$ = 136 Hz (*trans*), $^2J_{C-P}$ = 20 Hz (*cis*)), 107.1 (pseudo–d, $^3J_{C-P}$ = 28 Hz (*trans*)), 36.6 (pseudo–t, $^1J_{C-P}$ = 4.2 Hz), 25.3–24.6 (m), 18.8, 17.3 (pseudo–t, $^2J_{C-P}$ = 7.0 Hz), 11.7; ^{31}P {^{1}H} NMR (162 MHz, $CDCl_3$) δ 5.7 (pseudo–t, $^1J_{P-Pt}$ = 2134 Hz). ESI HRMS ($ClCH_2CH_2Cl$, AgOTf added) calcd. for $C_{51}H_{72}P_2PtSi_2$•Ag ([M + Ag]$^+$) 1104.3347, found 1104.3345. Anal. calcd. for $C_{51}H_{72}P_2PtSi_2$: C, 61.36; H, 7.27. Found: C, 61.52; H, 7.43.

***cis*–(*R,R*-Me-DUPHOS)Pt(C≡C–Si(*i*-Pr)$_3$)$_2$ (225)**

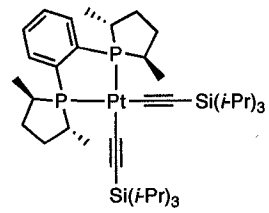

225

1,2-Bis[(2*R*,5*R*)-2,5-dimethylphospholano]benzene **221** (8.9 mg, 0.029 mmol) was added to a solution of **213** (31 mg, 0.029 mmol) in dry CH_2Cl_2 (5 mL). The mixture was stirred at rt for 48 h. Solvent removal followed by purification via gradient column chromatography (silica gel, CH_2Cl_2/hexanes 1:2 to CH_2Cl_2/hexanes 1:1) afforded **225** (22 mg, 88%) as a white solid. Mp 193–197 °C. R_f = 0.72 (CH_2Cl_2/hexanes 2:1). UV–vis (CH_2Cl_2) λ_{max} (ε) 268 (13600), 301 (11000) nm; IR (CH_2Cl_2, cast) 2938, 2860 cm^{-1}; ^1H NMR (400 MHz, $CDCl_3$) δ 7.67–7.63 (m, 2H), 7.56–7.52 (m, 2H), 3.50–3.38 (m, 2H), 2.74–2.61 (m, 2H), 2.36–2.16 (m, 6H), 1.73–1.62 (m, 2H), 1.48 (d, J = 7.0 Hz, 3H), 1.44 (d, J = 7.0 Hz, 3H), 1.12 (d, J = 3.0 Hz, 18H), 1.11 (d, J = 2.9 Hz, 18H), 1.08–0.99 (m, 6H), 0.86 (d, J = 7.2 Hz, 3H), 0.83 (d, J = 7.2 Hz, 3H); ^{13}C {^1H} NMR (100 MHz, $CDCl_3$) δ 143.8 (pseudo–t, J_{C-P}=36 Hz), 132.8 (pseudo–t, J_{C-P}=8.2 Hz), 130.9 (br), 128.9 (dd, $^2J_{C-P}$ = 133 Hz (*trans*), $^2J_{C-P}$ = 14 Hz (*cis*)), 109.2 (d, $^3J_{C-P}$ = 29 Hz (*trans*)), 40.8 (d, J_{C-P} = 34 Hz), 37.3–36.4 (m), 36.1, 19.04, 19.02, 17.7–17.3 (m), 14.1, 12.0; ^{31}P {^1H} NMR (162 MHz, $CDCl_3$) δ 65.3 (pseudo–t, $^1J_{P-Pt}$ = 2134 Hz). ESI HRMS ($ClCH_2CH_2Cl$) calcd. for $C_{40}H_{71}P_2PtSi_2$ ([M + H]$^+$) 864.4217, found 864.4220.

***cis*-(*R,R*-NORPHOS)Pt(C≡C-Si(*i*-Pr$_3$))$_2$ (226)**

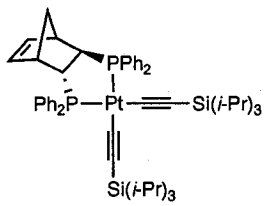

226

(*2R,3R*)-2,3-Bis(diphenylphosphino)bicyclo[2.2.1]hept-5-ene **222** (13 mg, 0.029 mmol) was added to a solution of **213** (23 mg, 0.022 mmol) in dry CH_2Cl_2 (10 mL). The mixture was stirred at rt for 14 h. Solvent removal followed by purification via gradient column chromatography (silica gel, CH_2Cl_2/hexanes 1:2 to CH_2Cl_2/hexanes 1:1) afforded **226** (20 mg, 90%) as a white solid. Mp 284 °C (dec.). R_f = 0.53 (CH_2Cl_2/hexanes 2:1). UV–vis (CH_2Cl_2) λ_{max} (ε) 257 (22100), 294 (11500) nm; IR (CH_2Cl_2, cast) 2938, 2860, 2049 cm^{-1}; ^{1}H NMR (400 MHz, $CDCl_3$) δ 8.10–8.05 (m, 2H), 7.96–7.85 (m, 4H), 7.79–7.70 (m, 2H), 7.55–7.35 (m, 12H), 6.14 (dd, J = 5.5, 3.2 Hz, 1H), 5.43 (dd, J = 5.5, 2.8 Hz, 1H), 3.09 (s, br, 1H), 2.96–2.88 (m, 1H), 2.82 (s, br, 1H), 2.44–2.36 (m, 1H), 1.86 (app d, J = 7.1 Hz, 1H), 1.16 (app d, J = 8.7 Hz, 1H), 0.91–0.81 (m, 42H); ^{13}C {^{1}H} NMR (100 MHz, $CDCl_3$) δ 140.2 (d, J_{C-P} = 7.0 Hz), 137.1 (d, J_{C-P} = 13 Hz), 136.6 (d, J_{C-P} = 12 Hz), 133.0 (d, J_{C-P} = 9.1 Hz), 132.8 (d, J_{C-P} = 9.1 Hz), 131.5 (d, J_{C-P} = 2.5 Hz), 131.5 (d, J_{C-P} = 2.1 Hz), 131.4 (d, J_{C-P} = 2.3 Hz), 131.0, 130.7, 130.5, 130.2, 130.1 (br), 128.4 (d, J_{C-P} = 11 Hz), 128.3 (d, J_{C-P} = 6.6 Hz), 128.2 (d, J_{C-P} = 6.4 Hz), 127.8 (d, J_{C-P} = 11 Hz), 126.0 (dd, $^2J_{C-P}$ = 169 Hz (*trans*), $^2J_{C-P}$ = 48 Hz (*cis*)), 122.3 (dd, $^2J_{C-P}$ = 135 Hz (*trans*), $^2J_{C-P}$ = 15 Hz (*cis*)), 107.4 (d, $^3J_{C-P}$ = 2.9 Hz (*trans*)), 107.1 (d, $^3J_{C-P}$ = 2.8 Hz (*trans*)), 52.0 (d, J_{C-P} = 8.7 Hz), 50.4 (dd, $^1J_{C-P}$ = 30 Hz, $^2J_{C-P}$ = 18 Hz), 48.5 (dd, $^1J_{C-P}$ = 36 Hz, $^2J_{C-P}$ = 20 Hz), 42.4 (dd, $^2J_{C-P}$ = 11 Hz, $^3J_{C-P}$ = 7.2 Hz), 39.9 (dd, $^2J_{C-P}$ = 13 Hz, $^3J_{C-P}$ = 6.4 Hz), 29.6,

18.95, 18.92, 18.88, 18.85, 11.8; ^{31}P {^{1}H} NMR (162 MHz, $CDCl_3$) δ 11.2 (pseudo–dt, $^{3}J_{P-P}$ = 15 Hz, $^{1}J_{P-Pt}$ = 2213 Hz), 10.3 (pseudo–dt, $^{3}J_{P-P}$ = 15 Hz, $^{1}J_{P-Pt}$ = 2211 Hz). ESI HRMS ($ClCH_2CH_2Cl$, AgOTf added) calcd. for $C_{53}H_{70}P_2PtSi_2$•Ag ([M + Ag]$^+$) 1126.3190, found 1126.3192. Anal. calcd. for $C_{53}H_{70}P_2PtSi_2$: C, 62.39; H, 6.92. Found: C, 62.14; H, 6.96.

***cis*–(dppee)Pt(C≡C–*p*–CH_3–C_6H_4)$_2$ (227)**

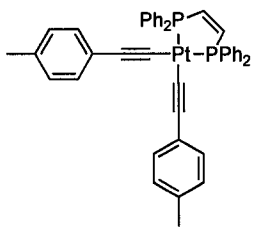

227

cis-1,2-Bis(diphenylphosphino)ethylene **200** (14 mg, 0.036 mmol) was added to a solution of **216** (27 mg, 0.028 mmol) in dry CH_2Cl_2 (10 mL). The mixture was stirred at rt for 21 h. Solvent removal followed by purification via gradient column chromatography (alumina, CH_2Cl_2/hexanes 1:1 to CH_2Cl_2) afforded **227** (11 mg, 48%) as a yellow solid. Mp 185 °C (dec.). R_f = 0.44 (CH_2Cl_2/hexanes 2:1). IR (CH_2Cl_2, cast) 3053, 2115 cm^{-1}; ^{1}H NMR (400 MHz, $CDCl_3$) δ 7.85–7.80 (m, 8H), 7.53–7.29 (m, 14H), 7.12 (d, J = 8.0 Hz, 4H), 6.92 (d, J = 7.8 Hz, 4H), 2.23 (s, 6H); ^{13}C {^{1}H} NMR (100 MHz, $CDCl_3$) δ 146.6 (dd, $^{1}J_{C-P}$=47 Hz, $^{2}J_{C-P}$=27 Hz), 134.6 (br), 133.5–133.2 (m), 131.1 (br), 129.9 (d, $^{1}J_{C-P}$ = 58 Hz), 128.7–128.6 (m), 128.1 (br), 125.2, 111.6 (d, $^{3}J_{C-P}$ = 32 Hz (*trans*)), 101.5 (dd, $^{2}J_{C-P}$ = 150 Hz (*trans*), $^{2}J_{C-P}$ = 15 Hz (*cis*)), 21.2; ^{31}P {^{1}H} NMR (162 MHz, $CDCl_3$) δ 53.1 (pseudo–t, $^{1}J_{P-Pt}$ = 2276 Hz). ESI HRMS ($ClCH_2CH_2Cl$, AgOTf added) calcd. for $C_{44}H_{36}P_2Pt$•Ag ([M + Ag]$^+$) 928.0991, found 928.0991.

***cis*-(*S*,*S*-CHIRAPHOS)Pt(C≡C-*p*-CH_3-C_6H_4)$_2$ (228)**

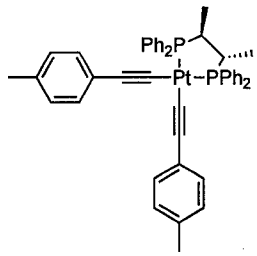

228

(2*S*,3*S*)-Bis(diphenylphosphino)butane **201** (11 mg, 0.026 mmol) was added to a solution of **216** (22 mg, 0.024 mmol) in dry CH_2Cl_2 (10 mL). The mixture was stirred at rt for 19 h. Solvent removal followed by purification via gradient column chromatography (alumina, CH_2Cl_2/hexanes 1:1 to CH_2Cl_2) afforded **228** (10 mg, 49%) as a yellow solid. Mp 143–147 °C. R_f = 0.30 (CH_2Cl_2/hexanes 2:1). UV–vis (CH_2Cl_2) λ_{max} (ε) 259 (46300), 318 (19500) nm; IR (CH_2Cl_2, cast) 2923, 2113 cm^{-1}; ^1H NMR (400 MHz, $CDCl_3$) δ 7.88–7.80 (m, 8H), 7.48–7.35 (m, 12H), 6.97 (d, J = 8.1 Hz, 4H), 6.86 (d, J = 8.2 Hz, 4H), 2.40 (s, br, 2H), 2.20 (s, 6H), 1.03–1.01 (m, 6H); ^{13}C {^1H} NMR (100 MHz, $CDCl_3$) δ 136.4 (pseudo–t, J_{C-P} = 6.1 Hz), 134.3, 132.9 (pseudo–t, J_{C-P} = 4.5 Hz), 131.4, 131.1 (pseudo–t, J_{C-P} = 4.6 Hz), 130.5 (br), 128.9 (d, J_{C-P} = 2.5 Hz), 128.3 (pseudo–t, J_{C-P} = 5.5 Hz), 128.1 (pseudo–t, J_{C-P} = 5.5 Hz), 128.0, 127.8 (d, J_{C-P} = 3.5 Hz), 127.2 (d, J_{C-P} = 3.5 Hz), 125.5, 110.3 (dd, $^3J_{C-P}$ = 35 Hz (*trans*), $^3J_{C-P}$ = 2.9 Hz (*cis*)), 105.3 (dd, $^2J_{C-P}$ = 145 Hz (*trans*), $^2J_{C-P}$ = 16 Hz (*cis*)), 37.2 (pseudo–t, $^1J_{C-P}$ = 25 Hz), 21.1, 14.9 (pseudo–t, $^2J_{C-P}$ = 5.6 Hz); ^{31}P {^1H} NMR (162 MHz, $CDCl_3$) δ 44.2 (pseudo–t, $^1J_{P-Pt}$ = 2234 Hz). ESI HRMS ($ClCH_2CH_2Cl$) calcd. for $C_{46}H_{43}P_2Pt$ ([M + H]$^+$) 852.2482, found 852.2478. Anal. calcd. for $C_{46}H_{42}P_2Pt$: C, 64.86; H, 4.97. Found: C, 64.96; H, 5.12.

***cis*-(*R*-PROPHOS)Pt(C≡C-*p*-CH_3-C_6H_4)$_2$ (229)**

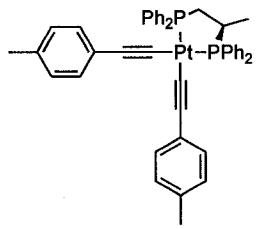

229

(*R*)-1,2-Bis(diphenylphosphino)propane **219** (11 mg, 0.027 mmol) was added to a solution of **216** (22 mg, 0.023 mmol) in dry CH_2Cl_2 (10 mL). The mixture was stirred at rt for 3 h. Solvent removal followed by purification via gradient column chromatography (alumina, hexanes to CH_2Cl_2/hexanes 1:1) afforded **229** (16 mg, 83%) as a yellow solid. Mp 134–137 °C. R_f = 0.39 (CH_2Cl_2/hexanes 2:1). UV–vis (CH_2Cl_2) λ_{max} (ε) 259 (52700), 319 (23500) nm; IR (CH_2Cl_2, cast) 3053, 2923, 2114, 1505, 1436 cm^{-1}; ^1H NMR (400 MHz, $CDCl_3$) δ 8.20–8.15 (m, 2H), 7.99–7.90 (m, 4H), 7.83–7.78 (m, 2H), 7.46–7.30 (m, 12H), 7.08 (d, J = 8.1 Hz, 2H), 7.01 (d, J = 8.1 Hz, 2H), 6.91 (d, J = 7.9 Hz, 2H), 6.89 (d, J = 8.0 Hz, 2H), 3.03–2.93 (m, 1H), 2.57–2.40 (m, 2H), 2.24 (s, 3H), 2.23 (s, 3H), 0.95 (dd, J = 13.7, 7.1 Hz, 3H); ^{13}C {^1H} NMR (100 MHz, $CDCl_3$) δ 135.6 (d, J_{C-P} = 12 Hz), 134.5 (d, J_{C-P} = 3.7 Hz), 133.8 (d, J_{C-P} = 11 Hz), 133.2 (d, J_{C-P} = 11 Hz), 133.1 (d, J_{C-P} = 8.7 Hz), 131.2 (d, J_{C-P} = 3.9 Hz), 130.9–130.6 (m), 130.1, 128.9, 128.6, 128.5, 128.4, 128.1, 128.0, 127.99, 127.89, 127.4, 125.4, 111.8 (dd, $^2J_{C-P}$ = 85 Hz (*trans*), $^2J_{C-P}$ = 3.0 Hz (*cis*)), 111.5 (dd, $^2J_{C-P}$ = 86 Hz (*trans*), $^2J_{C-P}$ = 2.7 Hz (*cis*)), 103.6 (d, $^3J_{C-P}$ = 15 Hz (*trans*)), 35.8 (dd, ^1J = 35 Hz, ^2J = 17 Hz), 34.2 (dd, ^1J = 34 Hz, ^2J = 13 Hz), 21.2, 15.9 (d, J = 10 Hz); ^{31}P {^1H} NMR (162 MHz, $CDCl_3$) δ 51.7 (pseudo–dt, $^3J_{P-P}$ = 8.4 Hz, $^1J_{P-Pt}$ = 2285 Hz), 34.3 (pseudo–t, $^3J_{P-P}$ = 8.4 Hz, $^1J_{P-Pt}$ = 2259 Hz). ESI HRMS ($ClCH_2CH_2Cl$, AgOTf

added) calcd. for $C_{45}H_{40}P_2Pt•Ag$ ([M + Ag]$^+$) 944.1304, found 944.1304. Anal. calcd. for $C_{45}H_{40}P_2Pt$: C, 64.51; H, 4.81. Found: C, 64.23; H, 5.05.

***cis*-(*S*,*S*-BDPP)Pt(C≡C-*p*-CH_3-C_6H_4)$_2$ (230/239)**

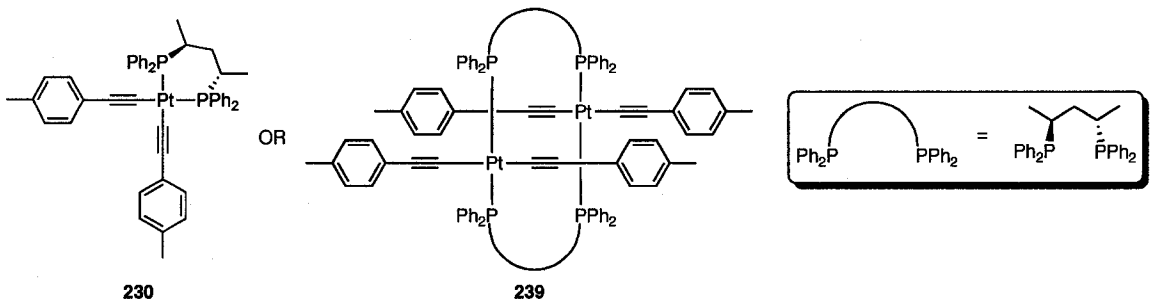

230 239

(2*S*,4*S*)-2,4-Bis(diphenylphosphino)pentane **220** (12 mg, 0.028 mmol) was added to a solution of **216** (25 mg, 0.026 mmol) in dry CH_2Cl_2 (10 mL). The mixture was stirred at rt for 19 h. Solvent removal followed by purification via gradient column chromatography (alumina, CH_2Cl_2/hexanes 1:1 to CH_2Cl_2) afforded **230/239** (20 mg, 89%) as a yellow solid. Mp 178–181 °C. R_f = 0.70 (CH_2Cl_2/hexanes 2:1). UV–vis (CH_2Cl_2) λ_{max} (ε) 268 (35600), 290 (21400), 349 (23000) nm; IR (CH_2Cl_2, cast) 2923, 2108, 1505 cm^{-1}; ^{1}H NMR (400 MHz, $CDCl_3$) δ 7.96–7.92 (m, 4H), 7.56–7.52 (m, 4H), 7.33–7.15 (m, 12H), 6.72 (d, J = 7.8 Hz, 4H), 6.35 (d, J = 8.0 Hz, 4H), 3.67 (s, br, 2H), 2.97 (s, br, 2H), 2.21 (s, 6H), 1.32 (d, J = 7.4 Hz, 3H), 1.29 (d, J = 7.5 Hz, 3H); ^{13}C {^{1}H} NMR (100 MHz, $CDCl_3$) δ 136.0 (pseudo–t, J_{C-P} = 6.1 Hz), 133.6, 132.7 (pseudo–t, $^1J_{C-P}$ = 26 Hz), 132.3 (pseudo–t, J_{C-P} = 4.6 Hz), 130.6, 129.9, 128.9, 128.2, 127.8, 127.6 (pseudo–t, J_{C-P} = 4.5 Hz), 127.2 (pseudo–t, J_{C-P} = 5.2 Hz), 126.1, 111.9, 107.9 (d, $^3J_{C-P}$ = 30 Hz (*trans*)), 37.4 (m), 28.4 (m), 21.1, 14.2; ^{31}P {^{1}H} NMR (162 MHz, $CDCl_3$) δ 26.9 (pseudo–t, $^1J_{P-Pt}$ = 2585 Hz). ESI HRMS ($ClCH_2CH_2Cl$, AgOTf added) calcd. for

$C_{94}H_{88}P_4Pt_2$•Ag ([2M + Ag]$^+$) 1837.4183, found 1837.4183. Anal. calcd. for $C_{47}H_{44}P_2Pt$: C, 65.19; H, 5.12. Found: C, 65.37; H, 5.33.

***cis*-(*R,R*-Me-DUPHOS)Pt(C≡C-*p*-CH_3-C_6H_4)$_2$ (231)**

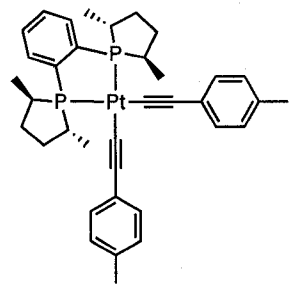

231

1,2-Bis[(2*R*,5*R*)-2,5-dimethylphospholano]benzene **221** (8.3 mg, 0.027 mmol) was added to a solution of **216** (26 mg, 0.027 mmol) in dry CH_2Cl_2 (10 mL). The mixture was stirred at rt for 16 h. Solvent removal followed by purification via column chromatography (alumina, hexanes) afforded **231** (16 mg, 81%) as a yellow solid. Mp 199 °C (dec.). R_f = 0.44 (CH_2Cl_2/hexanes 2:1). UV–vis (CH_2Cl_2) λ_{max} (ε) 263 (40900), 325 (16900) nm; IR (CH_2Cl_2, cast) 2923, 2108, 1504 cm^{-1}; ^{1}H NMR (400 MHz, $CDCl_3$) δ 7.72–7.67 (m, 2H), 7.60–7.57 (m, 2H), 7.35 (d, *J* = 8.1 Hz, 4H), 7.02 (d, *J* = 8.4, 4H), 3.54–3.38 (m, 2H), 2.81–2.71 (m, 2H), 2.40–2.23 (m, 4H), 2.30 (s, 6H), 2.15–2.05 (m, 2H), 1.76–1.65 (m, 2H), 1.54 (d, *J* = 7.0 Hz, 3H), 1.49 (d, *J* = 7.0 Hz, 3H), 0.88 (d, *J* = 7.2 Hz, 3H), 0.84 (d, *J* = 7.2 Hz, 3H); ^{13}C {^{1}H} NMR (100 MHz, $CDCl_3$) δ 143.6 (pseudo–t, J_{C-P} = 36 Hz), 134.6, 132.8 (pseudo–t, J_{C-P} = 8.3 Hz), 131.2 (br), 128.3, 125.4, 111.9 (d, $^3J_{C-P}$ = 35 Hz (*trans*)), 106.3 (dd, $^2J_{C-P}$ = 143 Hz (*trans*), $^2J_{C-P}$ = 15 Hz (*cis*)), 40.5 (d, J_{C-P} = 34 Hz), 37.5–36.9 (m), 36.3 (br), 21.2, 17.5 (pseudo–t, J_{C-P} = 3.5 Hz), 13.9; ^{31}P {^{1}H} NMR (162 MHz, $CDCl_3$) δ 66.4 (pseudo–t, $^1J_{P-Pt}$ = 2206 Hz). EIMS *m/z* 731.2 (M^+, 70), 501.1 ([M–

2(C≡C–*p*–Me–C_6H_4)]$^+$, 100); HRMS calcd. for $C_{36}H_{42}P_2Pt$ (M^+) 731.2410, found 731.2419.

Single crystals for X–ray crystallography were grown by layering a CH_2Cl_2 solution of **231** with acetone and allowing evaporation at rt. X–ray crystallographic data for **231**: $C_{36}H_{42}P_2Pt{\bullet}CH_2Cl_2$ (formula weight 816.65) crystallized in the orthorhombic space group $P2_12_12_1$ (No. 19) with a = 9.8524(9) Å, b = 18.9860(18) Å, c = 19.5240(18) Å; V = 3652.1(6) Å^3; Z = 4; ρ_{calcd} = 1.485 g cm^{-3}; μ = 4.099 mm^{-1}; T = –80 °C; $R_1(F)$ = 0.0203 (7186 reflections with $F_o^2 \geq 2\sigma(F_o^2)$, and $wR_2(F_o^2 \geq -3\sigma(F_o^2))$ = 0.0573 for all 28887 unique data.

***cis*–(*R,R*-NORPHOS)Pt(C≡C–*p*–CH_3–C_6H_4)$_2$ (232)**

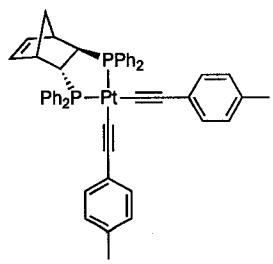

232

(2*R*,3*R*)-2,3-Bis(diphenylphosphino)bicyclo[2.2.1]hept-5-ene **222** (13 mg, 0.028 mmol) was added to a solution of **216** (28 mg, 0.030 mmol) in dry CH_2Cl_2 (10 mL). The mixture was stirred at rt for 36 h. Solvent removal followed by purification via gradient column chromatography (alumina, CH_2Cl_2/hexanes 2:1 to CH_2Cl_2) afforded **232** (18 mg, 72%) as a yellow solid. Mp 230 °C (dec.). R_f = 0.35 (CH_2Cl_2/hexanes 2:1). UV–vis (CH_2Cl_2) λ_{max} (ε) 257 (46300), 317 (18400) nm; IR (CH_2Cl_2, cast) 2923, 2113 cm^{-1}; ^{1}H NMR (400 MHz, $CDCl_3$) δ 8.09–8.04 (m, 2H), 7.98–7.93 (m, 2H), 7.83–7.73 (m, 4H), 7.56–7.37 (m, 12H), 7.05 (d, J = 8.1, 4H), 6.89 (d, J = 7.7 Hz, 4H), 6.20 (m, 1H), 5.48 (m, 1H), 3.15 (s,

br, 1H), 3.13–3.03 (m, 1H), 2.87 (s, br, 1H), 2.59–2.49 (m, 1H), 2.23 (s, 6H), 1.89 (br d, J = 7.6 Hz, 1H), 1.10 (br d, J = 8.6 Hz, 1H); ^{13}C {^{1}H, ^{31}P} NMR (100 MHz, $CDCl_3$) δ 140.1, 137.2, 136.5, 134.4, 134.4, 132.8, 132.7, 131.8, 131.7, 131.6, 131.2, 131.1, 130.4, 130.3, 128.7, 128.32, 128.27, 128.09, 128.0, 127.1, 125.5, 125.2, 109.88, 109.76, 101.5, 52.2, 49.6, 48.1, 42.5, 40.0, 21.4, 19.9; ^{31}P {^{1}H} NMR (162 MHz, $CDCl_3$) δ 12.0 (pseudo–dt, $^{3}J_{P-P}$ = 14 Hz, $^{1}J_{P-Pt}$ = 2280 Hz), 11.2 (pseudo–dt, $^{3}J_{P-P}$ = 14 Hz, $^{1}J_{P-Pt}$ = 2280 Hz). ESI HRMS ($ClCH_2CH_2Cl$) calcd. for $C_{49}H_{43}P_2Pt$ ([M + H]$^+$) 888.2488, found 888.2487. Anal. calcd. for $C_{49}H_{42}P_2Pt$: C, 66.28; H, 4.77. Found: C, 66.17; H, 4.82.

***cis*–(*S*,*S*-CHIRAPHOS)Pt(C≡C–C≡C–*p*–C_6H_5)$_2$ (234)**

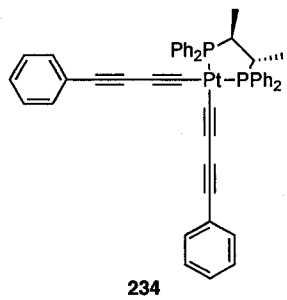

234

(2*S*,3*S*)-Bis(diphenylphosphino)butane **201** (11 mg, 0.025 mmol) was added to a solution of **233** (22 mg, 0.023 mmol) in dry CH_2Cl_2 (10 mL). The mixture was stirred at rt for 19 h. Solvent removal followed by purification via gradient column chromatography (silica gel, CH_2Cl_2/hexanes 1:2 to CH_2Cl_2) afforded **234** (15 mg, 75%) as a beige solid. Mp 224 °C (dec.). R_f = 0.40 (CH_2Cl_2/hexanes 2:1). UV–vis (CH_2Cl_2) λ_{max} (ε) 245 (35600), 251 (29500), 274 (53400), 292 (39500), 314 (34600), 337 (33800) nm; IR (CH_2Cl_2, cast) 3055, 2183, 2066 cm^{-1}; ^{1}H NMR (400 MHz, $CDCl_3$) δ 7.82–7.74 (m, 8H), 7.57–7.53 (m, 8H), 7.52–7.43 (m, 4H), 7.43–7.34 (m, 4H), 7.21–7.18 (m, 6H), 2.32 (s, br, 2H), 1.08 (d,

J = 5.4, 3H), 1.05 (d, J = 4.5, 3H); ^{13}C {^1H} NMR (100 MHz, $CDCl_3$) δ 136.4 (pseudo–t, J_{C-P} = 6.2 Hz), 132.7 (pseudo–t, J_{C-P} = 4.3 Hz), 132.1, 131.9, 131.0, 128.6 (pseudo–t, J_{C-P} = 5.2 Hz), 128.4 (pseudo–t, J_{C-P} = 5.4 Hz), 127.8, 127.1, 124.3, 115.0, 114.2, 106.2 (dd, $^2J_{C-P}$ = 144 Hz (*trans*), $^2J_{C-P}$ = 16 Hz (*cis*)), 92.3 (d, $^3J_{C-P}$ = 36 Hz (*trans*)), 78.5, 71.8, 36.0 (pseudo–t, $^1J_{C-P}$ = 25 Hz), 14.2 (pseudo–t, $^2J_{C-P}$ = 5.9 Hz); ^{31}P {^1H} NMR (162 MHz, $CDCl_3$) δ 41.9 (pseudo–t, $^1J_{P-Pt}$ = 2236 Hz). ESI HRMS ($ClCH_2CH_2Cl$) calcd. for $C_{48}H_{38}P_2Pt$•Na ([M + Na]$^+$) 894.1989, found 894.1991.

***cis*–(*S*,*S*-BDP*P*)Pt(C≡C–C≡C–*p*–C_6H_5)$_2$ (235/240)**

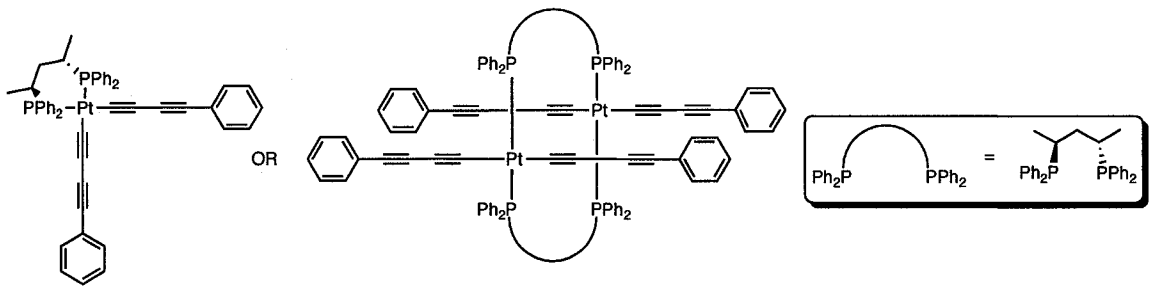

235 **240**

(2*S*,4*S*)-2,4-Bis(diphenylphosphino)pentane **220** (14 mg, 0.033 mmol) was added to a solution of **233** (30 mg, 0.031 mmol) in $CDCl_3$ (3 mL). The mixture was stirred at rt for 19 h. Subsequent to removal of ~90% of the solvent, precipitation by the addition of hexanes afforded **235/240** (18 mg, 66%) as a beige solid after filtration. Mp >155 °C (dec.). R_f = 0.53 (CH_2Cl_2/hexanes 2:1). UV–vis (CH_2Cl_2) λ_{max} (ε) 281 (33000), 302 (26600), 317 (23100), 355 (25200) nm; IR (CH_2Cl_2, cast) 3055, 2180, 2061 cm^{-1}; ^1H NMR (400 MHz, $CDCl_3$) δ 7.90–7.85 (m, 4H), 7.78–7.58 (m, 4H), 7.53–7.33 (m, 20H), 7.24–7.10 (m, 12H), 3.56 (s, br, 2H), 3.07 (s, br, 2H), 1.38 (d, J = 7.5 Hz, 3H), 1.34 (d, J = 7.5 Hz, 3H); ^{13}C {^1H} NMR (100 MHz, $CDCl_3$) δ 135.9 (pseudo–t, J_{C-P} = 5.6 Hz), 135.1

(pseudo–t, J_{C-P} = 6.1 Hz), 132.5 (pseudo–t, J_{C-P} = 4.7 Hz), 132.2–131.9 (m), 130.7 (s, br), 130.6, 129.7, 128.6, 128.5, 128.2–127.9 (m), 126.9, 124.6, 107.7 (d, $^3J_{C-P}$ = 15 Hz (*trans*)), 95.7 (d, $^2J_{C-P}$ = 103 Hz (*trans*)), 79.0, 70.9, 29.1 (m), 14.3; ^{31}P {^{1}H} NMR (162 MHz, $CDCl_3$) δ 26.9 (pseudo–t, $^1J_{P-Pt}$ = 2510 Hz). MALDI MS (DCTB) *m/z* 1771.2 ([2M]$^+$, 100).

***cis*–(*R*,*R*-NORPHOS)Pt(C≡C–C≡C–*p*–C_6H_5)$_2$ (236)**

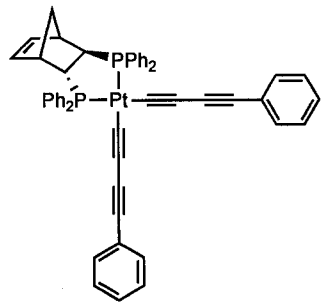

236

(2*R*,3*R*)-2,3-Bis(diphenylphosphino)bicyclo[2.2.1]hept-5-ene **222** (17 mg, 0.037 mmol) was added to a solution of **233** (33 mg, 0.034 mmol) in $CDCl_3$ (1 mL). The mixture was stirred at rt for 14 h. Solvent removal followed by purification via gradient column chromatography (silica gel, CH_2Cl_2/hexanes 2:1 to CH_2Cl_2) afforded **236** (15 mg, 49%) as a beige solid. Mp >240 °C (dec.). R_f = 0.38 (CH_2Cl_2/hexanes 2:1). UV–vis (CH_2Cl_2) λ_{max} (ε) 263 (87800) 273 (108000), 292 (83800), 314 (71000), 337 (65700) nm; IR (CH_2Cl_2, cast) 2924, 2182, 2068 cm^{-1}; ^{1}H NMR (400 MHz, $CDCl_3$) δ 8.02–7.96 (m, 2H), 7.91–7.85 (m, 2H), 7.81–7.69 (m, 4H), 7.61–7.41 (m, 12H), 7.38–7.34 (m, 4H), 7.21–7.18 (m, 6H), 6.19 (dd, *J* = 5.3, 3.5 Hz, 1H), 5.45 (dd, *J* = 5.2, 2.5 Hz, 1H), 3.14 (s, br, 1H), 3.09–2.98 (m, 1H), 2.87 (s, br, 1H), 2.85–2.44 (m, 1H), 1.88 (d, br, *J* = 10 Hz, 1H), 1.02 (d, *J* = 8.4 Hz, 1H); ^{13}C {^{1}H} NMR (100 MHz, $CDCl_3$) δ 140.0 (d, J_{C-P} = 7.4 Hz), 136.9 (d, J_{C-P} =

12 Hz), 136.2 (d, J_{C-P} = 12 Hz), 132.6 (d, J_{C-P} = 7.0 Hz), 132.5 (d, J_{C-P} = 7.0 Hz), 132.1–132.5 (m), 131.5 (br), 130.9 (br), 129.3, 129.1, 128.9 (d, J_{C-P} = 11 Hz), 128.5 (d, J_{C-P} = 5.4 Hz), 128.4 (d, J_{C-P} = 5.4 Hz), 128.2 (d, J_{C-P} = 11 Hz), 127.8, 126.6 (d, J_{C-P} = 51 Hz), 124.6 (d, J_{C-P} = 52 Hz), 124.2, 102.2 (dd, $^2J_{C-P}$ = 144 Hz (*trans*), $^2J_{C-P}$ = 6.9 Hz (*cis*)), 102.0 (dd, $^2J_{C-P}$ = 144 Hz (*trans*), $^2J_{C-P}$ = 7.0 Hz (*cis*)), 92.2 (dd, $^3J_{C-P}$ = 9.6 Hz (*trans*), $^3J_{C-P}$ = 2.8 Hz (*cis*)), 92.0 (dd, $^3J_{C-P}$ = 9.2 Hz (*trans*), $^3J_{C-P}$ = 2.8 Hz (*cis*)), 78.4, 71.9, 51.9 (d, J_{C-P} = 9.3 Hz), 48.7 (dd, J_{C-P} = 32 Hz, J_{C-P} = 18 Hz), 47.2 (dd, J_{C-P} = 38 Hz, J_{C-P} = 20 Hz), 42.2 (dd, J_{C-P} = 11 Hz, J_{C-P} = 6.8 Hz), 39.7 (dd, J_{C-P} = 13 Hz, J_{C-P} = 6.2 Hz); ^{31}P {^{1}H} NMR (162 MHz, $CDCl_3$) δ 11.3 (pseudo–dt, $^3J_{P-P}$ = 14 Hz, $^1J_{P-Pt}$ = 2294 Hz), 10.6 (pseudo–dt, $^3J_{P-P}$ = 14 Hz, $^1J_{P-Pt}$ = 2294 Hz). ESI HRMS ($ClCH_2CH_2Cl$) calcd. for $C_{51}H_{38}P_2Pt$•Na ($[M + Na]^+$) 930.1994, found 930.1997.

cis–(_S,S_-CHIRAPHOS)Pt(C≡C–C≡C–C≡C–Si(_i_-Pr)$_3$)$_2$ (238)

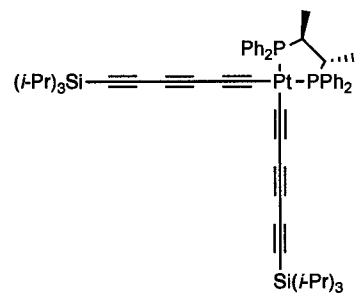

238

(2*S*,3*S*)-Bis(diphenylphosphino)butane **201** (11 mg, 0.025 mmol) was added to a solution of **237** (17 mg, 0.014 mmol) in CD_2Cl_2 (1 mL). The reaction was monitored by ^{31}P NMR spectroscopy and was complete after 30 min. Solvent removal followed by purification via gradient column chromatography (silica gel, CH_2Cl_2/hexanes 1:3 to CH_2Cl_2) afforded **238** (14 mg, 93%) as a beige solid. Mp 139–143 °C. R_f = 0.59 (CH_2Cl_2/hexanes 1:1).

UV–vis (CH_2Cl_2) λ_{max} (ε) 241 (137000), 257 (78300), 272 (64500), 291 (47400), 295 (49900), 315 (21500), 335 (20600), 359 (13500) nm; IR (CH_2Cl_2, cast) 3056, 2943, 2865, 2151, 2021 cm^{-1}; ^1H NMR (400 MHz, $CDCl_3$) δ 7.75–7.65 (m, 8H), 7.57–7.39 (m, 12H), 2.27 (s, br, 2H), 1.06–0.96 (m, 48H); ^{13}C {^1H} NMR (100 MHz, $CDCl_3$) δ 136.3 (pseudo–t, J_{C-P} = 6.1 Hz), 132.5 (pseudo–t, J_{C-P} = 4.3 Hz), 132.2, 131.2, 128.7 (pseudo–t, J_{C-P} = 5.0 Hz), 128.5 (pseudo–t, J_{C-P} = 5.5 Hz), 128.4, 127.1 (d, J_{C-P} = 3.5 Hz), 126.5–126.4 (m), 125.9 (d, J_{C-P} = 4.7 Hz), 103.3 (dd, $^2J_{C-P}$ = 143 Hz (*trans*), $^2J_{C-P}$ = 16 Hz (*cis*)), 92.3 (dd, $^3J_{C-P}$ = 40 Hz (*trans*), $^3J_{C-P}$ = 4.3 Hz (*cis*)), 91.7 (br), 80.1, 64.8, 57.7, 36.1 (pseudo–t, $^1J_{C-P}$ = 25 Hz), 18.5, 14.0 (pseudo–t, $^2J_{C-P}$ = 6.1 Hz), 11.3; ^{31}P {^1H} NMR (162 MHz, $CDCl_3$) δ 41.9 (pseudo–t, $^1J_{P-Pt}$ = 2236 Hz). ESI HRMS ($ClCH_2CH_2Cl$) calcd. for $C_{58}H_{70}P_2PtSi_2$•Na ([M + Na]$^+$) 1102.4031, found 1102.4035.

6.3 Experimental Details for Chapter 3

Compound 300

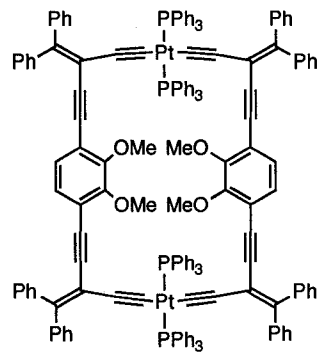

300

Compound **301** (56 mg, 0.069 mmol) was desilylated with TBAF (90 mg, 0.10 mL, 0.34 mmol) in wet THF (10 mL) as described in the general procedure A. After solvent reduction to 2 mL the terminal alkyne was added with Et_2NH (4 mL) to a degassed mixture of Et_2NH (300 mL) and *cis*-$PtCl_2(PPh_3)_2$ (56 mg, 0.071 mmol). CuI (20 mg, 0.1

mmol) was added and the flask was sealed under N_2 according to general procedure C. The solution stirred for 48 h at 55 °C. Et_2O (50 mL) and CH_2Cl_2 (50 mL) were added, the organic phase separated, washed with H_2O (3 × 50 mL), and then with saturated aqueous NH_4Cl (3 × 50 mL). An insoluble yellow solid formed between the organic and aqueous layer which was filtered to give a product tentatively assigned as **300** (9 mg, 10%). Mp >250 °C (dec.). R_f = 0.46 (CH_2Cl_2/hexanes 1:1). IR (CH_2Cl_2, cast) 3058, 2941, 2194, 2092 cm^{-1}; ^1H NMR (400 MHz, $CDCl_3$) δ 7.76–7.71 (m, 24H), 7.30–7.21 (m, 60H), 7.02–6.95 (m, 16H), 6.69 (s, br, 4H), 3.57 (s, br, 12H). ^{31}P {^1H} NMR (162 MHz, $CDCl_3$) δ 19.1 (pseudo–t, $^1J_{P\text{-}Pt}$ = 2634 Hz). MALDI MS (DCTB) *m/z* 2616.8 ([M]$^+$, 100).

Compound 301

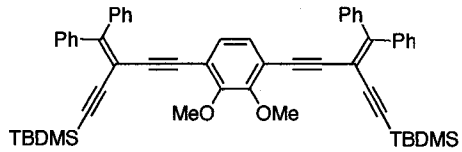

301

Compound **306** (218 mg, 0.659 mmol) was desilylated with TBAF (450 mg, 0.50 mL, 1.7 mmol) in wet THF (10 mL) as described in the general procedure A. After solvent reduction to 2 mL the terminal alkyne was added with Et_2NH (4 mL) to a degassed mixture of dry THF (50 mL), triflate **307** (670 mg, 1.4 mmol), $Pd(PPh_3)_4$ (82 mg, 0.071 mmol) and CuI (0.025 g, 0.13 mmol) according to general procedure B. The solution stirred for 72 h at 50 °C. Et_2O (100 mL) was added, the organic phase separated, washed with saturated aqueous NH_4Cl (3 × 50 mL) and dried ($MgSO_4$). Solvent removal and purification by gradient column chromatography (silica gel, CH_2Cl_2/hexanes 1:3 to 1:1) afforded **301** (320 mg, 59%) as a bright yellow solid. Mp 134–137 °C. R_f = 0.41 (CH_2Cl_2/hexanes 1:1). IR (CH_2Cl_2, cast) 2928, 2142 cm^{-1}; ^1H NMR (400 MHz, $CDCl_3$) δ

7.50–7.46 (m, 8H), 7.36–7.30 (m, 12H), 6.83 (s, br, 2H), 3.77 (s, 6H), 0.88 (s, 18H), 0.079 (s, 12H); ^{13}C {^{1}H} NMR (100 MHz, $CDCl_3$) δ 156.3, 153.8, 140.1, 140.0, 130.3, 130.2, 128.42, 128.38, 127.6, 127.55, 127.48, 118.4, 103.5, 102.1, 96.2, 94.4, 87.9, 61.0, 26.0, 16.6, –4.9. ESI HRMS ($ClCH_2CH_2Cl$) calcd. for $C_{56}H_{58}O_2Si_2$•Na ([M + Na]$^+$) 841.3868, found 841.3869. Anal. calcd. for $C_{56}H_{58}O_2Si_2$: C, 82.10; H, 7.14. Found: C, 81.67; H, 7.24.

1,4-bis(trimethylsilyl)-2,3-dimethoxybenzene (303)

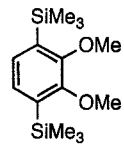

303

Compound **303** was prepared as previously reported[2] and full characterization is reported here. (2,3-Dimethoxyphenyl)trimethylsilane **304** (26.8 g, 0.129 mol) was added to a solution of dry hexanes (50 mL) and TMEDA (25 mL, 19 g, 0.17 mol). The mixture was stirred at 0 °C under N_2. After 30 min, BuLi (2.5 M in hexanes, 62 mL, 0.15 mol) was added and the reaction mixture was allowed to stir 14 h at rt. The solution was then cooled to –78 °C and TMSCl (22 mL, 19 g, 0.17 mol) was added slowly, and the reaction warmed to rt over 6 h. H_2O (125 mL) and hexanes (100 mL) were added, the organic phase separated, washed with H_2O (2 × 100 mL), and dried ($MgSO_4$, charcoal). Solvent removal and purification by column chromatography (silica gel, CH_2Cl_2/hexanes 1:2) afforded **303** (35 g, 96%) as a white solid. Mp 36–40 °C. R_f = 0.62 (CH_2Cl_2/hexanes 1:2). IR (CH_2Cl_2, cast) 2955, 1378 cm^{-1}; ^{1}H NMR (400 MHz, $CDCl_3$) δ 7.18 (s, 2H), 3.89 (s, 6H), 0.36 (s, 18H); ^{13}C {^{1}H} NMR (100 MHz, $CDCl_3$) δ 156.7, 135.8, 129.3, 59.4, –0.5.

EIMS *m/z* 282.1 (M^+, 75), 193.1 ([M–C_3H_9OSi]$^+$, 100); HRMS calcd. for $C_{14}H_{26}O_2Si_2$ (M^+) 282.1471, found 282.1466. Anal. calcd. for $C_{14}H_{26}O_2Si_2$: C, 59.52; H, 9.28. Found: C, 59.45; H, 9.49.

(2,3-dimethoxyphenyl)trimethylsilane (304)

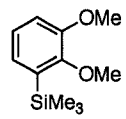

304

Compound **304** was prepared as previously reported[2] and full characterization is reported here. 1,2-Dimethoxybenzene (veratrole, **302**) (20.3 g, 0.147 mol) was added to a solution of dry hexanes (50 mL) and TMEDA (20 mL, 15 g, 0.13 mol). The mixture was stirred at rt under N_2. After 30 min BuLi (2.5 M in hexanes, 64 mL, 0.16 mol) was added and allowed to stir 14 h at rt. The solution was then cooled to –78 °C and TMSCl (22 mL, 19 g, 0.18 mol) was added slowly, and the reaction warmed to rt. H_2O (100 mL) and hexanes (100 mL) were added, the organic phase separated, washed with H_2O (3 × 100 mL), and dried ($MgSO_4$, charcoal). Solvent removal and purification by column chromatography (silica gel, CH_2Cl_2/hexanes 1:1) afforded **304** (28 g, 91%) as a colourless oil. R_f = 0.40 (CH_2Cl_2/hexanes 1:1). IR (CH_2Cl_2, cast) 3061, 2954, 1458 cm^{-1}; ^1H NMR (400 MHz, $CDCl_3$) δ 7.11 (t, *J* = 7.6 Hz, 1H), 7.04 (dd, *J* = 7.4, 1.7 Hz, 1H), 7.00 (dd, *J* = 7.8, 1.7 Hz, 1H), 3.94 (s, 3H), 3.91 (s, 3H), 0.36 (s, 9H); ^{13}C {^1H} NMR (100 MHz, $CDCl_3$) δ 153.7, 151.8, 133.1, 126.2, 123.9, 113.9, 60.4, 55.4, –0.5. EIMS *m/z* 210.1 (M^+, 62), 195.1 ([M–CH_3]$^+$, 66), 165.1 ([M–OC_2H_5)]$^+$, 100); HRMS calcd. for $C_{11}H_{18}O_2Si$ (M^+) 210.1076, found 210.1076. Anal. calcd. for $C_{11}H_{18}O_2Si$: C, 62.81; H, 8.63. Found: C, 62.83; H, 8.72.

Compound 306

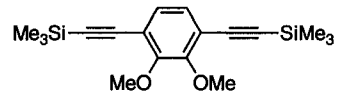

306

1,4-Diiodo-2,3-dimethoxybenzene **305** (500 mg, 1.3 mmol) was cross-coupled with TMS–acetylene (0.40 mL, 280 mg, 2.8 mmol) in the presence of $Pd(PPh_3)_4$ (76 mg, 0.066 mmol) and CuI (14 mg, 0.076 mmol) in degassed toluene/Et_2NH (20 mL, 3:1) for 72 h at 65 °C according to general procedure B. Et_2O (50 mL) and 10% aqueous HCl (50 mL) were added, the organic phase separated, washed with saturated aqueous $NaHCO_3$ (50 mL), H_2O (2 × 50 mL), and dried ($MgSO_4$, charcoal). Solvent reduction and purification by column chromatography (silica gel, CH_2Cl_2/hexanes 1:3) led to the isolation of pure **306** (220 mg, 51%) as a yellow oil. R_f = 0.63 (CH_2Cl_2/hexanes, 1:1). IR (CH_2Cl_2 cast) 2960, 2156 cm^{-1}; ^1H NMR (400 MHz, $CDCl_3$) δ 7.07 (s, 2H), 3.94 (s, 6H), 0.25 (s, 18H); ^{13}C {^1H} NMR (100 MHz, $CDCl_3$) δ 154.4, 128.0, 118.9, 100.5, 100.3, 60.9, –0.2. EI HRMS calcd. for $C_{18}H_{26}O_2Si_2$ (M^+) 330.1471, found 330.1468. Anal. calcd. for $C_{18}H_{26}O_2Si_2$: C, 65.40; H, 7.93. Found: C, 65.82; H, 8.08.

Compound 308

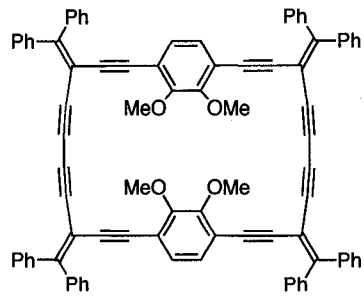

308

Compound **301** (49 mg, 0.060 mmol) was desilylated with TBAF (90 mg, 0.10 mL, 0.34 mmol) in wet THF (10 mL) as described in the general procedure A. After solvent reduction to ~2 mL, the terminal alkyne was added in dry CH_2Cl_2 (4 mL) to degassed

CH_2Cl_2 (150 mL). A solution of CuCl (123 mg, 1.24 mmol), TMEDA (115 mg, 0.15 mL, 0.99 mmol) in CH_2Cl_2 (10 mL) was slowly added and the resulting solution stirred for 72 h at rt. Et_2O (150 mL) was added, the organic phase separated, washed with saturated aqueous NH_4Cl (4 × 100 mL), saturated aqueous $NaHCO_3$ (2 × 100 mL), brine (2 × 100 mL) and dried ($MgSO_4$). Solvent reduction to ~5 mL and purification by precipitation via the addition of acetone afforded a bright yellow solid that was filtered to give **308** (20 mg, 56%). Mp >300 °C. R_f = 0.47 (CH_2Cl_2/hexanes 2:1). IR (CH_2Cl_2, cast) 3055, 2937, 2190 cm^{-1}; ^1H NMR (400 MHz, CD_2Cl_2) δ 7.52–7.37 (m, 44H), 7.07 (s, 4H), 3.79 (s, 12H). Insufficient solubility to obtain a ^{13}C NMR spectrum and mass spectrometry.

Compound 309

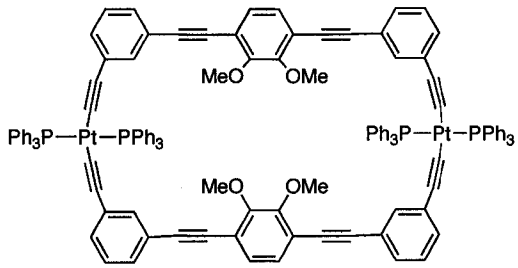

309

Compound **312** (78 mg, 0.15 mmol) was desilylated with TBAF (90 mg, 0.10 mL, 0.34 mmol) in wet THF (10 mL) as described in the general procedure A. After solvent reduction to ~2 mL the terminal alkyne was added with Et_2NH (4 mL) to a degassed mixture of Et_2NH (250 mL) and *cis*-$PtCl_2(PPh_3)_2$ (124 mg, 0.157 mmol). CuI (5 mg, 0.03 mmol) was added and the flask was sealed under N_2 according to general procedure C and allowed to stir for 7 d at 55 °C. Et_2O (50 mL) and CH_2Cl_2 (50 mL) were added, the organic phase separated, washed with H_2O (2 × 100 mL), saturated aqueous NH_4Cl (4 × 100 mL) and dried (Na_2SO_4). Solvent reduction to ~4 mL and precipitation with Et_2O

afforded crude compound **309** as a yellow solid (31 mg, 19%). ^{31}P {^{1}H} NMR (162 MHz, $CDCl_3$) δ 19.8 (pseudo–t, $^{1}J_{P-Pt}$ = 2646 Hz).

Compound 311

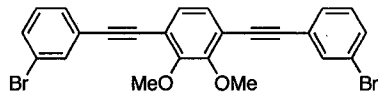

311

Compound **306** (288 mg, 0.871 mmol) was desilylated with TBAF (450 mg, 0.50 mL, 1.7 mmol) in wet THF (10 mL) as described in the general procedure A. After solvent reduction to ~2 mL the terminal alkyne was added with Et_2NH (3 mL) to a degassed mixture of dry THF (50 mL), 3-bromoiodobenzene (**310**) (0.25 mL, 550 mg, 2.0 mmol), $Pd(PPh_3)_4$ (208 mg, 0.180 mmol) and CuI (84 mg, 0.44 mmol) according to general procedure B. The solution was stirred for 24 h at 55 °C, and Et_2O (50 mL) and CH_2Cl_2 (50 mL) were then added. The organic phase separated, washed with H_2O (2 × 100 mL), saturated aqueous NH_4Cl (3 × 100 mL) and dried (Na_2SO_4). Solvent removal and purification by precipitation from a CH_2Cl_2 solution by the addition of Et_2O and hexanes afforded **311** (390 mg, 91%) as a pale yellow solid. Mp 129–132 °C. R_f = 0.37 (CH_2Cl_2/hexanes 1:1). IR (CH_2Cl_2, cast) 3054, 2213 cm^{-1}; ^{1}H NMR (400 MHz, $CDCl_3$) δ 7.70 (t, *J* = 1.7 Hz, 2H), 7.50–7.46 (m, 4H), 7.23 (t, *J* = 7.9 Hz, 2H), 7.20 (s, 2H), 4.03 (s, 6H); ^{13}C {^{1}H} NMR (100 MHz, $CDCl_3$) δ 154.2, 134.3, 131.7, 130.1, 129.8, 128.0, 125.1, 122.2, 118.8, 93.6, 86.4, 61.4. EIMS *m/z* 496.0 (M^+, 12); EI HRMS calcd. for $C_{24}H_{16}{}^{79}Br^{81}BrO_2$ (M^+) 495.9497, found 495.9502 Anal. calcd. for $C_{24}H_{16}Br_2O_2$: C, 58.09; H, 3.25. Found: C, 57.70; H, 3.36.

Compound 312

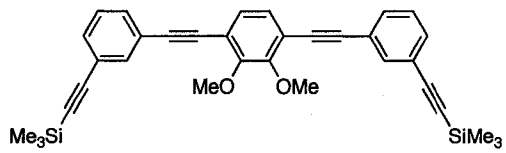

312

Compound **311** (191 mg, 0.385 mmol) was cross coupled according to general procedure B with TMS–acetylene (0.13 mL, 90 mg, 0.92 mmol) in the presence of $Pd(PPh_3)_4$ (48 mg, 0.042 mmol) and CuI (30 mg, 0.16 mmol) in a solution of degassed Et_2NH (5 mL) and THF (40 mL) for 5 d at 55 °C. Et_2O (50 mL) and CH_2Cl_2 (50 mL) were added, the organic phase separated, washed with H_2O (2 × 50 mL), saturated aqueous NH_4Cl (4 × 50 mL), dried ($MgSO_4$). Solvent reduction and purification by gradient column chromatography (silica gel, CH_2Cl_2/hexanes 1:3 to CH_2Cl_2/hexanes 1:1) led to the isolation of pure **312** (78 mg, 38%) as a brown oil. ^1H NMR (400 MHz, $CDCl_3$) δ 7.67 (td, J = 1.7, 0.56 Hz, 2H), 7.62 (dt, J = 7.8, 1.2 Hz, 2H), 7.44 (dt, J = 7.8, 1.2 Hz, 2H), 7.30 (td, J = 7.8, 0.6 Hz, 2H), 7.19 (s, 2H), 4.04 (s, 6H), 0.27 (s, 18H). Product was carried on without further characterization.

Compound 313

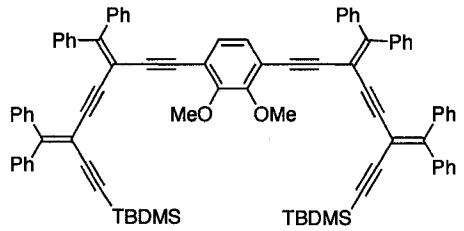

313

Compound **301** (54 mg, 0.065 mmol) was desilylated with TBAF (90 mg, 0.10 mL, 0.34 mmol) in wet THF (10 mL) as described in the general procedure A. After solvent reduction to 2 mL the terminal alkyne was added with Et_2NH (2 mL) to a degassed mixture of THF (25 mL) and an excess of vinyl triflate **307** (115 mg, 0.247 mmol). $Pd(PPh_3)_4$ (17 mg, 0.015 mmol) and CuI (6 mg, 0.03 mmol) were added and the flask was sealed under N_2 according to general procedure B. The solution was stirred for 24 h at 60 °C. Et_2O (50 mL) and CH_2Cl_2 (50 mL) were added, the organic phase separated, washed with H_2O (2 × 100 mL), saturated aqueous NH_4Cl (4 × 100 mL) and dried with $MgSO_4$. Solvent reduction and purification by column chromatography (silica gel, CH_2Cl_2/hexanes 1:2) led to the isolation of **313** (38 mg, 48%) as a bright yellow solid. R_f = 0.52 (CH_2Cl_2/hexanes, 1:1). IR (CH_2Cl_2, cast) 3056, 2925, 2854, 2198 (vw), 2145 (vw) cm^{-1}; ^1H NMR (400 MHz, $CDCl_3$) δ 7.48–7.21 (m, 40H), 6.79 (s, 2H), 3.62 (s, 6H), 0.84 (s, 18H), 0.05 (s, 12H). Product was carried on without further characterization.

Compound 314

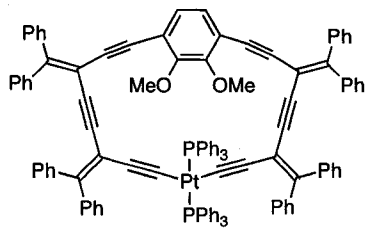

314

Compound **313** (30 mg, 0.029 mmol) was desilylated with TBAF (90 mg, 0.10 mL, 0.34 mmol) in wet THF (10 mL) as described in the general procedure A. After solvent reduction to 2 mL the terminal alkyne was added with Et_2NH (4 mL) to a degassed mixture of Et_2NH (50 mL) and $PtCl_2(PPh_3)_2$ (29 mg, 0.036 mmol). CuI (12 mg, 0.063 mmol) was added and the flask was sealed under N_2 according to general procedure C. The solution was stirred for 5 d at 55 °C. Et_2O (50 mL) and CH_2Cl_2 (50 mL) were added, the organic phase separated, washed with H_2O (2 × 50 mL), saturated aqueous NH_4Cl (2 × 50 mL) and dried ($MgSO_4$). Solvent removal and column chromatography (silica gel, CH_2Cl_2/hexanes 1:1) led to the isolation of two unknown compounds (8.3 mg, 19% and 6.5 mg, 15%) as bright yellow solids. R_f = 0.47 and 0.27 (CH_2Cl_2/hexanes, 1:3). First unknown: ^1H NMR (400 MHz, $CDCl_3$) δ 7.76–7.70 (m, 2H), 7.54–7.27 (m, 3H); $^{31}P\{^1H\}$ NMR (162 MHz, $CDCl_3$) δ 44.4. Second unknown: too insoluble for meaningful spectroscopic analysis.

Compound 316

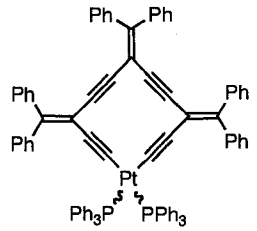

316

Compound **315** (76 mg, 0.088 mmol) was desilylated with TBAF (90 mg, 0.10 mL, 0.34 mmol) in wet THF (10 mL) as described in the general procedure A. After solvent reduction to 2 mL the terminal alkyne was added with Et_2NH (2 mL) to a degassed mixture of Et_2NH (50 mL) and $PtCl_2(PPh_3)_2$ (71 mg, 0.090 mmol). CuI (5 mg, 0.03 mmol) was added and the flask was sealed under N_2 according to general procedure C. The solution was stirred for 48 h at 55 °C. Et_2O (50 mL) and CH_2Cl_2 (50 mL) were added, the organic phase separated, washed with H_2O (2 × 100 mL), saturated aqueous NH_4Cl (4 × 100 mL), and dried ($MgSO_4$). Solvent removal and gradiant column chromatography (silica gel, CH_2Cl_2/hexanes 3:1 to EtOAc) led to the isolation of a yellow solid (7.8 mg). ^{31}P $\{^1H\}$ NMR (162 MHz, $CDCl_3$) δ 19.6 (pseudo–t, $^1J_{P-Pt}$ = 2072 Hz). MALDI MS (DCTB) *m/z* 2086.6 ($[M + H]^+$, 100). The same procedure was followed again with compound **315** (59 mg, 0.068 mmol), $PtCl_2(PPh_3)_2$ (105 mg, 0.133 mmol) and CuI (5 mg, 0.03 mmol) in 50 mL of degassed Et_2NH at 55 °C for 4 d. Precipitation from a CH_2Cl_2 solution with hexanes led to the isolation of a brown solid (58 mg). ^{31}P $\{^1H\}$ NMR (162 MHz, $CDCl_3$) δ 15.4 (pseudo–t, $^1J_{P-Pt}$ = 3672 Hz). MALDI MS (DCTB) *m/z* 2088.1 ($[M + H]^+$, 100).

Compound 317

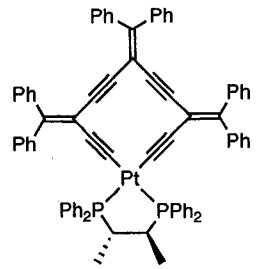

317

The second unknown compound assumed to be **316** (24 mg, 0.018 mmol) and *S,S*-CHIRAPHOS **201** (10 mg, 0.025 mmol) were dissolved in CD_2Cl_2 (1 mL) and sonicated for 30 min. After the ^{31}P NMR spectrum indicated the reaction was complete, solvent removal and purification via gradient column chromatography (silica gel, CH_2Cl_2/hexanes 1:1 to CH_2Cl_2) was attempted but did not result in the isolation of compound **317**. Reaction mixture ^{31}P $\{^1H\}$ NMR (162 MHz, $CDCl_3$) δ 47.4 (pseudo–t, $^1J_{P-Pt} = 2289$ Hz).

6.4 Experimental Details for Chapter 4

Compound 410

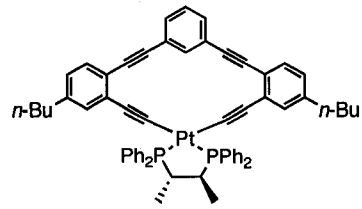

410

(*2S,3S*)-Bis(diphenylphosphino)butane **201** (14 mg, 0.033 mmol) was added to a solution of **400** (30 mg, 0.026 mmol) in dry CH_2Cl_2 (10 mL). After the mixture was stirred under N_2 at rt for 72 h. Additional **201** (11 mg, 0.026 mmol) was added since **400** was still present. The resulting solution was stirred for 7 d. Solvent removal followed by purification via gradient column chromatography (silica gel, CH_2Cl_2/hexanes 1:3 to

EtOAc/hexanes 1:1) afforded **410** (12 mg, 44%) as a white solid. Mp >213 °C (dec.). R_f = 0.52 (CH_2Cl_2/hexanes 2:1). UV–vis (CH_2Cl_2) λ_{max} (ε) 245 (30400), 253 (33900), 259 (41100), 271 (60400), 306 (32400), 348 (13000) nm; IR (CH_2Cl_2, cast) 3055, 2926, 2228, 2093 cm^{-1}; ^1H NMR (400 MHz, $CDCl_3$) δ 8.66 (s, br, 1H), 7.93–7.86 (m, 10H), 7.44–7.41 (m, 4H), 7.35–7.28 (m, 9H), 7.12 (d, J = 7.9 Hz, 2H), 6.73 (d, br, J = 7.7, 2H), 6.23 (s, br, J = 1.4 Hz, 2H), 2.52 (s, br, 2H), 2.30 (t, J = 7.5 Hz, 4H), 1.42–1.34 (m, 4H), 1.29–1.19 (m, 4H), 0.95 (d, J = 6.6, 3H), 0.93 (d, J = 6.6, 3H), 0.87 (t, J = 7.3 Hz, 6H); ^{13}C {^1H} NMR (100 MHz, $CDCl_3$) δ 143.3, 141.7, 136.1 (pseudo–t, J_{C-P} = 5.9 Hz), 133.8 (pseudo–t, J_{C-P} = 4.6 Hz), 132.4 (pseudo–t, $^1J_{C-P}$ = 29 Hz), 131.2, 131.0, 130.5, 129.0, 128.3 (pseudo–t, J_{C-P} = 5.0 Hz), 128.0 (pseudo–t, J_{C-P} = 5.4 Hz), 127.6, 127.0, 124.7, 124.6, 120.8, 112.8 (m), 93.0, 92.3, 39.5 (pseudo–t, $^1J_{C-P}$ = 25 Hz), 35.2, 33.1, 22.1, 15.7 (pseudo–t, $^2J_{C-P}$ = 4.8 Hz), 13.8; ^{31}P {^1H} NMR (162 MHz, $CDCl_3$) δ 46.4 (pseudo–t, $^1J_{P-Pt}$ = 2232 Hz). ESI HRMS ($ClCH_2CH_2Cl$) calcd. for $C_{62}H_{56}P_2Pt$•Na ([M + Na]$^+$) 1080.3397, found 1080.3389.

Compound 411

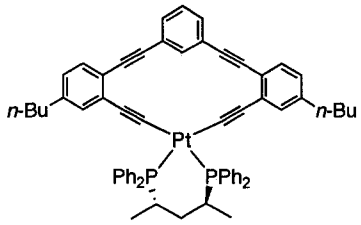

or **dimer**

411

(2*S*,4*S*)-2,4-Bis(diphenylphosphino)pentane **220** (22 mg, 0.051 mmol) was added to a solution of **400** (50 mg, 0.043 mmol) in dry CH_2Cl_2 (2 mL). The mixture was stirred under N_2 at rt for 5 d. The ^{31}P NMR spectrum indicated that the reaction was not

complete, therefore after the addition of excess **220** (24 mg, 0.055 mmol) the reaction mixture was heated to 50 °C under N_2 for 22 d. The ^{31}P NMR spectrum indicated that the reaction may be complete, but other peaks were also observed. Solvent reduction and gradient column chromatography (silica gel, CH_2Cl_2/hexanes 1:2 to EtOAc) and/or precipitation with hexanes or Et_2O from a CH_2Cl_2 solution did not lead to the isolation of **411**. ^{31}P {^1H} NMR (162 MHz, $CDCl_3$) δ 26.0 (pseudo–t, $^1J_{P-Pt}$ = 2572 Hz).

Compound 412

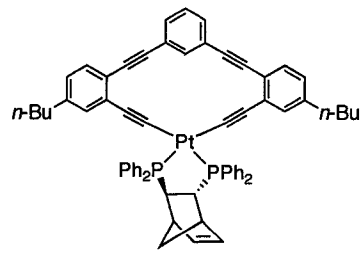

412

(*2R,3R*)-2,3-Bis(diphenylphosphino)bicyclo[2.2.1]hept-5-ene **222** (10 mg, 0.022 mmol) was added to a solution of **400** (25 mg, 0.022 mmol) in dry CH_2Cl_2 (5 mL). The mixture was stirred under N_2 at rt for 5 d. The ^{31}P NMR spectrum indicated that the reaction was not complete, therefore after the addition of additional **222** (10 mg, 0.022 mmol) the reaction mixture was heated to 50 °C under N_2 for 1 d. After the addition of additional **222** (6 mg, 0.013 mmol) and another 11 days at 50 °C under N_2, the ^{31}P NMR spectrum did not show any improvement above ~40% conversion to product. Solvent reduction and gradient column chromatography (silica gel, CH_2Cl_2/hexanes 1:2 to EtOAc) and/or precipitation from a CH_2Cl_2 solution with hexanes or Et_2O did not lead to the isolation of **412**. ^{31}P {^1H} NMR (162 MHz, CD_2Cl_2) δ 14.5 (pseudo–dt, $^1J_{P-Pt}$ = 2277 Hz, $^3J_{P-P}$ = 9.5 Hz), 13.2 (pseudo–dt, $^1J_{P-Pt}$ = 2268 Hz, $^3J_{P-P}$ = 9.6 Hz).

Compound 413

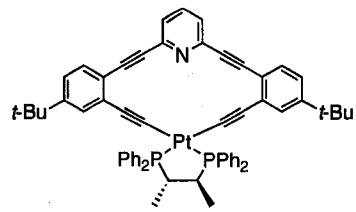

413

(*2S,3S*)-Bis(diphenylphosphino)butane **201** (13 mg, 0.032 mmol) was added to a solution of **401** (31 mg, 0.027 mmol) in dry CH_2Cl_2 (2 mL). The mixture was stirred at rt for 10 days under N_2, additional **201** was added (12 mg, 0.029 mmol), and the reaction was allowed to stir for 10 more days. Solvent removal from the greenish/black mixture followed by purification via a silica plug (silica CH_2Cl_2/hexanes 1:1 to CH_2Cl_2 to EtOAc) afforded a brown solution. Precipitation with hexanes from a CH_2Cl_2 solution afforded **413** (9.8 mg, 29%) as a beige solid that was quite insoluble in $CDCl_3$ and CD_2Cl_2. Mp >245 °C (dec.). R_f = 0.56 (CH_2Cl_2/hexanes 1:1). UV–vis (CH_2Cl_2) λ_{max} (ε) 264 (65200), 297 (48600), 316 (57700), 337 (26900) nm; IR (CH_2Cl_2, cast) 3055, 2962, 2926, 2212, 2091 cm^{-1}; ^1H NMR (400 MHz, $CDCl_3$) δ 8.39–8.35 (m, 4H), 8.06–8.02 (m, 4H), 7.54 (t, J = 7.8 Hz, 2H), 7.41–7.39 (m, 6H), 7.30–7.19 (m, 9H), 6.91 (dd, J = 8.2, 1.9 Hz, 2H), 6.24 (d, J = 1.9 Hz, 2H), 2.88 (s, br, 2H), 0.87 (s, 18H), 0.68 (d, J = 7.2 Hz, 3H), 0.65 (d, J = 6.9 Hz, 3H); ^{13}C {^1H} NMR (100 MHz, $CDCl_3$) δ 150.4, 144.6, 135.53, 135.48 (pseudo–t, J_{C-P} = 5.6 Hz), 134.1 (pseudo–t, J_{C-P} = 5.1 Hz), 132.8, 130.7, 130.0, 129.9, 128.4 (pseudo–t, J_{C-P} = 4.9 Hz), 128.0 (pseudo–t, J_{C-P} = 5.4 Hz), 122.3, 121.6, 119.6, 92.0, 90.7, 42.0–41.5 (m), 34.0, 30.7, 17.6 (pseudo–t, J_{C-P} = 3.4 Hz); ^{31}P {^1H} NMR (162 MHz, $CDCl_3$) δ 52.2 (pseudo–t, $^1J_{P-Pt}$ = 2271 Hz). ESI HRMS ($ClCH_2CH_2Cl$) calcd. for $C_{61}H_{56}NP_2Pt$ ($[M + H]^+$) 1059.3530, found 1059.3533.

Compound 414

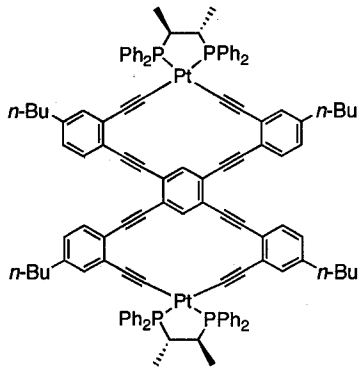

414

(*2S,3S*)-Bis(diphenylphosphino)butane **201** (25 mg, 0.057 mmol) was added to a solution of **402** (57 mg, 0.025 mmol) in dry $CDCl_3$ (3 mL). The mixture was stirred at rt under N_2 for 7 d until the majority of **402** was consumed as determined from the ^{31}P NMR spectrum. Solvent reduction and gradient column chromatography (silica CH_2Cl_2/hexanes 1:1 to CH_2Cl_2 to EtOAc) did not lead to the isolation of **414** but to the recovery of **402** (3 mg). ^{31}P $\{^1H\}$ NMR (162 MHz, $CDCl_3$) δ 47.0 (pseudo–t, $^1J_{P-Pt} = 2291$ Hz).

6.5 REFERENCES

1. Stone, M. T.; Fox, J. M.; Moore, J. S. *Org. Lett.* **2004**, *6*, 3317-3320.

2. Zhu, Z. G.; Swager, T. M. *Org. Lett.* **2001**, *3*, 3471-3474.

3. Stang, P. J.; Fisk, T. E. *Synthesis* **1979**, 438-440.

Appendix A

SELECTED SPECTRA*

*all spectra were run in $CDCl_3$ at 400 MHz

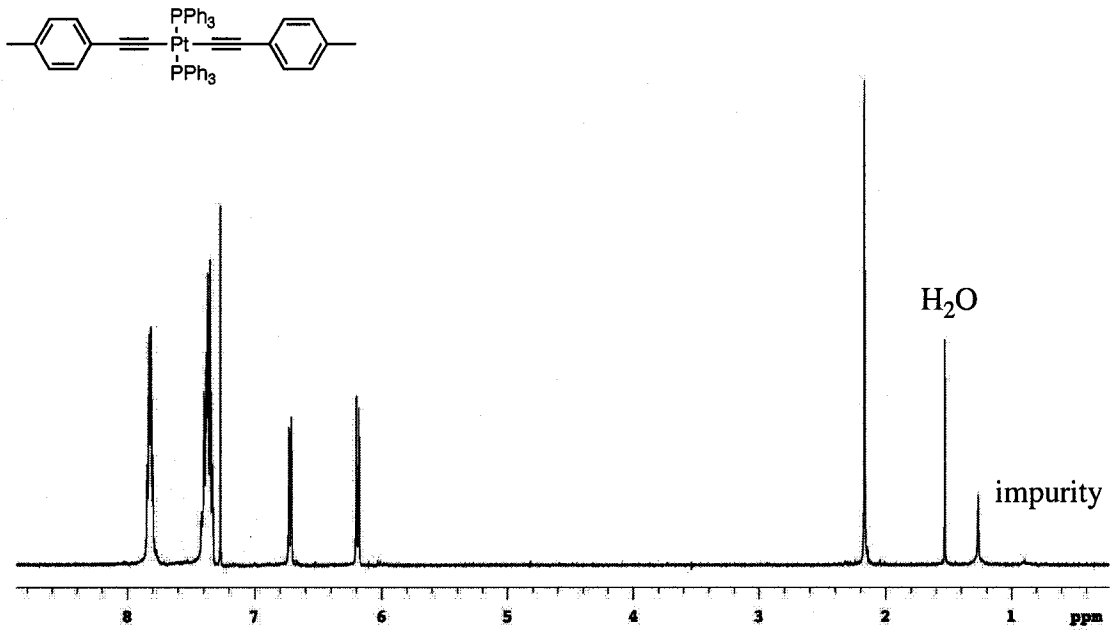

Figure A.1 ^{1}H NMR spectrum of **216**

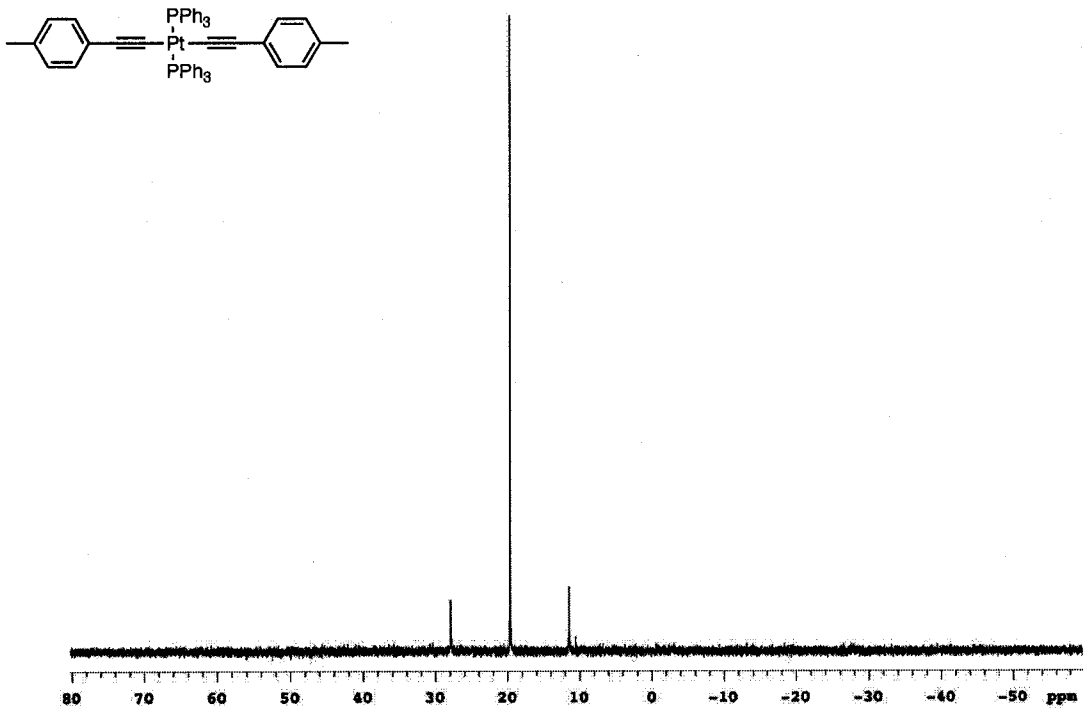

Figure A.2 ^{31}P $\{^{1}H\}$ NMR spectrum of **216**

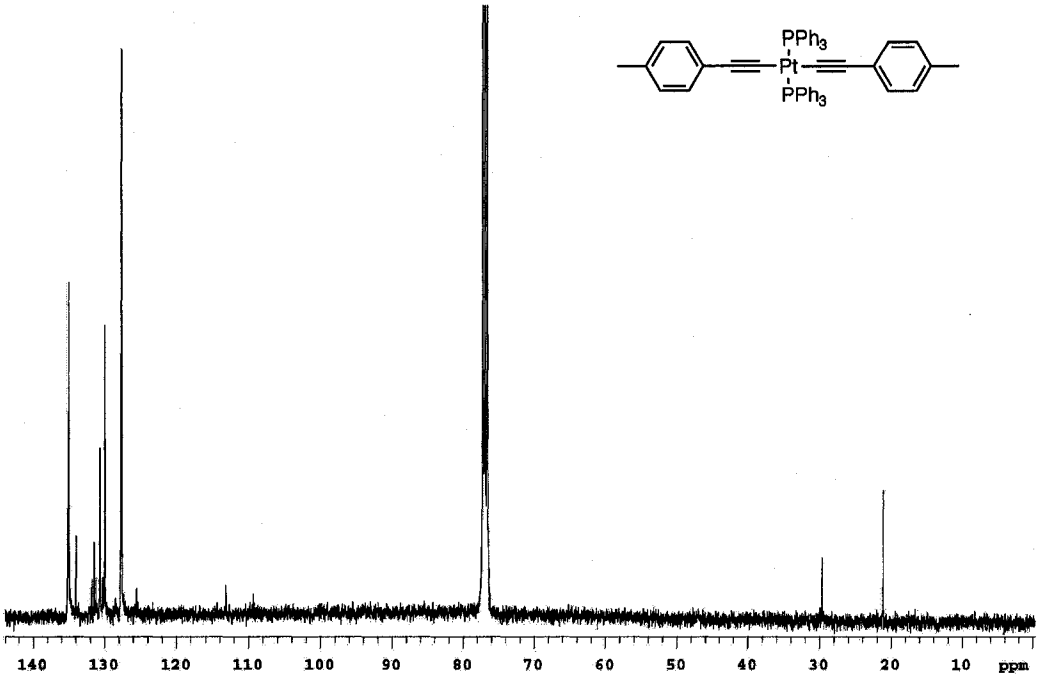

Figure A.3 ^{13}C {^{1}H} NMR spectrum of **216**

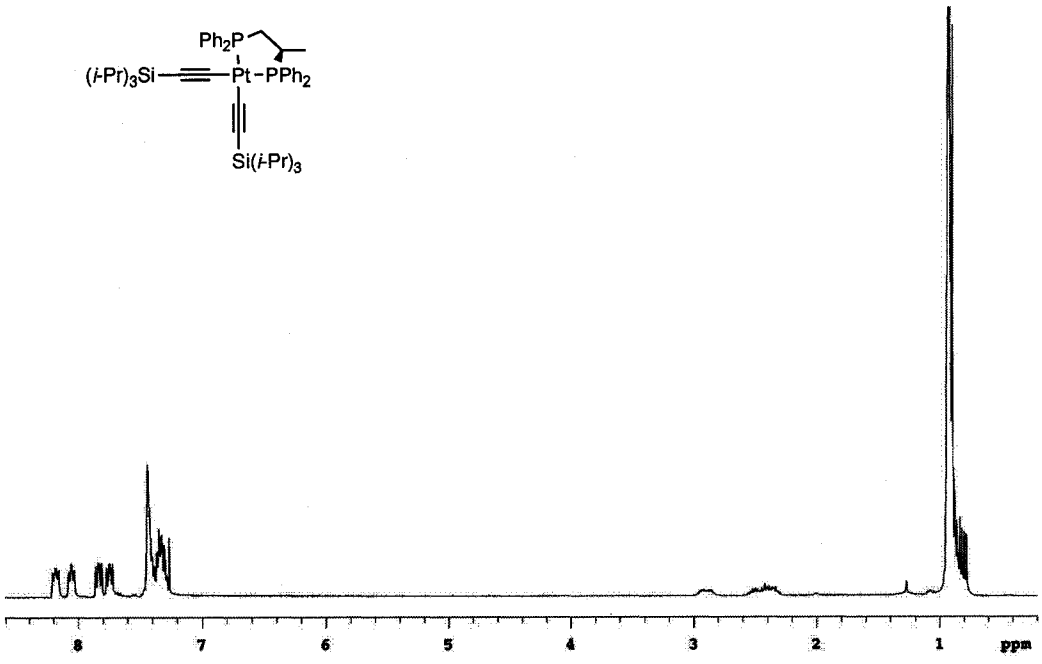

Figure A.4 ^{1}H NMR spectrum of **223**

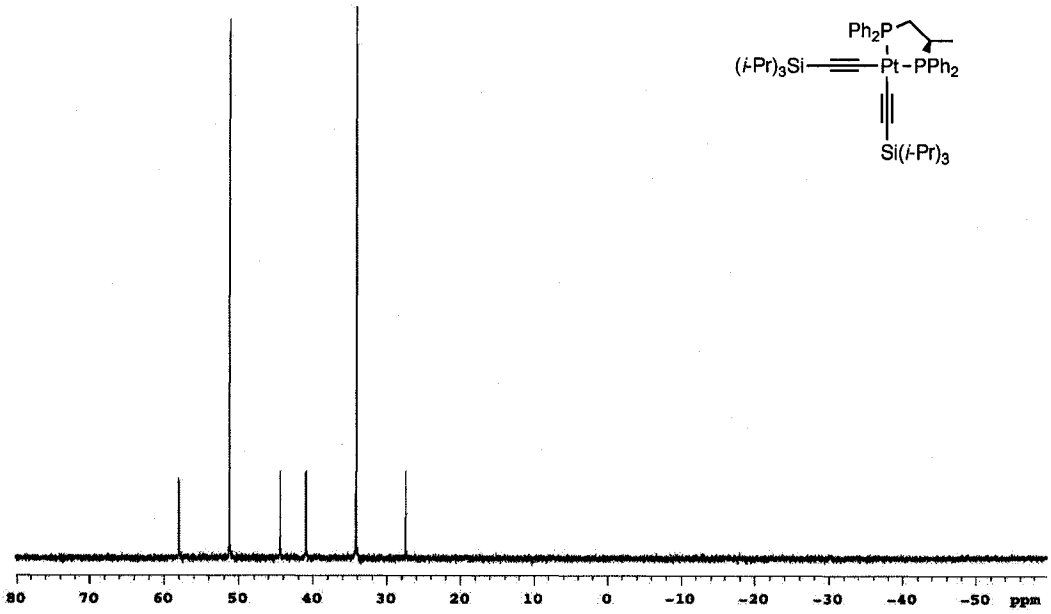

Figure A.5 ^{31}P $\{^{1}H\}$ NMR spectrum of **223**

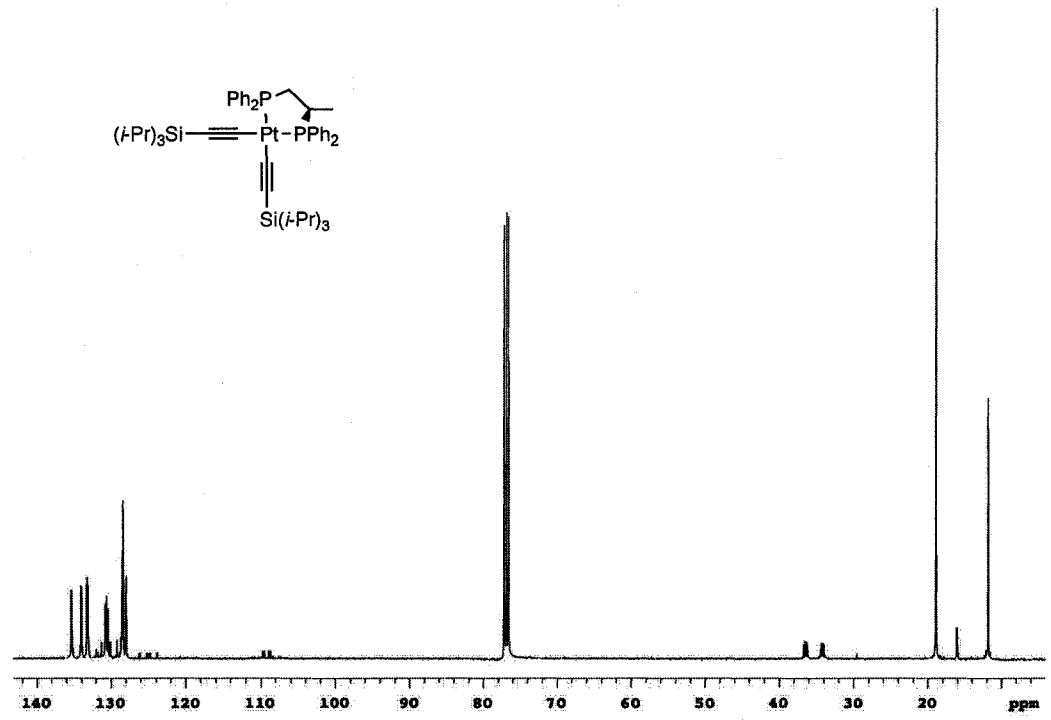

Figure A.6 ^{13}C $\{^{1}H\}$ NMR spectrum of **223**

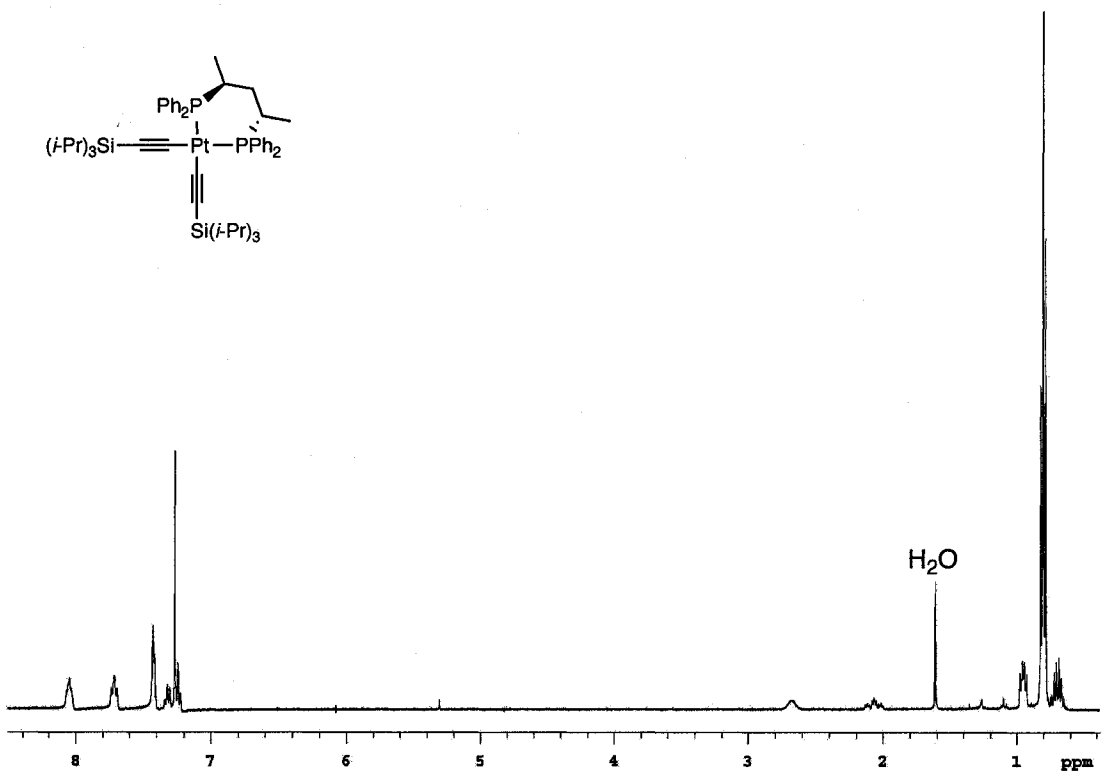

Figure A.7 ^{1}H NMR spectrum of **224**

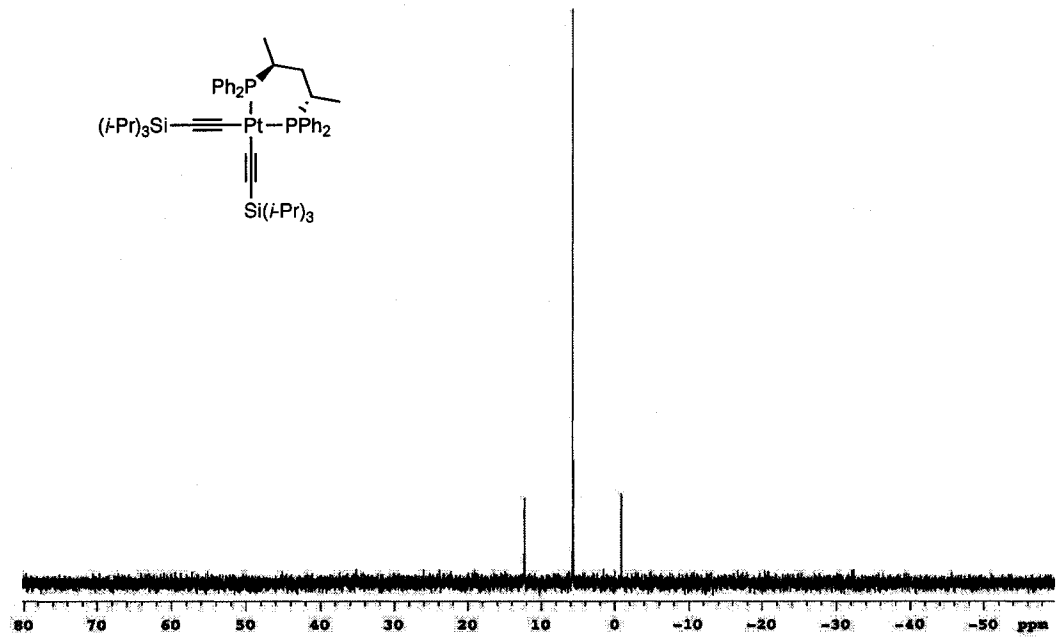

Figure A.8 ^{31}P $\{^{1}H\}$ NMR spectrum of **224**

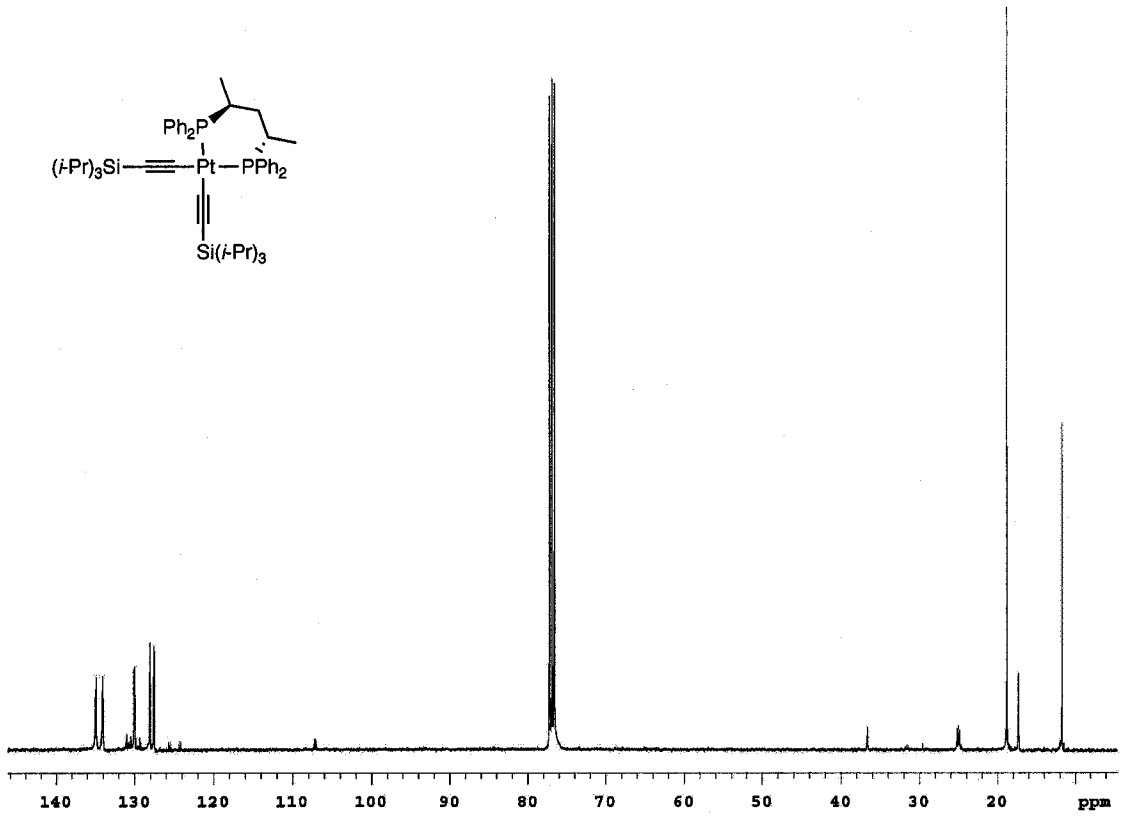

Figure A.9 ^{13}C {^{1}H} NMR spectrum of **224**

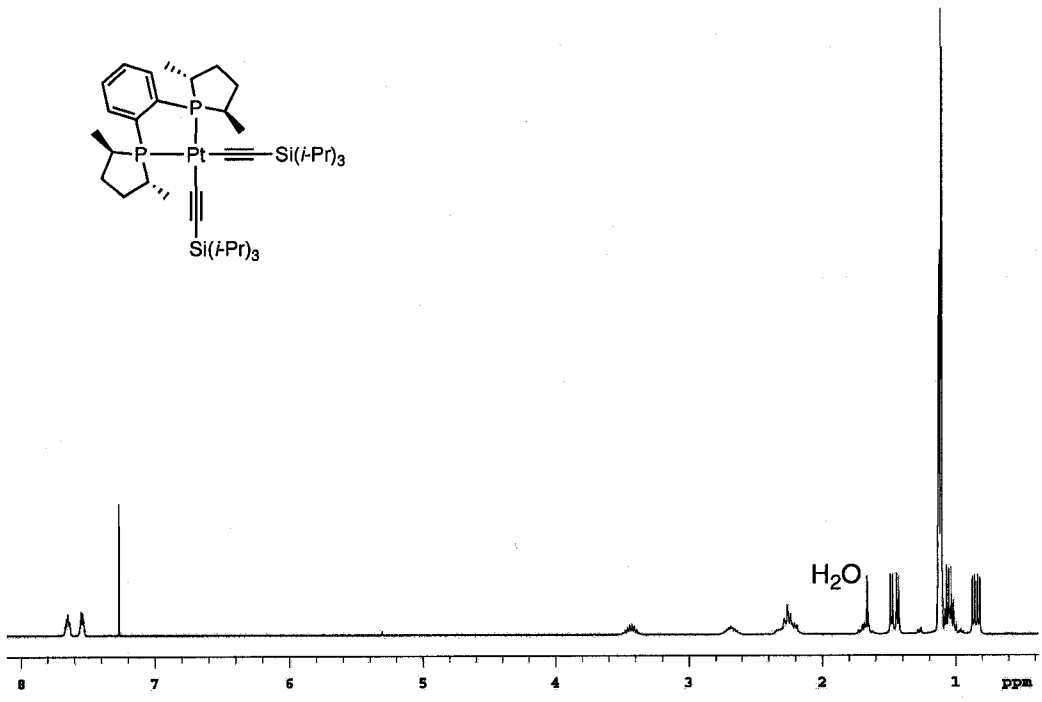

Figure A.10 ^{1}H NMR spectrum of **225**

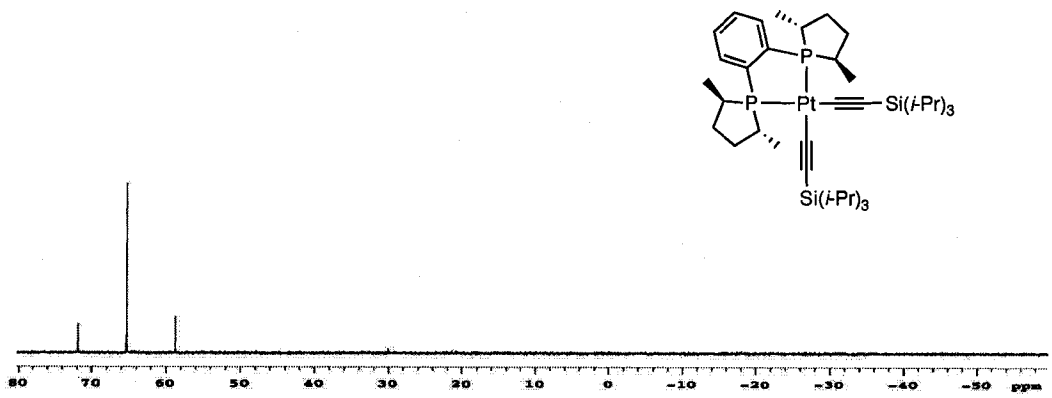

Figure A.11 ^{31}P $\{^{1}H\}$ NMR spectrum of **225**

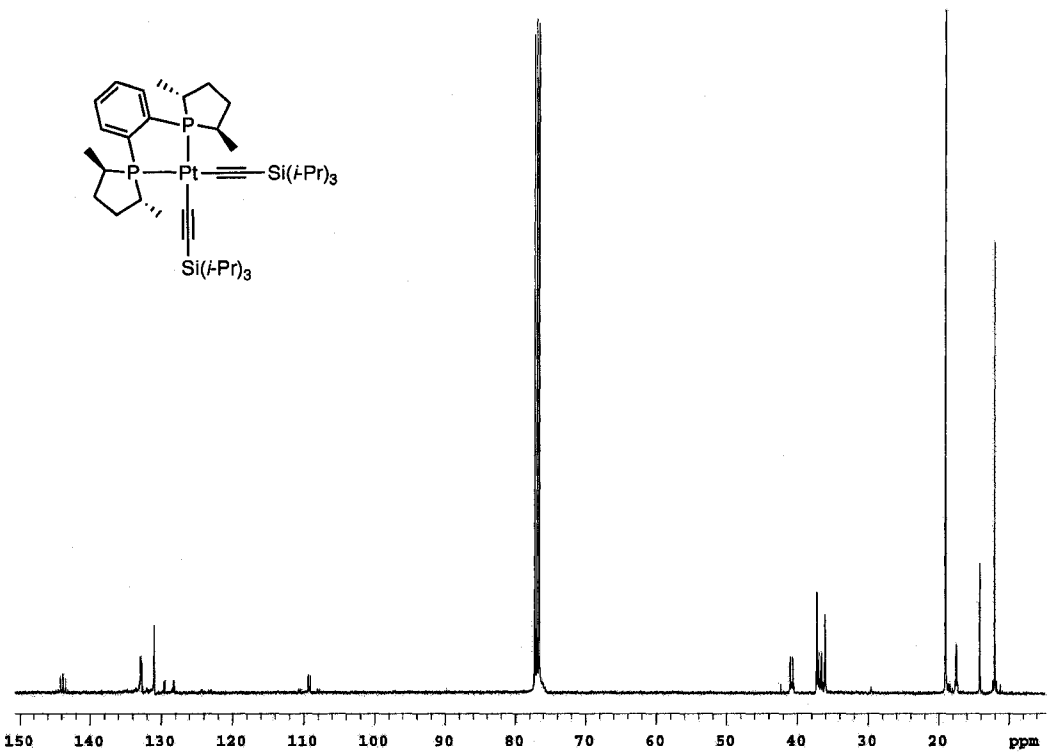

Figure A.12 ^{13}C $\{^{1}H\}$ NMR spectrum of **225**

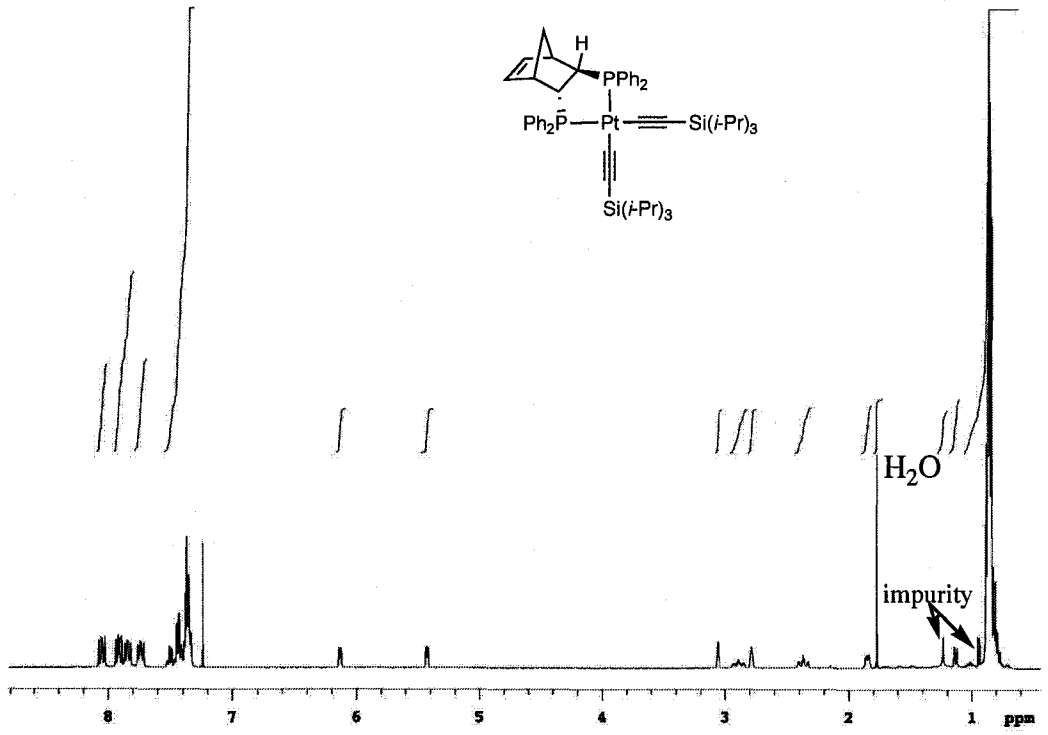

Figure A.13 ^{1}H NMR spectrum of **226**

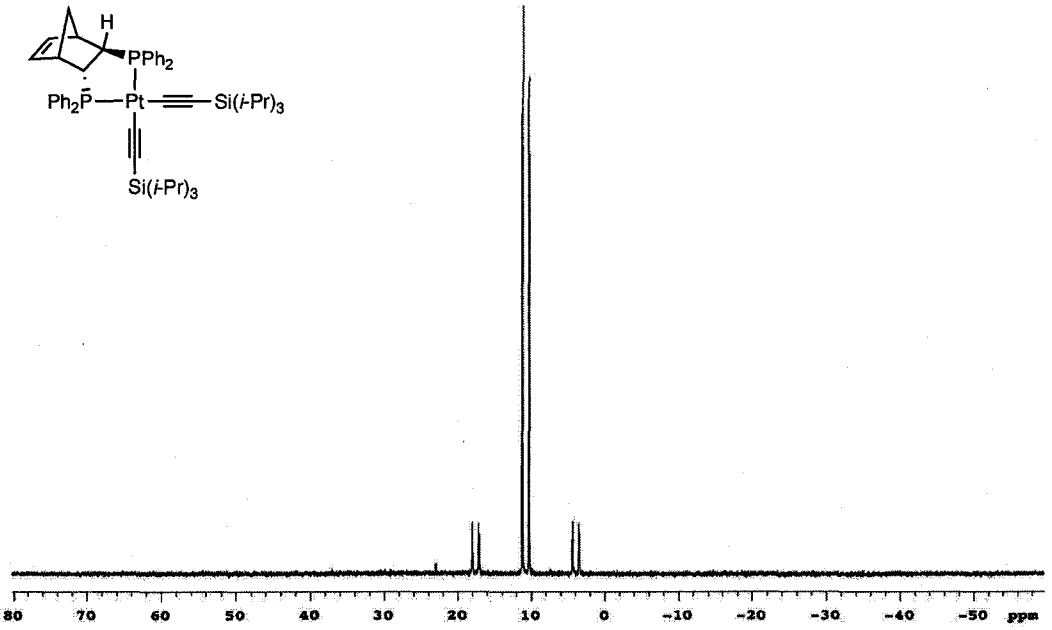

Figure A.14 ^{31}P $\{^{1}H\}$ NMR spectrum of **226**

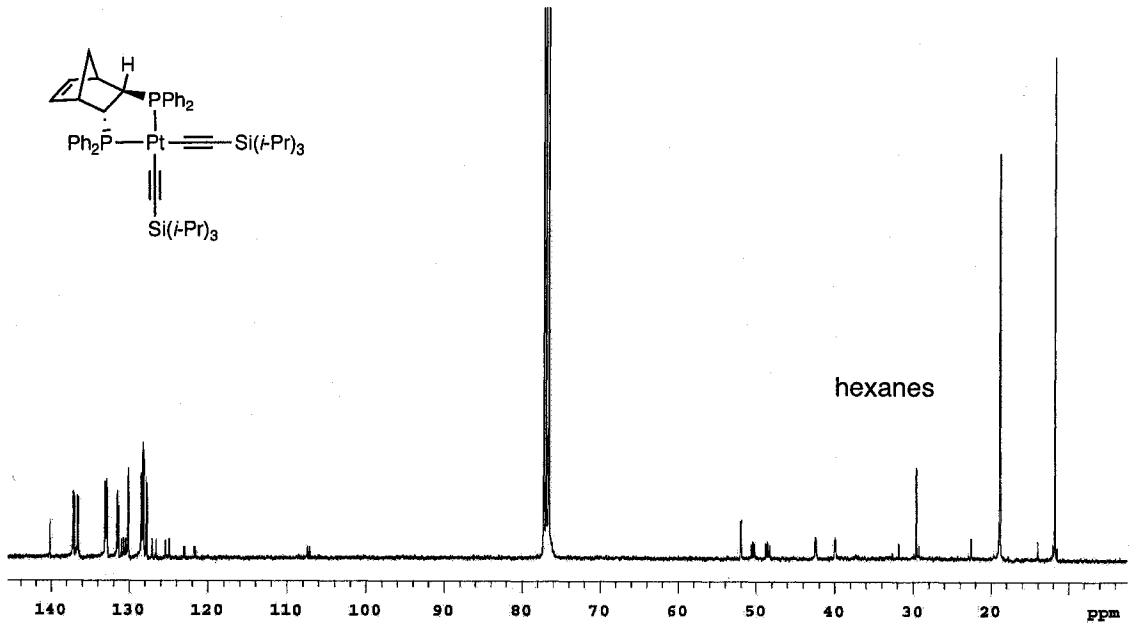

Figure A.15 ^{13}C {^{1}H} NMR spectrum of **226**

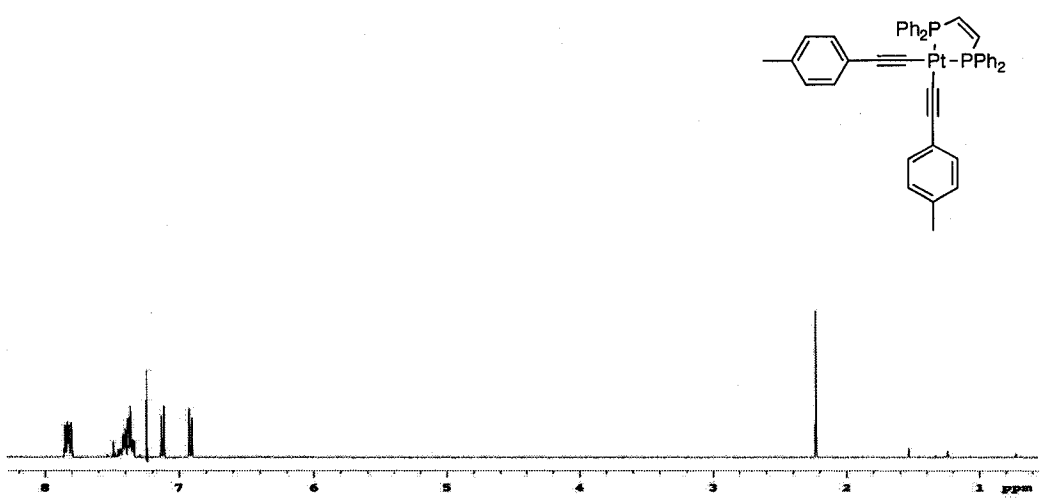

Figure A.16 ^{1}H NMR spectrum of **227**

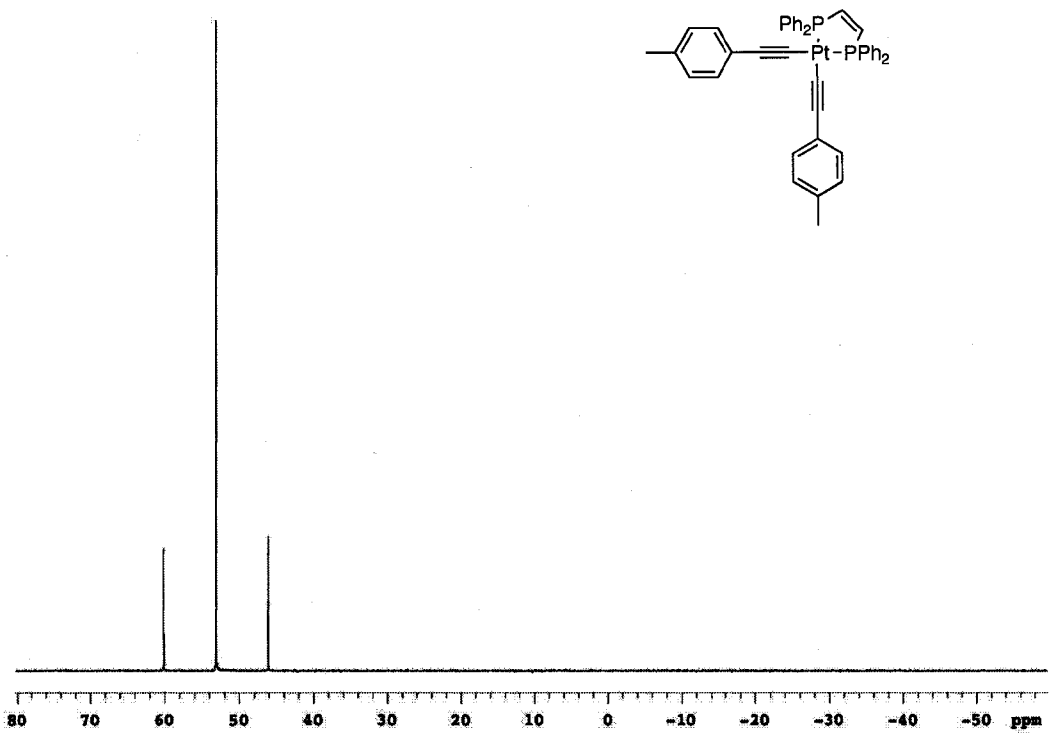

Figure A.17 ^{31}P $\{^{1}H\}$ NMR spectrum of **227**

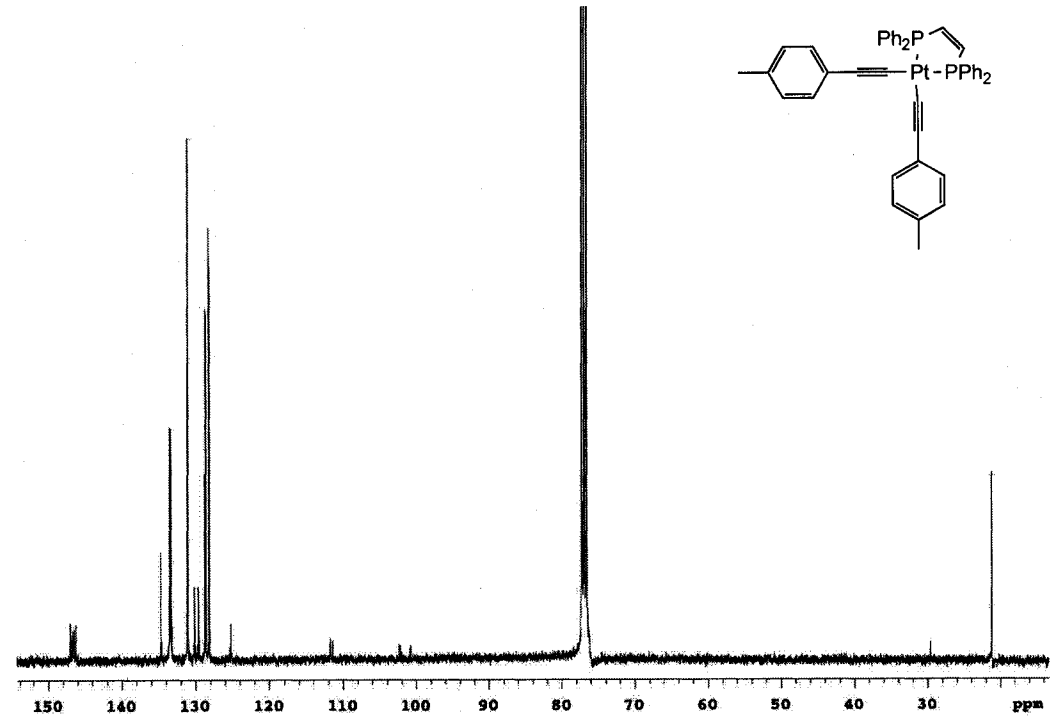

Figure A.18 ^{13}C $\{^{1}H\}$ NMR spectrum of **227**

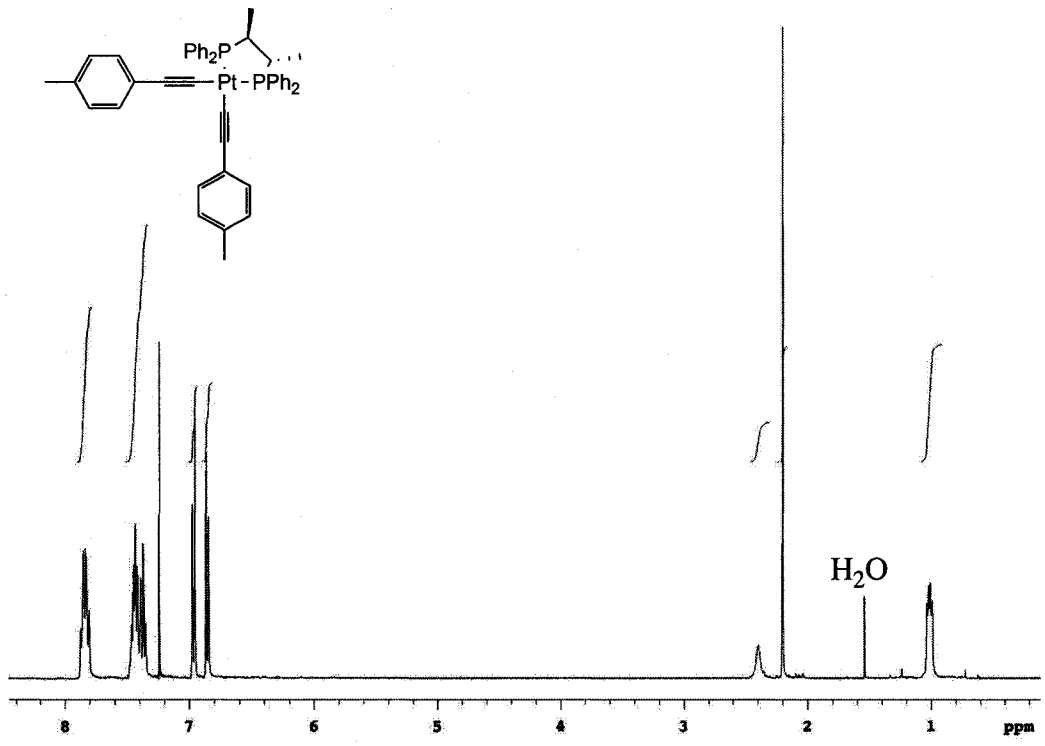

Figure A.19 ^{1}H NMR spectrum of **228**

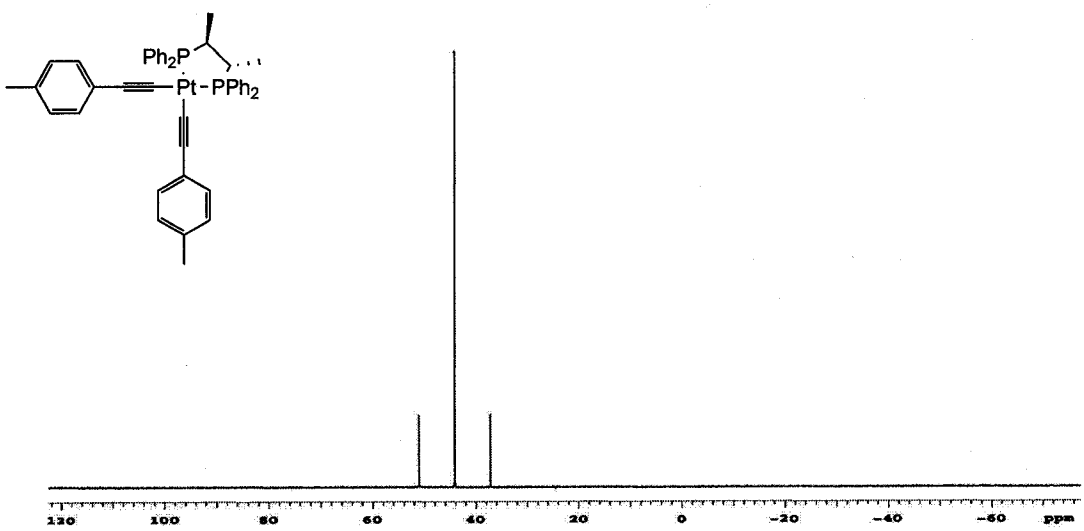

Figure A.20 ^{31}P $\{^{1}H\}$ NMR spectrum of **228**

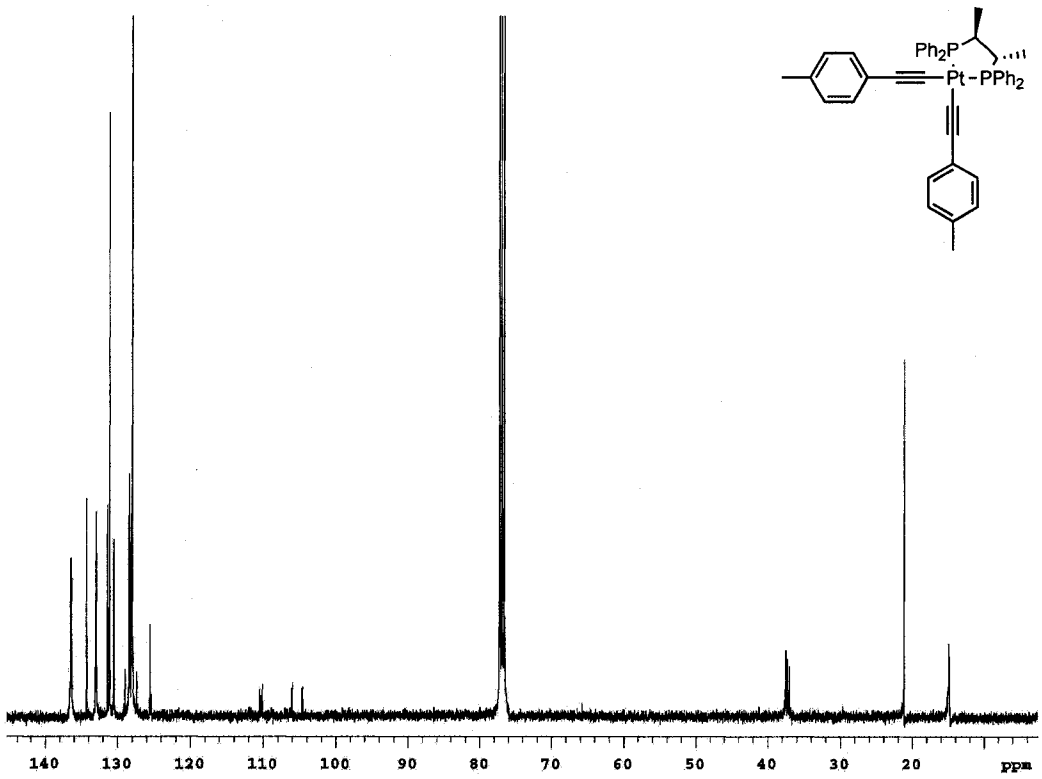

Figure A.21 ^{13}C {^{1}H} NMR spectrum of **228**

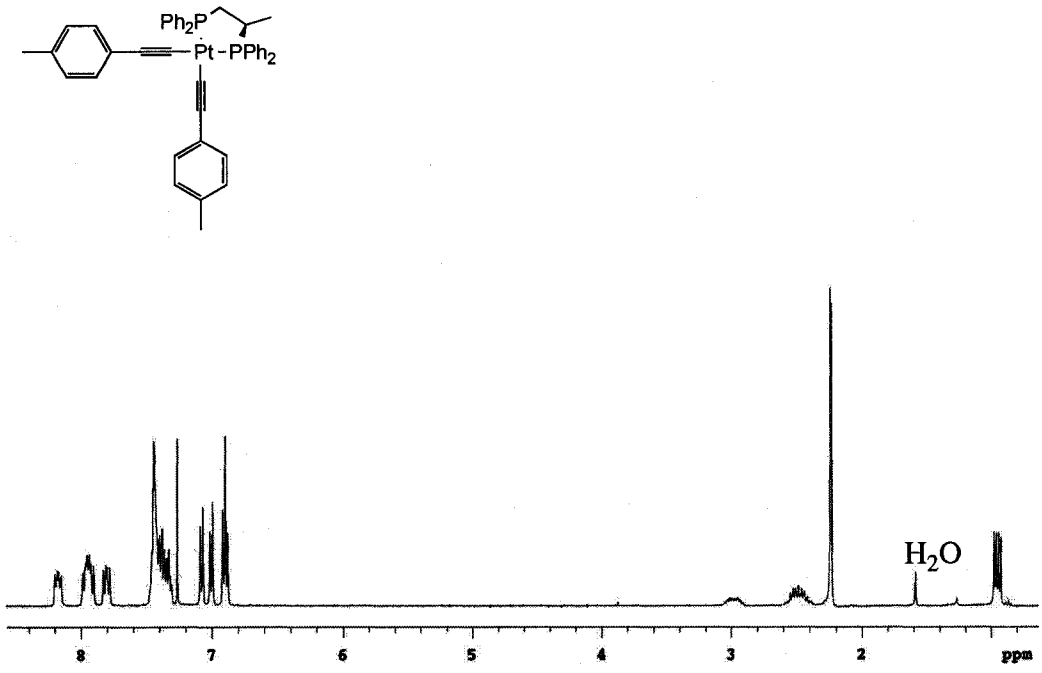

Figure A.22 ^{1}H NMR spectrum of **229**

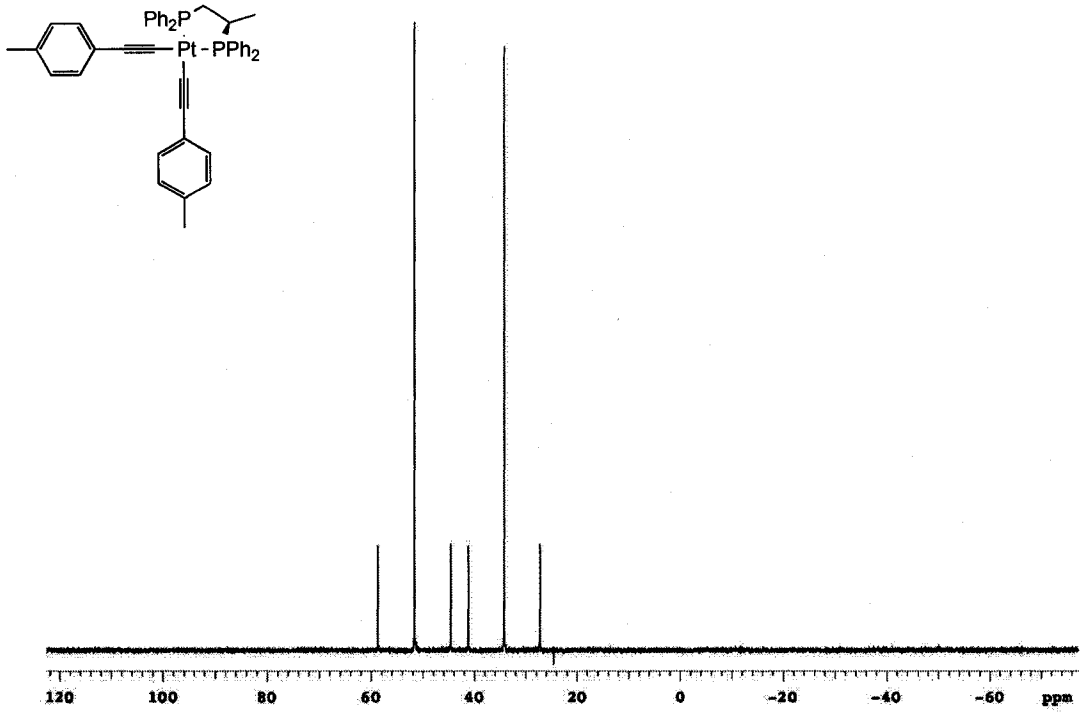

Figure A.23 ^{31}P $\{^{1}H\}$ NMR spectrum of **229**

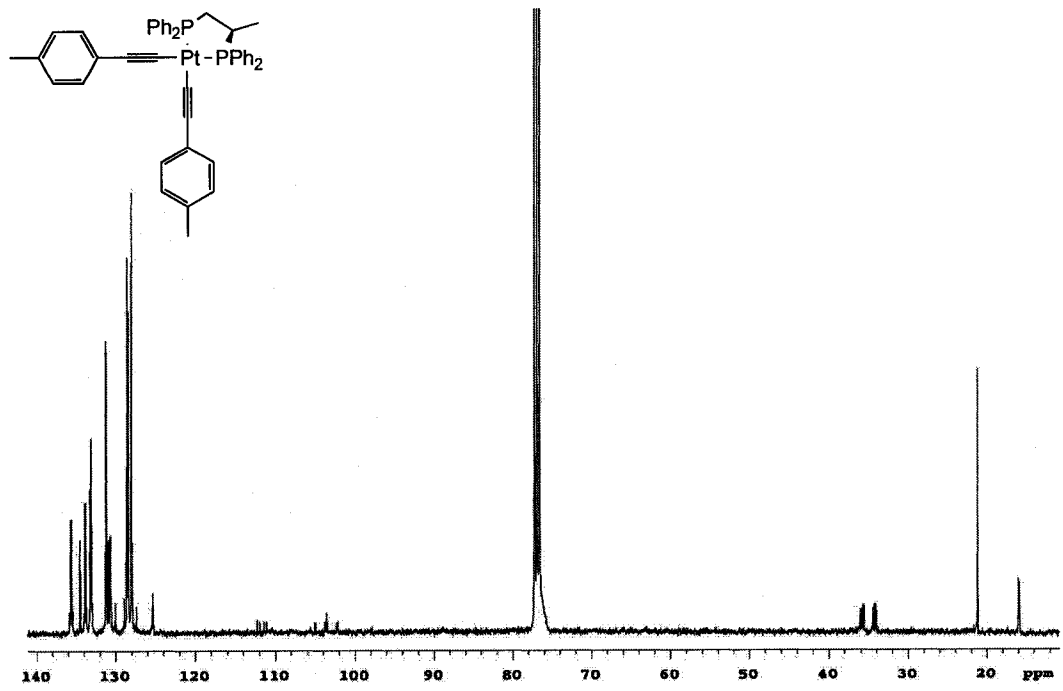

Figure A.24 ^{13}C $\{^{1}H\}$ NMR spectrum of **229**

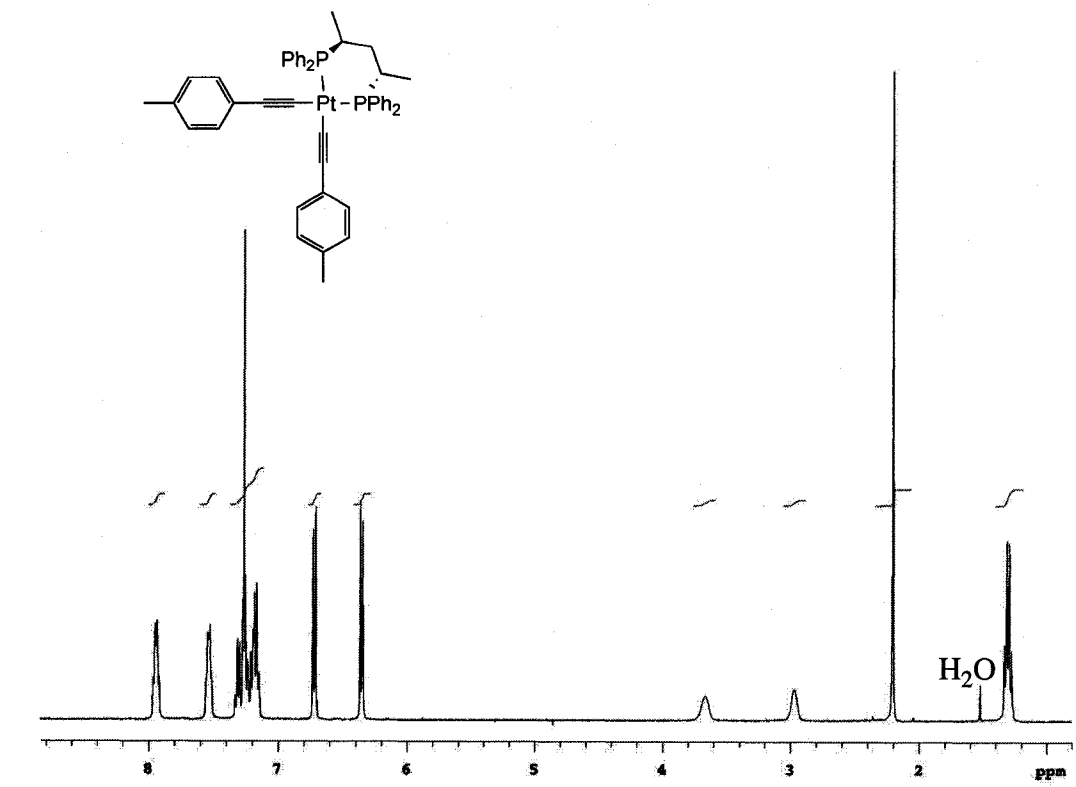

Figure A.25 ^{1}H NMR spectrum of **230**

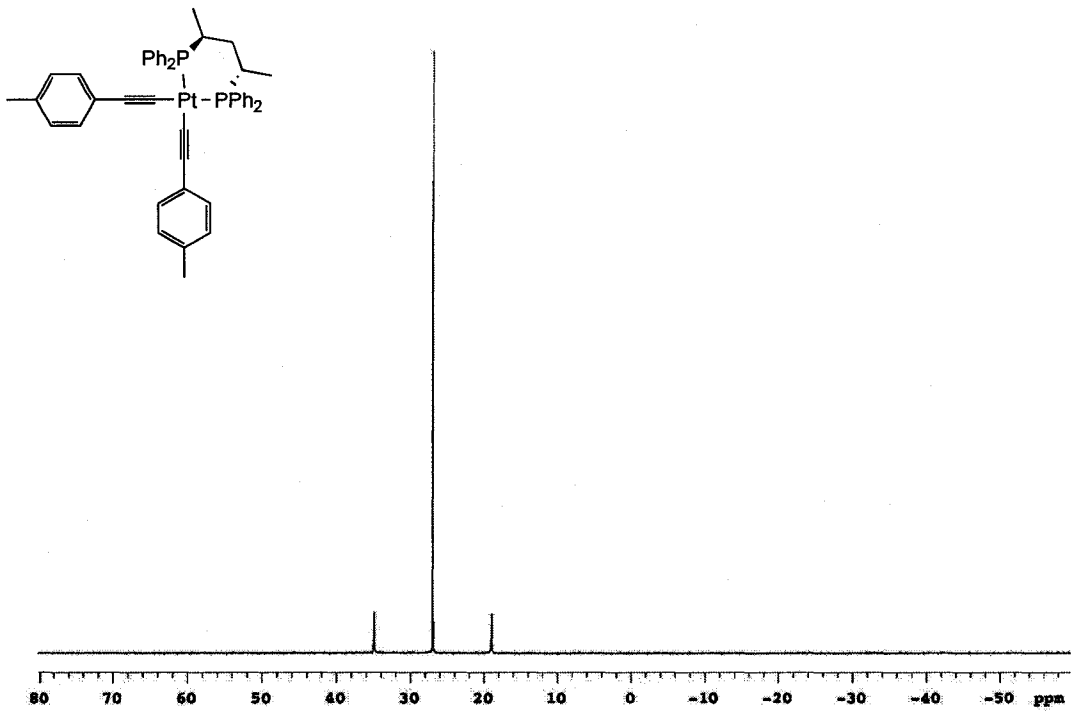

Figure A.26 ^{31}P $\{^{1}H\}$ NMR spectrum of **230**

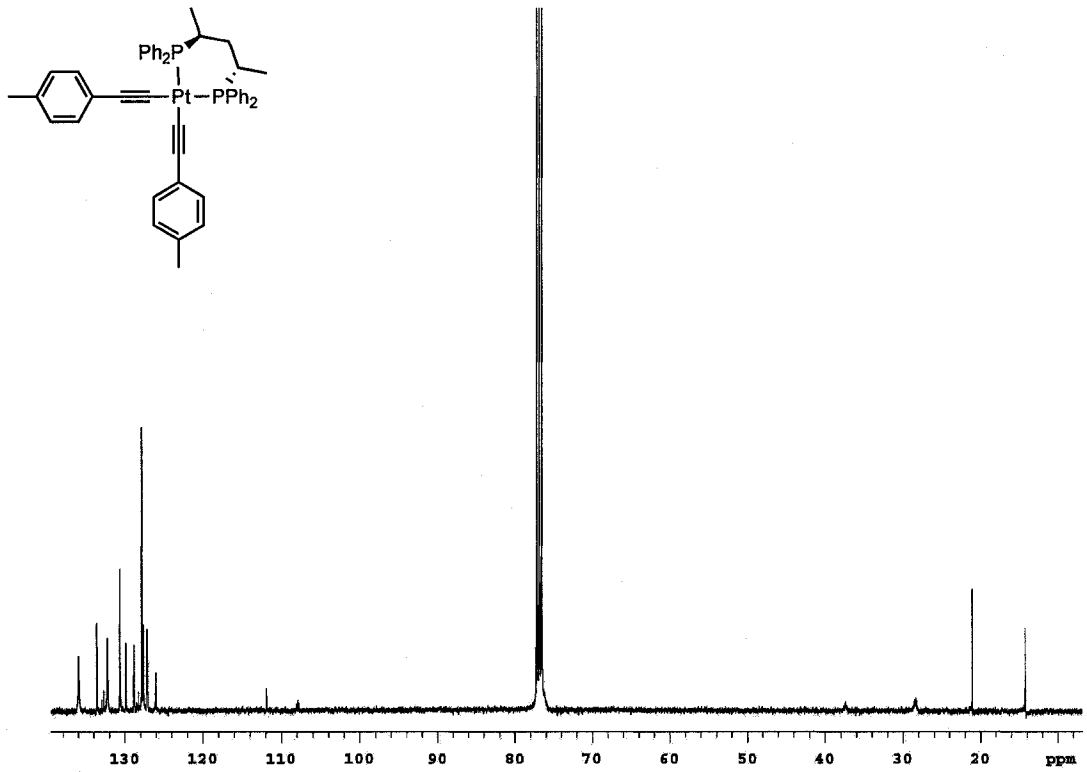

Figure A.27 ^{13}C {^{1}H} NMR spectrum of **230**

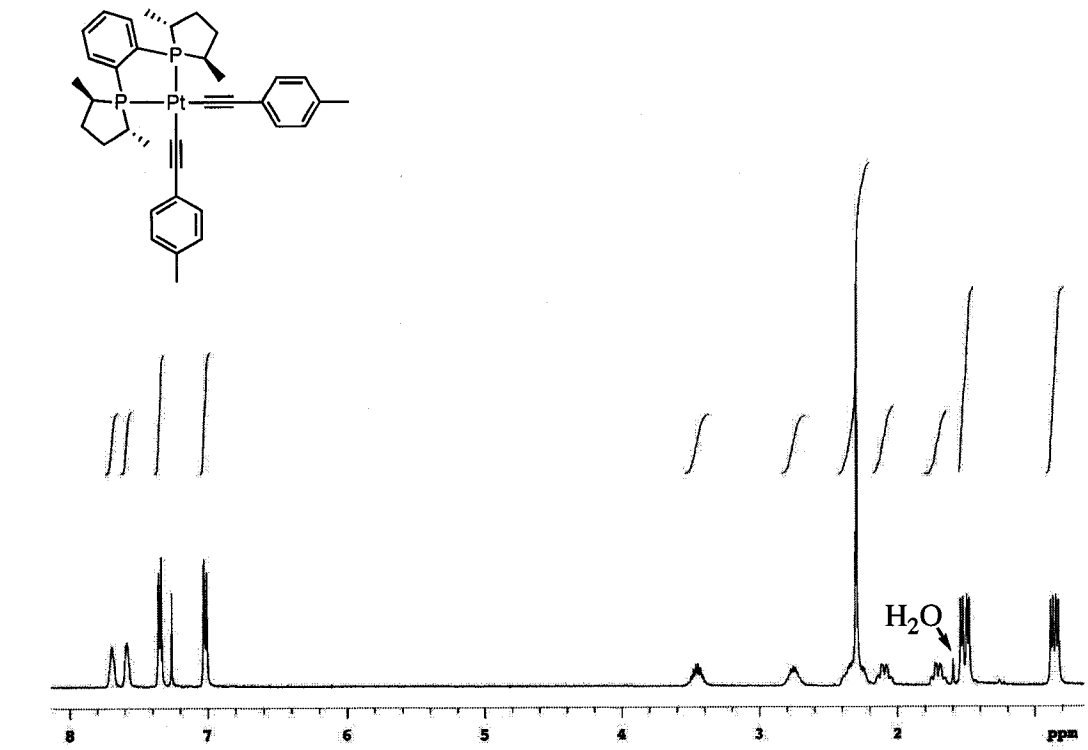

Figure A.28 ^{1}H NMR spectrum of **231**

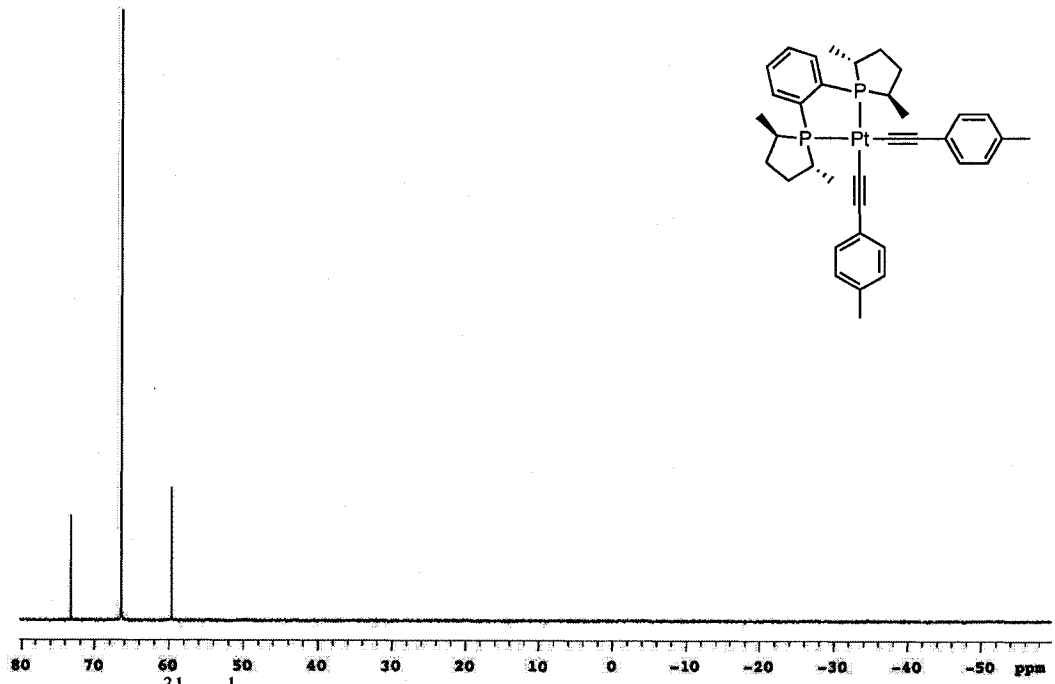

Figure A.29 ^{31}P $\{^{1}H\}$ NMR spectrum of **231**

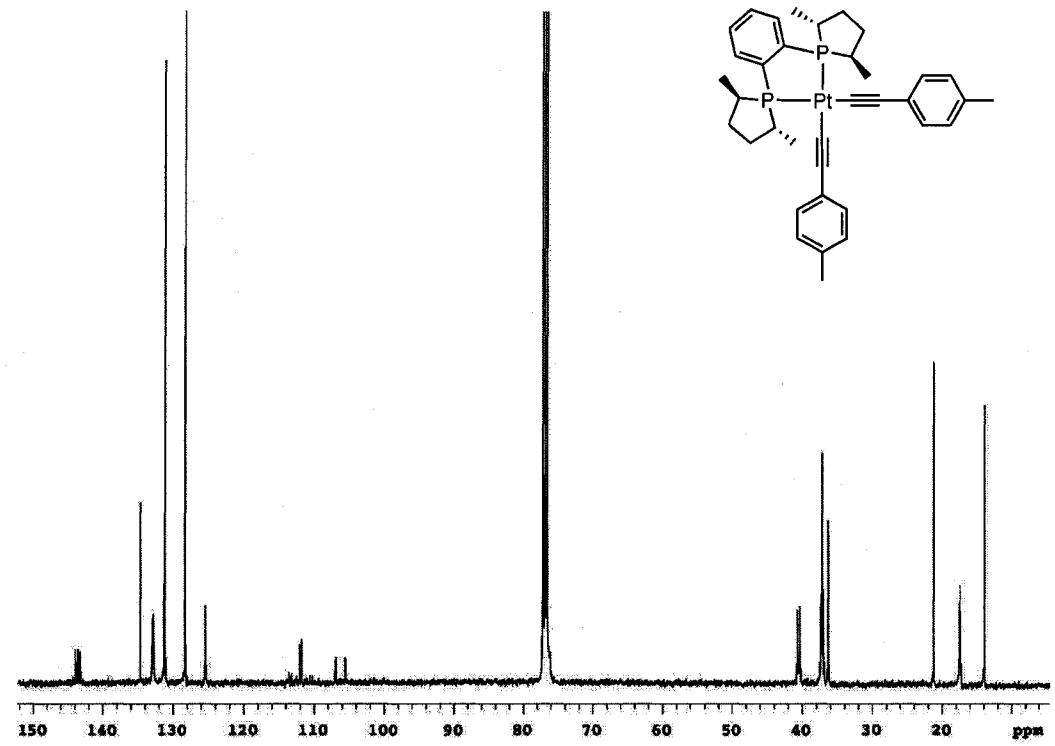

Figure A.30 ^{13}C $\{^{1}H\}$ NMR spectrum of **231**

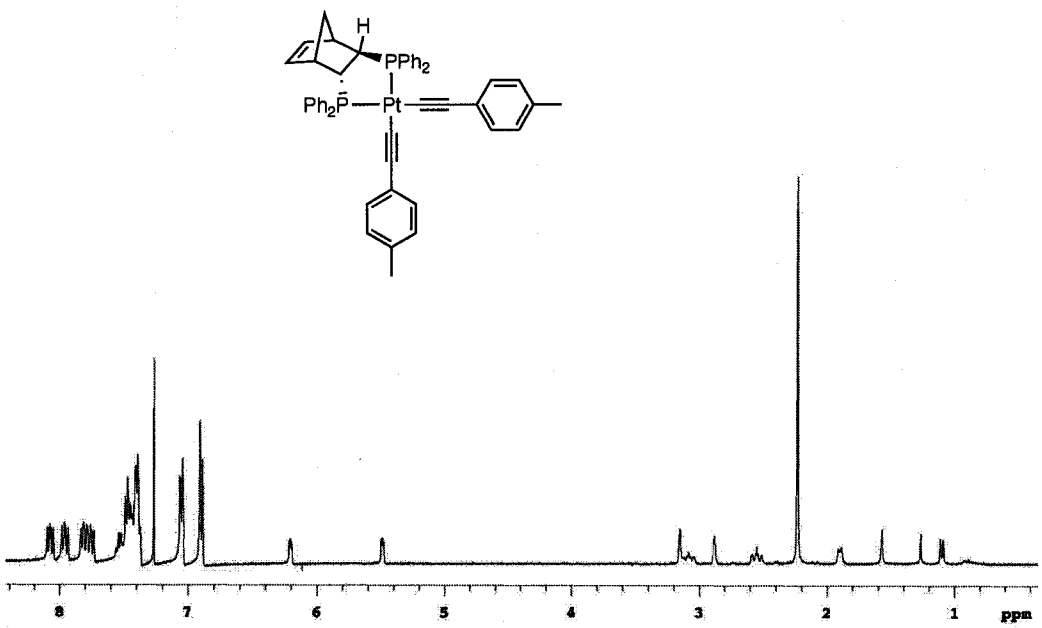

Figure A.31 ^{1}H NMR spectrum of **232**

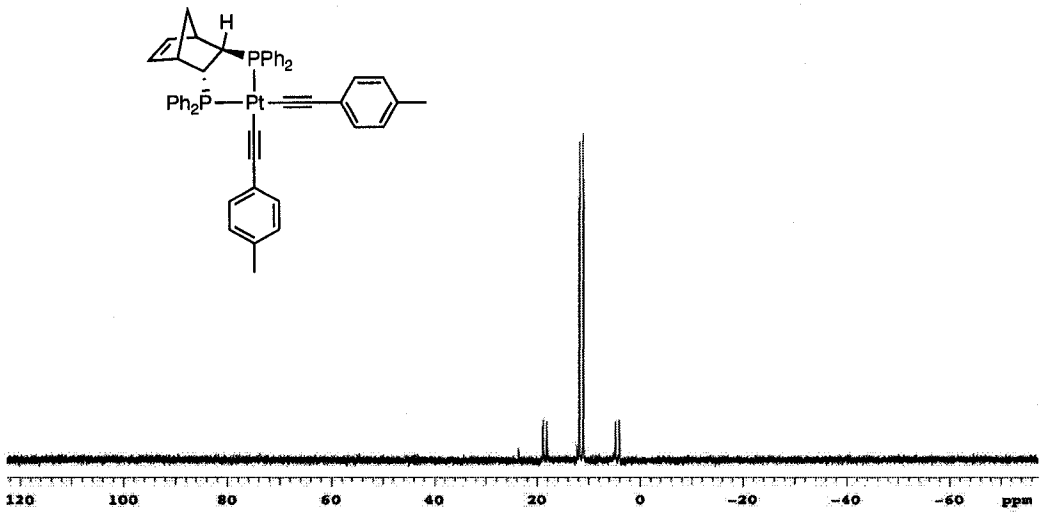

Figure A.32 ^{31}P $\{^{1}H\}$ NMR spectrum of **232**

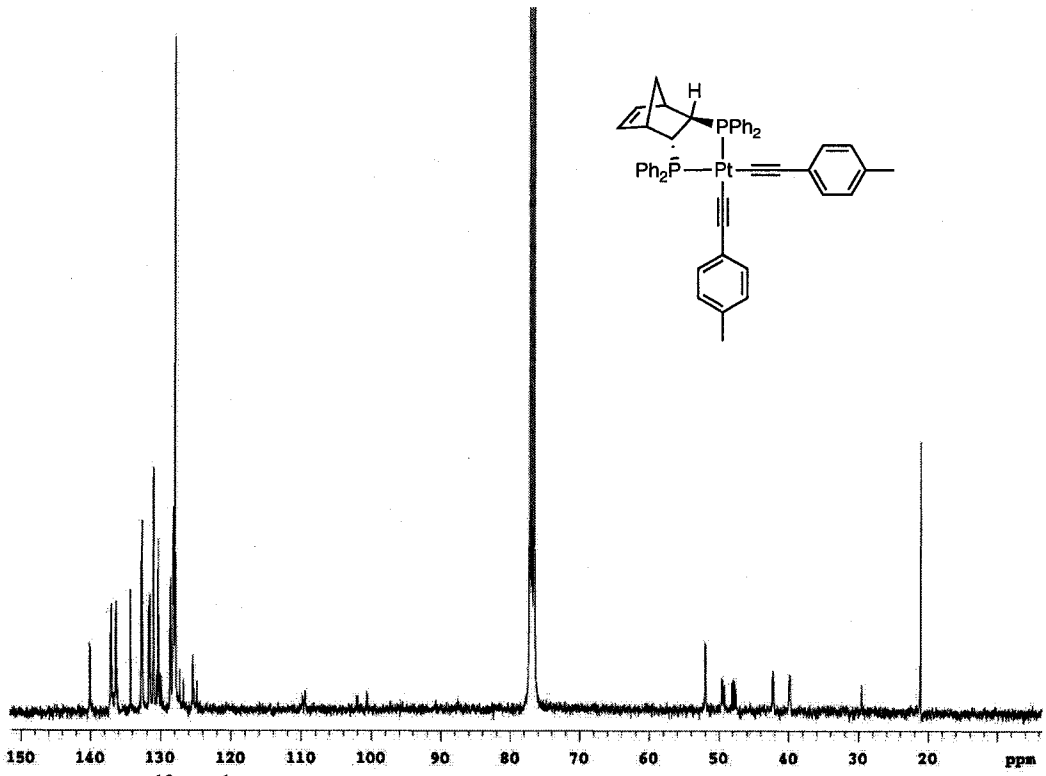

Figure A.33 ^{13}C {^{1}H} NMR spectrum of **232**

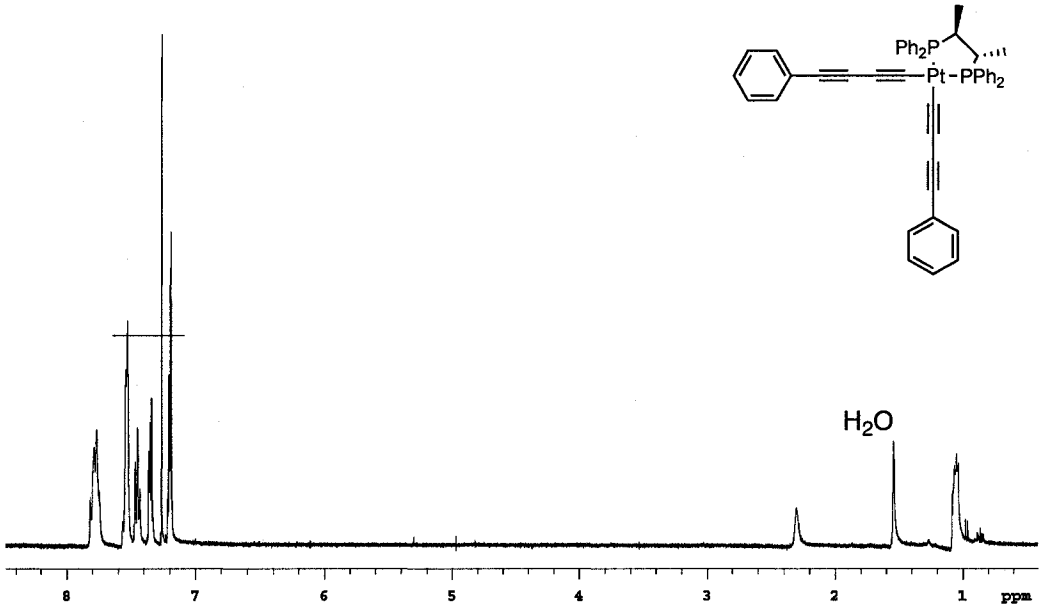

Figure A.34 ^{1}H NMR spectrum of **234**

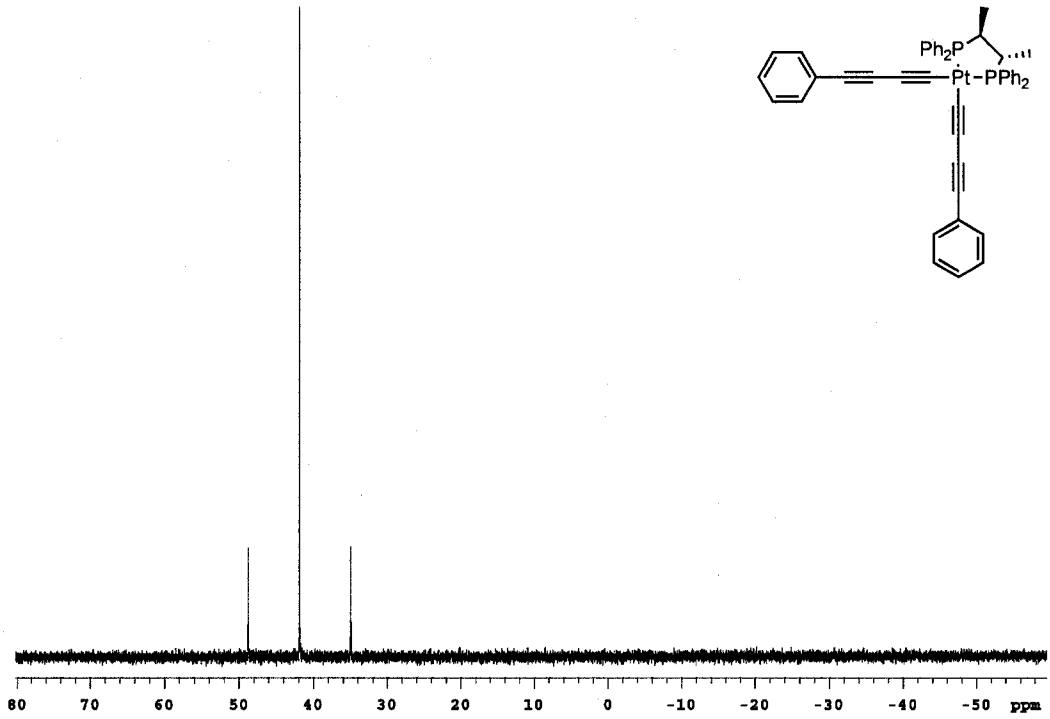

Figure A.35 ^{31}P $\{^{1}H\}$ NMR spectrum of **234**

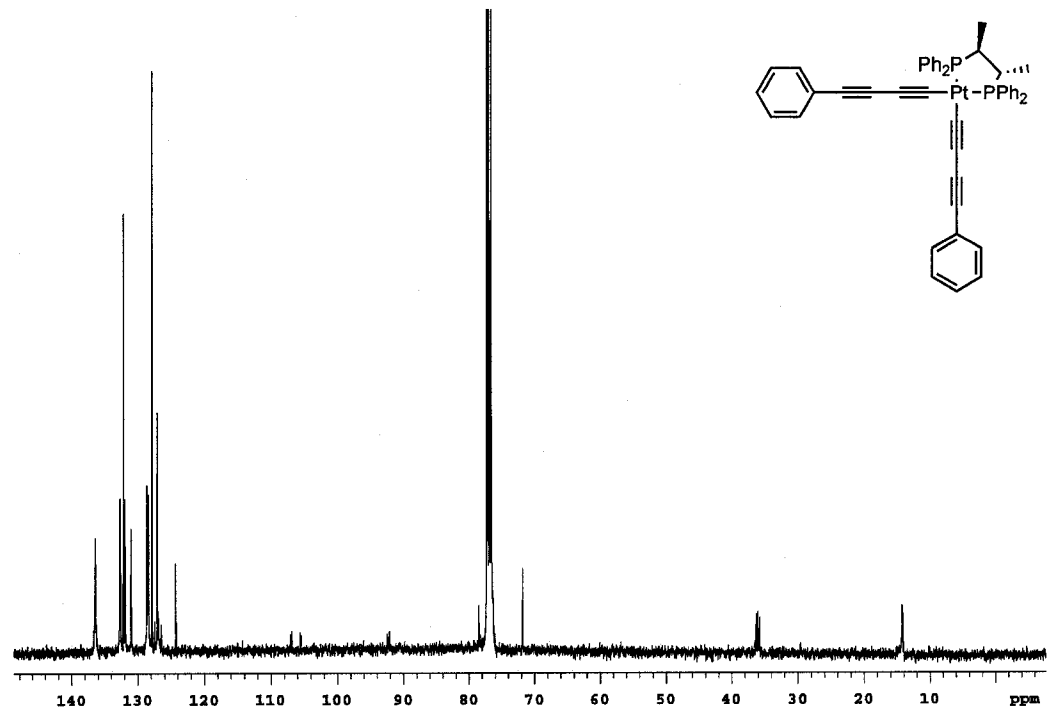

Figure A.36 ^{13}C $\{^{1}H\}$ NMR spectrum of **234**

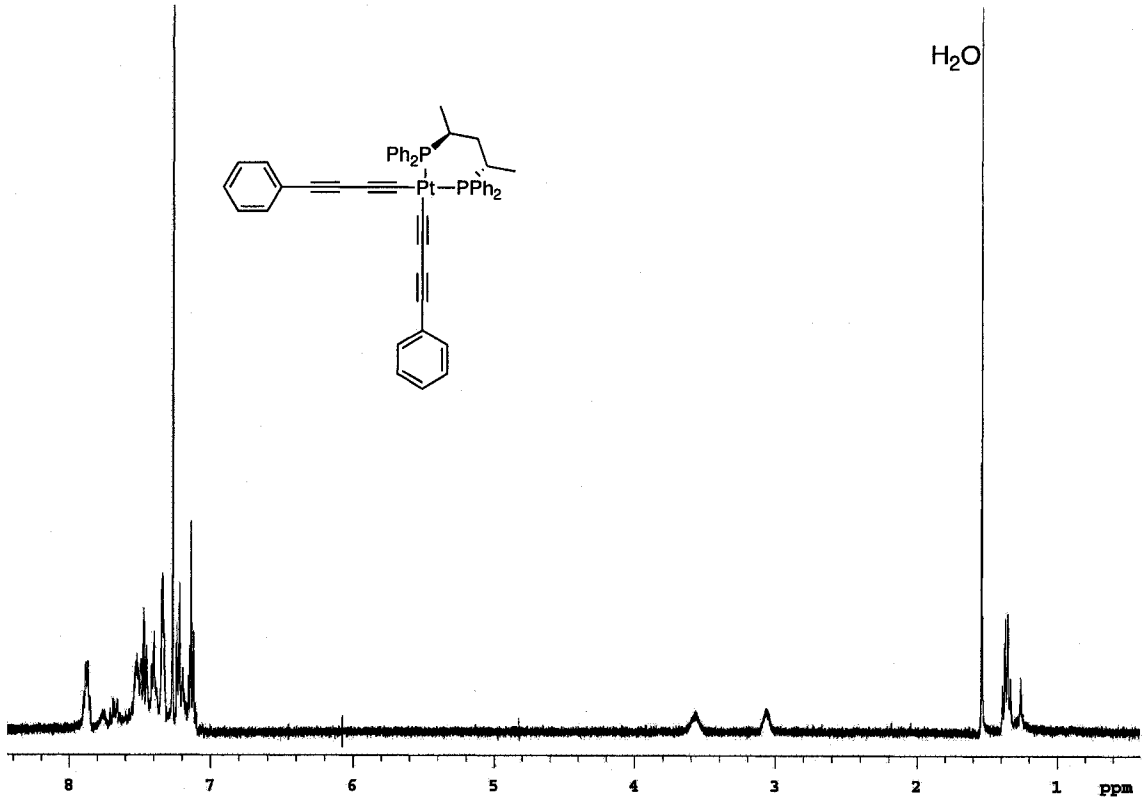

Figure A.37 ^{1}H NMR spectrum of **235**

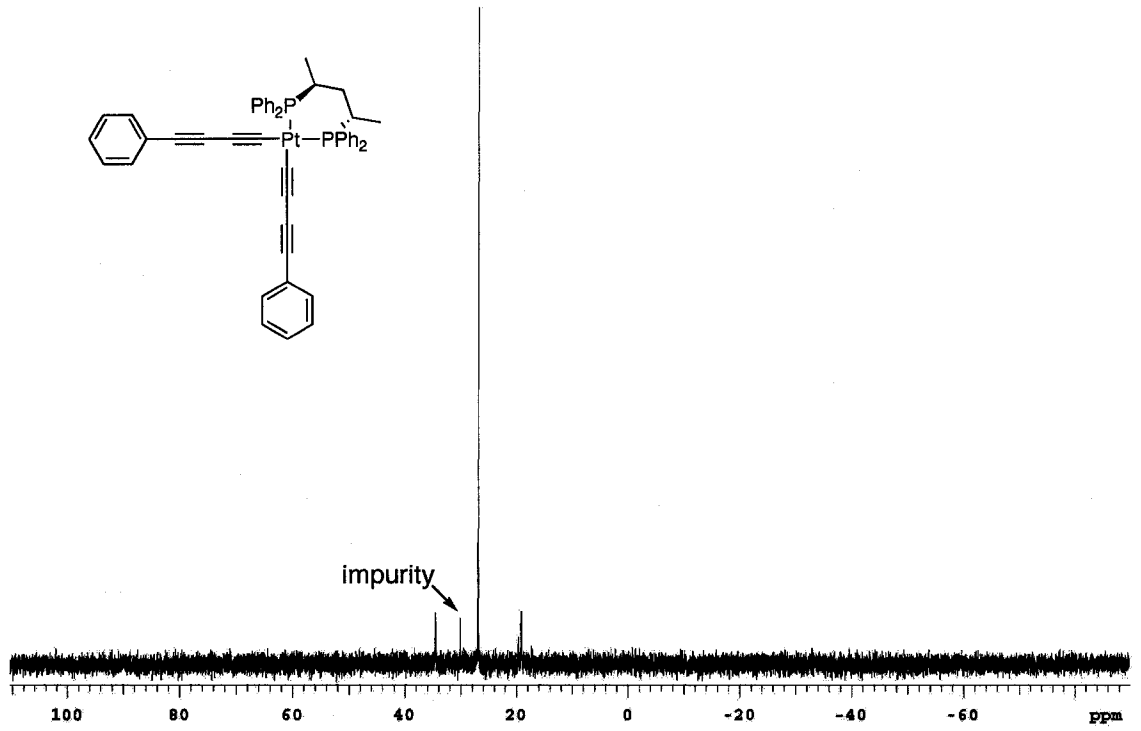

Figure A.38 ^{31}P $\{^{1}H\}$ NMR spectrum of **235**

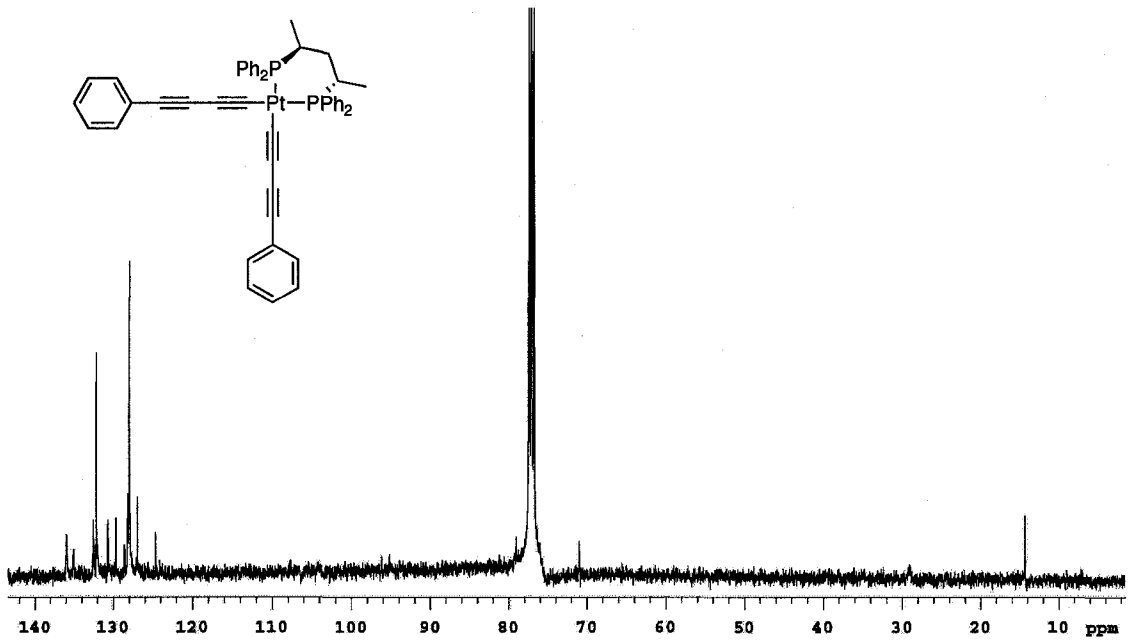

Figure A.39 ^{13}C $\{^{1}H\}$ NMR spectrum of **235**

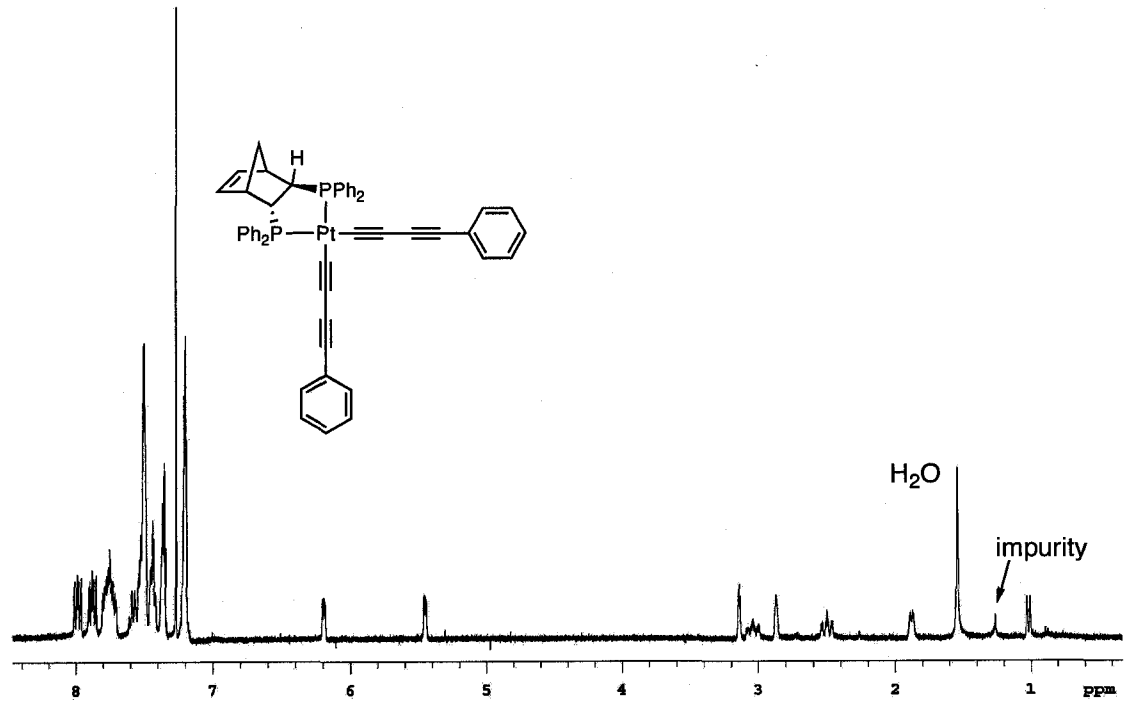

Figure A.40 ^{1}H NMR spectrum of **236**

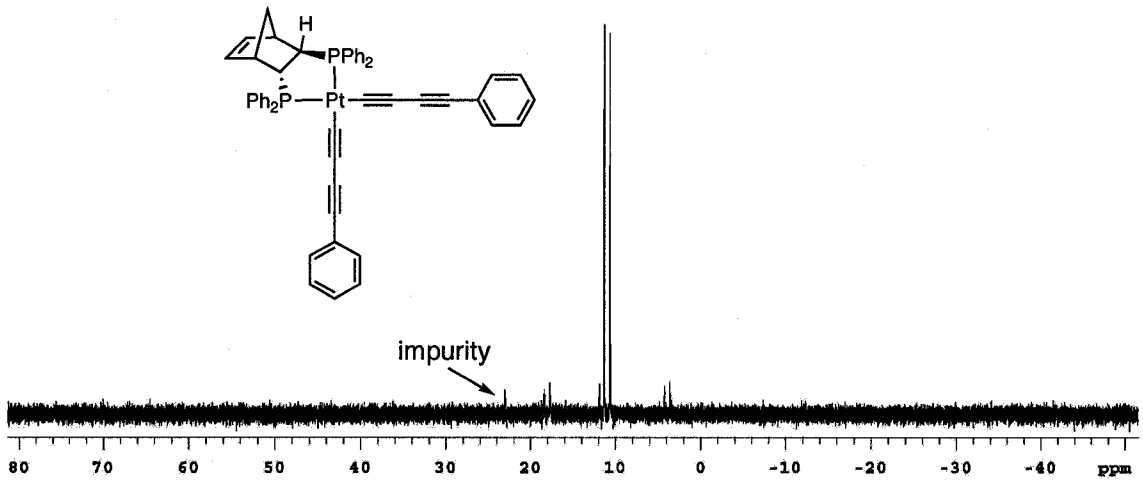

Figure A.41 ^{31}P $\{^{1}H\}$ NMR spectrum of **236**

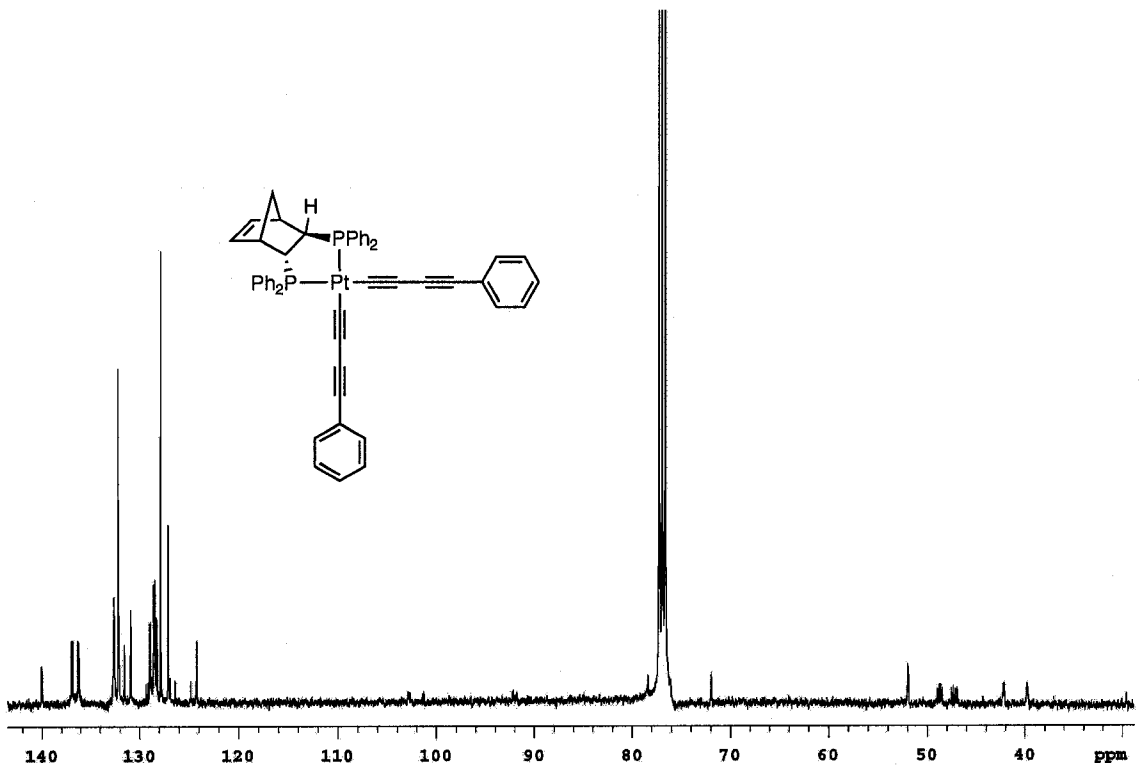

Figure A.42 ^{13}C $\{^{1}H\}$ NMR spectrum of **236**

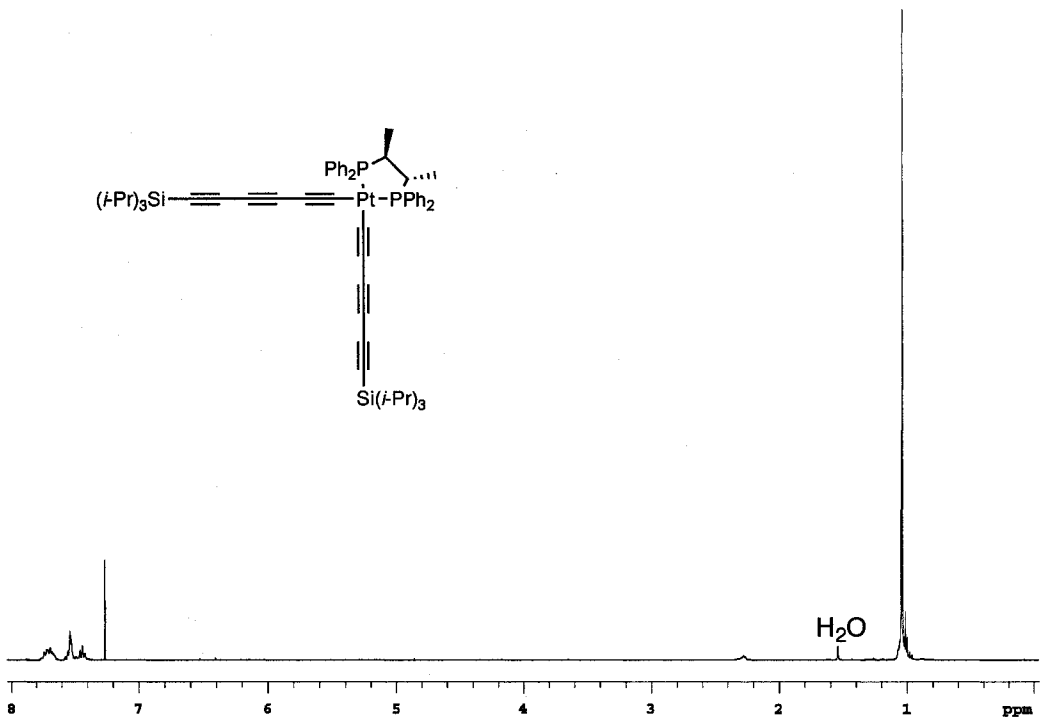

Figure A.43 ^{1}H NMR spectrum of **238**

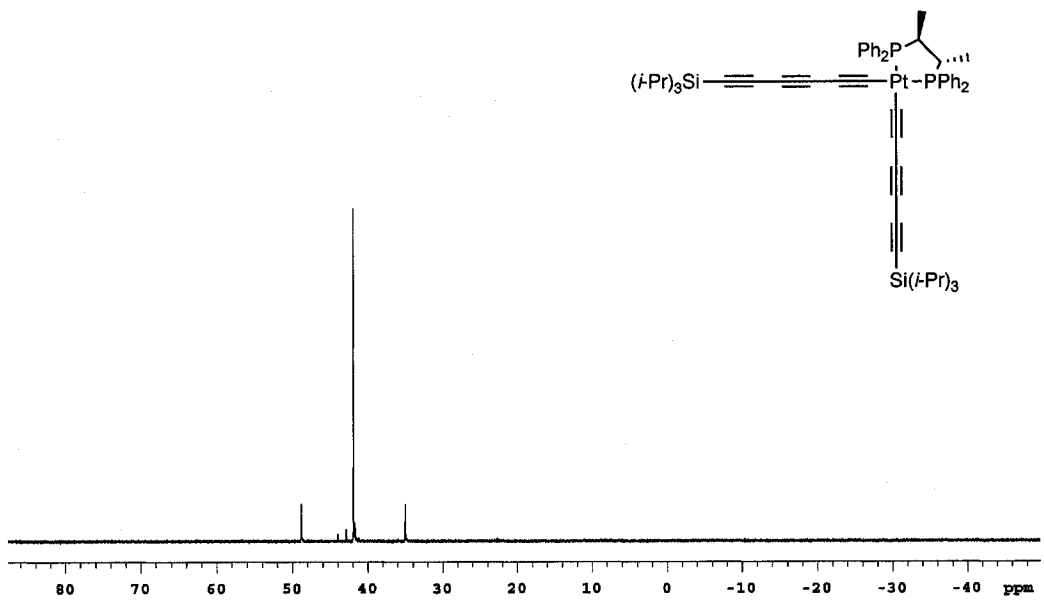

Figure A.44 ^{31}P $\{^{1}H\}$ NMR spectrum of **238**

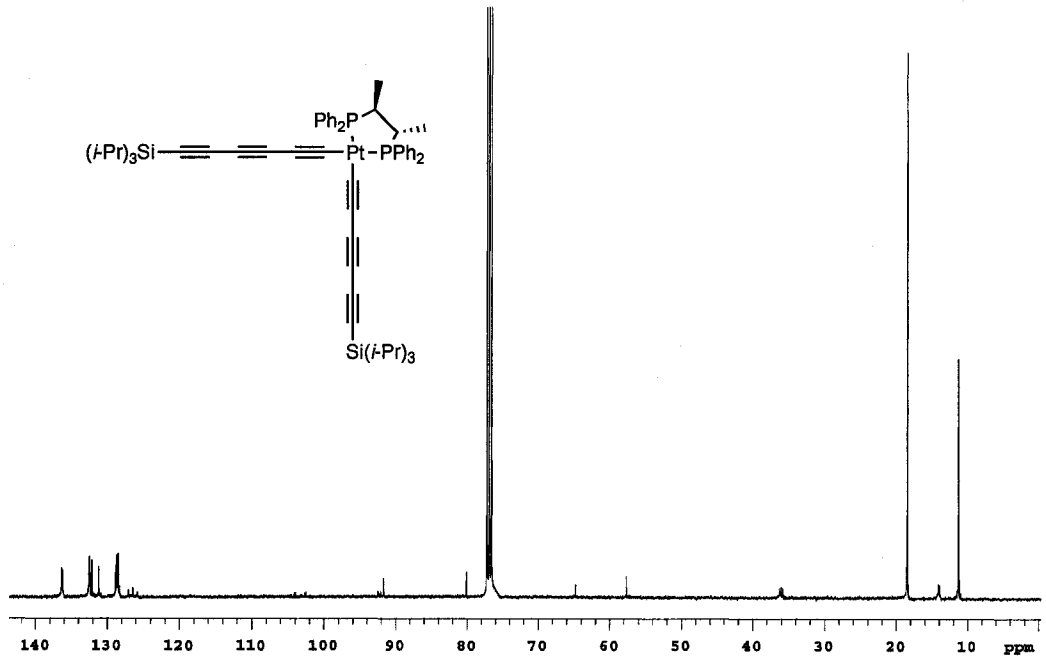

Figure A.45 ^{13}C {^{1}H} NMR spectrum of **238**

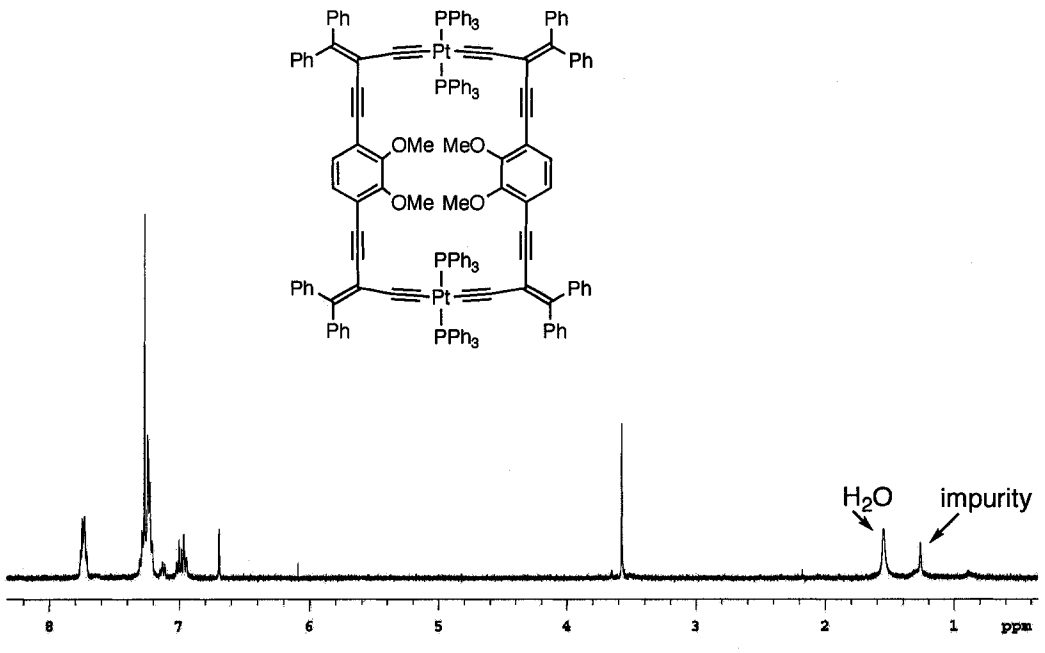

Figure A.46 ^{1}H NMR spectrum of **300**

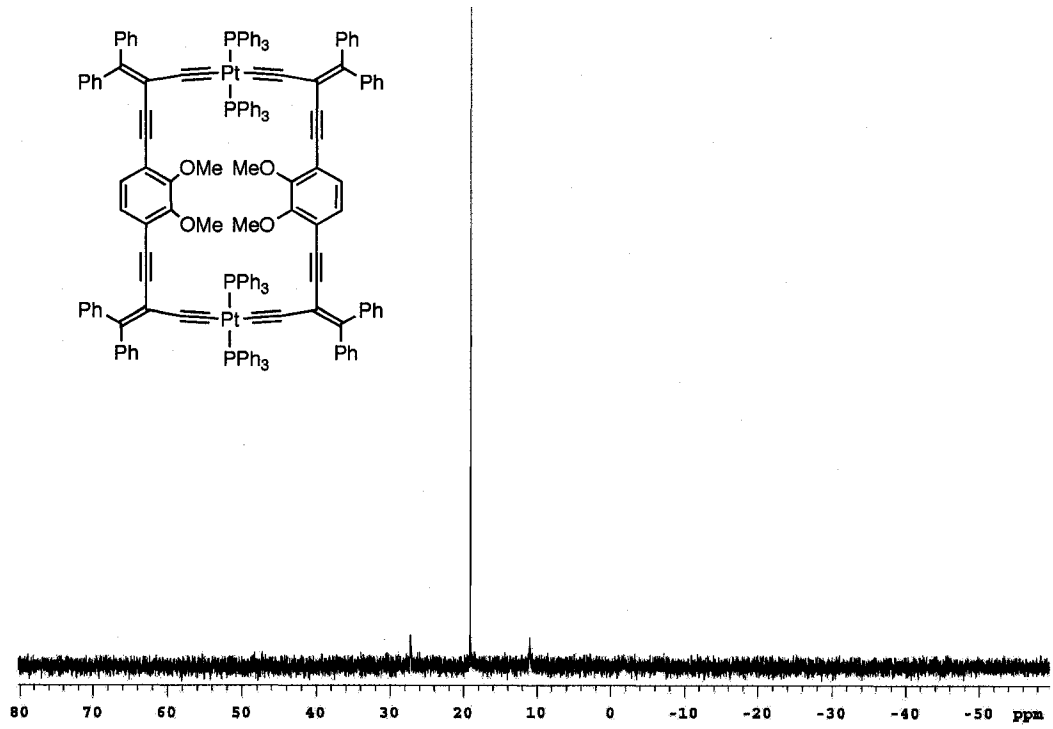

Figure A.47 $^{31}P\ \{^{1}H\}$ NMR spectrum of **300**

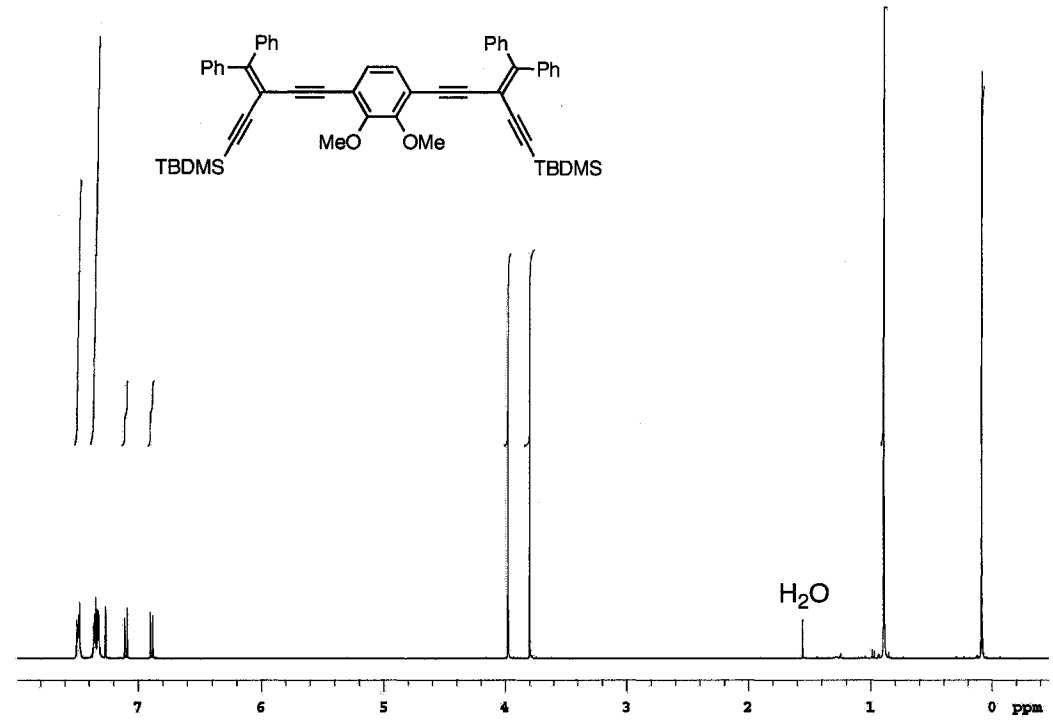

Figure A.48 ^{1}H NMR spectrum of **301**

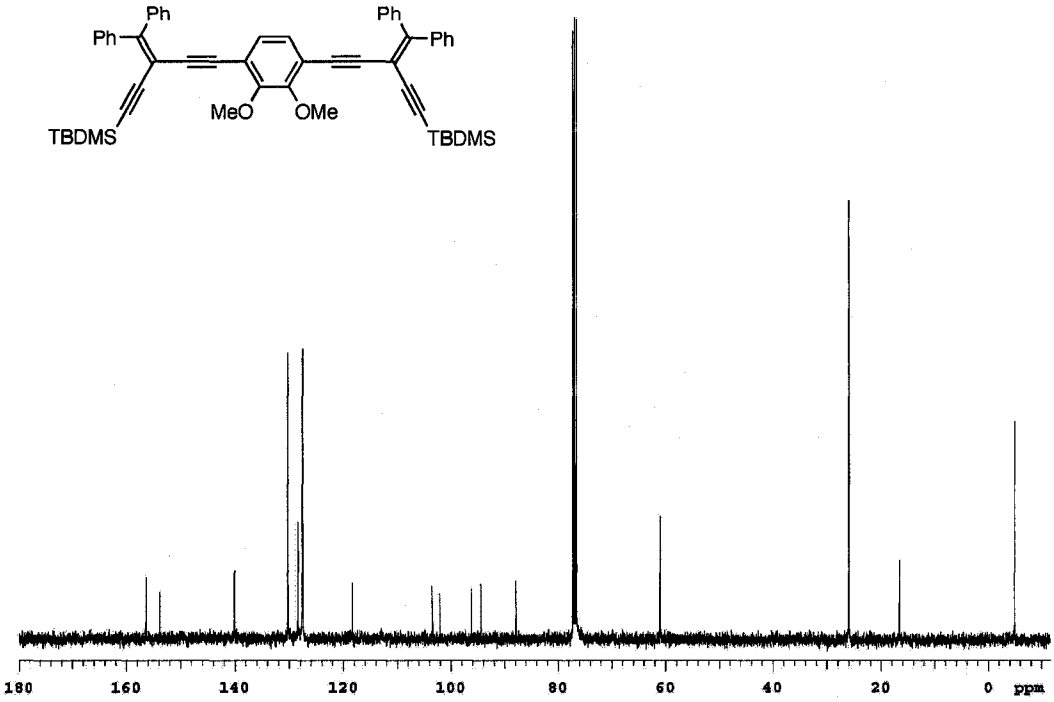

Figure A.49 ^{13}C {^{1}H} NMR spectrum of **301**

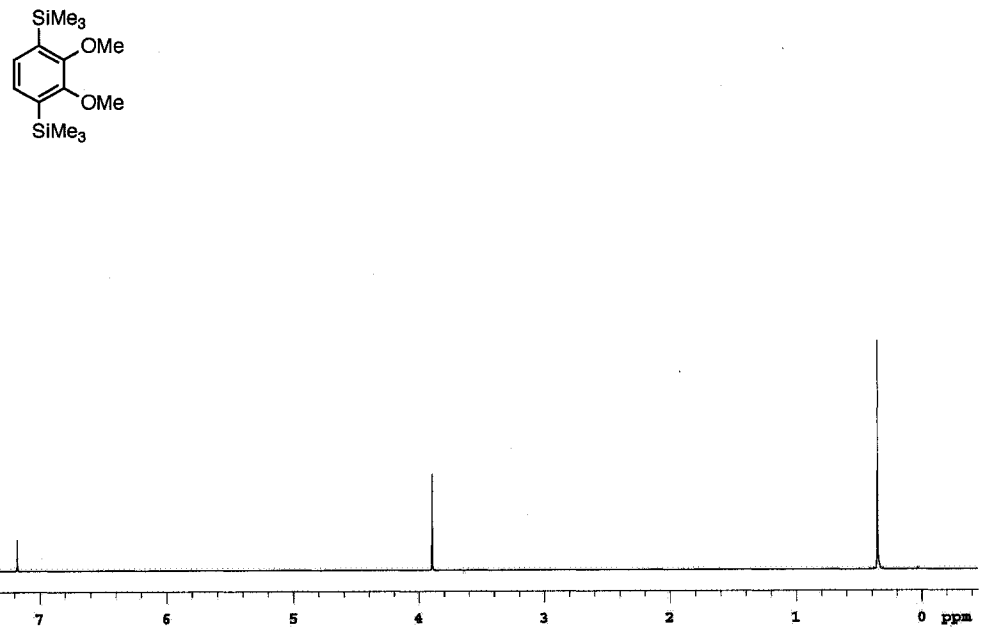

Figure A.50 ^{1}H NMR spectrum of **303**

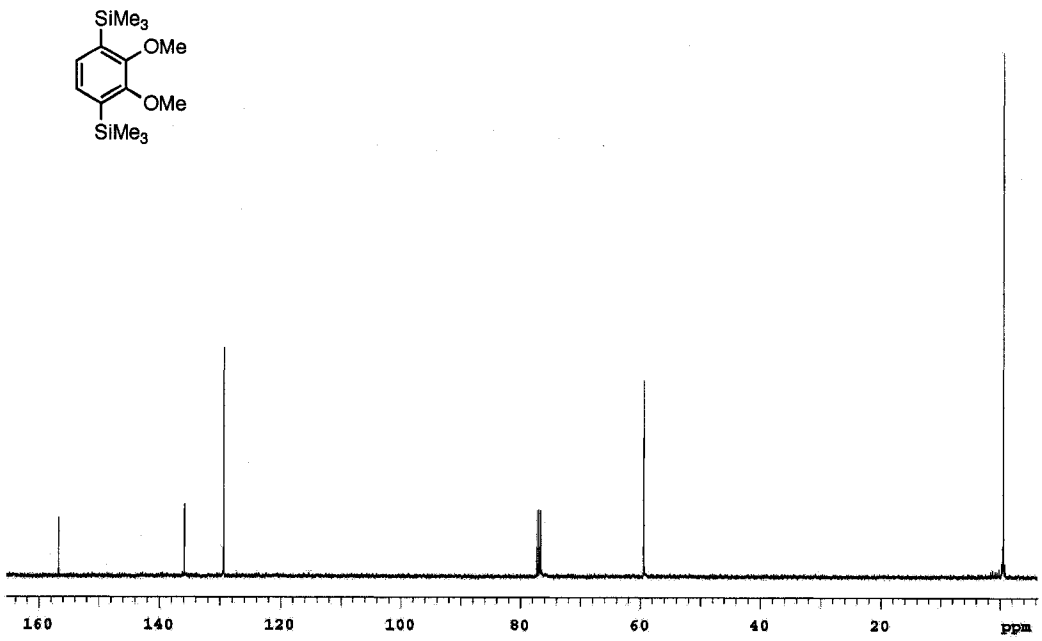

Figure A.51 ^{13}C {^{1}H} NMR spectrum of **303**

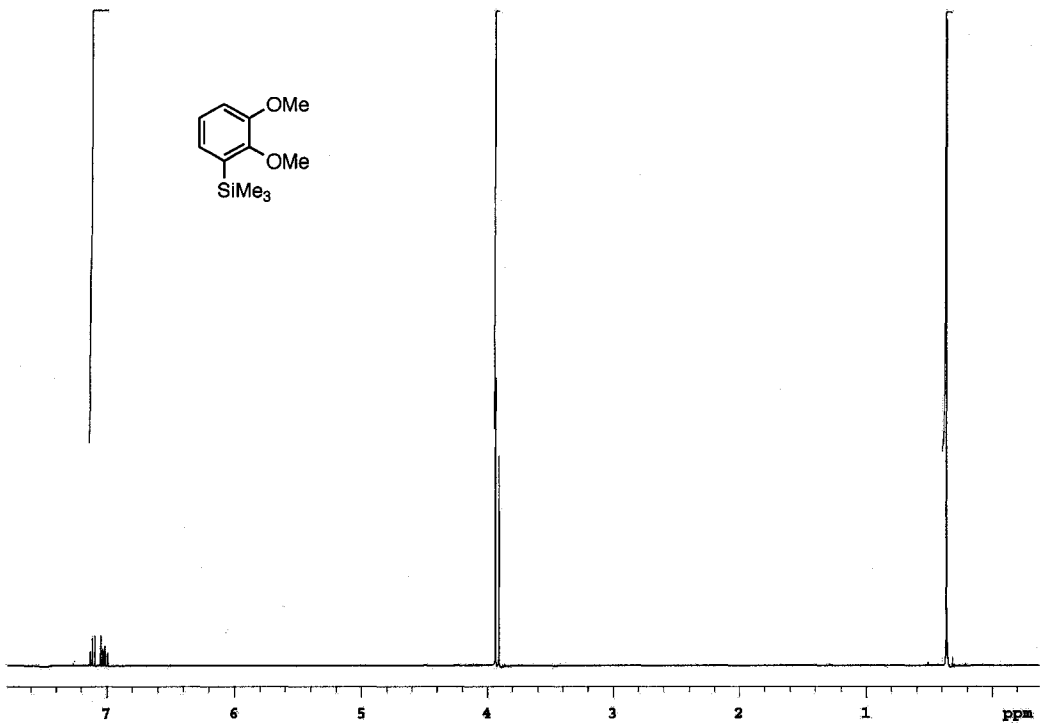

Figure A.52 ^{1}H NMR spectrum of **304**

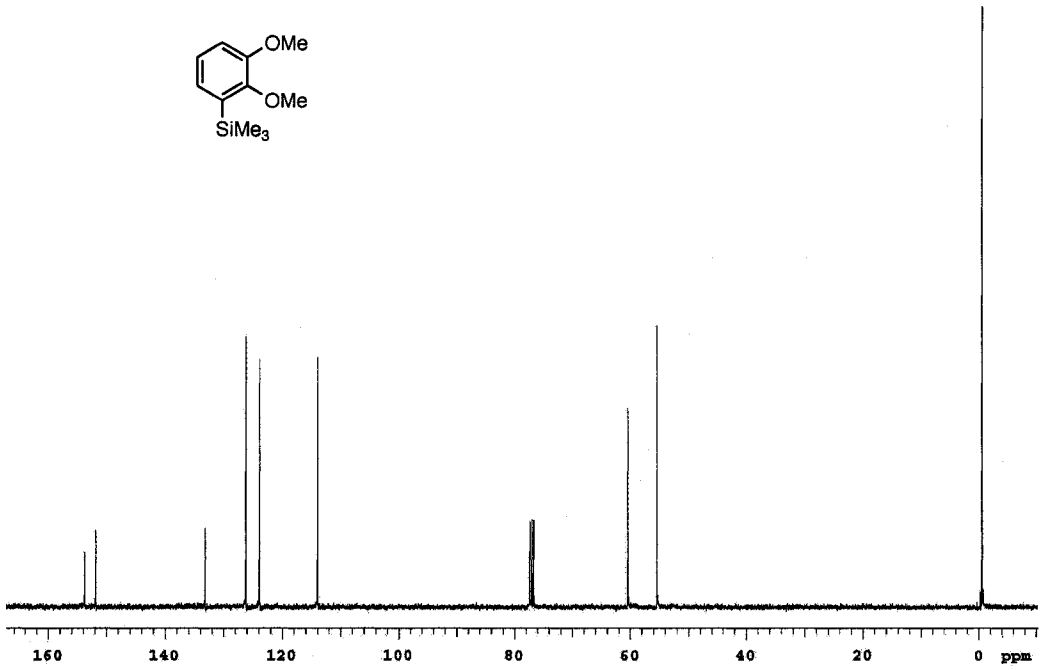

Figure A.53 ^{13}C {^{1}H} NMR spectrum of **304**

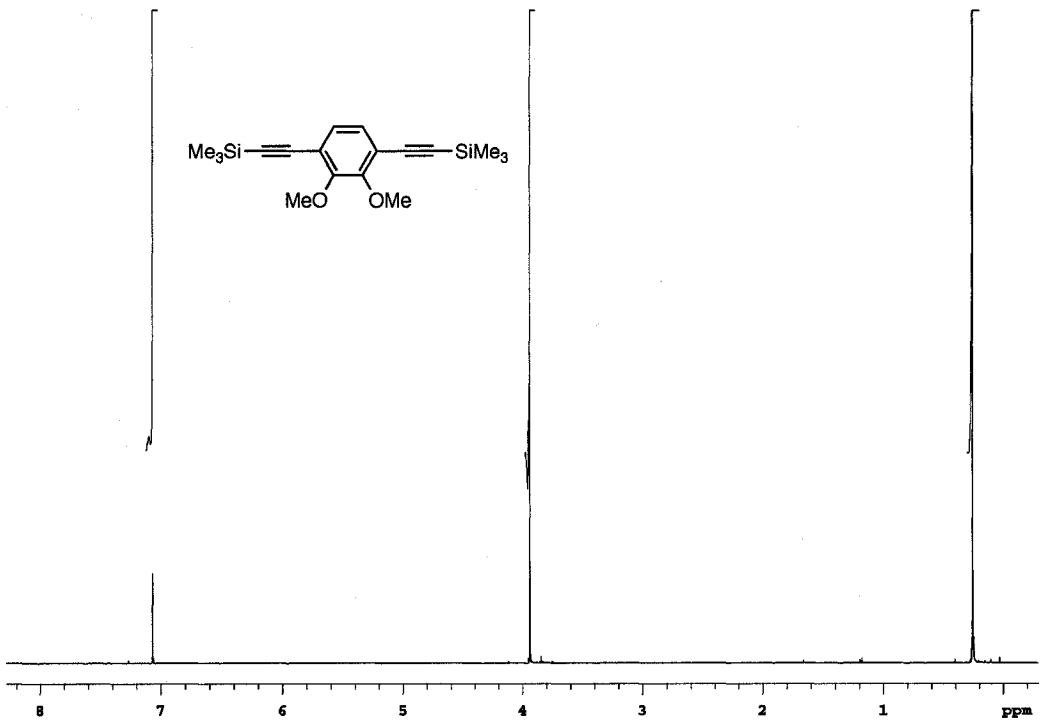

Figure A.54 ^{1}H NMR spectrum of **306**

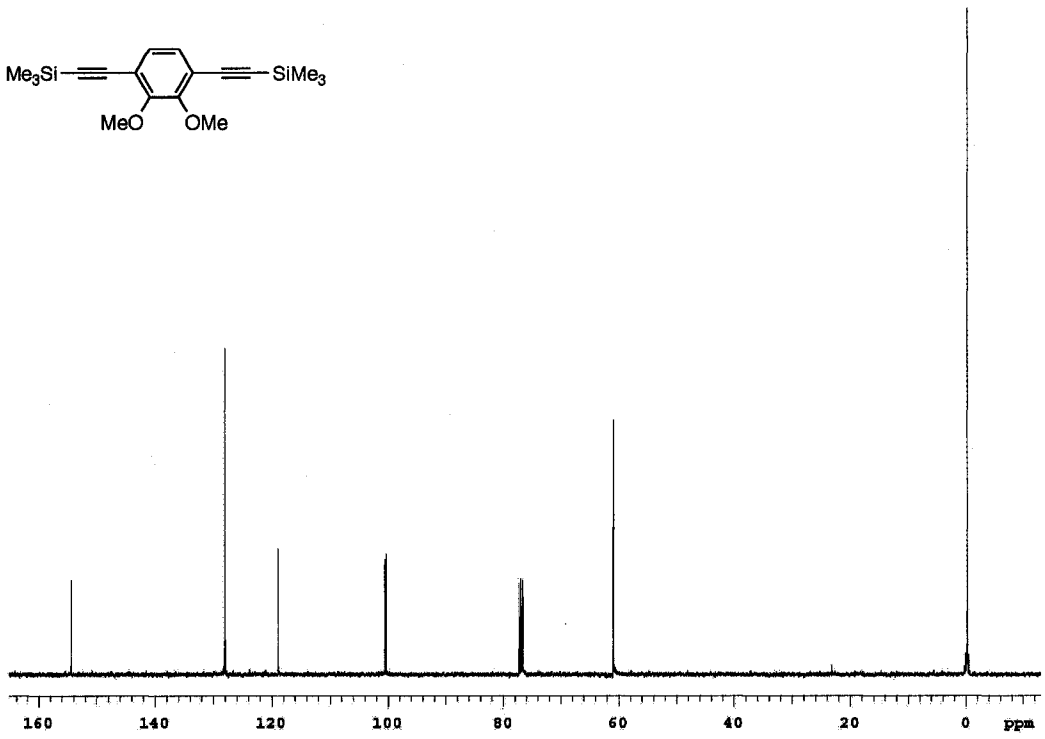

Figure A.55 ^{13}C {^{1}H} NMR spectrum of **306**

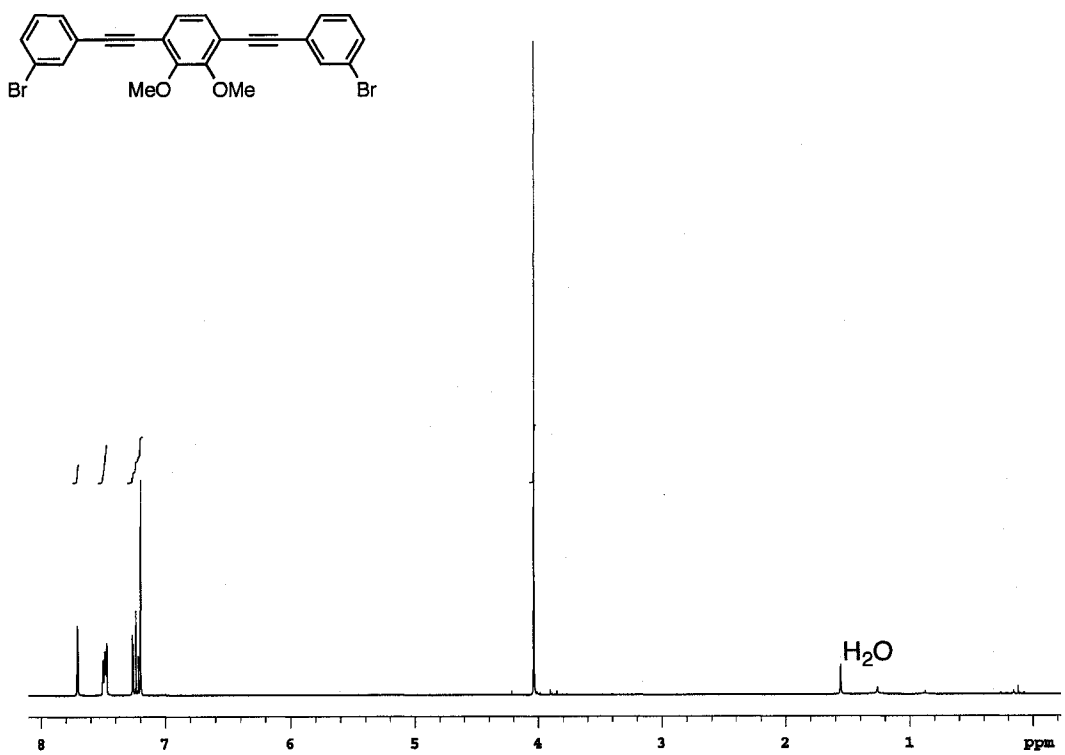

Figure A.56 ^{1}H NMR spectrum of **311**

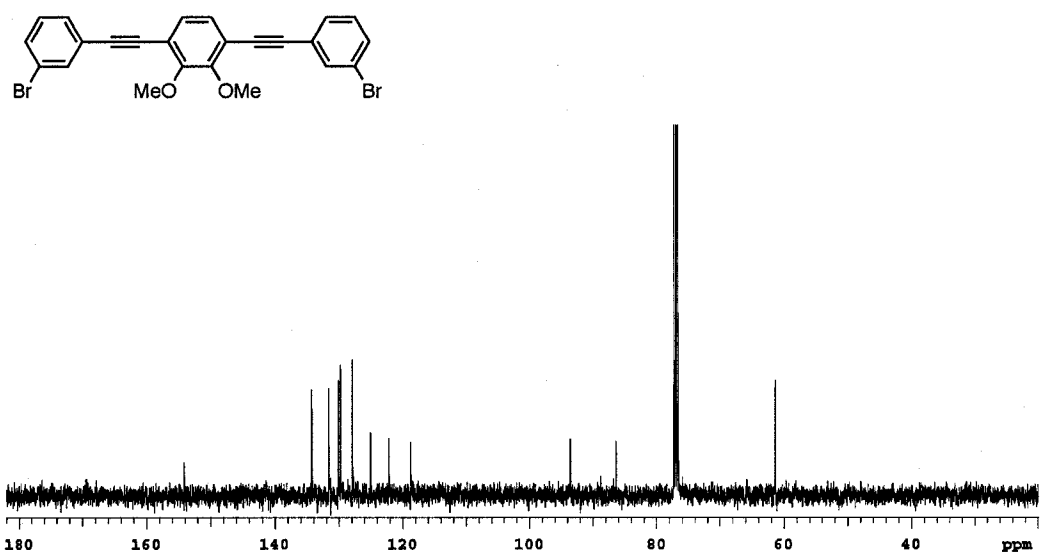

Figure A.57 ^{13}C {^{1}H} NMR spectrum of **311**

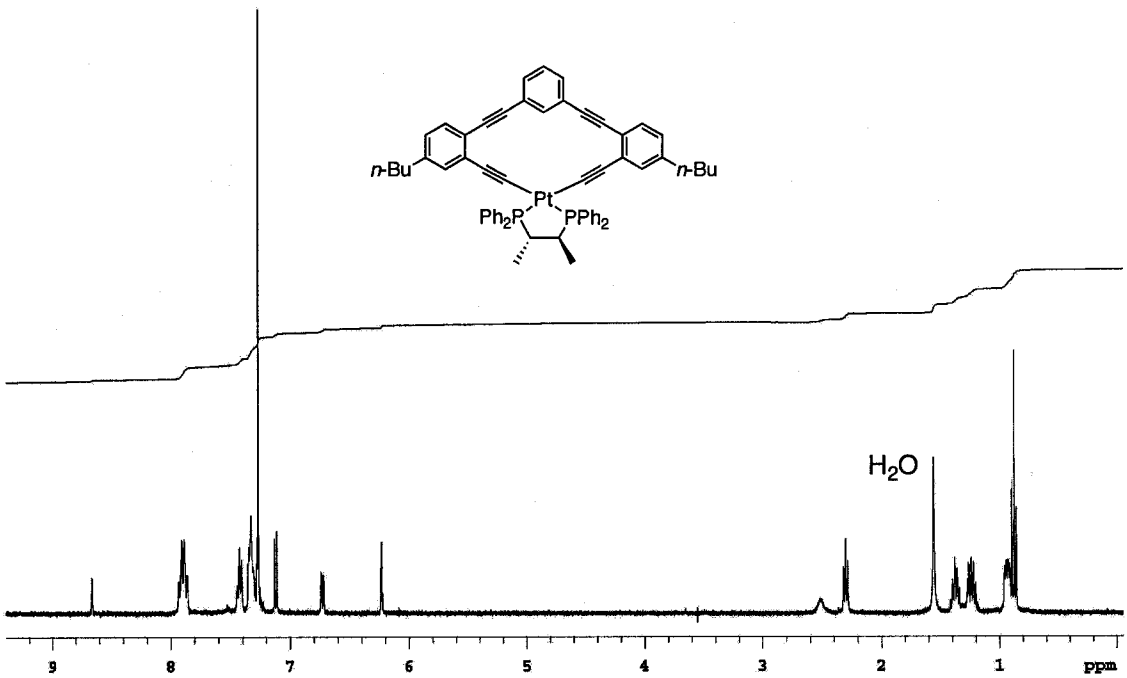

Figure A.58 ^{1}H NMR spectrum of **410**

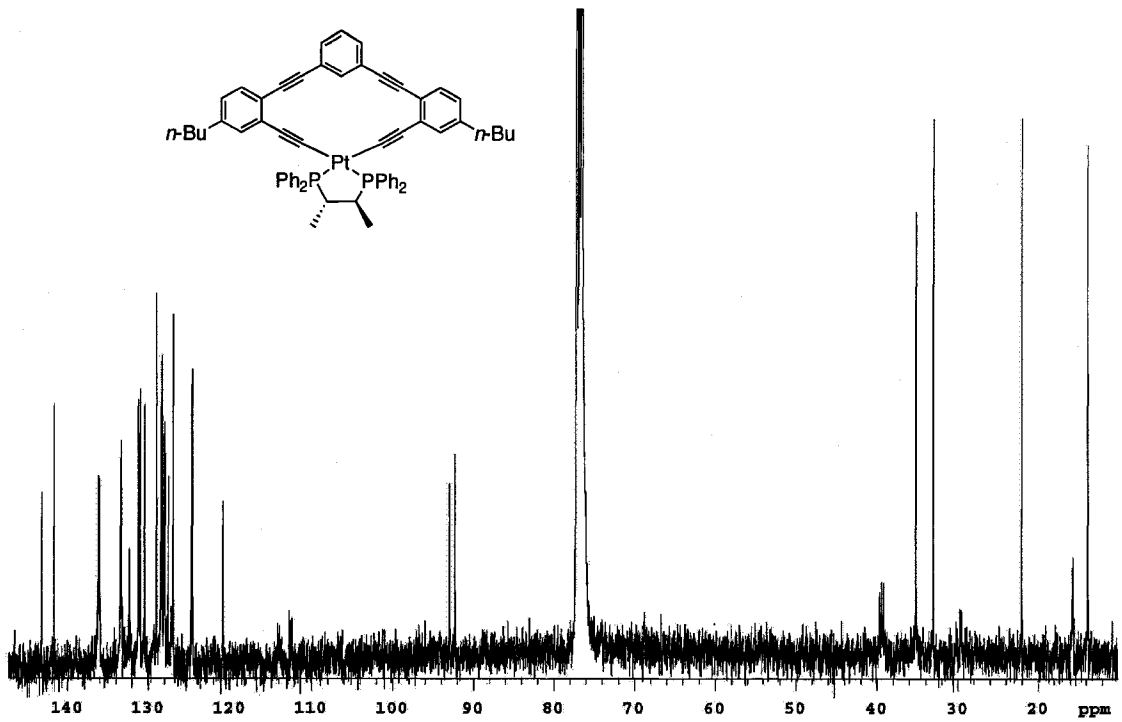

Figure A.59 ^{13}C {^{1}H} NMR spectrum of **410**

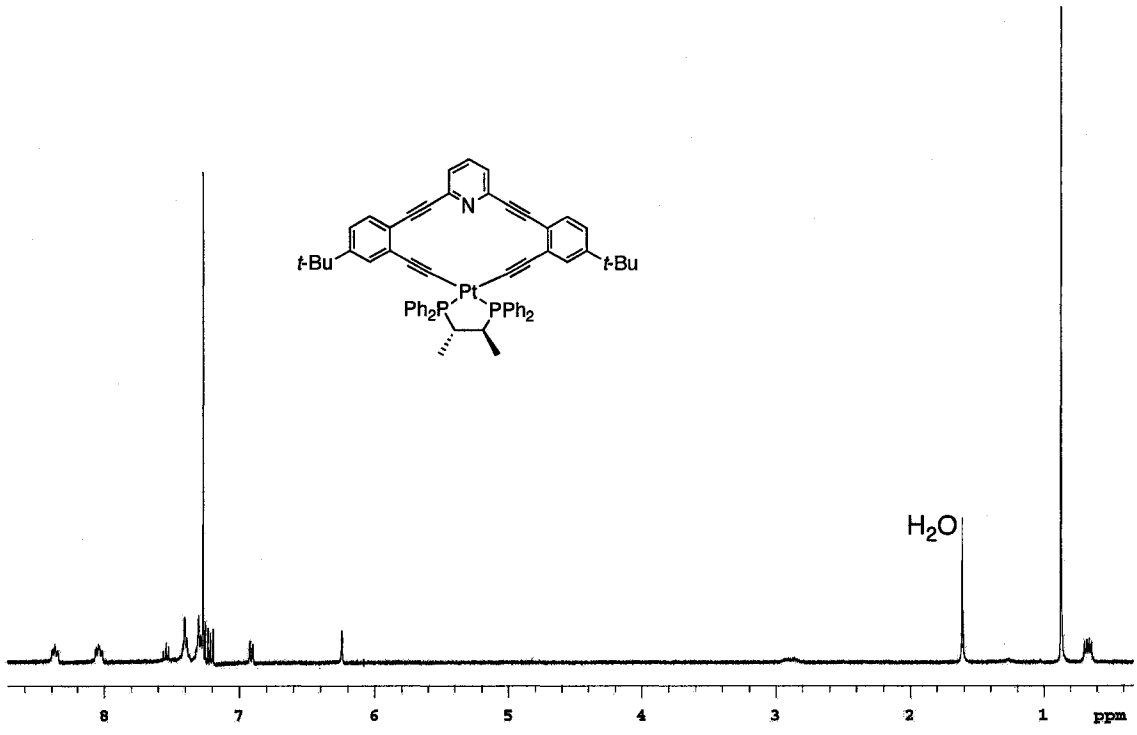

Figure A.60 ^{1}H NMR spectrum of **413**

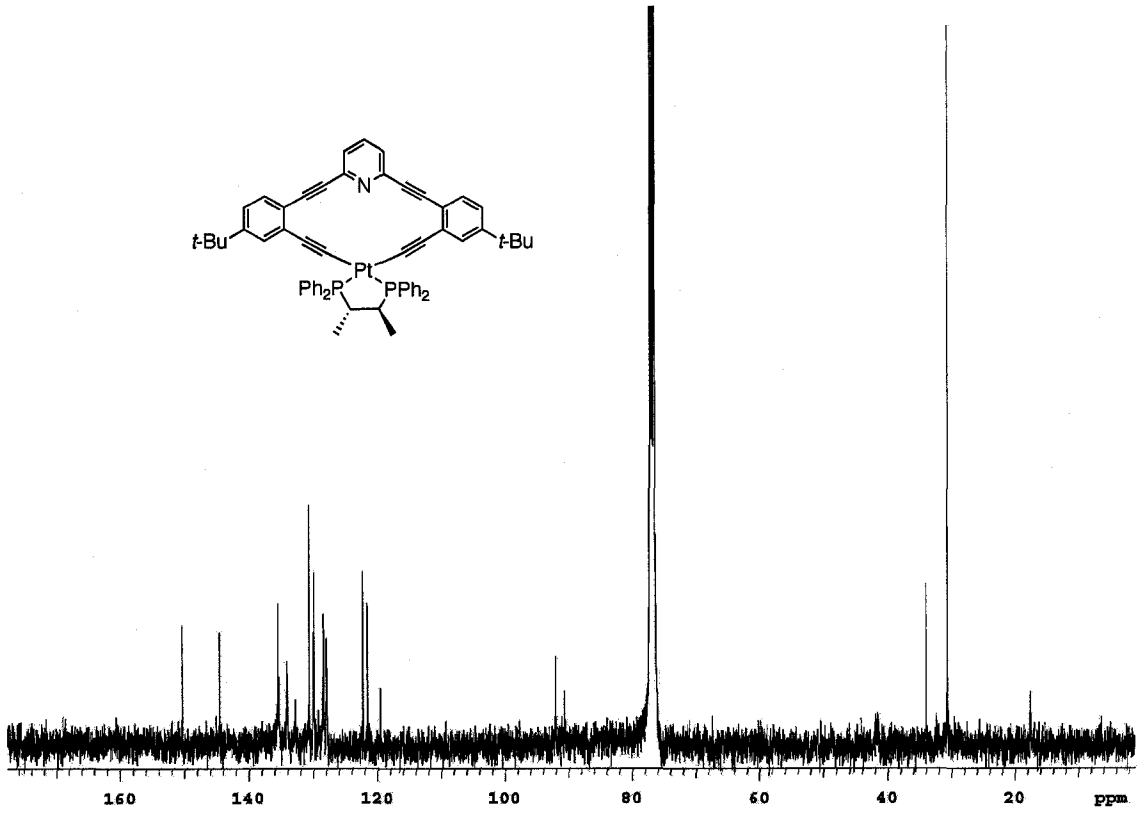

Figure A.61 ^{13}C {^{1}H} NMR spectrum of **413**

APPENDIX B

CIRCULAR DICHROISM SPECTROMETER DIRECTIONS FOR THE TYKWINSKI GROUP
Operation of CARY-17 Spectrophotometer and Olis Circular Dichroism Module

Turning On the Instrument and Computer

1. Turn nitrogen gas ON.

2. Turn cooling box ON.
   a. Must see RED light ON.
   b. If red light not ON, switch tubes to flush, then return to original postion.
   c. If bubbles present, switch tubes and flush.

3. Turn on Xenon lamp.
   a. Must see GREEN light ON.

4. Use manual trigger and wait until 150 W before scanning.

5. Turn on Main Computer.

6. Turn on Computer.

Using OLIS Globalworks

1. Open OLIS Globalworks icon.
2. Choose Data Collection.
3. Choose Conv CD.
4. Create Protocol.
   a. Temp Conroller
      i. Set to 20 °C
   b. Parameter
      i. Check PMT1 and PMT2
      ii. Select CD units in millidegrees
   c. X and Y axes
      i. X axis min 240
      ii. Y axis max 700
      iii. Check Auto scale Y
      iv. Check Auto scale Raw Data
   d. Repeated Scans
      i. Select: Auto
      ii. # scans = 1
      iii. Repeat: none
   e. Operational Modes
      i. Select: Fixed Bandwidth, Scan, CD, minutes, Integration as a Function of High Volts

f. Increments
    i. Choose number of scans to do in scan range.
    (ie. 700–240nm = 460 nm)
        1. For quick scan, every 5 nm choose 460/5 = 92 scans
        2. For slow scan, every 1 nm choose 460/1 = 460 scans
        3. Choose Bandwidth = 2.00 [k]nm

5. To save this protocol:
    a. Go to FILE.
    b. Select Save Protocol As.

Obtaining a Spectrum

1. Use a circular cuvette.
2. Scan sample of solvent to use as a background. (Note: Make sure wavelength range and increments match that of your sample runs.)
3. Scan sample.
4. To subtract background:
    a. Select sample spectrum file.
    b. Then select solvent spectrum file.
    c. Right click mouse and choose SUBTRACT DATASETS. (Note: Every sample scanned must have the background subtracted.)
5. Data has been collected as millidegrees vs. wavelength. To convert to $\Delta\varepsilon$:
    a. Select spectrum that you want the units converted.
    b. Right click mouse and choose CONVERT CD UNITS.
    c. Choose MOLAR EXTINCTION.
    d. Enter in MW, concentration (g/L) and path length (cm). ENTER.
6. To smooth data:
    a. Select spectrum to smooth.
    b. Right click mouse and select DIGITAL FILTER.
    c. Enter 25. ENTER.
7. To save any spectrum:
    a. Select spectrum to save.
    b. Go to FILE.
    c. Select Save Dataset As.
8. To transfer data to Excel:
    a. Right click on spectrum, it should change from red to yellow.
    b. Select Move file to Excel.
    c. Use Excel to graph data.

To Plot CD and UV–vis Spectra on the Same Graph in Excel

1. Select one data series on graph.
2. In the Format Menu select: Selected Data Series.
3. In the Axis tab select: Secondary axis.

APPENDIX C

DERIVATION OF EXPONENTIAL ABSORPTION INDEX, k: For Circular Dichroism Spectroscopy[1]

Achiral Absorption

Beer's Law at a fixed wavelength, λ (nm)

$A = \log (I_o / I) = \varepsilon bc$

where
A = absorbance
ε = molar absorptivity (L mol^{-1} cm^{-1})
b = path length (cm)
c = concentration (mol L^{-1})
I = intensity of light leaving sample cell
I_o = intensity of light incident upon sample cell

$I = I_o 10^{-\varepsilon bc}$ or $I = I_o e^{-4\pi kb/\lambda}$

k = exponential absorption index (dimensionless)

$I_o 10^{-\varepsilon bc} = I_o e^{-4\pi kb/\lambda}$ I_o cancels

$10^{-\varepsilon bc} = e^{-4\pi kb/\lambda}$ Natural log

$-\varepsilon bc(\ln 10) = \frac{-4\pi kb}{\lambda} (\ln e)$ ln e = 1, b cancels

$\varepsilon c(\ln 10) = \frac{4\pi k}{\lambda}$ Solve for k

$$k = \frac{(\ln 10)\, c\lambda\varepsilon}{4\pi}$$

Chiral Absorption (circular dichroism at a fixed wavelength)

$$k_l - k_r = \frac{(\ln 10)\, c\lambda}{4\pi} (\varepsilon_l - \varepsilon_r)$$

Ellipticity (ψ) = $\frac{\pi b (k_l - k_r)}{\lambda}$ in radians

Solve for ($k_l - k_r$)

l = left circularly polarized light,
r = right circularly polarized light

$$k_l - k_r = \frac{(\ln 10)\, c\lambda}{4\pi} (\varepsilon_l - \varepsilon_r) = \frac{\psi\lambda}{\pi b}$$

λ and π cancel
Solve for ellipticity (ψ) in radians

$$\psi = \frac{(\ln 10)\, cb}{4} (\varepsilon_l - \varepsilon_r)$$

Convert to elipitcity (θ) in millidegrees, m°
$\Delta\varepsilon = (\varepsilon_l - \varepsilon_r)$

$$\theta = \frac{(\ln 10) 360\ °(1000\ m°) cb\, \Delta\varepsilon}{4(2\pi)}$$

$$\theta = 32982 cb\, \Delta\varepsilon$$

$$\Delta\varepsilon = \frac{\theta}{32982 cb}$$

$\Delta\varepsilon$ = molar extinction or molar CD, $M^{-1}\ cm^{-1}$

$$\therefore \quad k = 32982$$

Reference

1. Charney, E. *A Molecular Basis of Optical Activity;* Wiley-Interscience: New York, NY, **1979**; pp 351–353.

APPENDIX D

CHELATING DIPHOSPHINE LIGAND VS. NATURAL BITE ANGLE (β_n) CALCULATIONS

Table 1 Calculated, modeled and X–ray natural bite angles of diphosphine ligands.

Chelating Ligand	Natural Bite Angle, β_n / °		
	Calculated[d]	Modeled	X–ray
dppee	–	–	89 (4)[a]
PROPHOS (dppe)	85.03 (3.11)[b]	84.4 (70–95)[b]	85 (3)[a]
CHIRAPHOS (dppe)	85[c]	–	–
BDPP (dppp)	91.08 (4.00)[b]	86.2[b]	91.56 (3.70)[b]
DUPHOS	82.61[b]	84.7[b]	–
NORPHOS	–	123 (110–145)[a]	–
DIOP	97.63 (4.72)[b]	98 (90–120)[a]	100.0 (4.3)[b]
BINAP	92.43 (2.6)[b]	–	92(3)[a]

For calculated data and crystal structure, the values in parentheses are the standard deviations and for modeled data the values in parentheses indicate the range of bite angles a ligand can accommodate with no more than 3 kcal mol^{-1} strain energy (flexibility range). [a] Ref. 1 [b] Ref. 2 [c] Ref. 3 [d] Standardized ligand bite angle with M–P distances of 2.315 Å calculated from the P···P distance as found in the CSD {=2arcsin1/2($r_{P...P}$/2.315)}. dppe = $Ph_2PCH_2CH_2PPh_2$, dppp = $Ph_2PCH_2CH_2CH_2PPh_2$

Table 2 *cis*-Pt-TIPS-monoyne Data

Compound	Ligand	δ /ppm	$^3J_{P-P}$ / Hz	$^1J_{P-Pt}$ / Hz	β_n /°	Absolute Δε / M^{-1} cm^{-1}
225	*R,R*-Me-DUPHOS	65.3		2134	83	3
223	*R*-PROPHOS	51.3		2206	85	5
223	*R*-PROPHOS	34.2		2191	85	5
215	*S,S*-CHIRAPHOS	46.4	13	2194	85	13
214	dppee	52.0		2208	89	N/A
224	*S,S*-BDPP	5.7		2134	91	2
226	*R,R*-NORPHOS	11.2	28	2213	123	28
226	*R,R*-NORPHOS	10.3		2211	123	28

Table 3 *cis*-Pt-tolyl-monoyne Data

Compound	Ligand	δ /ppm	$^{3}J_{P-P}$ / Hz	$^{1}J_{P-Pt}$ / Hz	β_n /°	Absolute Δε / M^{-1} cm^{-1}
231	*R,R*-Me-DUPHOS	66.4		2206	83	6
229	*R*-PROPHOS	44.2	25	2234	85	9
229	*R*-PROPHOS	51.7	9	2285	85	9
228	*S,S*-CHIRAPHOS	34.3		2259	85	25
226	dppee	53.1		2276	89	N/A
230	*S,S*-BDPP	26.9		2585	91	12
232	*R,R*-NORPHOS	11.8	53	2280	123	53
232	*R,R*-NORPHOS	11.1		2280	123	53

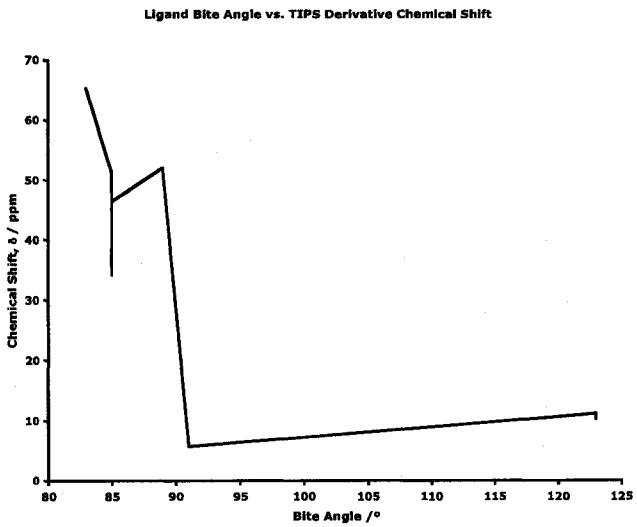

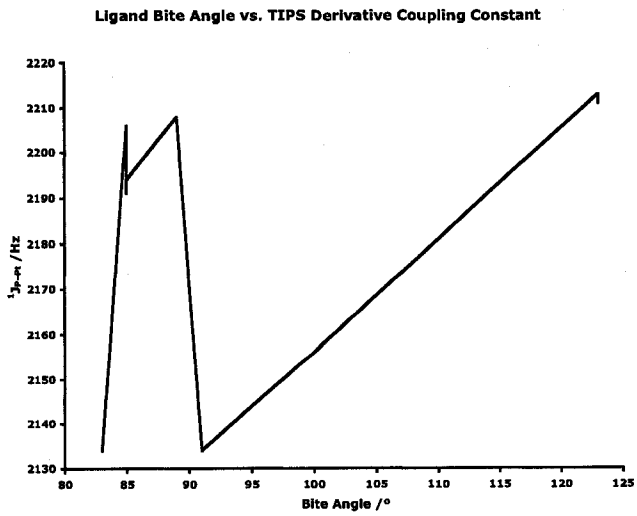

Ligand Bite Angle vs. Tolyl Derivative Chemical Shift

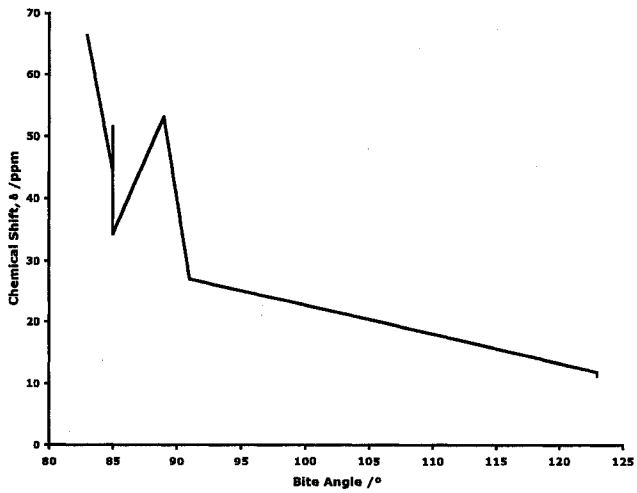

Ligand Bite Angle vs. Tolyl Derivative Coupling Constant

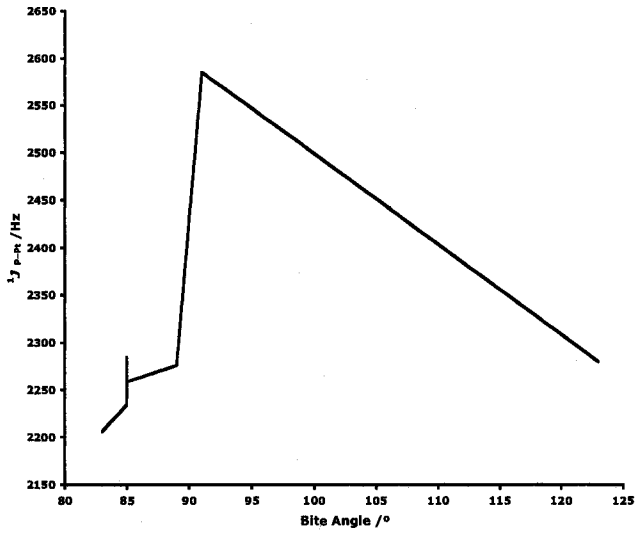

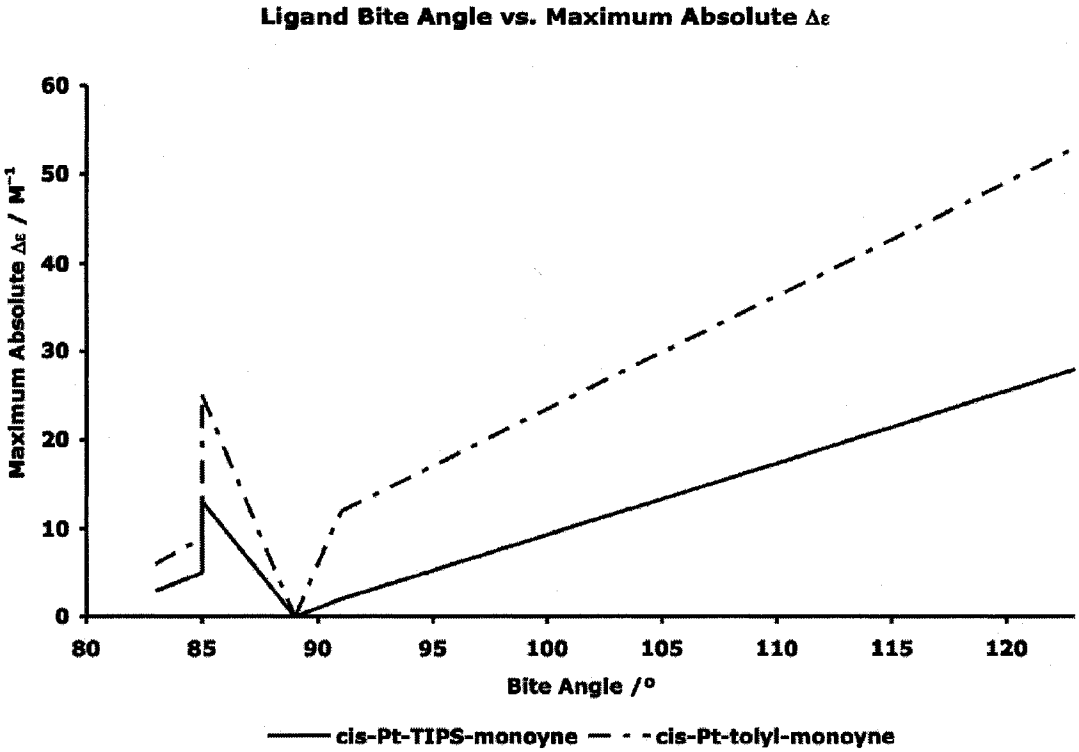

References:

1. van Leeuwen, P.; Kamer, P. C. J.; Reek, J. N. H.; Dierkes, P. *Chem. Rev.* **2000**, *100*, 2741-2769.
2. Dierkes, P.; van Leeuwen, P. *J. Chem. Soc., Dalton Trans.* **1999**, 1519-1529.
3. del Rio, I.; de Lange, W. G. J.; van Leeuwen, P.; Claver, C. *J. Chem. Soc., Dalton Trans.* **2001**, 1293-1300.